Rod-like Brownian Particles in Shear Flow

Jan K.G. Dhont, W.J. Briels

WILEY-VCH Verlag Berlin GmbH
December 22, 2004

Preface

This chapter is a self-contained treatment of various aspects concerning suspensions of uniaxial rod-like colloidal particles in flow. First of all, friction coefficients of rods in an otherwise unbounded fluid will be calculated and the motion of a single rod in flow will be discussed, both for a non-Brownian and a Brownian rod. The generalized diffusion equation for interacting rods, the so-called N-particle Smoluchowski equation is then discussed, on the basis of which the Doi-Edwards equation of motion for the orientational order parameter tensor is derived. This microscopic derivation reveals the approximations that are involved in the Doi-Edwards theory. One of the approximations involves the neglect of dynamical correlations. Computer simulations indicate that such correlations might be important. On the basis of the Doi-Edwards equation (supplemented with an appropriate closure relation) together with experimental results, the phase behaviour of rods in simple shear flow is addressed. A microscopic expression for the stress tensor for suspensions of rigid colloidal particles is then derived, and subsequently expressed in terms of the orientational order parameter tensor. The viscoelastic response of suspensions of stiff rods is discussed, and theory is compared with experiments and simulations. In the last section, current research interests will be briefly discussed, including banding transitions, the non-equilibrium phase diagram under flow conditions and phase separation kinetics.

0.1 Introduction

Flow affects microstructural order of colloidal systems in two respects : center-to-center correlations are affected by flow and flow can induce changes in orientational order. For spherical colloids, flow-induced changes of macroscopic properties find their origin entirely in shear-induced changes of center-to-center correlations. For non-spherical colloidal particles, there is the additional effect that flow tends to align single colloidal particles due to the torques that the flowing solvent exerts on their cores. For very elongated colloidal cores, single particle alignment is dominant over shear-induced changes of center-to-center correlations. For such systems, equations for one-particle orientational distribution functions, with the neglect of flow-induced distortions of center-to-center correlations, are sufficient to predict their macroscopic behaviour under flow. For spherical colloidal particles, however, one-particle distribution functions are not affected by flow, so that theory for spheres should be based on equations for correlation functions.

This chapter deals with stiff, uni-axial colloidal rods with a very large aspect ratio in shear flow. It will be assumed throughout the chapter that the center-to-center correlation function is not affected by flow, and is thus equal to the corresponding correlation function in equilibrium, in the absence of flow. In addition, the singlet function of rods surrounding a given rod is taken equal to the singlet function of that given rod at the same instant of time. As will be discussed, these two simplifications are equivalent to the neglect of dynamical correlations. There are indications from computer simulations, however, that dynamical correlations might play a role.

Examples of flow-affected macroscopic phenomena which will be discussed in the present chapter are the shear-induced shift of the isotropic-nematic phase transition and the shear-rate dependent viscoelastic response. The effect of shear flow on microstructural order, which is at the origin of shear-induced macroscopic phenomena, will be considered in detail. In addition, shear flow induces phenomena which do not occur in the absence of flow, such as pattern formation (or more specific, shear banding) and dynamical states under stationary applied flow. These will be addressed only briefly at the end of this chapter.

The aim of this chapter is to set up, in a self contained fashion, a microscopic theory of the behaviour of rods in flow. Some of the results presented here are on a text book level, some are re-derivations of well-known equations and some are at the edge of current research interests. Much of the introductory material on colloids is also discussed by Doi and Edwards (1986), Russel, Saville, and Schowalter (1991) and Dhont (1996).

First of all, the so-called *velocity gradient tensor* will be defined in section 2. This tensor describes the type of flow that is applied. Two types of flow are of particular importance : simple shear flow and elongational (or, extensional) flow. Simple shear flow is a velocity profile where the gradient in the fluid flow velocity is constant, whereas for elongational flow the sample is compressed in one direction and elongated in the other direction. Such flows can be either stationary or oscillatory.

Colloidal rods tend to align in a flow field due to the interaction of the solvent with the surface of the core of the rods. As a first step to understand how orientational order is affected

by flow, the force and torque of the solvent on a single rod in an otherwise unbounded fluid must be calculated. Since the linear dimensions of the rods is much larger than the size of solvent molecules, the solvent can be described on the basis of hydrodynamics. The rod is treated as a macroscopic object as far as its interactions with solvent molecules is concerned. The basic knowledge of hydrodynamics relevant for colloids is developed in section 3. The main result here is that inertial effects can be neglected on a time scale that is relevant for colloids, leading to the so-called *creeping flow equations* for the solvent flow velocity. These are linear equations of motion for which the Greens function, known as *the Oseen tensor*, is derived in section 3. Friction of rods in a flowing solvent is then treated on basis of these basic hydrodynamic equations in section 4. Friction coefficients can be calculated exactly for ellipsoidal rods of arbitrary aspect ratio, which involves an exact solution of the creeping flow equations, Happel and Brenner (1983). Alternatively, friction coefficients are derived in section 4 on the basis of the bead model for a rod, by analyzing forces that act on beads.

Once the hydrodynamic friction coefficients are known, orbits of the orientation of a non-Brownian rod in a flow field can be analyzed. These so-called *Jeffery orbits* are discussed in section 5. Here, interactions between rods are not incorporated, that is, the orbits of a single rod in an otherwise unbounded fluid are considered.

Brownian motion in the absence of flow is then analyzed in section 6 on the basis of Newton's equation of motion. This equation of motion includes a random force which describes forces originating from collisions of solvent molecules with the surface of the colloidal particle. Such equations of motion containing a fluctuating term are referred to as *Langevin equations*. Specifying certain statistical properties of the random force allows to distinguish between several important time scales and the calculation of the *mean squared displacement*. Again, this analysis is performed for a single rod in an otherwise unbounded solvent.

For the description of Brownian motion and diffusion of rods at higher rod concentration, where interactions between rods are important, it is more convenient to employ equations of motion for probability density functions. The fundamental equation of motion of this sort, the so-called *Smoluchowski equation* is derived in section 7. In the same section it is shown that the diffusive properties as obtained in section 6 on the basis of the Langevin equation are reproduced by the Smoluchowski equation.

At higher concentrations and when a flow field is applied, the orientational order can be quantified by means of the *orientational order parameter tensor* $\mathbf{S}$. This tensor is introduced in section 8. It is shown that the largest eigenvalue of this tensor is a measure for the degree of orientational order and that the corresponding eigenvector defines the preferred orientation of the rods.

Orientational order for very dilute rod-suspensions under flow are discussed in section 9. Interactions between rods are neglected here. Solutions of the Smoluchowski equation are shown to be in accordance with computer simulations.

Orientational order and phase behaviour of concentrated suspensions in flow is analyzed by means of an equation of motion for the order parameter tensor $\mathbf{S}$, which is known as *the Doi-Edwards equation*. In section 10 this equation of motion is derived from the Smoluchowski equation. This derivation is a microscopic basis of the Doi-Edwards equation, which reveals the approximations that are implicit in the Doi-Edwards equation. To obtain a closed equation of motion for the second order tensor $\mathbf{S}$, a closure relation must be used for a fourth order tensor. There are a number of propositions for such a closure relation. A simple closure

relation will be discussed in section 10, which is shown to be accurate to within about $10\,\%$. This particular closure relation, however, can not describe non-stationary states under stationary flow conditions like tumbling and wagging. To describe such states, the Smoluchowski equation itself should be solved numerically. This will not be discussed in the present chapter.

The isotropic-nematic phase transition is discussed in section 11, both without and with simple shear flow. The bifurcation diagram is introduced and the paranematic-to-nematic and nematic-to-paranematic spinodals in the shear-rate versus concentration plane are calculated. The prediction of the shear-rate dependent location of binodals is much more complicated, and requires equations of motion for the orientational order parameter tensor *and* the flow field velocity, which should accurately account for strong inhomogeneities in concentration, orientational order parameter and shear rate. Such equations of motion will not be derived in this chapter, but only briefly discussed in the last section on current research.

In the derivation of the Doi-Edwards equation of motion from the Smoluchowski equation, dynamical correlations are neglected. Computer simulations indicate, however, that such correlations are important for the description of diffusion. The discrepancy between the analytically obtained effective collective diffusion coefficients within the Doi-Edwards theory and that found in computer simulations is discussed in section 12.

A microscopic derivation of the stress tensor in terms of the concentration and the orientational order parameter tensor is given in section 13. Within certain approximations, a very similar expression as in the Doi-Edwards-Kuzuu theory is obtained. On the basis of this expression for the stress tensor, (non-linear) viscoelastic elastic response of rod suspensions is discussed in section 14. Analytical and numerical predictions are compared to experiments and computer simulations. A surprising finding is that the zero-shear, zero-frequency shear viscosity is a linear function of the concentration up to very high concentrations, in accordance with computer simulations. Comparison with experiments indicates a sensitive dependence of the viscoelastic behaviour on the flexiblity of the core of the rods. So far, no theory on the dynamics and viscoelastic response is available that incorporates flexibility.

Section 15 is a (certainly biased) overview of the current research interests in the field of rod suspensions under shear flow. The possible non-equilibrium phase diagram is addressed, together with banding transitions, non-stationary states and kinetics of phase separation and band formation.

0.2 The Velocity Gradient Tensor

A linear flow profile is characterized by means of the so-called velocity gradient tensor $\mathbf{G}$, where the flow velocity $\mathbf{U}$ at position $\mathbf{r}$ is written as $\mathbf{U} = \mathbf{G} \cdot \mathbf{r}$. For spatially varying flow profiles, velocities can locally be described by such a linear flow profile, provided that gradients are small on the length scale set by the size of the colloidal particles. The velocity gradient tensor can have several different forms. In case of so-called *simple shear flow*, the gradient velocity tensor is usually denoted as $\mathbf{\Gamma}$, and is equal to,

$$\mathbf{\Gamma} \;=\; \dot{\gamma} \begin{pmatrix} 0 & 1 & 0 \\ 0 & 0 & 0 \\ 0 & 0 & 0 \end{pmatrix} \quad , \quad \text{simple shear flow} \; . \tag{1}$$

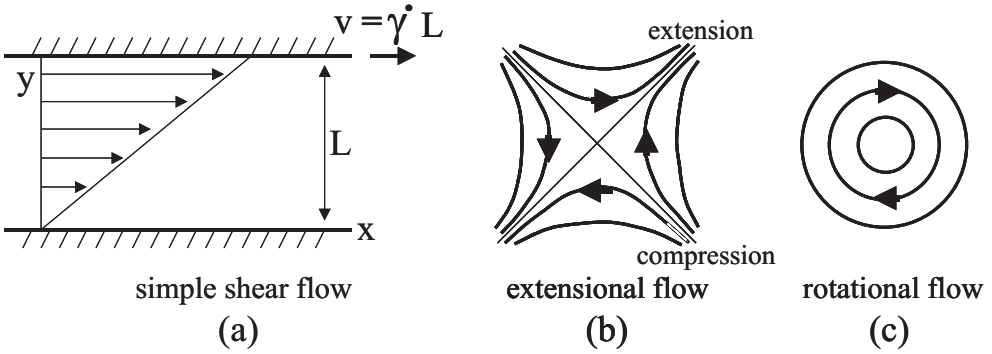

Figure 1: (a) Simple shear flow, where L is the gapwidth. (b) Depicts elongational flow, sometimes also referred to as extensional flow (where the elongational and compression axes are indicated), and (c) depicts rotational flow. Arrows indicate the flow direction.

The corresponding flow profile is a flow in the x-direction, with its gradient in the y-direction, as sketched in fig.1a. The z-direction is commonly referred to as the vorticity direction. The strength of the flow is characterized by the *shear rate* $\dot{\gamma}$, which equals the spatial gradient $\partial U_x/\partial y$ of the flow velocity U_x in the x-direction. For so-called *elongational or extensional flow*, where the velocity gradient tensor is denoted as $\mathbf{E}$, we have,

$$\mathbf{E} \;=\; \dot{\gamma} \begin{pmatrix} 0 & 1 & 0 \\ 1 & 0 & 0 \\ 0 & 0 & 0 \end{pmatrix} \quad , \quad \text{elongational flow} \; , \tag{2}$$

which flow is sketched in fig.1b. In such an elongational flow, deformable objects tend to elongate along the so-called extensional axis, and suppressed along the compressional axis. These two directions are indicated in fig.1b. Whenever it is not specified whether simple shear flow or elongational flow is considered, the velocity gradient tensor will be denoted as $\mathbf{G}$.

We will encounter the symmetric part $\mathbf{E} = \frac{1}{2}\left[\mathbf{G} + \mathbf{G}^T\right]$ of the velocity gradient tensor, where the superscript "T" stands for the transpose of the corresponding tensor. For elongational flow, the velocity gradient tensor is already symmetric : this is why we denoted the velocity gradient tensor for elongational flow by an $\mathbf{E}$ in eq.(2). For simple shear flow we have,

$$\mathbf{E} \;=\; \tfrac{1}{2}\dot{\gamma} \begin{pmatrix} 0 & 1 & 0 \\ 1 & 0 & 0 \\ 0 & 0 & 0 \end{pmatrix} \quad , \quad \text{simple shear flow} \; . \tag{3}$$

We will sometimes also encounter the anti-symmetric part $\mathbf{\Omega} = \frac{1}{2}\left[\mathbf{G} - \mathbf{G}^T\right]$ of the velocity gradient tensor. For elongational flow the anti-symmetric part is zero, while for simple shear flow we have,

$$\mathbf{\Omega} \;=\; \tfrac{1}{2}\dot{\gamma} \begin{pmatrix} 0 & 1 & 0 \\ -1 & 0 & 0 \\ 0 & 0 & 0 \end{pmatrix} \quad , \quad \text{simple shear flow} \; . \tag{4}$$

The flow velocities corresponding to flow with a velocity gradient tensor equal to $\mathbf{E}$ in eq.(3) or eq.(4) are sketched in fig.1b and c, respectively. The former case is an elongational flow, also referred to as extensional flow, while the second is pure rotational flow. Note that,

$$\mathbf{\Gamma} \;=\; \mathbf{E} + \mathbf{\Omega}\;, \tag{5}$$

so that simple shear flow can be decomposed into a linear combination of elongational and rotational flow.

In laboratory experiments, the shear rate is either independent of time, or the shear rate can be sinusoidally oscillating,

$$\begin{aligned} \dot{\gamma} \;&=\; \text{time independent} \quad , \;\; \text{stationary flow}\;, \\ \dot{\gamma}(t) \;&=\; \dot{\gamma}_0\, \cos\{\omega\, t\} \qquad , \;\; \text{oscillatory flow}\;, \end{aligned} \tag{6}$$

where ω is the frequency of oscillation and $\dot{\gamma}_0$ is referred to as the *shear-rate amplitude*. Oscillatory experiments can be employed to probe the dynamics of a system of Brownian particles.

0.3 Hydrodynamics

Consider a system containing large rod-like particles immersed in a fluid. There are three types of interactions to be distinguished in such a system : interactions of rods with rods, solvent molecules with solvent molecules and rods with solvent molecules. The latter two types of interactions can be described on the basis of phenomenological equations for fluid flow, provided that the linear dimensions of the rods are much larger than the size of solvent molecules. Such solutions of large molecules are referred to as *Brownian or colloidal systems*. The large difference in relevant length scales between the solvent and the assembly of Brownian rods allows to describe the solvent on a phenomenological level, without losing the microscopics for the assembly of Brownian particles. In such a phenomenological treatment, only macroscopic quantities of the fluid like its viscosity and mass density enter the equations of interest. In the present section, friction coefficients of rods are calculated, which will be used later in this chapter in microscopic equations of motion for rod-like Brownian particles.

The mechanical state of the solvent is characterized by the local velocity $\mathbf{u}(\mathbf{r}, t)$ at position $\mathbf{r}$ at time t, the pressure $p(\mathbf{r}, t)$ and the mass density $\rho(\mathbf{r}, t)$. All these fields are averages over small volume elements that are located at the various positions $\mathbf{r}$. These volume elements must be so small that the state of the fluid hardly changes within the volume elements. At the same time, the volume elements should contain many fluid molecules, to be able to properly define such averages. In particular we wish to define the thermodynamic state of volume elements, which is possible when they contain a large amount of solvent molecules, and when they are in internal equilibrium, that is, when there is *local equilibrium*. In this way the temperature field $T(\mathbf{r}, t)$ may be defined. The temperature dependence of, for example, the mass density is then described by thermodynamic relations. These thermodynamic relations are an important ingredient in a general theory of hydrodynamics. For our purposes, however, the temperature and mass density may be considered constant. Temperature variations due to viscous dissipation in the solvent are assumed to be negligible. At constant temperature, the only mechanism to change the mass density of the solvent is to vary the pressure. For fluids,

however, exceedingly large pressures are needed to change the density significantly, that is, fluids are quite *incompressible*. Brownian motion is not so vigorous to induce such extreme pressure differences, so that the density will also be assumed constant. The assumption of constant temperature and density is also a matter of time scales. Relaxation times for local temperature and pressure differences in the solvent are much faster than typical time scales relevant for Brownian motion.

Assuming constant temperature and mass density leaves just two variables which describe the state of the fluid : the fluid flow velocity $\mathbf{u}(\mathbf{r},t)$ and the pressure $p(\mathbf{r},t)$. Thermodynamic relations need not be considered in this case, simplifying the phenomenological analysis considerably.

0.3.1 The continuity equation

The rate of change of the mass of fluid contained in some arbitrary volume $\mathcal{W}$ is equal to the mass of fluid flowing through its boundary $\partial\mathcal{W}$. The local velocity at surface elements on $\partial\mathcal{W}$ can be written as the sum of its component parallel and perpendicular to the surface. The parallel component does not contribute to in and out flux of mass through the boundary $\partial\mathcal{W}$. Only the component $\mathbf{u}\cdot\hat{\mathbf{n}}$ of the flow perpendicular to the surface gives rise to in and out flux of mass, where $\hat{\mathbf{n}}$ is the unit normal of the corresponding surface element. Hence,

$$\frac{d}{dt}\int_{\mathcal{W}} d\mathbf{r}\,\rho(\mathbf{r},t) \;=\; -\oint_{\partial\mathcal{W}} d\mathbf{S}\cdot\{\rho(\mathbf{r},t)\mathbf{u}(\mathbf{r},t)\}\;,$$

where $d\mathbf{S}=\hat{\mathbf{n}}\,dS$, with dS an infinitesimal surface area. The minus sign on the right hand-side is added, because the mass in $\mathcal{W}$ decreases when $\mathbf{u}$ is along the outward normal. The time derivative on the left hand-side can be taken inside the integral, while the integral on the right hand-side can be written as an integral over the volume $\mathcal{W}$, using Gauss's integral theorem. This leads to,

$$\int_{\mathcal{W}} d\mathbf{r}\,\left[\frac{\partial}{\partial t}\rho(\mathbf{r},t) \;+\; \nabla\cdot\{\rho(\mathbf{r},t)\mathbf{u}(\mathbf{r},t)\}\right] \;=\; 0\;,$$

where ∇ is the gradient operator with respect to $\mathbf{r}$. Since the volume $\mathcal{W}$ is an arbitrary volume, the integrand must be equal to zero. This can be seen by choosing $\mathcal{W}$ as a sphere centered at some position $\mathbf{r}$, with a (infinitesimally) small radius. Within that small sphere the integrand in the above integral is constant, so that the integral reduces to the product of the volume of $\mathcal{W}$ and the value of the integrand at the point $\mathbf{r}$. Hence,

$$\frac{\partial}{\partial t}\,\rho(\mathbf{r},t) \;+\; \nabla\cdot\{\rho(\mathbf{r},t)\mathbf{u}(\mathbf{r},t)\} \;=\; 0\;.$$

This equation expresses conservation of mass, and is referred to as the *continuity equation*.

For a fluid with a constant mass density, the continuity equation reduces to,

$$\nabla\cdot\mathbf{u}(\mathbf{r},t) \;=\; 0\;. \tag{7}$$

Fluids with an essentially constant mass density are referred to as *incompressible fluids*, and eq.(7) is therefore sometimes referred to as the *incompressibility equation*. Being nothing more than the condition to ensure conservation of mass, this single equation is not sufficient to calculate the fluid flow velocity. It must be supplemented by Newton's equation of motion to obtain a closed set of equations.

0.3.2 The Navier-Stokes equation

The Navier-Stokes equation is Newton's equation of motion for a small amount of mass contained in a volume element within the fluid. Consider such an infinitesimally small volume element, the volume of which is denoted as $\delta\mathbf{r}$. The position $\mathbf{r}$ of that volume element as a function of time is set by Newton's equation of motion. The momentum that is carried by the mass element is equal to $\rho(\mathbf{r},t)\,(\delta\mathbf{r})\mathbf{u}(\mathbf{r},t)$, so that Newton's equation of motion reads,

$$\rho(\mathbf{r},t)\;\delta\mathbf{r}\;\frac{d\mathbf{u}(\mathbf{r},t)}{dt}\;=\;\mathbf{f}\;,$$

where $\mathbf{f}$ is the total force that is exerted on the mass element. Since in Newton's equations of motion $\mathbf{r}$ is the time dependent position coordinate of the volume element, and $d\mathbf{r}/dt = \mathbf{u}$ is the velocity of the volume element, the above equation can be written as,

$$\rho(\mathbf{r},t)\;\delta\mathbf{r}\;\left[\frac{\partial\mathbf{u}(\mathbf{r},t)}{\partial t}+\mathbf{u}(\mathbf{r},t)\cdot\nabla\mathbf{u}(\mathbf{r},t)\right]\;=\;\mathbf{f}\;.$$

Here, $\nabla\mathbf{u}$ is a dyadic product, that is, it is a tensor of which the ij^{th} component is equal to $\nabla_i\mathbf{u}_j$, with ∇_i the differentiation with respect to r_i, the i^{th} component of $\mathbf{r}$.

The total force $\mathbf{f}$ on the volume element consists of two parts. First of all, there may be external fields which exert forces on the fluid. These forces are denoted by $(\delta\mathbf{r})\,\mathbf{f}^{ext}(\mathbf{r})$, that is, $\mathbf{f}^{ext}$ is the external force on the fluid per unit volume. The second part arises from interactions of the volume element with the surrounding fluid.

The forces due to interactions with the surrounding fluid are formally expressed in terms of the *stress tensor* $\mathbf{\Sigma}(\mathbf{r},t)$, which is defined as follows. Consider an infinitesimally small surface area in the fluid, with surface area dS and a normal unit vector $\hat{\mathbf{n}}$. The force per unit area exerted by the fluid located at the side of the surface area to which the unit normal is directed, on the fluid on the opposite side of the surface area, is by definition equal to $d\mathbf{S}\cdot\mathbf{\Sigma}$, with $d\mathbf{S}{=}\hat{\mathbf{n}}\,dS$ (see fig.2).

Hence, by definition, the force of surrounding fluid on the volume element $\delta\mathbf{r}$ is equal to,

$$\oint_{\partial\delta\mathbf{r}} d\mathbf{S}'\;\cdot\mathbf{\Sigma}(\mathbf{r}',t)\;=\;\int_{\delta\mathbf{r}} d\mathbf{r}'\,\nabla'\cdot\mathbf{\Sigma}(\mathbf{r}',t)\;=\;\delta\mathbf{r}\;\nabla\cdot\mathbf{\Sigma}(\mathbf{r},t)\;,$$

where $\partial\delta\mathbf{r}$ is the boundary of the volume element. We used Gauss's integral theorem to rewrite the surface integral as a volume integral. The last equation is valid due to the infinitesimal size $\delta\mathbf{r}$ of the volume element at position $\mathbf{r}$. The force $\mathbf{f}^h$ on the volume element due to interaction with the surrounding fluid is thus given by,

$$\mathbf{f}^h(\mathbf{r},t)\;=\;(\delta\mathbf{r})\,\nabla\cdot\mathbf{\Sigma}(\mathbf{r},t)\;. \tag{8}$$

There are two contributions to the stress tensor : a contribution resulting from gradients in the fluid flow velocity, and a contribution due to pressure gradients.

Consider first the forces due to pressure gradients. Let us take the volume element $\delta\mathbf{r}$ cubic, with sides of length δl. The pressure p is a force per unit area, so that the force on the volume element in the x-direction is equal to,

$$(\delta l)^2\left(p(x-\frac{1}{2}\delta l,y,z,t)-p(x+\frac{1}{2}\delta l,y,z,t)\right)=-(\delta l)^3\;\frac{\partial}{\partial x}\,p(x,y,z,t),$$

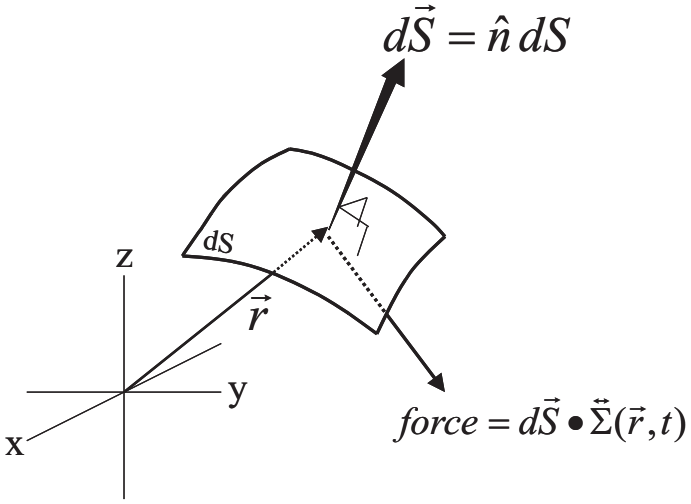

Figure 2: Definition of the stress tensor $\mathbf{\Sigma}$.

where $(\delta l)^2$ is the area of the faces of the cube. The force on the volume element is thus $-(\delta \mathbf{r})\nabla p(\mathbf{r}, t)$. We therefore arrive at, $\nabla \cdot \mathbf{\Sigma} = -\nabla p$. The contribution of pressure gradients to the stress tensor is thus easily seen to be equal to,

$$\mathbf{\Sigma}(\mathbf{r}, t) \; = \; -p(\mathbf{r}, t)\, \hat{\mathbf{I}}\,,$$

with $\hat{\mathbf{I}}$ the 3×3-dimensional unit tensor. This contribution to the stress tensor is referred to as *the isotropic part of the stress tensor*, since it is proportional to the unit tensor and therefore does not have a preferred spatial direction.

Next, consider the forces on the volume element due to gradients in the fluid flow velocity. When the fluid flow velocity is uniform, that is, when there are no gradients in the fluid flow velocity, the only forces on the volume element are due to pressure and possibly external forces. There are friction forces in addition, only in case the volume element attains a velocity which differs from that of the surrounding fluid. The contribution to the stress tensor due to friction forces is therefore a function of spatial derivatives of the flow velocity, not of the velocity itself. This contribution to the stress tensor can be formally expanded in a power series with respect to the gradients in the fluid flow velocity. For not too large gradients (such that the fluid velocity is approximately constant over distances of many times the molecular dimension) the leading term in such an expansion suffices to describe friction forces. The contribution of gradients in the fluid flow velocity to the stress tensor is thus a linear combination of the derivatives $\nabla_i u_j(\mathbf{r}, t)$, where ∇_i is the derivative with respect to the i^{th} component of $\mathbf{r}$, and $u_j(\mathbf{r}, t)$ is the j^{th} component of $\mathbf{u}(\mathbf{r}, t)$.

There are also no friction forces when the fluid is in uniform rotation, in which case the flow velocity is equal to $\mathbf{u} = \mathbf{\Omega} \times \mathbf{r}$, with $\mathbf{\Omega}$ the angular velocity. Such a fluid flow corresponds to rotation of the vessel containing the fluid, relative to the observer. Linear combinations of the form,

$$\nabla_i u_j(\mathbf{r}, t) + \nabla_j u_i(\mathbf{r}, t)\,, \tag{9}$$

are easily verified to vanish in case $\mathbf{u} = \mathbf{\Omega} \times \mathbf{r}$. The stress tensor is thus proportional to such linear combinations of gradients in the fluid velocity field.

For isotropic fluids, with no preferred spatial direction, the most general expression for the components Σ_{ij} of the stress tensor as a result of friction is therefore,

$$\Sigma_{D,ij} \;=\; \eta_0 \left\{ \nabla_i u_j + \nabla_j u_i - \frac{2}{3}\delta_{ij} \nabla \cdot \mathbf{u}(\mathbf{r},t) \right\} + \zeta_0 \, \delta_{ij} \nabla \cdot \mathbf{u} \,, \tag{10}$$

where the subscript "D" stands for *the deviatoric part of the stress tensor*. The terms $\sim \nabla \cdot \mathbf{u}(\mathbf{r},t)$ on the right hand-side are due to the linear combinations (9) with $i = j$. The term $-\frac{2}{3}\nabla \cdot \mathbf{u}(\mathbf{r},t)$ is introduced to make the expression between the curly brackets traceless (meaning that the sum of the diagonal elements of that contribution is zero). It could also have been absorbed in the last term on the right hand-side. The constants η_0 and ζ_0, which are scalar quantities for isotropic fluids, are the *shear viscosity* and *bulk viscosity* of the fluid, respectively. Notice that all terms proportional to $\nabla \cdot \mathbf{u}(\mathbf{r},t)$ are zero for incompressible fluids.

We thus find the following expression for the total stress tensor for an isotropic fluid,

$$\begin{aligned} \mathbf{\Sigma}(\mathbf{r},t) \;\; &= \;\; \eta_0 \left\{ \nabla \mathbf{u}(\mathbf{r},t) + [\nabla \mathbf{u}(\mathbf{r},t)]^T - \frac{2}{3}\,\hat{\mathbf{I}}\,\nabla \cdot \mathbf{u}(\mathbf{r},t) \right\} \\ &\qquad + \left\{ \zeta_0 \, \nabla \cdot \mathbf{u}(\mathbf{r},t) - p(\mathbf{r},t) \right\} \hat{\mathbf{I}} \,, \end{aligned} \tag{11}$$

where the superscript T stands for transposition.

The above expression for the stress tensor leads to the *Navier-Stokes equation*,

$$\begin{aligned} \rho \, \frac{\partial \mathbf{u}(\mathbf{r},t)}{\partial t} + \rho \, \mathbf{u}(\mathbf{r},t) \cdot \nabla \mathbf{u}(\mathbf{r},t) \;\; &= \;\; \eta_0 \, \nabla^2 \mathbf{u}(\mathbf{r},t) - \nabla p(\mathbf{r},t) \\ &\quad + \left(\zeta_0 + \frac{1}{3}\eta_0 \right) \nabla \left(\nabla \cdot \mathbf{u}(\mathbf{r},t) \right) + \mathbf{f}^{ext}(\mathbf{r}) \,, \end{aligned} \tag{12}$$

where the mass density, and the shear- and bulk viscosity are now taken independent of position. For incompressible fluids, for which $\nabla \cdot \mathbf{u}(\mathbf{r},t) = 0$ (see eq.(7)), the Navier-Stokes equation reduces to,

$$\rho \, \frac{\partial \mathbf{u}(\mathbf{r},t)}{\partial t} + \rho \, \mathbf{u}(\mathbf{r},t) \cdot \nabla \mathbf{u}(\mathbf{r},t) = \nabla \cdot \mathbf{\Sigma}(\mathbf{r},t) + \mathbf{f}^{ext}(\mathbf{r},t) = \eta_0 \nabla^2 \mathbf{u}(\mathbf{r},t) - \nabla p(\mathbf{r},t) + \mathbf{f}^{ext}(\mathbf{r}) \,. \tag{13}$$

Together with the continuity equation (7) for incompressible fluids, this equation fully determines the fluid flow and pressure once the external force and boundary conditions are specified.

0.3.3 The creeping flow equations

The different terms in the Navier-Stokes equation (13) can be very different in magnitude, depending on the problem at hand. In the present case we are interested in fluid flow around small sized objects (the colloidal particles). Let us estimate the magnitude of the various terms in the Navier-Stokes equation for this case. A typical value for the fluid flow velocity is the velocity v of the colloidal objects. The fluid flow velocity decreases from a value v, close to

a Brownian particle, to a much smaller value, over a distance of the order of a typical linear dimension a of the particles (for spherical particles a is the radius, for a rotating rod a is the length of the rod). Hence, typically, $\mid \nabla^2 \mathbf{u} \mid \approx v/a^2$. Similarly, $\mid \mathbf{u} \cdot \nabla \mathbf{u} \mid \approx v^2/a$. The rate of change of $\mathbf{u}$ is v divided by the time it takes the colloidal particle to lose its velocity due to friction with the fluid. This time interval is equal to a few times M/γ, with M the mass of the colloidal particle and γ its friction coefficient (this will be discussed in more detail later in this chapter). Introducing the rescaled variables,

$$\begin{aligned} \mathbf{u}' &= \mathbf{u}/v \,, \\ \mathbf{r}' &= \mathbf{r}/a \,, \\ t' &= t/(M/\gamma) \,, \end{aligned}$$

transforms the Navier-Stokes equation (13) to,

$$\frac{\rho\,\gamma\,v}{M}\,\frac{\partial \mathbf{u}'}{\partial t'} + \frac{\rho\,v^2}{a}\,\mathbf{u}'\cdot\nabla'\mathbf{u}' \;=\; \frac{\eta_0 v}{a^2}\nabla'^{\,2}\mathbf{u}' - \frac{1}{a}\nabla' p + \mathbf{f}^{ext} \,,$$

where ∇' is the gradient operator with respect to $\mathbf{r}'$. Introducing further the dimensionless pressure and external force,

$$\begin{aligned} p' &= \frac{a}{\eta_0 v}\, p \,, \\ \mathbf{f}'^{\,ext} &= \frac{a^2}{\eta_0 v}\, \mathbf{f}^{ext} \,, \end{aligned}$$

transforms the Navier-Stokes equation further to,

$$\rho\,\frac{a^2\gamma}{M\eta_0}\,\frac{\partial \mathbf{u}'}{\partial t'} + Re\;\mathbf{u}'\cdot\nabla'\mathbf{u}' \;=\; \nabla'^{\,2}\mathbf{u}' - \nabla' p' + \mathbf{f}'^{\,ext} \,. \tag{14}$$

The dimensionless number Re is the so-called *Reynolds number*, which is equal to,

$$Re \;=\; \frac{\rho\,a\,v}{\eta_0} \,. \tag{15}$$

By construction we have,

$$\mid \mathbf{u}'\cdot\nabla'\mathbf{u}' \mid \approx \mid \nabla'^{\,2}\mathbf{u}' \mid \approx\; 1.$$

Hence, for very small values of the Reynolds number, the term proportional to $\mathbf{u}\cdot\nabla\mathbf{u}$ in the left hand-side in eq.(14) may be neglected. Furthermore, for spherical particles we have $\gamma = 6\pi\eta_0 a$ so that $\rho\,a^2\gamma/M\eta_0 = 9\rho/2\rho_p \approx 9/2$, with ρ_p the mass density of the Brownian particle. The prefactor of $\partial\mathbf{u}'/\partial t'$ is thus approximately equal to $9/2$. The time derivative should generally be kept as it stands, also for small Reynolds numbers. Now suppose, however, that one is interested in a description on the diffusive time scale $\tau_D \gg M/\gamma$ (the significance of the diffusive time scale will be discussed later in this chapter). For such times, the time derivative $\partial\mathbf{u}'/\partial t'$ is long zero, since $\mathbf{u}$ goes to zero as a result of friction during the time interval M/γ. One may then neglect the contribution to the time derivative which is due to relaxation of momentum of the Brownian particle as a result of friction with the solvent. The remaining time dependence of $\mathbf{u}$ on the diffusive time scale is due to the possible time dependence of the external force and to interactions with other Brownian rods, which vary

significantly only over time intervals larger than the diffusive time scale. The value of the corresponding derivative $\partial \mathbf{u}/\partial t$ can now be estimated as above : the only difference is that the time should not be rescaled with respect to the time M/γ, but with respect to the diffusive time scale τ_D. We now have, $t' = t/\tau_D$, $\mathbf{u}' = \mathbf{u}/v$, and $\mid \partial \mathbf{u}'/\partial t' \mid \approx 1$. The transformed Navier-Stokes equation in this case reads,

$$\frac{9}{2}\,\frac{\rho}{\rho_p}\,\frac{M/\gamma}{\tau_D}\,\frac{\partial \mathbf{u}'}{\partial t'} + Re\,\mathbf{u}'\cdot\nabla'\mathbf{u}' \;=\; \nabla'^{\,2}\mathbf{u}' - \nabla' p' + \mathbf{f}'^{\,ext}\;,$$

where all derivatives of the fluid flow velocity $\mathbf{u}'$ are of the order 1. Since $\tau_D \gg M/\gamma$, the time derivative due to changes of the fluid flow velocity as a result of the time varying external force and interactions with other Brownian particles may now be neglected in addition.

For small Reynolds numbers and on the diffusive time scale, the Navier-Stokes equation (16), written in terms of the original unprimed quantities, therefore simplifies to,

$$\nabla p(\mathbf{r},t) - \eta_0 \nabla^2\,\mathbf{u}(\mathbf{r},t) \;=\; \mathbf{f}^{ext}(\mathbf{r})\;. \tag{16}$$

This equation, together with the incompressibility equation (7), are the *creeping flow equations*. "Creeping" refers to the fact that the Reynolds number is small, which is the case when the typical fluid flow velocity v is small.

A typical value for the velocity of a Brownian particle can be estimated from the equipartition theorem, $\frac{1}{2}M < v^2 > = \frac{3}{2}k_B T$ (k_B is Boltzmann's constant and T is the temperature). Estimating $v \approx \sqrt{< v^2 >}$, using a typical mass of $10^{-17}\,kg$ for a spherical particle with a radius of $100\,nm$ and the density and viscosity of water, the Reynolds number is found to be equal to 10^{-2}. Hydrodynamics of a fluid in which colloidal particles are embedded can thus be described on the basis of the creeping flow equations.

For small Reynolds numbers and on the Brownian time scale, inertial forces on fluid elements are thus small in comparison to pressure- and friction forces. The neglect of inertial contributions in the Navier-Stokes equation leads to the linear equation (16), which can be solved analytically in some cases.

0.3.4 The Oseen tensor

An external force acting only in a single point $\mathbf{r}'$ on the fluid is mathematically described by a delta distribution,

$$\mathbf{f}^{ext}(\mathbf{r}) \;=\; \mathbf{f}_0\,\delta(\mathbf{r}-\mathbf{r}')\;. \tag{17}$$

The prefactor $\mathbf{f}_0$ is the total force $\int d\mathbf{r}'\,\mathbf{f}^{ext}(\mathbf{r}')$ acting on the fluid. Since the creeping flow equations are linear, the fluid flow velocity at some point $\mathbf{r}$ in the fluid, due to the point force in $\mathbf{r}'$, is directly proportional to that point force. Hence,

$$\mathbf{u}(\mathbf{r}) \;=\; \mathbf{T}(\mathbf{r}-\mathbf{r}')\cdot\mathbf{f}_0\;.$$

The tensor $\mathbf{T}$ is commonly referred to as the *Oseen tensor*, named after the scientist who first derived an explicit expression for this tensor, Oseen (1927). The Oseen tensor connects the point force at a point $\mathbf{r}'$ to the resulting fluid flow velocity at a point $\mathbf{r}$. Note that $\mathbf{T}$ is only a

function of the difference coordinate $\mathbf{r} - \mathbf{r}'$ due to translational invariance of a homogeneous fluid. Similarly, the pressure at a point $\mathbf{r}$ is linearly related to the point force,

$$p(\mathbf{r}) \;=\; \mathbf{g}(\mathbf{r} - \mathbf{r}') \cdot \mathbf{f}_0 \,.$$

The vector $\mathbf{g}$ is referred to here as the *pressure vector*.

Consider an external force which is continuously distributed over the entire fluid. Due to the linearity of the creeping flow equations, the fluid flow velocity at some point $\mathbf{r}$ is simply the superposition of the fluid flow velocities resulting from the forces acting in each point on the fluid. Hence,

$$\mathbf{u}(\mathbf{r}) \;=\; \int d\mathbf{r}' \, \mathbf{T}(\mathbf{r} - \mathbf{r}') \cdot \mathbf{f}^{ext}(\mathbf{r}') \,. \tag{18}$$

The same holds for the pressure,

$$p(\mathbf{r}) \;=\; \int d\mathbf{r}' \, \mathbf{g}(\mathbf{r} - \mathbf{r}') \cdot \mathbf{f}^{ext}(\mathbf{r}') \,. \tag{19}$$

In mathematical language, the Oseen tensor and the pressure vector are the Green's functions of the creeping flow equations for the fluid flow velocity and pressure, respectively. Once these Green's functions are known and the external force is specified, the resulting fluid velocity and pressure can be calculated through the evaluation of the above integrals. The calculation of the Green's functions is thus equivalent to solving the creeping flow equations, provided that the external forces are known.

Let us calculate the Oseen tensor and pressure vector. To this end, substitute eqs.(18,19) into the creeping flow equations (7,16). This leads to,

$$\begin{aligned} \int d\mathbf{r}' \; [\nabla \cdot \mathbf{T}(\mathbf{r} - \mathbf{r}')] \cdot \mathbf{f}^{ext}(\mathbf{r}') \;&=\; 0 \,, \\ \int d\mathbf{r}' \; \Big[\nabla \mathbf{g}(\mathbf{r} - \mathbf{r}') - \eta_0 \nabla^2 \mathbf{T}(\mathbf{r} - \mathbf{r}') - \hat{\mathbf{I}} \, \delta(\mathbf{r} - \mathbf{r}')\Big] \cdot \mathbf{f}^{ext}(\mathbf{r}') \;&=\; \mathbf{0} \,, \end{aligned}$$

where, as before, $\hat{\mathbf{I}}$ is the 3×3-dimensional unit tensor. Since the external force is arbitrary, the expressions in the square brackets must be equal to zero, so that the Green's functions satisfy the following differential equations,

$$\begin{aligned} \nabla \cdot \mathbf{T}(\mathbf{r}) \;&=\; \mathbf{0} \,, \\ \nabla \mathbf{g}(\mathbf{r}) - \eta_0 \nabla^2 \mathbf{T}(\mathbf{r}) \;&=\; \hat{\mathbf{I}} \, \delta(\mathbf{r}) \,. \end{aligned} \tag{20}$$

A single equation for the pressure vector is obtained by taking the divergence of the second equation, with the use of the first equation,

$$\nabla^2 \, \mathbf{g}(\mathbf{r}) \;=\; \nabla \cdot \hat{\mathbf{I}} \, \delta(\mathbf{r}) \;=\; \nabla \delta(\mathbf{r}) \,.$$

Using,

$$\frac{1}{4\pi} \, \nabla^2 \, \frac{1}{r} \;=\; -\, \delta(\mathbf{r}) \,, \tag{21}$$

it follows that,

$$\mathbf{g}(\mathbf{r}) \;=\; -\frac{1}{4\pi}\,\nabla\frac{1}{r} \;+\; \mathbf{G}(\mathbf{r})\;.$$

Here, $\mathbf{G}$ is a vector for which $\nabla^2\mathbf{G}{=}\mathbf{0}$, while $\mathbf{G} \rightarrow \mathbf{0}$ as $r \rightarrow \infty$. It can be shown that such a vector is $\mathbf{0}$. Hence,

$$\mathbf{g}(\mathbf{r}) \;=\; -\frac{1}{4\pi}\nabla\frac{1}{r} \;=\; \frac{1}{4\pi}\,\frac{\mathbf{r}}{r^3}\;. \tag{22}$$

The differential equation to be satisfied by the Green's function for the fluid flow velocity (the Oseen tensor), is found by substitution of eq.(22) into eq.(20),

$$\nabla^2\left[\frac{1}{4\pi}\frac{1}{r}\,\hat{\mathbf{I}} - \eta_0\mathbf{T}(\mathbf{r})\right] \;=\; \frac{1}{4\pi}\left[3\frac{\mathbf{r}\,\mathbf{r}}{r^5} - \frac{1}{r^3}\,\hat{\mathbf{I}}\right]\;.$$

An obvious choice for the term between the square brackets on the left hand-side of the above expression is of the form,

$$\frac{1}{4\pi}\frac{1}{r}\,\hat{\mathbf{I}} - \eta_0\mathbf{T}(\mathbf{r}) \;=\; \alpha_0\frac{1}{r^n}\hat{\mathbf{I}} + \alpha_1\frac{1}{r^m}\frac{\mathbf{r}\,\mathbf{r}}{r^2}\;,$$

with $\alpha_{0,1}$, n and m constants. These constants can indeed be chosen such that this Ansatz is the solution of the differential equation (with the boundary condition that $\mathbf{T}(\mathbf{r}) \rightarrow \mathbf{0}$ as $r \rightarrow \infty$). A somewhat lengthy, but straightforward calculation yields,

$$\mathbf{T}(\mathbf{r}) \;=\; \frac{1}{8\pi\eta_0}\frac{1}{r}\left[\hat{\mathbf{I}} + \frac{\mathbf{r}\,\mathbf{r}}{r^2}\right]\;. \tag{23}$$

This concludes the determination of the Green's functions for the creeping flow equations.

0.4 Hydrodynamic Friction of a Single Rod

The behaviour of rod-like colloids in shear flow is strongly coupled to friction of solvent with the rod's surface. In the present section, friction coefficients for very long and thin rods will be calculated on the basis of the creeping flow equations. This is most easily done by considering a rod consisting of spherical beads with diameter D (as depicted in fig.3). For very long and thin rods, friction coefficients for such necklaces are the same as for cylindrical rods with thickness D. The number of spherical beads is equal to $n+1 = L/D$ (with L the length of the rod), where the bead index number ranges from $-\frac{1}{2}n$ to $+\frac{1}{2}n$. The position of the central bead (for which $n = 0$) defines the position coordinate of the rod.

The flow velocity around a moving rod in shear flow is given, according to eq.(18), by,

$$\mathbf{u}(\mathbf{r}) \;=\; \mathbf{G}\cdot\mathbf{r} + \oint_{\partial V} dS'\,\mathbf{T}(\mathbf{r}-\mathbf{r}')\cdot\mathbf{f}(\mathbf{r}')\;, \tag{24}$$

where the integral ranges over the surface ∂V of the rod. Here, the force $\mathbf{f}(\mathbf{r}')$ is the force per unit area that a surface element at $\mathbf{r}'$ exerts on the fluid. The first term on the right-hand side in eq.(24) is the flow that would have existed in the absence of the rod, the second term is the contribution due to the presence of the rod. For stick boundary conditions we have that,

$$\mathbf{u}(\mathbf{r}) \;=\; \mathbf{v}_c + \boldsymbol{\Omega}\times(\mathbf{r}-\mathbf{r}_c) \quad,\quad \text{for} \quad \mathbf{r}\in\partial V\;, \tag{25}$$

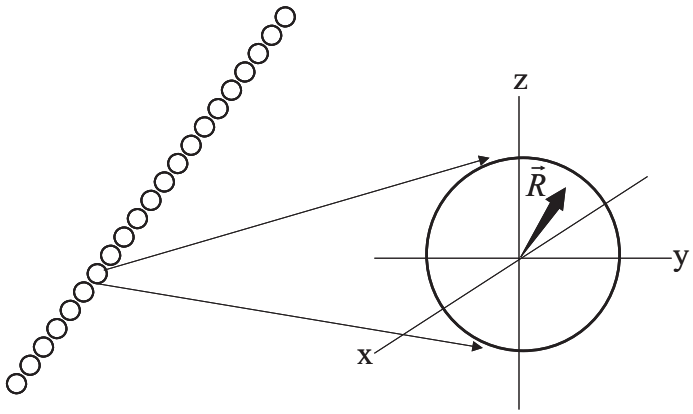

Figure 3: The necklace representation of a very long and thin rod, and the definition of the vector $\mathbf{R}$ on the surface of a bead, relative to the position of that bead.

where $\mathbf{v}_c$ is the translational velocity of the center of the rod, $\mathbf{r}_c$ the position of the center of the rod, and $\mathbf{\Omega}$ is the rod's angular velocity relative to its center.

Within the bead model discussed above, ∂V is the sum of the surfaces ∂V_j of the beads, with j ranging from $-\frac{1}{2}n$ to $+\frac{1}{2}n$. The center position of the j^{th} bead will be denoted as $\mathbf{r}_j = \mathbf{r}_c + j\, D\, \hat{\mathbf{u}}$, where $\hat{\mathbf{u}}$ is the unit vector along the long axis of the rod, which specifies its orientation. Within the bead model, eq.(24) reads,

$$\mathbf{u}(\mathbf{R}+\mathbf{r}_j) \;=\; \mathbf{G}\cdot(\mathbf{R}+\mathbf{r}_j) + \sum_{i\,=\,-\frac{1}{2}n}^{\frac{1}{2}n} \oint_{\partial V^0} dS'\, \mathbf{T}(\mathbf{R}-\mathbf{R}'+\mathbf{r}_{ji})\cdot\mathbf{f}_i(\mathbf{R}')\,, \qquad (26)$$

with $\mathbf{R} = \mathbf{r} - \mathbf{r}_j$ and $\mathbf{R}' = \mathbf{r}' - \mathbf{r}_i$ position vectors with length $D/2$ on the surface ∂V^0 of a bead with its center at $\mathbf{r}_i$ (see fig.(3)). The stick boundary condition (25) now becomes,

$$\begin{aligned} \mathbf{u}(\mathbf{R}+\mathbf{r}_j) &= \mathbf{v}_c + \mathbf{\Omega}\times(\mathbf{R}+\mathbf{r}_j-\mathbf{r}_c) \\ &= \mathbf{v}_c + \mathbf{\Omega}\times(\mathbf{R}+jD\mathbf{u}) \quad , \quad \text{for} \quad R = D/2 \text{ and all } \; j\,. \end{aligned} \qquad (27)$$

In the next two subsections we consider translation (without rotation) and rotation (without translation). Motion of a translating *and* rotating rod is a linear superposition of the results for these two special cases, due to the linearity of the creeping flow equations and its boundary condition.

0.4.1 Translational friction

Let us first consider a translating rod in an otherwise quiescent fluid, without shear flow. The boundary condition (27) reduces simply to, $\mathbf{u}(\mathbf{R}+\mathbf{r}_j) = \mathbf{v}_c$. The representation (26) for $\mathbf{u}$ thus yields,

$$\mathbf{v}_c \;=\; \sum_{i\,=\,-\frac{1}{2}n}^{\frac{1}{2}n} \oint_{\partial V^0} dS'\, \mathbf{T}(\mathbf{R}-\mathbf{R}'+\mathbf{r}_{ji})\cdot\mathbf{f}_i(\mathbf{R}') \quad , \quad \text{for} \quad R = D/2 \quad \text{and all } j\,. \qquad (28)$$

Integration of both sides over the surface of the entire rod, that is, operating on both sides with $\sum_{j\,=\,-\frac{1}{2}n}^{\frac{1}{2}n} \oint_{\partial V^0} dS$, yields,

$$\mathbf{v}_c \;=\; \frac{1}{\pi L D} \sum_{j\,=\,-\frac{1}{2}n}^{\frac{1}{2}n} \sum_{i\,=\,-\frac{1}{2}n}^{\frac{1}{2}n} \oint_{\partial V^0} dS \oint_{\partial V^0} dS' \, \mathbf{T}(\mathbf{R}-\mathbf{R}'+\mathbf{r}_{ji}) \cdot \mathbf{f}_i(\mathbf{R}') \,. \tag{29}$$

Using that,

$$\oint_{\partial V^0} dS' \, \mathbf{T}(\mathbf{r}-\mathbf{R}') \;=\; \frac{D}{4\,\eta_0} \left\{ \left[\frac{D}{2r} + \frac{1}{3} \left(\frac{D}{2r} \right)^3 \right] \hat{\mathbf{I}} + \left[\frac{D}{2r} - \left(\frac{D}{2r} \right)^3 \right] \frac{\mathbf{r}\mathbf{r}}{r^2} \right\} , \tag{30}$$

it is found that, for $i=j$, the surface integrals in eq.(29) are equal to,

$$\oint_{\partial V^0} dS \, \mathbf{T}(\mathbf{R}-\mathbf{R}'+\mathbf{r}_{ji}) \;=\; \frac{D}{3\eta_0} \hat{\mathbf{I}} \;\;, \;\; \text{for} \;\; i=j \,. \tag{31}$$

For $i \neq j$, the Oseen tensor may be Taylor expanded as,

$$\mathbf{T}(\mathbf{R}-\mathbf{R}'+\mathbf{r}_{ji}) \;=\; \mathbf{T}(\mathbf{r}_{ij}) + (\mathbf{R}-\mathbf{R}') \cdot \nabla_i \mathbf{T}(\mathbf{r}_{ij}) + \cdots \,, \tag{32}$$

with ∇_i the gradient operator with respect to $\mathbf{r}_i$. Only the leading order term in this Taylor expansion must be retained to obtain expressions for friction coefficients that are valid to leading order in L/D (if you wish you may include the next higher order Taylor terms and convince yourself that these terms do not contribute in leading order). Using eq.(31) and eq.(32) to leading order in eq.(29) gives,

$$\mathbf{v}_c \;\approx\; -\frac{1}{3\pi\eta_0 L} \sum_{i\,=\,-\frac{1}{2}n}^{\frac{1}{2}n} \mathbf{F}_i^h - \frac{D}{L} \left[\sum_{j\,=\,-\frac{1}{2}n}^{\frac{1}{2}n} \sum_{i\,=\,-\frac{1}{2}n\,,\;i\neq j}^{\frac{1}{2}n} \mathbf{T}(\mathbf{r}_{ij}) \right] \cdot \mathbf{F}_i^h \,. \tag{33}$$

where,

$$\oint_{\partial V^0} dS' \, \mathbf{f}_i(\mathbf{R}') \;=\; -\mathbf{F}_i^h \,, \tag{34}$$

is the total force of the fluid on bead i. The first term on the right-hand side is simply the sum of Stokesian friction forces on the beads, while the second term represents the contribution due to hydrodynamic interaction between the beads. For very long rods, all forces $\mathbf{F}_i^h$ may be taken equal, that is, end-effects may be neglected, since the majority of beads (away from the ends of the rod) experience approximately the same force. Substituting $\mathbf{F}_i^h = \frac{D}{L}\mathbf{F}^h$, with $\mathbf{F}^h$ the total force on the rod, yields,

$$\mathbf{v}_c \;=\; -\frac{1}{3\pi\eta_0 L} \mathbf{F}^h - \left(\frac{D}{L} \right)^2 \left[\sum_{j\,=\,-\frac{1}{2}n}^{\frac{1}{2}n} \sum_{i\,=\,-\frac{1}{2}n\,,\;i\neq j}^{\frac{1}{2}n} \mathbf{T}(\mathbf{r}_{ij}) \right] \cdot \mathbf{F}^h \,. \tag{35}$$

The double bead index summation can be calculated up to leading order by replacing sums by integrals (for details see appendix A). It is thus found that,

$$\begin{aligned} \sum_{j\,=\,-\frac{1}{2}n}^{\frac{1}{2}n} \sum_{i\,=\,-\frac{1}{2}n\,,\;i\neq j}^{\frac{1}{2}n} \mathbf{T}(\mathbf{r}_{ij}) \;&=\; \frac{1}{8\pi\eta_0 D} \left[\hat{\mathbf{I}} + \hat{\mathbf{u}}\hat{\mathbf{u}} \right] \sum_{j\,=\,-\frac{1}{2}n}^{\frac{1}{2}n} \sum_{i\,=\,-\frac{1}{2}n\,,\;i\neq j}^{\frac{1}{2}n} \frac{1}{|\,i-j\,|} \\ &\approx\; \frac{1}{4\pi\eta_0 D} \left[\hat{\mathbf{I}} + \hat{\mathbf{u}}\hat{\mathbf{u}} \right] \frac{L}{D} \ln\!\left\{ \frac{L}{D} \right\} . \end{aligned} \tag{36}$$

We finally obtain, to leading order,

$$\begin{aligned} \mathbf{v}_c &= -\frac{1}{3\pi\eta_0 L}\mathbf{F}^h - \frac{1}{4\pi\eta_0 L}\ln\left\{\frac{L}{D}\right\}\left[\hat{\mathbf{I}}+\hat{\mathbf{u}}\hat{\mathbf{u}}\right]\cdot\mathbf{F}^h \\ &\approx -\frac{1}{4\pi\eta_0 L}\ln\left\{\frac{L}{D}\right\}\left[\hat{\mathbf{I}}+\hat{\mathbf{u}}\hat{\mathbf{u}}\right]\cdot\mathbf{F}^h\,. \end{aligned} \tag{37}$$

Notice that the Stokesian friction of each bead does not contribute in leading order : the major contribution comes from hydrodynamic fields near each bead generated by the remaining beads. Hydrodynamic interaction between the beads is thus essential for the friction of a translating rod.

Inversion of eq.(37) yields,

$$\mathbf{F}^h = -\mathbf{\Gamma}_f\cdot\mathbf{v}_c\ ,\ \text{with}\ \mathbf{\Gamma}_f = \frac{4\pi\eta_0 L}{\ln\{L/D\}}\left[\hat{\mathbf{I}}-\frac{1}{2}\hat{\mathbf{u}}\hat{\mathbf{u}}\right]\ , \tag{38}$$

where the tensor $\mathbf{\Gamma}_f$ is referred to as the *friction tensor*. Contrary to a spherical particle, the friction force is generally not co-linear with its velocity. When the motion of the rod is parallel to its orientation, the friction force of the rod with the fluid is found from eq.(38) to be equal to,

$$\mathbf{F}^h = -\gamma_\parallel\,\mathbf{v}_c\,, \tag{39}$$

with $\gamma_\parallel$ *the friction coefficient for parallel motion,*

$$\gamma_\parallel = \frac{2\pi\eta_0 L}{\ln\{L/D\}}\,. \tag{40}$$

For motion perpendicular to the center line it is likewise found that,

$$\mathbf{F}^h = -\gamma_\perp\,\mathbf{v}_c\,, \tag{41}$$

with $\gamma_\perp$ *the friction coefficient for parallel motion,*

$$\gamma_\perp = \frac{4\pi\eta_0 L}{\ln\{L/D\}}\,. \tag{42}$$

Notice that this friction constant is twice as large as for parallel motion. This is only true for very long and thin rods. For rods with smaller aspect ratios, corrections to the limiting expressions (40) and (42) were considered by de la Torre and Bloomfield (1981). Also note that the friction tensor can be written as,

$$\mathbf{\Gamma}_f = \gamma_\parallel\,\hat{\mathbf{u}}\hat{\mathbf{u}} + \gamma_\perp\left[\hat{\mathbf{I}}-\hat{\mathbf{u}}\hat{\mathbf{u}}\right]\ , \tag{43}$$

where the dyadic product $\hat{\mathbf{u}}\hat{\mathbf{u}}$ is the projection operator parallel to the orientation direction of the rod and $\hat{\mathbf{I}}-\hat{\mathbf{u}}\hat{\mathbf{u}}$ is the projection operator in the direction perpendicular to $\hat{\mathbf{u}}$. This expression for the friction tensor is generally valid, also for shorter rods, in which case, however, correction terms should be added to the limiting expressions (40,42), as discussed by de la Torre and Bloomfield (1981).

Consider now the additional contribution of shear flow. The forces $\mathbf{F}_i^h$ as a function of the bead index i may be obtained directly from the above considerations as follows. Each bead i has a velocity, relative to the externally imposed fluid flow velocity, equal to $\mathbf{v}_c - \mathbf{G}\cdot\mathbf{r}_i =$

$\mathbf{v}_c - \mathbf{G}\cdot\mathbf{r}_c - iD\mathbf{G}\cdot\hat{\mathbf{u}}$. The *relative* change of this velocity between neighbouring beads is thus $\sim 1/i$, and is small for beads away from the center. Large groups of beads therefore experience a friction force as in the case of a uniformly translating rod in an otherwise quiescent fluid. Beads away from the center therefore experience a friction force parallel to the center line equal to,

$$\mathbf{F}^h_{i\,,\,\parallel} \;=\; -\frac{D}{L}\,\gamma_{\parallel}\,\hat{\mathbf{u}}\hat{\mathbf{u}}\cdot(\mathbf{v}_c - \mathbf{G}\cdot\mathbf{r}_c - iD\mathbf{G}\cdot\hat{\mathbf{u}})\;,$$

and perpendicular to the center line,

$$\mathbf{F}^h_{i\,,\,\perp} \;=\; -\frac{D}{L}\,\gamma_{\perp}\,\left[\hat{\mathbf{I}} - \hat{\mathbf{u}}\hat{\mathbf{u}}\right]\cdot(\mathbf{v}_c - \mathbf{G}\cdot\mathbf{r}_c - iD\mathbf{G}\cdot\hat{\mathbf{u}})\;.$$

Here, the apparent local velocity of the fluid is decomposed in its component parallel and perpendicular to the rods center line, and the friction coefficient on the bead is equal to that of an entire rod divided by the number $n+1 = L/D$ of beads. The total force that the fluid exerts on the rod is now simply found by summation over all beads,

$$\begin{aligned}\mathbf{F}^h \;&=\; \sum_{i\,=\,-\frac{1}{2}n}^{\frac{1}{2}n}\left[\mathbf{F}^h_{i\,,\,\parallel} + \mathbf{F}^h_{i\,,\,\perp}\right] \;=\; -\left(\gamma_{\parallel}\hat{\mathbf{u}}\hat{\mathbf{u}} + \gamma_{\perp}\left[\hat{\mathbf{I}} - \hat{\mathbf{u}}\hat{\mathbf{u}}\right]\right)\cdot(\mathbf{v}_c - \mathbf{G}\cdot\mathbf{r}_c)\\ &=\; -\frac{4\pi\eta_0 L}{\ln\{L/D\}}\left[\hat{\mathbf{I}} - \frac{1}{2}\hat{\mathbf{u}}\hat{\mathbf{u}}\right]\cdot(\mathbf{v}_c - \mathbf{G}\cdot\mathbf{r}_c)\;. \qquad (44)\end{aligned}$$

The last equation is only valid for very long and thin rods. The first equation is also valid for shorter rods, where expressions for the two friction coefficients were calculated by de la Torre and Bloomfield (1981). This result is precisely eq.(38) for translational motion in an otherwise quiescent fluid, where the velocity of the rods center is taken relative to the local shear flow velocity. Such a result is intuitively clear, as additional friction forces due to the shear flow on the beads with a positive bead index simply cancel with the same forces on beads with a negative index.

0.4.2 Rotational friction

Consider a rod in shear flow with its center at the origin (so that $\mathbf{v}_c = \mathbf{0} = \mathbf{r}_c$) and with a prescribed angular velocity $\boldsymbol{\Omega}$ perpendicular to its center line. The rotational friction coefficient may be obtained directly from the above results on translational friction, with arguments similar to the ones given at the end of the previous subsection where the effect of shearing motion of the fluid on translational friction is considered. The velocity of bead i relative to the local fluid flow velocity is equal to $\boldsymbol{\Omega}\times\mathbf{r}_i - \mathbf{G}\cdot\mathbf{r}_i = iD\,\boldsymbol{\Omega}\times\hat{\mathbf{u}} - -iD\,\mathbf{G}\cdot\hat{\mathbf{u}}$. The *relative* change of this velocity between neighbouring beads is thus $\sim 1/i$, and is small for beads away from the origin. Large groups of beads therefore experience a friction force as in case of a uniformly translating rod in an otherwise quiescent fluid. Beads away from the origin therefore experience a friction force parallel to the center line equal to,

$$\mathbf{F}^h_{i\,,\,\parallel} \;=\; -\frac{D}{L}\,\gamma_{\parallel}\,\hat{\mathbf{u}}\hat{\mathbf{u}}\cdot(iD\,\boldsymbol{\Omega}\times\hat{\mathbf{u}} - iD\,\mathbf{G}\cdot\hat{\mathbf{u}})\;, \qquad (45)$$

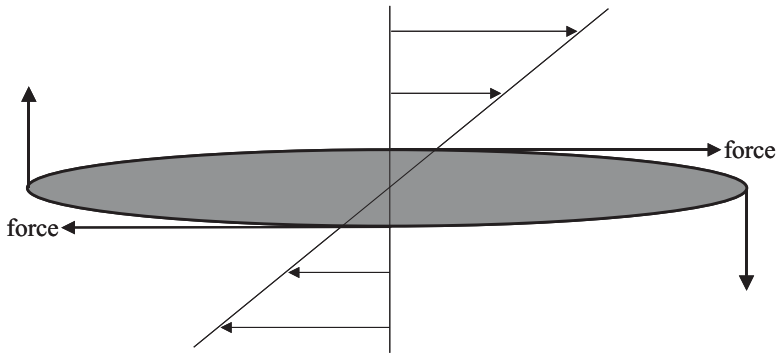

Figure 4: A rod in simple shear flow with its center line parallel to the flow direction experiences a non-zero torque entirely due to its non-zero thickness.

and perpendicular to the center line,

$$\mathbf{F}^h_{i\,,\,\perp} \;=\; -\frac{D}{L}\,\gamma_\perp\,\Big[\hat{\mathbf{I}} - \hat{\mathbf{u}}\hat{\mathbf{u}}\Big]\cdot(iD\,\mathbf{\Omega}\times\hat{\mathbf{u}} - iD\,\mathbf{G}\cdot\hat{\mathbf{u}})\;. \tag{46}$$

The torque on the rod is thus equal to,

$$\begin{aligned}\mathcal{T}^h \;&=\; \sum_{i\,=\,-\frac{1}{2}n}^{\frac{1}{2}n}\mathbf{r}_i\times\Big[\mathbf{F}^h_{i\,,\,\parallel}+\mathbf{F}^h_{i\,,\,\perp}\Big]\\ &=\; -\frac{D^3}{L}\,\gamma_\perp\,[\hat{\mathbf{u}}\times(\mathbf{\Omega}\times\hat{\mathbf{u}})-\hat{\mathbf{u}}\times(\mathbf{G}\cdot\hat{\mathbf{u}})]\sum_{i\,=\,-\frac{1}{2}n}^{\frac{1}{2}n} i^2\,,\end{aligned} \tag{47}$$

where it is used that $\gamma_\perp = 2\gamma_\parallel$ (see eqs.(40,42)). Since $\hat{\mathbf{u}}\perp\mathbf{\Omega}$, and using that $\sum_{i=1}^k i^2 = \frac{1}{6}k(k+1)(2k+1)\approx\frac{1}{3}k^3$ for large k, it is thus found that,

$$\mathcal{T}^h \;=\; -\gamma_r\,[\,\mathbf{\Omega}-\hat{\mathbf{u}}\times(\mathbf{G}\cdot\hat{\mathbf{u}})\,]\;, \tag{48}$$

where,

$$\gamma_r \;=\; \frac{1}{12}L^2\,\gamma_\perp \;=\; \frac{\pi\eta_0 L^3}{3\ln\{L/D\}}\;, \tag{49}$$

is the *rotational friction coefficient*. Notice that a torque-free rod in shear flow thus attains an angular velocity equal to $\hat{\mathbf{u}}\times(\mathbf{G}\cdot\hat{\mathbf{u}})$. For rods with smaller aspect ratios, corrections to the limiting expression (49) are given by de la Torre and Bloomfield (1981).

For the special case of simple shear flow, where $\mathbf{G}=\mathbf{\Gamma}$ as given in eq.(1), the above result predicts a zero torque on the rod when it is oriented along the flow direction, since then $\hat{\mathbf{u}}\times(\mathbf{\Gamma}\cdot\hat{\mathbf{u}})=\mathbf{0}$. From symmetry it follows that for such orientations the total force $\mathbf{F}^h_i$ of the fluid on each bead is zero, so that the torque is indeed $\mathbf{0}$. What is neglected in eq.(47) is the variation of the fluid flow velocity over the surface of each bead, which is a good approximation for orientations away from alignment along the flow direction. When the rod

is oriented along the flow direction, however, the fluid flow variation over the surfaces of the beads give rise to a small but non-zero torque. The torque is only non-zero when the finite thickness of the rod is taken into account, and its magnitude is at least an order D/L smaller than the torque $\gamma_r \hat{\mathbf{u}} \times (\mathbf{\Gamma} \cdot \hat{\mathbf{u}})$ for orientations not parallel to the flow direction.

As will be seen in the section on Jeffery orbits, which are the orbits described by $\hat{\mathbf{u}}$ of a non-Brownian rod in shear flow, the small torque on a rod that is oriented along the flow direction is essential to obtain the realistic periodic motion for $\hat{\mathbf{u}}$: without this small contribution, $\hat{\mathbf{u}}$ would simply end up in the direction parallel to the flow. Let us therefore consider this small, but essential contribution to the torque for non-Brownian rods.

The additional contribution to the torque is due to variations of the fluid forces over the bead surfaces. Taking these variations into account, the torque is by definition equal to (∂V is again the surface of the rod),

$$\begin{aligned} \mathcal{T}^h &= -\oint_{\partial V} dS'\, \mathbf{r}' \times \mathbf{f}(\mathbf{r}') = -\sum_{i\,=\,-\frac{1}{2}n}^{\frac{1}{2}n} \oint_{\partial V^0} dS'\, (\mathbf{R}' + \mathbf{r}_i) \times \mathbf{f}_i(\mathbf{R}') \\ &= \sum_{i\,=\,-\frac{1}{2}n}^{\frac{1}{2}n} \mathbf{r}_i \times \mathbf{F}_i^h - \sum_{i\,=\,-\frac{1}{2}n}^{\frac{1}{2}n} \oint_{\partial V^0} dS'\, \mathbf{R}' \times \mathbf{f}_i(\mathbf{R}')\,. \end{aligned} \tag{50}$$

The last term on the right-hand side is now extra as compared to the case where the additional torque due to variations of the hydrodynamic forces over the rods surface is neglected. This is the term that is responsible for a finite torque when the rod is oriented along the flow direction. The first term on the right-hand side is already considered before with the neglect of end-effects. In calculating the additional contribution $\Delta\mathcal{T}^h$ (the last term on the right-hand side) end-effects will also be neglected, meaning that the variation of the hydrodynamic forces over the bead surface is taken equal for all beads. The variation of the fluid flow in which a bead is embedded is given by $\mathbf{\Gamma} \cdot \mathbf{R}'$. We are only interested in the component of this flow in the direction along $\hat{\mathbf{u}}$, since the complementary perpendicular component gives rise to rotation about the center line, which does not affect $\hat{\mathbf{u}}$. This parallel component of the flow along the surface of the rod is equal to $\hat{\mathbf{u}}\hat{\mathbf{u}} \cdot \mathbf{\Gamma} \cdot \mathbf{R}'$, and the corresponding parallel force is proportional to this flow velocity. Hence,

$$\mathbf{f}_i(\mathbf{R}') \;=\; C\, \hat{\mathbf{u}}\hat{\mathbf{u}} \cdot \mathbf{\Gamma} \cdot \mathbf{R}'\,, \tag{51}$$

where C is an as yet unknown constant. It now follows that,

$$\Delta\mathcal{T}^h \;=\; -\,C \sum_{i\,=\,-\frac{1}{2}n}^{\frac{1}{2}n} \oint_{\partial V^0} dS'\, \mathbf{R}' \times (\mathbf{\Gamma} \cdot \mathbf{R}') \;=\; C\, \frac{L}{D}\, \frac{\pi D^4}{12}\, \hat{\mathbf{u}} \times \left(\mathbf{\Gamma}^T \cdot \hat{\mathbf{u}}\right)\,, \tag{52}$$

where the superscript "T" stands for transposition. The constant C can now be determined by comparing this result to solutions of the creeping flow equations for the simple case that the rod is oriented along the flow direction. For the case of a cylinder without end-effects and for a long and thin ellipsoidal particles it can be shown that,

$$C \;=\; -\frac{6\,\eta_0}{D} \qquad , \quad \text{for cylinders without end-effects}\,, \tag{53}$$

$$\;=\; -\frac{4\,\eta_0}{D \ln\{L/D\}} \quad , \quad \text{for long and thin ellipsoids}\,. \tag{54}$$

The different results are not just the result of neglect of end-effects in case of the cylindrical particle. The precise value of C is sensitive to the precise shape of the surface of the rod : the torque on a rod aligned along the flow direction depends on how the fluid is "pushed away" or "sucked in" as it flows along its surface.

We thus finally find the following expression for the torque,

$$\mathcal{T}^h \;=\; -\gamma_r \left[\, \mathbf{\Omega} - \hat{\mathbf{u}} \times (\mathbf{\Gamma} \cdot \hat{\mathbf{u}}) + \kappa^2\, \hat{\mathbf{u}} \times \left(\mathbf{\Gamma}^T \cdot \hat{\mathbf{u}}\right) \right] \;, \tag{55}$$

where the dimensionless constant κ^2 is equal to,

$$\kappa^2 \;=\; \frac{3}{2}\left(\frac{D}{L}\right)^2 \ln\!\left\{\frac{L}{D}\right\} \quad , \quad \text{for cylinders without end-effects} \;, \tag{56}$$

$$\;=\; \left(\frac{D}{L}\right)^2 \qquad\qquad , \quad \text{for long and thin ellipsoid}s \;. \tag{57}$$

Since for colloidal rods the precise geometry of their surface is usually not known, and κ^2 is sensitive to that geometry, the constant κ^2 should be considered as a fitting parameter when performing experiments. This parameter tends to zero with decreasing values of D/L.

0.5 Motion of Non-Brownian Rods in Shear Flow : Jeffery Orbits

The first thing that comes to mind when beginning to study the effect of shear flow on dilute suspensions of rods is to ask about their motion without considering Brownian motion. The trajectory of motion of a Brownian rod will be the smooth trajectory of a non-Brownian rod that is randomly corrugated due to Brownian motion. In this section we ask for the orientational orbits that a non-Brownian rod (a "fiber") traverses when subjected to shear flow. These orbits are commonly the referred to as *Jeffery orbits*, named after the scientist Jefferey (1922) who first considered this problem (a more compact formulation as compared to the original work of Jeffery has been formulated by Hinch and Leal (1972) and Leal and Hinch (1972)). We shall consider Jeffery orbits of rods in elongational flow and simple shear flow, respectively.

The expressions derived in the previous section for very long and thin rods will be used to calculate such Jeffery orbits. Jefferey (1922) derived exact expressions for ellipsoidal rods, while Bretherton (1962) showed that the same equations of motion can be applied to arbitrary shaped, cylindrically symmetric, slender bodies, provided that the body is modelled as an equivalent ellipsoid. The expressions obtained in the following are the asymptotic limits for large aspect ratios of those derived by Jeffery and Bretherton. It turns out, however, that for aspect ratios L/D larger than about 3-4, errors that are made in using these asymptotic expressions (but employing the correct value for the rotational friction coefficient) are typically less about 5% (asymptotic limits are obtained when, typically, $1/(1+r^2)$ is approximated by $1/r^2$, where $r = L/D$). This is confirmed by simulations (see for example Ingber and Mondy (1994)).

Interactions between fibers at high fiber concentration and intrinsic flexibility of fibers does of course have an effect on the orbits described by a rod. Simulations on Jeffery orbits

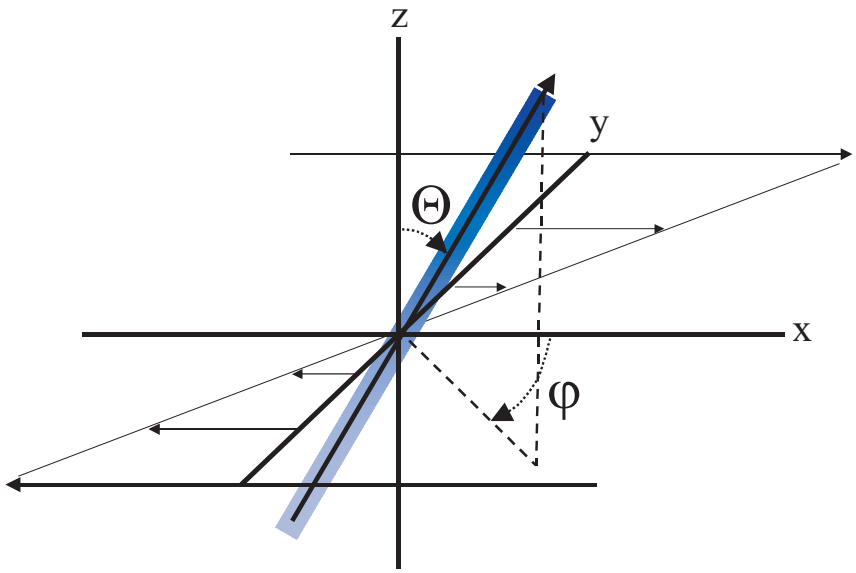

Figure 5: Definition of the spherical coordinates φ and Θ, relative to the flow and gradient direction in case of simple shear flow. The flow is in the x-direction while the gradient is in the y-direction. In this example, $\varphi < 0$.

where interactions and flexibility are considered have been performed by Yamamoto and Matsuoka (1995). The theory described here assumes rigid rods. A discussion and references on the effect of interactions between fibers, wall effects and rheology of fiber suspensions can be found in the book by Papathanasiou and Guell (1997). The treatment here describes the motion of a single fiber, which is not affected by interactions with other fibers or a wall.

Jeffery orbits are most conveniently described in terms of the spherical coordinates φ and Θ of the unit vector $\hat{\mathbf{u}}$ that specifies the orientation of the rod. These coordinates, relative to the flow and gradient direction in case of simple shear flow are sketched in fig.5. In case of elongational flow, the elongation axis is oriented along $\{\varphi, \Theta\} = \{\pi/4, \pi/2\}$ (compare figs.1a,b). In fig.5, φ for the corresponding rod is negative.

0.5.1 Jeffery orbits in elongational flow

According to eq.(48), the torque $\mathcal{T}^h$ that the fluid exerts on a very long and thin rod with an angular velocity $\mathbf{\Omega}$ in a shear field with velocity gradient tensor $\mathbf{G} = \mathbf{E}$ (see eq.(2)) is equal to,

$$\mathcal{T}^h \;=\; -\gamma_r \left[\, \mathbf{\Omega} - \hat{\mathbf{u}} \times (\mathbf{E} \cdot \hat{\mathbf{u}}) \,\right] \;, \tag{58}$$

where γ_r is the rotational friction coefficient. It will turn out that for elongational flow, the torque exerted on the rod when it is orientated parallel to the flow direction (the last term in eq.(55)) is of no relevance, contrary to simple shear flow. When no external torque acts on the rod, the hydrodynamic torque in eq.(58) is $\mathbf{0}$, so that,

$$\mathbf{\Omega} \;=\; \hat{\mathbf{u}} \times (\mathbf{E} \cdot \hat{\mathbf{u}}) \;. \tag{59}$$

On the other hand, by definition,

$$\frac{d\hat{\mathbf{u}}}{dt} \;=\; \mathbf{\Omega} \times \hat{\mathbf{u}} \;. \tag{60}$$

Substitution of eq.(59) into eq.(60), using that $\hat{\mathbf{u}} \times (\hat{\mathbf{u}} \times \mathbf{a}) = (\hat{\mathbf{u}} \cdot \mathbf{a})\hat{\mathbf{u}} - \mathbf{a}$ for arbitrary vectors $\mathbf{a}$, yields,

$$\frac{d\hat{\mathbf{u}}}{dt} \;=\; \mathbf{E} \cdot \hat{\mathbf{u}} - (\hat{\mathbf{u}} \cdot \mathbf{E} \cdot \hat{\mathbf{u}})\, \hat{\mathbf{u}} \;. \tag{61}$$

This equation of motion for the orientation $\hat{\mathbf{u}}$ describes the rotational orbits of a long and thin rod, without Brownian motion, in elongational flow. Expressing the orientation in terms of spherical angular coordinates, and substitution of the explicit form of $\mathbf{E}$ in eq.(2), the following equations of motion for these coordinates are obtained,

$$\begin{aligned}
\frac{d\Theta}{dt}\cos\{\Theta\}\cos\{\varphi\} - \frac{d\varphi}{dt}\sin\{\Theta\}\sin\{\varphi\} &= -\dot{\gamma}\sin^3\{\Theta\}\sin\{\varphi\}\cos^2\{\varphi\} + \frac{\dot{\gamma}}{2}\sin\{\Theta\}\sin\{\varphi\}, \\
\frac{d\Theta}{dt}\cos\{\Theta\}\sin\{\varphi\} + \frac{d\varphi}{dt}\sin\{\Theta\}\cos\{\varphi\} &= -\dot{\gamma}\sin^3\{\Theta\}\sin^2\{\varphi\}\cos\{\varphi\} + \frac{\dot{\gamma}}{2}\sin\{\Theta\}\cos\{\varphi\}, \\
\frac{d\Theta}{dt} &= \dot{\gamma}\sin\{\Theta\}\cos\{\Theta\}\sin\{\varphi\}\cos\{\varphi\} \;.
\end{aligned} \tag{62}$$

It may seem that we have here three equations for two unknowns (Θ and φ) : each one of these equations, however, may be derived from the remaining two. Elimination of $d\Theta/dt$ from one of the first two equations, using the third equation, yields the following seemingly simple set of two equations of motion for the spherical angular coordinates,

$$\begin{aligned}
\frac{d\varphi}{dt} &= -\dot{\gamma}\left[\sin^2\{\varphi\} - \tfrac{1}{2}\right] \;, \\
\frac{d\Theta}{dt} &= \dot{\gamma}\,\sin\{\Theta\}\cos\{\Theta\}\sin\{\varphi\}\cos\{\varphi\} \;.
\end{aligned} \tag{63}$$

The first of these equations is easily integrated, to yield,

$$\int_{\varphi(t=0)}^{\varphi(t)} \frac{d\varphi'}{\sin^2\{\varphi'\} - \frac{1}{2}} \;=\; \ln\left\{\frac{(\tan\{\varphi(t)\} - 1)\;\;(\tan\{\varphi(t=0)\} + 1)}{(\tan\{\varphi(t)\} + 1)\;\;(\tan\{\varphi(t=0)\} - 1)}\right\} \;=\; -\dot{\gamma}\,t \;. \tag{64}$$

Solving for $\tan\{\varphi(t)\}$ leads to,

$$\tan\{\varphi(t)\} \;=\; \left\{\frac{1 + C(t)}{1 - C(t)}\right\} \quad , \quad \text{with} \quad , \quad C(t) \;=\; \frac{\tan\{\varphi(t=0)\} - 1}{\tan\{\varphi(t=0)\} + 1}\,\exp\{-\dot{\gamma}\,t\} \;. \tag{65}$$

At infinite time, the spherical coordinate φ of $\hat{\mathbf{u}}$ thus becomes equal to $\pi/4$ (or equivalently $5\pi/4$). Hence, the projection of $\hat{\mathbf{u}}$ onto the xy-plane (the flow-gradient plane) is along the

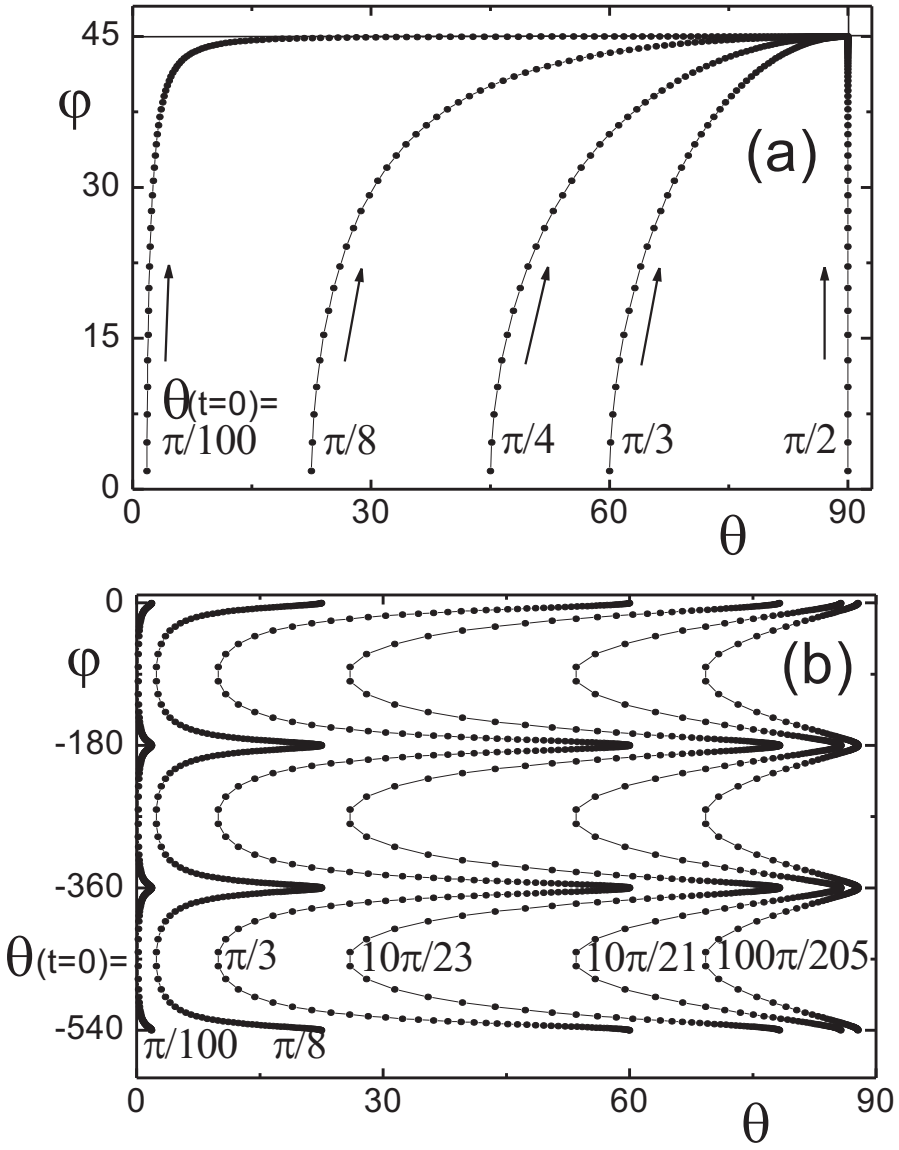

Figure 6: (a) Jeffery orbits for elongational flow for initial values $\varphi(t=0) = \pi/100$ and various values for $\Theta(t=0)$, as indicated in the figure. Data points • correspond to time steps equal to $1/(10\,\dot{\gamma})$. The arrows indicate the direction of the temporal evolution of the spherical coordinates. (b) Jeffery orbits for simple shear flow with $\kappa = 0.1$, for various values of $\Theta(t=0)$, as indicated in the figure. The points • on the orbits mark time intervals of $T/200$. $\varphi(t)$ decreases with time.

direction of the the extensional axis of the elongational flow. The reason for this is easily inferred from fig.1b.

Dividing the two equations of motion in eq.(63) yields,

$$\frac{d\Theta}{\sin\{\Theta\}\cos\{\Theta\}} \;=\; -\,\frac{d\varphi\;\sin\{\varphi\}\cos\{\varphi\}}{\sin^2\{\varphi\}-\frac{1}{2}}\;.$$

Integration of both sides now leads to,

$$\tan\{\Theta(t)\} \;=\; \tan\{\Theta(t=0)\}\,\sqrt{\frac{\sin^2\{\varphi(t=0)\}-\frac{1}{2}}{\sin^2\{\varphi(t)\}-\frac{1}{2}}}\;, \tag{66}$$

where $\varphi(t)$ can be obtained from eq.(65). Since $\varphi(t)$ tends to $\pi/4$ (or $5\pi/4$), the above solution predicts that $\tan\{\Theta\}$ tends to infinity, and hence $\Theta(t)\rightarrow\pi/2$. Hence, independent of the initial condition, a rod will end up in the velocity-gradient plane along the extensional axis. This is verified in fig.6a, which shows numerical results for the spherical coordinates. Here, the distance between each data point is $1/(10\,\dot\gamma)$. Data are shown for small values of $\varphi(t\,=\,0)$. For larger initial values for φ, the orbit just starts on one of the curves shown and then traces the same orbit. As can be seen from the most upper-left curve in fig.6a, when the initial value of Θ is small, the rod spends a relatively long time around the unstable stationary solution $\{\Theta,\varphi\}=\{0,\pi/4\}$ of the equations of motion, before reaching the final stable state $\{\Theta,\varphi\}=\{\pi/2,\pi/4\}$. That is, $\hat{\mathbf{u}}$ first rotates to the extensional direction where $\varphi\,=\,\pi/4$, keeping its angle Θ with the vorticity direction relatively small. This angle then slowly increases, after which there is an acceleration towards the final orientation.

0.5.2 Jeffery orbits in simple shear flow

As we have seen in the section on hydrodynamics, the torque $\mathcal{T}^h$ that the fluid exerts on a very long and thin rod with an angular velocity $\mathbf{\Omega}$ in a shear field with velocity gradient tensor $\mathbf{G}=\mathbf{\Gamma}$ (see eq.(1)) is equal to,

$$\mathcal{T}^h \;=\; -\gamma_r\left[\,\mathbf{\Omega}-\hat{\mathbf{u}}\times(\mathbf{\Gamma}\cdot\hat{\mathbf{u}})+\kappa^2\,\hat{\mathbf{u}}\times\left(\mathbf{\Gamma}^T\cdot\hat{\mathbf{u}}\right)\,\right]\;, \tag{67}$$

where γ_r is the rotational friction coefficient. The parameter κ^2 tends to zero for decreasing values of D/L, and measures the torque of the rod when aligned such that $\varphi=0$, for which case $\hat{\mathbf{u}}\times(\mathbf{\Gamma}\cdot\hat{\mathbf{u}})=\mathbf{0}$. Neglecting this small contribution results in an orientation of the rod in the flow direction for long times, while for a rod of finite thickness, where κ^2 is small but non-zero, a periodic motion results. Contrary to the case of elongational flow, considered in the previous subsection, the small but finite contribution $\sim\kappa^2$ is essential for a correct description in case of simple shear flow.

When no other torque is acting on the rod, the hydrodynamic torque is $\mathbf{0}$, so that,

$$\mathbf{\Omega} \;=\; \hat{\mathbf{u}}\times(\mathbf{\Gamma}\cdot\hat{\mathbf{u}})-\kappa^2\,\hat{\mathbf{u}}\times\left(\mathbf{\Gamma}^T\cdot\hat{\mathbf{u}}\right)\;. \tag{68}$$

Precisely as for elongational flow, this implies that,

$$\frac{d\hat{\mathbf{u}}}{dt} \;=\; \mathbf{\Gamma}\cdot\hat{\mathbf{u}}-\kappa^2\,\mathbf{\Gamma}^T\cdot\hat{\mathbf{u}}-(\hat{\mathbf{u}}\cdot\mathbf{\Gamma}\cdot\hat{\mathbf{u}})\,\hat{\mathbf{u}}\,. \tag{69}$$

In terms of spherical coordinates, this is equivalent to,

$$\frac{d\Theta}{dt}\cos\{\Theta\}\cos\{\varphi\}-\frac{d\varphi}{dt}\sin\{\Theta\}\sin\{\varphi\}=-\dot\gamma(1-\kappa^2)\sin^3\{\Theta\}\sin\{\varphi\}\cos^2\{\varphi\}+\dot\gamma\sin\{\Theta\}\sin\{\varphi\},$$
$$\frac{d\Theta}{dt}\cos\{\Theta\}\sin\{\varphi\}+\frac{d\varphi}{dt}\sin\{\Theta\}\cos\{\varphi\}=-\dot\gamma(1-\kappa^2)\sin^3\{\Theta\}\sin^2\{\varphi\}\cos\{\varphi\}-\dot\gamma\kappa^2\sin\{\Theta\}\cos\{\varphi\},$$
$$\frac{d\Theta}{dt}=\dot\gamma(1-\kappa^2)\sin\{\Theta\}\cos\{\Theta\}\sin\{\varphi\}\cos\{\varphi\}\,. \tag{70}$$

Precisely as in the previous case of elongational flow, we thus arrive at the following equations of motion for the spherical angular coordinates,

$$\begin{aligned}\frac{d\varphi}{dt} &= -\dot\gamma\left[\sin^2\{\varphi\}+\kappa^2\cos^2\{\varphi\}\right]\,,\\ \frac{d\Theta}{dt} &= \dot\gamma(1-\kappa^2)\,\sin\{\Theta\}\cos\{\Theta\}\sin\{\varphi\}\cos\{\varphi\}\,.\end{aligned} \tag{71}$$

The first of these equations is easily integrated to yield,

$$\int_{\varphi(t=0)}^{\varphi(t)}\frac{d\varphi'}{\sin^2\{\varphi'\}+\kappa^2\cos^2\{\varphi'\}} \;=\; \frac{1}{\kappa}\left[\arctan\left\{\frac{1}{\kappa}\tan\{\varphi(t)\}\right\}-C'\right] \;=\; -\dot\gamma\,t\,, \tag{72}$$

where C' is an integration constant, equal to,

$$C' \;=\; \arctan\left\{\frac{1}{\kappa}\tan\{\varphi(t=0)\}\right\}\,. \tag{73}$$

Hence,

$$\tan\{\varphi(t)\} \;=\; \kappa\,\tan\{C'-\dot\gamma\kappa\,t\}\,. \tag{74}$$

Since $\varphi(t)$ is periodic, trajectories of $\hat{\mathbf{u}}$ do not depend on $\varphi(t=0)$, so that, without loss of generality, we may take $\varphi(t=0)=0$. For this choice, according to eq.(73), $C'=0$. The solution (74) thus simplifies to,

$$\tan\{\varphi(t)\} \;=\; -\kappa\,\tan\{\dot\gamma\kappa\,t\}\,. \tag{75}$$

It follows that $\varphi(t)$ is a periodic function of time, with a period T which is independent of the initial value of $\hat{\mathbf{u}}$, and is equal to,

$$T \;=\; \frac{2\pi}{\dot\gamma\,\kappa}\,. \tag{76}$$

It should be noted that terms of order $(D/L)^2$ are neglected in the equation of motion (69) for the orientation (except for the important contribution $\sim\kappa^2$ to the torque), so that the expression for the period T here is valid to within terms of that order.

Division of the two equations of motion in eq.(71) yields,

$$\frac{d\Theta}{\sin\{\Theta\}\cos\{\Theta\}} \;=\; (\kappa^2-1)\frac{d\varphi\,\sin\{\varphi\}\cos\{\varphi\}}{\sin^2\{\varphi\}+\kappa^2\cos^2\{\varphi\}}\,.$$

Integration of both sides leads to,

$$\tan\{\Theta(t)\} \;=\; \tan\{\Theta(t=0)\}\,\sqrt{\frac{1+(\kappa^2-1)\cos^2\{\varphi(t=0)\}}{1+(\kappa^2-1)\cos^2\{\varphi(t)\}}}\,, \tag{77}$$

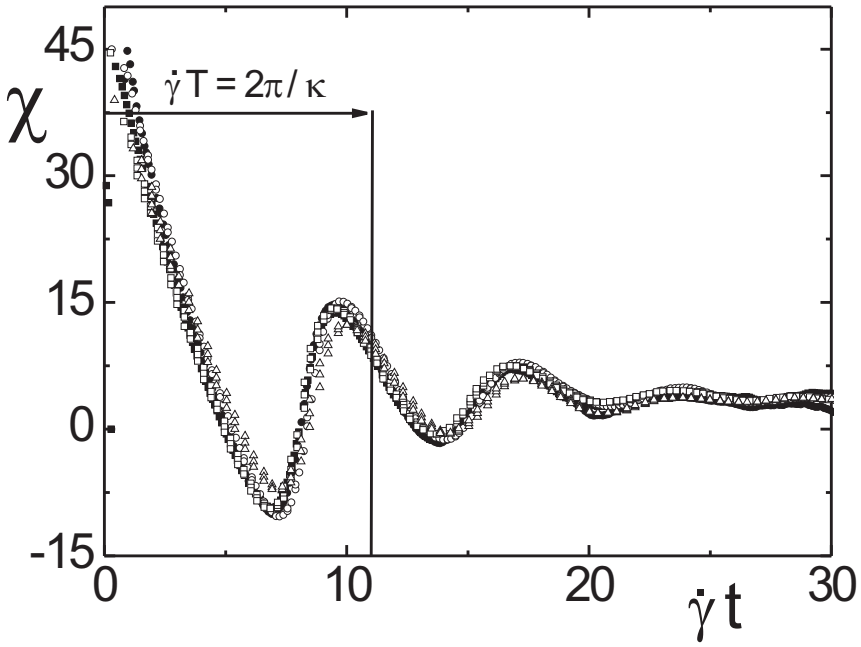

Figure 7: The angle χ between the projection of the director onto the gradient-velocity plane and the flow direction as a function of strain $\dot{\gamma}\, t$, for five different shear rates : $\dot{\gamma} = 1\,\bullet,\ 1.7\,\blacksquare\ ,3\,O,\ 5\,\square$ and $7\,s^{-1}\ \triangle$, as obtained from dichroism measurements by Vermant et al. (2001). The sample consists of ellipsoidal hematite rods with an aspect ratio of 2.5 with a polydispersity of about $25\,\%$, dissolved in a slightly acidic water/glycerin $5/95$ mixture. The average length of the rods is $430\,nm$ and their thickness $170\,nm$. The vertical line indicates the period of time T as obtained from eq.(76).

where $\varphi(t)$ follows from eq.(75). Jeffery orbits are plotted in fig.6b for various values of $\Theta(t=0)$ and for $\kappa = 0.1$. As already mentioned above, the parameter κ is a measure for the torque on the rod when aligned in the velocity-gradient plane, and tends to 0 for $D/L \to 0$. For long and thin rods, for which κ is small, this torque is small, and the rod spends a relatively long time around this particular orientation. For $\kappa = 0$, that is, in the unrealistic case of zero thickness of the rod, the above result predicts that the rod ends up at an orientation where $\varphi = 0$ (or a multiple of π). The small, but finite value of κ, however, results in periodic motion of the rod. In the present case of simple shear flow, the small torque as a result of the finite thickness of the rod in the equation of motion (69) is thus essential, since this small contribution will lead to a continuing motion of the rod, not ending in an orientation in the flow direction at infinite time. As can be seen from fig.6, the rod spends a relatively long time

at orientations where φ is a multiple of π. For smaller values of κ, this would be even more pronounced.

An experiment

Experimental results for the angle χ between the director in the gradient-velocity plane and the flow direction as obtained from dichroism measurements on hematite suspensions are shown in fig.7 (data are taken from Vermant et al. (2001)). The laser beam is along the vorticity direction, so that dichroism in the gradient-velocity plane is probed. The flow is imposed at time $t = 0$, from an initially isotropic dispersion. The geometrical aspect ratio of the hematite rods is 2.5 with a polydispersity of about $25\,\%$. For small times, rods are preferentially oriented with an angle of 45^o with the flow direction, due to the orientational effect of the elongational part of the simple shear flow. For a single rod, the angle χ is equal to φ in eq.(75). Hence, according to eq.(75), χ should scale with the strain $\dot{\gamma}\,t$, which is indeed confirmed by these experiments. The temporal oscillations of χ are damped because of the polydispersity in aspect ratio. The shear rates are chosen large enough so that during the time interval where damping occurs, orientational Brownian motion of the rods does not play a role. According to eqs.(76,56), each different aspect ratio leads to a different period T of oscillation of $\varphi(t)$, so that after some time different rods are "out of phase", which gives rise to damping of the oscillations of the measured angle χ. Since the dispersions are very dilute, so that the rods do not interact with each other, the angle χ can be calculated taking polydispersity into account (details can be found in Vermant et al. (2001)). Using the equations derived in the present section and properly averaging with respect to polydispersity in aspect ratio fits the experimental master curve in fig.7. The effective aspect ratio as obtained from this fit is 1.75 (instead of the geometrical aspect ratio 2.5) and a polydispersity of $65\,\%$ (instead of $25\,\%$). These differences between the effective and geometrical values are due to deviation of the rod shapes from an ideal ellipsoidal shape. The period of oscillation as given by eq.(76) is seen to be of the right magnitude (despite the fact that eq.(76) is only valid for long and thin rods, while the present hematite rods are quite short and thick).

0.6 Brownian Motion of a Free Rod (without shear flow)

Before going to Brownian rods in shear flow, we shall consider translational and rotational Brownian motion of a long and thin rod in the absence of flow. Brownian motion can be studied on the basis of Newton's equation of motion, supplemented with fluctuating forces and torques resulting from collisions of solvent molecules with the rod. Such equations of motion with a fluctuating component are referred to as *Langevin equations*. We shall first review Newton's equations of motion before formulating the Langevin equations for a long and thin rod. On the basis of these equations, important time scales can be defined. Due to the very large size and mass of the rod in comparison to the solvent molecules, the rod moves on a time scale that is much larger than typical relaxation times of solvent molecules. In addition it will turn out that velocities relax quite fast due to friction with the solvent. This enables us to coarse grain equations of motion to the so-called Brownian time scale, on which velocities and

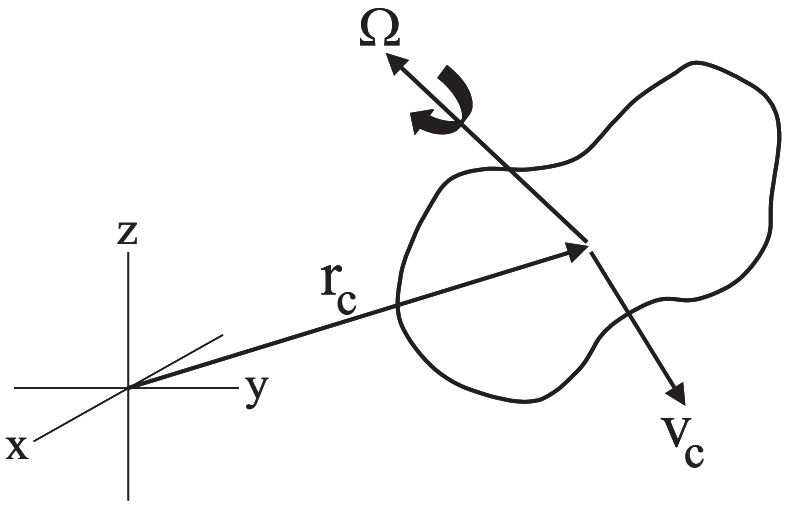

Figure 8: Motion of a rigid body. $\mathbf{\Omega}$ is the angular velocity and $\mathbf{v}_c$ is the translational velocity of the reference point $\mathbf{r}_c$.

angular momenta have long relaxed to equilibrium with the heat bath of solvent molecules.

In an experiment, the time scale is set by the time interval over which observables are averaged during a measurement. For example, taking photographs of a Brownian particle is an experiment on a time scale that is set by the shutter time of the camera. Subsequent photographs reveal the motion of the Brownian particle averaged over a time interval equal to the shutter time. Any theory considering the motion of the Brownian particle obtained in such a way should of course be aimed at the calculation of observables, averaged over that time interval. A time scale is thus the minimum time resolution of an experiment or theory.

0.6.1 Newton's equations of motion for a rigid body

Let us first recall Newton's equations of motion for non-spherical rigid particles. The rigid body contains a large number of molecules, with positions $\mathbf{r}_n$, momenta $\mathbf{p}_n$, and masses m_n, where $n = 1, 2, 3, \cdots$. The positions of the molecules are fixed relative to each other, that is, the body is rigid as a result of inter-molecular interactions. The velocity $\mathbf{v}_n$ of molecule n is composed of two parts : the rigid body can rotate and translate. To make the distinction between the two contributions, the velocities are written as,

$$\mathbf{v}_n \;=\; \mathbf{\Omega} \times (\mathbf{r}_n - \mathbf{r}_c) \;+\; \mathbf{v}_c, \tag{78}$$

where $\mathbf{r}_c$ is an arbitrary point inside the rigid body with a translational velocity $\mathbf{v}_c$, and $\mathbf{\Omega}$ is the angular velocity with respect to the point $\mathbf{r}_c$ (see fig.8).

Newton's equation of motion for the total momentum $\mathbf{p}$ reads,

$$\frac{d\mathbf{p}}{dt} \equiv \frac{d}{dt}\sum_n \mathbf{p}_n = \mathbf{\Omega}\times\sum_n m_n\left[\mathbf{v}_n - \mathbf{v}_c\right] + \frac{d\mathbf{\Omega}}{dt}\times\sum_n m_n\left[\mathbf{r}_n - \mathbf{r}_c\right] + M\frac{d\mathbf{v}_c}{dt} = \mathbf{F}\,, \tag{79}$$

where $\mathbf{F}$ is the total *external force* on the particle, and $M = \sum_n m_n$ is the total mass of the particle. With the following choice for the point $\mathbf{r}_c$,

$$\mathbf{r}_c \;=\; \sum_n m_n \mathbf{r}_n / \sum_n m_n, \tag{80}$$

which is the *center of mass* of the rigid body, eq.(79) becomes similar to Newton's equation of motion for a spherical particle,

$$\frac{d\mathbf{p}_c}{dt} \;=\; \mathbf{F}, \tag{81}$$

where $\mathbf{p}_c \;=\; M\mathbf{v}_c$. The rotational motion of the particle is characterized by the angular momentum $\mathbf{J}$,

$$\mathbf{J} \;\equiv\; \sum_n \mathbf{r}_n^c \times \mathbf{p}_n^c, \tag{82}$$

where the superscript c refers to coordinates relative to the center of mass coordinate ($\mathbf{r}_n^c \;=\; \mathbf{r}_n - \mathbf{r}_c$ and $\mathbf{p}_n^c \;=\; \mathbf{p}_n - \mathbf{p}_c$). The equation of motion of the angular momentum $\mathbf{J}$ follows simply by differentiating the defining equation (82), and using Newton's equation of motion for each molecule separately,

$$\frac{d\mathbf{J}}{dt} \;=\; \sum_n \mathbf{r}_n^c \times \mathbf{F}_n \;\equiv\; \mathcal{T}, \tag{83}$$

with $\mathbf{F}_n$ the force on the n^{th} molecule. The last equality in this equation defines the *torque* $\mathcal{T}$ on the particle. Equations (81) and (83) are Newton's equations of motion for translational and rotational motion, respectively.

Notice that the angular momentum is a linear function of the angular velocity $\mathbf{\Omega}$, since, according to eqs.(78,80,82),

$$\mathbf{J} \;=\; \sum_n m_n \mathbf{r}_n^c \times (\mathbf{\Omega} \times \mathbf{r}_n^c)\,. \tag{84}$$

The right-hand side can be written as a tensor multiplication of $\mathbf{\Omega}$,

$$\mathbf{J} \;=\; \mathbf{I}^c \cdot \mathbf{\Omega}, \tag{85}$$

with $\mathbf{I}^c$ the *inertia tensor*, the ij^{th} component of which is,

$$I_{ij}^c \;\equiv\; \sum_n m_n \left[(r_n^c)^2\,\delta_{ij} \;-\; (r_n^c)_i (r_n^c)_j\right], \tag{86}$$

with δ_{ij} the Kronecker delta ($\delta_{ij} \;=\; 0$ for $i \neq j$, and $\delta_{ij} \;=\; 1$ for $i \;=\; j$). The torque, angular momentum, angular velocity and inertia tensor may be considered as the rotational counterparts of force, momentum, translational velocity and mass, respectively.

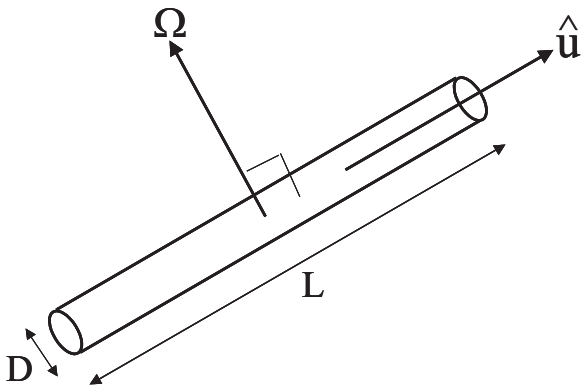

Figure 9: For a long and thin rod, the angular velocity may be thought of as being perpendicular to its orientation.

For the analysis of time scales, we shall need the expression for the kinetic energy E_{kin} of a rotating rod. Using eqs.(78,80,86), one finds,

$$\begin{aligned} E_{kin} &= \sum_n \frac{1}{2} m_n \mathbf{v}_n \cdot \mathbf{v}_n \\ &= \sum_n \frac{1}{2} m_n [\mathbf{\Omega} \times \mathbf{r}_n^c + \mathbf{v}_c] \cdot [\mathbf{\Omega} \times \mathbf{r}_n^c + \mathbf{v}_c] \\ &= \sum_n \frac{1}{2} m_n v_c^2 + \sum_n \frac{1}{2} m_n (\mathbf{\Omega} \times \mathbf{r}_n^c) \cdot (\mathbf{\Omega} \times \mathbf{r}_n^c) \\ &= \frac{1}{2} M v_c^2 \; + \; \sum_n \frac{1}{2} m_n \left[\Omega^2 (r_n^c)^2 - (\mathbf{\Omega} \cdot \mathbf{r}_n^c)^2 \right] \\ &\equiv \frac{1}{2} M v_c^2 \; + \; \frac{1}{2} \, \mathbf{\Omega} \cdot \mathbf{I}^c \cdot \mathbf{\Omega} \; . \end{aligned} \tag{87}$$

The first term on the right-hand side in the last line is the translational kinetic energy, the second term is the kinetic energy associated with rotation about the center of mass.

0.6.2 The Langevin equation for a long and thin rod

Clearly, thermal collisions of solvent molecules with the Brownian particle result in both stochastic motion of the position of its center of mass as well as its orientation. The Langevin equations are Newton's equations of motion (81) for translational motion and (83) for rotational motion supplemented with a fluctuating force and torque, respectively, which account for collisions of the rod with solvent molecules.

In the following, we specialize to a long and thin cylindrically symmetric rod. For such a long and thin rod, the rotational motion around the cylinder axis of symmetry need not be considered. The components of the inertia tensor related to rotational motion around the

long cylinder axis are very small in comparison to its remaining components, and may be disregarded. The angular velocity $\mathbf{\Omega}$ is therefore understood to denote the component of the angular velocity perpendicular to the cylinder axis of symmetry (see fig9). The component $\mathbf{\Omega}$ of the angular velocity that changes the orientation of the rod is equal to,

$$\mathbf{\Omega} \;=\; \hat{\mathbf{u}} \times \frac{d\hat{\mathbf{u}}}{dt} \;. \tag{88}$$

This can be seen as follows. By definition we have,

$$\frac{d\hat{\mathbf{u}}}{dt} \;=\; \mathbf{\Omega} \times \hat{\mathbf{u}} \;, \tag{89}$$

Operating on both sides with $\hat{\mathbf{u}}\times$, using that $\hat{\mathbf{u}} \times (\mathbf{\Omega} \times \hat{\mathbf{u}}) = (\hat{\mathbf{u}} \cdot \hat{\mathbf{u}})\mathbf{\Omega} - (\hat{\mathbf{u}} \cdot \mathbf{\Omega})\hat{\mathbf{u}}$, and noting that $\hat{\mathbf{u}} \cdot \hat{\mathbf{u}} = 1$ and $\hat{\mathbf{u}} \cdot \mathbf{\Omega} = 0$, eq.(88) is recovered.

The force and torque of the solvent on the rod consists of two parts. Once the rods attained a finite translational and rotational velocity, there is a systematic force equal to $-\mathbf{\Gamma}_f \cdot \mathbf{p}/M$ (see eq.(38)) and a systematic torque equal to $-\gamma_r \mathbf{\Omega}$ (see eq.(48)) on the rod due to friction. The second part is the fluctuating force and torque discussed before. Denoting the fluctuating force by $\mathbf{f}$ and the fluctuating torque by $\mathbf{T}$, the complete set of Langevin equations reads (we omit the superscripts "c" in the following),

$$\begin{aligned} d\mathbf{p}/dt &= -\frac{\mathbf{\Gamma}_f}{M} \cdot \mathbf{p} + \mathbf{f}(t), \\ d\mathbf{r}/dt &= \mathbf{p}/M, \\ d\mathbf{J}/dt &= -\gamma_r\, \mathbf{\Omega} + \mathbf{T}(t), \\ \mathbf{I} \cdot \mathbf{\Omega} &= \mathbf{J}. \end{aligned} \tag{90}$$

Since systematic interactions with the solvent molecules are made explicit through friction contributions, the ensemble average of the fluctuating force and torque are zero,

$$\begin{aligned} < \mathbf{f}(t) > &= \mathbf{0} \;, \\ < \mathbf{T}(t) > &= \mathbf{0} \;. \end{aligned} \tag{91}$$

Due to the fore mentioned large separation in time scales on which the solvent molecules relax and the rod moves, it is sufficient for the calculation of the thermal movement of the Brownian particle to use a delta correlated fluctuating force and torque in time, that is,

$$\begin{aligned} < \mathbf{f}(t)\mathbf{f}(t') > &= \mathbf{G}_{trans}\, \delta(t - t') \;, \\ < \mathbf{T}(t)\mathbf{T}(t') > &= \mathbf{G}_{rot}\, \delta(t - t') \;, \end{aligned} \tag{92}$$

where δ is the delta distribution and $\mathbf{G}_{trans}$ and $\mathbf{G}_{rot}$ are constant 3×3-dimensional tensors (where the subscripts stand for "translation" and "rotation"), which may be regarded as a measure for the strength of the fluctuating force and torque. They are referred to as the *translational and rotational fluctuation strength*, respectively. Such delta correlations limit the description to a time resolution which is large with respect to the solvent time scale of $10^{-13}s$.

Note that for the rods with a large aspect ratio L/D considered here, the inertia tensor in eq.(86) is easily calculated, replacing the sum over molecules by an integral. For a constant

local mass density ρ of the rod material, the inertia tensor becomes,

$$\mathbf{I} = \int d\mathbf{r}'\, \rho\, [r'^2 \hat{\mathbf{I}} - \mathbf{r}'\mathbf{r}'] \;\approx\; \pi \left(\frac{D}{2}\right)^2 \rho \int_{-\frac{1}{2}L}^{\frac{1}{2}L} dl\, l^2\, [\hat{\mathbf{I}} - \hat{\mathbf{u}}\hat{\mathbf{u}}] \;=\; \frac{1}{12} M L^2\, [\hat{\mathbf{I}} - \hat{\mathbf{u}}\hat{\mathbf{u}}]\,. \quad (93)$$

The typical magnitude for the inertia tensor is thus $\frac{1}{12} M L^2$. Note that since $\mathbf{\Omega}$ is perpendicular to $\hat{\mathbf{u}}$ (see eq.(88)), it follows from eq.(93) that,

$$\mathbf{I} \cdot \mathbf{\Omega} = \tfrac{1}{12}\, M L^2\, \mathbf{\Omega}\,. \quad (94)$$

This result will be convenient in our further analysis of the Langevin equation.

0.6.3 The Brownian time scale : Relaxation rates of the translational and rotational velocity

The Langevin equation (90) can be used to estimate the time scale on which the translational and rotational velocity decay to equilibrium with the heat bath of solvent molecules. First consider the translational velocity. Ensemble averaging the first equation in (90), using eq.(92) gives,

$$\frac{d <\mathbf{p}>}{dt} \;=\; - < \frac{\mathbf{\Gamma}_f}{M} \cdot \mathbf{p} > \;. \quad (95)$$

Remember that the friction tensor $\mathbf{\Gamma}_f$ depends on the orientation of the rod, and can therefore not be taken outside the ensemble averaging brackets $< \cdots >$. However, the interest here is in an *estimate* of the relaxation time of the translational velocity. Since the magnitude of the friction coefficient of a rod varies only a factor of two depending on its orientation, one can use a typical magnitude of the elements of $\mathbf{\Gamma}_f$ in eq.(95). This typical magnitude follows from the expression in eq.(38) as $2\pi\eta_0 L/\ln\{L/D\}$. The time scale on which the translational velocity relaxes can thus be estimated from,

$$\frac{d <\mathbf{p}>}{dt} \;\approx\; -\frac{2\,\pi\,\eta_0\,L}{M\,\ln\{L/D\}} \;<\mathbf{p}> \;. \quad (96)$$

It follows that (with $\mathbf{p}(0)$ the initial translational momentum),

$$<\mathbf{p}>(t) \;\approx\; \mathbf{p}(0) \exp\{-t/\tau_{trans}\} \quad , \quad \text{with} \;\; \tau_{trans} \;=\; \frac{M\,\ln\{L/D\}}{2\,\pi\,\eta_0\,L} \;\approx\; 1 \text{ ns}\,. \quad (97)$$

A typical value for the relaxation time τ_{trans} of the translational velocity of a rod is thus found to be of the order of a nano second.

The time scale on which rotational velocities relax can be estimated from the last two of the equations in (90). Ensemble averaging gives, using eq.(91),

$$\begin{aligned} \frac{d <\mathbf{J}>}{dt} &= -\gamma_r \;<\mathbf{\Omega}>\,, \\ <\mathbf{I} \cdot \mathbf{\Omega}> &= <\mathbf{J}> \;. \end{aligned} \quad (98)$$

Using eq.(94) in the second equation, and substitution of the result into the first equation leads to,

$$\frac{d <\mathbf{\Omega}>}{dt} \;=\; -\frac{12\,\gamma_r}{M\,L^2} \;<\mathbf{\Omega}>\,, \quad (99)$$

and hence (with $\mathbf{\Omega}(0)$ the initial angular velocity),

$$<\mathbf{\Omega}>(t) \,=\, \mathbf{\Omega}(0)\exp\{-t/\tau_{rot}\}\ ,\ \text{with}\ \ \tau_{rot} = \frac{12\,M\,L^2}{\gamma_r} = \frac{M\ \ln\{L/D\}}{4\,\pi\,\eta_0\,L} \approx 1\ \text{ns}\,. \quad (100)$$

where the expression (49) for the rotational friction coefficient has been used. Relaxation times for translational and rotational velocities are thus both of the order of a nano second.

Within a description where time is coarse grained to a time much larger than τ_{trans} and τ_{rot}, *inertial forces and torques on the rod can be neglected*. This will turn out to be an important fact in further theoretical developments discussed later in this chapter. The corresponding coarsening in length scale and orientational angle will be discussed in the following section. The time scale that is much larger than τ_{trans} and τ_{rot}, but still small enough to resolve position and orientation in sufficient detail, is referred to as *the Brownian or diffusive time scale*.

0.6.4 The Brownian length scale and Brownian angle

As discussed in the beginning of this section, a coarsening in time implies a coarsening of position and angular orientation. On the Brownian time scale the spatial and angular resolution is not better than the distance over which the Brownian particle moves and the angle over which a rod typically rotates, respectively, during a time interval equal to the Brownian time scale.

Consider first the length Δl that the rod traverses during the time $\tau \gg \tau_{trans}$. This so-called *Brownian length scale* is easily obtained by integration of eqs.(97),

$$\Delta l \,=\, \int_0^\tau dt\,\frac{|<\mathbf{p}(t)>|}{M} \,=\, \frac{|\mathbf{p}(0)|}{M}\,\tau_{trans}\,(1-\exp\{-\tau/\tau_{trans}\}) \,\approx\, \frac{|\mathbf{p}(0)|}{M}\,\tau_{trans}\,. \quad (101)$$

A typical value for $|\,\mathbf{p}(0)\,|$ is obtained from the equipartition theorem,

$$|\,\mathbf{p}(0)\,| \approx\, \sqrt{<|\,\mathbf{p}\,|^{\,2}>} \,=\, \sqrt{3Mk_BT}. \quad (102)$$

The Brownian length scale is thus estimated as,

$$\Delta l \,\approx\, \sqrt{3\,M\,k_B\,T}\,\frac{\ln\{L/D\}}{2\,\pi\,\eta_0\,L}\,. \quad (103)$$

Using typical numerical values for the several quantities gives,

$$\frac{\Delta l}{L} \,\approx\, 10^{-4}\ -\ 10^{-3}\,. \quad (104)$$

The conclusion is that displacements that are very small in comparison to the length of the rod are still resolved on the Brownian time scale. When $\Delta L/L$ would have been a large number, it would have made no sense to coarsen to the Brownian time scale, since it is then not possible to accurately describe the motion of the rod.

Next consider the typical angle $\Delta\Theta$ over which a rod rotates during a time $\tau \gg \tau_{rot}$. This is the so-called *Brownian angle*. Integration of eq.(100) gives,

$$\Delta\Theta \,=\, \int_0^\tau dt\ \ |<\mathbf{\Omega}(t)>| = |\,\mathbf{\Omega}(0)|\ \,\tau_{rot}\,(1-\exp\{-\tau/\tau_{rot}\}) \,\approx |\,\mathbf{\Omega}(\mathbf{0})|\ \,\tau_{rot}\,. \quad (105)$$

According to eq.(94), the rotational contribution to the kinetic energy in eq.(87) is equal to $\frac{1}{24} M L^2 \, |\boldsymbol{\Omega}|^2$. Hence, according to the equipartition theorem, a typical value for $|\boldsymbol{\Omega}_0|$ can be estimated as,

$$|\boldsymbol{\Omega}(0)| \;\approx\; \sqrt{<|\boldsymbol{\Omega}|^2>} \;=\; 6\sqrt{\frac{k_B\,T}{M\,L^2}}\;. \tag{106}$$

The Brownian angle is thus of the order,

$$\Delta\Theta \;\approx\; 6\sqrt{M\,k_B\,T}\;\frac{\ln\{L/D\}}{4\,\pi\,\eta_0\,L^2}\;. \tag{107}$$

For typical numerical values we have (note that, according to eq.(103), the right-hand side is equal to $\sqrt{3}\,\Delta L/L$),

$$\frac{\Delta\Theta}{\pi} \;\approx\; 10^{-4} - 10^{-3}\;. \tag{108}$$

Very small angular displacements can thus still be resolved on the Brownian time scale.

For the study of processes where a significant translational and rotational displacement of the Brownian particle is essential, a statistical description on the Brownian time scale is therefore sufficient.

0.6.5 Calculation of fluctuation strengths

Analyzing the Langevin equation requires the determination of the fluctuation strengths in eq.(92). This can be done using the equipartition theorem for translational and rotational motion, after having solved the Langevin equation for $\mathbf{p}(t)$ and $\boldsymbol{\Omega}(t)$.

First consider the translational velocity. Integration of the first equation of motion in (90) yields,

$$\mathbf{p}(t) \;=\; \exp\left\{-\frac{\boldsymbol{\Gamma}_f}{M}t\right\}\cdot\mathbf{p}(0) + \int_0^t dt'\,\exp\left\{-\frac{\boldsymbol{\Gamma}_f}{M}(t-t')\right\}\cdot\mathbf{f}(t')\,. \tag{109}$$

The exponent of a tensor, $\mathbf{A}$ say, is defined through the Taylor expansion,

$$\exp\{\mathbf{A}\} \;\equiv\; \sum_{n=0}^{\infty}\frac{1}{n!}\,\mathbf{A}^n\;, \tag{110}$$

where $\mathbf{A}^n$ is $\mathbf{A}\cdot\mathbf{A}\cdots\mathbf{A}$, n times, and $\mathbf{A}^0 \equiv \hat{\mathbf{I}}$, the identity tensor. Now, from eq.(43) it is easily shown by induction that,

$$\boldsymbol{\Gamma}_f^n \;=\; \gamma_\parallel^n\,\hat{\mathbf{u}}\hat{\mathbf{u}} \;+\; \gamma_\perp^n\,[\,\hat{\mathbf{I}} - \hat{\mathbf{u}}\hat{\mathbf{u}}\,]\;, \tag{111}$$

and hence, from the defining expression (110) for the tensor exponential,

$$\exp\left\{-\frac{\boldsymbol{\Gamma}_f}{M}(t-t')\right\} \;=\; \exp\left\{-\frac{\gamma_\parallel}{M}(t-t')\right\}\hat{\mathbf{u}}\hat{\mathbf{u}} \;+\; \exp\left\{-\frac{\gamma_\perp}{M}(t-t')\right\}[\hat{\mathbf{I}} - \hat{\mathbf{u}}\hat{\mathbf{u}}]\;. \tag{112}$$

Equation (109) can thus be written as,

$$\mathbf{p}(t) \;=\; \mathbf{p}_\parallel(t) + \mathbf{p}_\perp(t)\;,\;\text{with}\;\mathbf{p}_\parallel \equiv \hat{\mathbf{u}}\hat{\mathbf{u}}\cdot\mathbf{p}\;,\;\text{and}\;\mathbf{p}_\perp \equiv [\,\hat{\mathbf{I}} - \hat{\mathbf{u}}\hat{\mathbf{u}}\,]\cdot\mathbf{p}\;, \tag{113}$$

with,

$$\mathbf{p}_{\parallel}(t) \equiv \exp\left\{-\frac{\gamma_{\parallel}}{M}t\right\}\,\mathbf{p}_{\parallel}(0) + \int_0^t dt' \exp\left\{-\frac{\gamma_{\parallel}}{M}(t-t')\right\}\mathbf{f}_{\parallel}(t')\;,$$
$$\mathbf{p}_{\perp}(t) \equiv \exp\left\{-\frac{\gamma_{\perp}}{M}t\right\}\mathbf{p}_{\perp}(0) + \int_0^t dt' \exp\left\{-\frac{\gamma_{\perp}}{M}(t-t')\right\}\mathbf{f}_{\perp}(t')\;, \qquad (114)$$

where the components of the random force parallel and perpendicular to the rods orientation are respectively defined as,

$$\mathbf{f}_{\parallel}(t) \;\equiv\; \hat{\mathbf{u}}(t)\hat{\mathbf{u}}(t)\cdot\mathbf{f}(t) \;\;,\;\; \text{and} \;\; \mathbf{f}_{\perp}(t) \;\equiv\; [\,\hat{\mathbf{I}} - \hat{\mathbf{u}}(t)\hat{\mathbf{u}}(t)\,]\cdot\mathbf{f}(t)\;. \qquad (115)$$

Instead of using the full tensor form in eq.(95) for the fluctuating force, we shall only need correlation functions of inner products of its two components $\mathbf{f}_{\parallel}$ and $\mathbf{f}_{\perp}$. Since $\mathbf{f}(t)$ varies with time much faster than $\hat{\mathbf{u}}(t)$, the latter is virtually constant over time intervals equal to many times the correlation time of the former. The conditional ensemble averages of $\mathbf{f}_{\parallel,\perp}$, with a prescribed $\hat{\mathbf{u}}$, are therefore still $\mathbf{0}$, and their correlation functions are still delta correlated on a time scale much larger than the solvent time scale. For the same reason,

$$< \mathbf{f}_{\parallel}(t)\cdot\mathbf{f}_{\perp}(t') > = \;0\;. \qquad (116)$$

We shall therefore define two independent fluctuation strengths for the fluctuating force parallel and perpendicular to the rods orientation,

$$\begin{aligned} < \mathbf{f}_{\parallel}(t)\cdot\mathbf{f}_{\parallel}(t') > &= G_{\parallel}\,\delta(t-t'), \\ < \mathbf{f}_{\perp}(t)\cdot\mathbf{f}_{\perp}(t') > &= G_{\perp}\,\delta(t-t'). \end{aligned} \qquad (117)$$

Notice that we are working here with inner products instead of dyadic products as for the spherical particle, so that both $G_{\parallel}$ and $G_{\perp}$ are scalars. Since $< \mathbf{p}_{\parallel}(t)\cdot\mathbf{p}_{\perp}(t) >= 0$, the kinetic energy corresponding to translational motion of the Brownian rod is a sum of two quadratic terms related to the perpendicular velocity and a single quadratic term related to the parallel velocity. From the equipartition theorem it is thus found that,

$$\begin{aligned} \lim_{t\to\infty} < \mathbf{p}_{\parallel}(t)\cdot\mathbf{p}_{\parallel}(t) > &= M/\beta, \\ \lim_{t\to\infty} < \mathbf{p}_{\perp}(t)\cdot\mathbf{p}_{\perp}(t) > &= 2\,M/\beta. \end{aligned} \qquad (118)$$

Substitution of eq.(114) into the above expressions, using eqs.(116,117), it is readily found that,

$$\begin{aligned} G_{\parallel} &= 2\gamma_{\parallel}/\beta\,, \\ G_{\perp} &= 4\gamma_{\perp}/\beta\,. \end{aligned} \qquad (119)$$

This concludes the determination of the translational fluctuation strengths, which will be used to investigate the translational Brownian motion of the rod in the following section.

Next consider the fluctuation strength for the correlation function in eq.(92) of the torque. Using eq.(94) in the last equation in (90), substituting the result into the third equation and integration yields,

$$\mathbf{\Omega}(t) \;=\; \mathbf{\Omega}(0)\,\exp\left\{-\frac{12\gamma_r}{ML^2}t\right\} + \frac{12}{ML^2}\int_0^t dt'\,\mathbf{T}(t')\,\exp\left\{-\frac{12\gamma_r}{ML^2}(t-t')\right\}\;. \qquad (120)$$

Using the second equation in (92) thus leads to,

$$\lim_{t\to\infty} < \mathbf{\Omega}(t)\,\mathbf{\Omega}(t) > = \frac{6}{\gamma_r M L^2}\mathbf{G}_r. \tag{121}$$

From eq.(87) for the kinetic energy together with eq.(94) and one finds that the kinetic energy due to rotational motion is equal to $\frac{1}{24}ML^2\Omega^2(t)$. The equipartition theorem implies that $\frac{1}{24}ML^2\Omega^2(t) = \frac{3}{2}k_BT$. Hence,

$$\lim_{t\to\infty} < \mathbf{\Omega}(t)\,\mathbf{\Omega}(t) > = 12\,\hat{\mathbf{I}}\,\frac{k_BT}{ML^2}\ . \tag{122}$$

Combining this with eq.(121) identifies the rotational fluctuation strength,

$$\mathbf{G}_r \ = \ \hat{\mathbf{I}}\,\frac{2\gamma_r}{\beta}\ . \tag{123}$$

This expression allows for the analysis of the rotational part of the Langevin equation.

0.6.6 Translational Brownian motion of a rod

The simplest quantity that characterizes translational Brownian motion is the *mean squared displacement*, defined as,

$$W(t) \ \equiv <|\mathbf{r}(t) - \mathbf{r}(t=0)|^2>\ , \tag{124}$$

where the brackets denote ensemble averaging. This quantity can be calculated from the Langevin equation as follows.

We shall calculate the mean squared displacement on the Brownian time scale. As mentioned before, inertial forces can be neglected on the Brownian time scale. Neglecting the inertial force $d\mathbf{p}/dt$ on the left hand-side of the first equation in (90) gives,

$$d\mathbf{r}/dt \ = \ \mathbf{\Gamma}_f^{-1}\cdot\mathbf{f}(t)\ , \tag{125}$$

where $\mathbf{\Gamma}_f^{-1}$ is the inverse of $\mathbf{\Gamma}_f$. The reason for neglecting the inertial force can be made more explicit as follows. Let $t' = t/\tau$ be the dimensionless time in units of the Brownian time scale τ. Rescaling the first equation in eq.(90) gives,

$$\frac{\tau_{trans}}{\tau}\,\frac{d\mathbf{p}}{dt'} \ = \ -\,\tau_{trans}\,\frac{\mathbf{\Gamma}_f}{M}\cdot\mathbf{p} + \tau_{trans}\,\mathbf{f}(\tau\,t')\ . \tag{126}$$

Since the typical magnitude of the elements of the tensor $\mathbf{\Gamma}_f/M$ is $1/\tau_{trans}$ (see eqs.(38,97)), so that $\tau_{trans}\,\mathbf{\Gamma}_f/M$ is of order unity, and $\tau \gg \tau_{trans}$ on the Brownian time scale, this is a singularly perturbed differential equation. That is, the inertial term is important only over a very small time interval in t', which is the mathematical boundary layer connected to the singular perturbation. During this time interval the momentum coordinate relaxes to equilibrium with the solvent. Beyond this small time interval, where $d\mathbf{p}/dt'$ is not very large anymore, so that the inertial contribution can be neglected. This immediately leads to eq.(125).

The inverse of the friction tensor appearing in eq.(125) is easily calculated,

$$\mathbf{\Gamma}_f^{-1} \ = \ \frac{1}{\gamma_\parallel}\hat{\mathbf{u}}\hat{\mathbf{u}} \ + \ \frac{1}{\gamma_\perp}[\,\hat{\mathbf{I}} - \hat{\mathbf{u}}\hat{\mathbf{u}}\,]\ . \tag{127}$$

The Langevin equation can thus be written in terms of the parallel and perpendicular components of the random force (see eq.(115)),

$$d\mathbf{r}/dt \;=\; \frac{1}{\gamma_{\parallel}}\mathbf{f}_{\parallel}(t) + \frac{1}{\gamma_{\perp}}\mathbf{f}_{\perp}(t)\;, \tag{128}$$

hence,

$$\mathbf{r}(t) = \mathbf{r}(t=0) + \int_0^t dt' \;\left[\frac{1}{\gamma_{\parallel}}\mathbf{f}_{\parallel}(t') + \frac{1}{\gamma_{\perp}}\mathbf{f}_{\perp}(t')\right]\;. \tag{129}$$

Using that the fluctuating forces are delta correlated with fluctuation strengths given in eq.(119), one readily finds that,

$$W(t) \;=\; 6\,\bar{D}\,t\;, \tag{130}$$

where,

$$\bar{D} \;=\; \frac{1}{3}\left(D_{\parallel} + 2D_{\perp}\right). \tag{131}$$

Here we introduced the Einstein translational diffusion coefficients for parallel and perpendicular motion,

$$\begin{aligned} D_{\parallel} &= k_B T/\gamma_{\parallel}\;, \\ D_{\perp} &= k_B T/\gamma_{\perp}\;. \end{aligned} \tag{132}$$

For times $t \ll \tau_{trans}$, where friction with the solvent has not been effective, the velocity of the center of mass of a rod is constant. The mean squared displacement then varies like $\sim t^2$. On the Brownian time scale, that is for times $t \gg \tau_{trans}$, many independent collisions of the rod with solvent molecules have occurred. This apparently leads to a linear variation of $W(t)$ with time. Such dynamic behaviour is called *diffusive*.

0.6.7 Orientational correlations

The simplest quantity that characterizes rotational Brownian motion is the *rotational mean squared displacement*,

$$W_{rot}(t) \;\equiv <|\;\hat{\mathbf{u}}(t) - \hat{\mathbf{u}}(t=0)\;|^2> = \;2\,[\,1 - <\hat{\mathbf{u}}(t)> \cdot\, \hat{\mathbf{u}}(t=0)\,]\;. \tag{133}$$

This rotational displacement is calculated on the Brownian time scale. For the same reason as for translational motion, the inertial term for the rotational langevin equation of motion can be neglected on the Brownian time scale. The third of the equations of motion in (90) thus reduces to,

$$\mathbf{\Omega} \;= \hat{\mathbf{u}} \times \frac{d\hat{\mathbf{u}}}{dt} \;=\; \frac{1}{\gamma_r}\,\mathbf{T}(t)\;. \tag{134}$$

where eqs.(88,94) have been used. As a first step to obtain an expression for the rotational mean squared displacement (133), the differential equation (134) should be solved for $\hat{\mathbf{u}}(t)$ in terms of the fluctuating torque $\mathbf{T}$. To this end, eq.(134) is rewritten as,

$$d\hat{\mathbf{u}}/dt \;=\; \frac{1}{\gamma_r}\,\mathbf{T}(t) \times \hat{\mathbf{u}}\;. \tag{135}$$

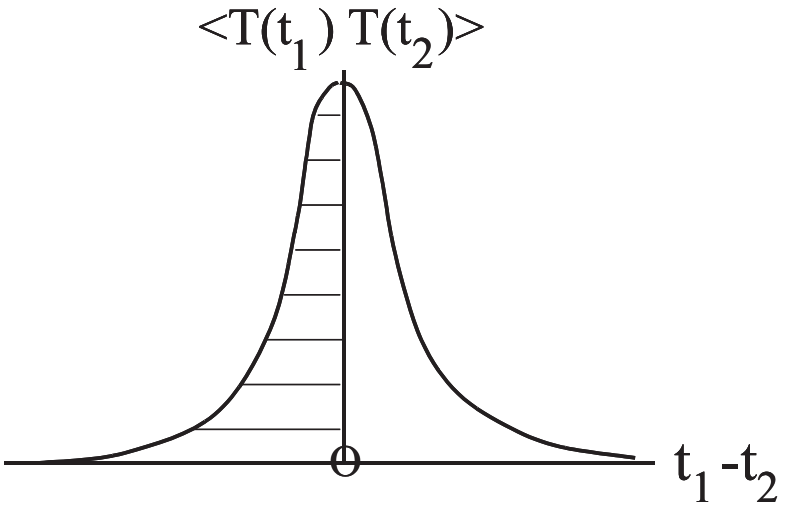

Figure 10: Integration of the correlation function of the torque over half the domain of its argument.

To integrate this equation, the right-hand side is written as a tensor multiplication,

$$d\hat{\mathbf{u}}/dt \;=\; \mathbf{A}(t)\cdot\hat{\mathbf{u}}\,, \tag{136}$$

with,

$$\mathbf{A}(t) \;\equiv\; \frac{1}{\gamma_r}\begin{pmatrix} 0 & -T_3(t) & T_2(t) \\ T_3(t) & 0 & -T_1(t) \\ -T_2(t) & T_1(t) & 0 \end{pmatrix}, \tag{137}$$

where T_j is the j^{th} component of $\mathbf{T}$. The differential equation (136) is equivalent to the integral equation,

$$\hat{\mathbf{u}}(t) \;=\; \hat{\mathbf{u}}(0) + \int_0^t dt'\,\mathbf{A}(t')\cdot\hat{\mathbf{u}}(t')\,, \tag{138}$$

which is solved by iteration,

$$\begin{aligned}\hat{\mathbf{u}}(t) \quad = \quad \hat{\mathbf{u}}(0) + \sum_{n=1}^{\infty}\int_0^t dt_1\int_0^{t_1} dt_2\int_0^{t_2} dt_3\cdots\int_0^{t_{n-2}} dt_{n-1}\int_0^{t_{n-1}} dt_n \\ \mathbf{A}(t_1)\cdot\mathbf{A}(t_2)\cdot\;\cdots\;\cdot\mathbf{A}(t_n)\cdot\hat{\mathbf{u}}(0)\,.\end{aligned} \tag{139}$$

For the calculation of the ensemble average of $\hat{\mathbf{u}}(t)$, the ensemble averages of the multiple integrals over products of $\mathbf{A}$'s must be evaluated explicitly. From the definition of the tensor

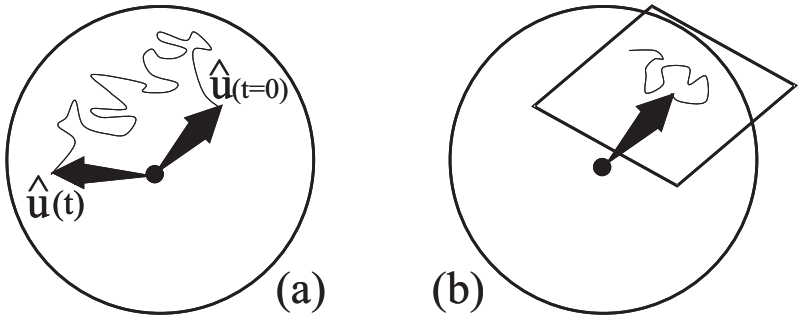

Figure 11: (a) Rotational diffusion visualized as diffusion of a point on the unit sphere. (b) For small time this is equivalent to diffusion of a point on a two-dimensional surface.

$\mathbf{A}$ it follows immediately that,

$$\mathbf{A}(t)\cdot\hat{\mathbf{u}}(0) \;=\; \frac{1}{\gamma_r}\mathbf{T}(t)\times\hat{\mathbf{u}}(0)\,, \tag{140}$$

$$\begin{aligned}\mathbf{A}^2(t)\cdot\hat{\mathbf{u}}(0) &= \frac{1}{\gamma_r^2}\mathbf{T}(t)\times(\mathbf{T}(t)\times\hat{\mathbf{u}}(0)) \\ &= \frac{1}{\gamma_r^2}\left[-T^2(t)\hat{\mathbf{I}}+\mathbf{T}(t)\mathbf{T}(t)\right]\cdot\hat{\mathbf{u}}(0)\,.\end{aligned} \tag{141}$$

Since the ensemble average of the random torque, and hence of $\mathbf{A}$, is zero, and its correlation function is delta correlated in time, the first two terms in the ensemble averaged iterated solution are found from eqs.(123,137),

$$\int_0^t dt_1 \;<\mathbf{A}(t_1)>\cdot\hat{\mathbf{u}}(0) \;=\; \mathbf{0}\,, \tag{142}$$

$$\int_0^t dt_1\int_0^{t_1} dt_2 \;<\mathbf{A}(t_1)\cdot\mathbf{A}(t_2)>\cdot\hat{\mathbf{u}}(0) \;=\; -\,2\,\frac{k_BT}{\gamma_r}\,t\,\hat{\mathbf{u}}(0)\,. \tag{143}$$

Here we used that,

$$\int_0^{t_1} dt_2\,\delta(t_1-t_2) \;=\; \frac{1}{2}\,.$$

Since t_1 is not in the interior of the integration range here, this integral is *not* equal to 1. That its value is equal to $\frac{1}{2}$ can be seen as follows. On the smallest time scale, the correlation function $<\mathbf{T}(t_1)\mathbf{T}(t_2)>$ of the random torque, and hence of $\mathbf{A}$, is a symmetric function of the difference t_1-t_2. The integral with respect to t_2 in eq.(139) ranges over half of the symmetric correlation function (see fig.10), and is thus equal to $\frac{1}{2}\times$ the integral ranging over the entire range of the argument. To evaluate the ensemble averages over higher order products of $\mathbf{A}$ in the iterated solution (139), we use that, on the Brownian time scale, $\mathbf{T}$ and hence also $\mathbf{A}$ is a Gaussian variable. On the Brownian time scale, $\mathbf{T}$ is an average over many independent realizations, so that, according to the central limit theorem, it is a Gaussian variable. All the ensemble averages of products of an odd number of $\mathbf{A}$'s are thus zero. The ensemble averages

of products of an even number of $\mathbf{A}$'s can be written as a sum of products of averages of only two $\mathbf{A}$'s. Consider for example the ensemble average of the $n = 4$ term in the iterated solution (summation over the repeated indices p, q, r, s is understood here, A_{ij} is the ij^{th} component of $\mathbf{A}$ and $\hat{u}_s(0)$ is the s^{th} component of $\hat{\mathbf{u}}(0)$),

$$\int_0^t dt_1 \int_0^{t_1} dt_2 \int_0^{t_2} dt_3 \int_0^{t_3} dt_4 < A_{ip}(t_1)A_{pq}(t_2)A_{qr}(t_3)A_{rs}(t_4) > \hat{u}_s(0) =$$
$$\int_0^t dt_1 \int_0^{t_1} dt_2 \int_0^{t_2} dt_3 \int_0^{t_3} dt_4 \, [< A_{ip}(t_1)A_{pq}(t_2) >< A_{qr}(t_3)A_{rs}(t_4) > \hat{u}_s(0)$$
$$+ < A_{ip}(t_1)A_{qr}(t_3) >< A_{pq}(t_2)A_{rs}(t_4) > \hat{u}_s(0)$$
$$+ < A_{ip}(t_1)A_{rs}(t_4) >< A_{pq}(t_2)A_{qr}(t_3) > \hat{u}_s(0) \,] \, .$$

For the respective products of ensemble averages in the above equation we need to evaluate the following integrations over delta distributions,

$$\int_0^t dt_1 \int_0^{t_1} dt_2 \int_0^{t_2} dt_3 \int_0^{t_3} dt_4 \, \delta(t_1 - t_2) \, \delta(t_3 - t_4) \, ,$$
$$\int_0^t dt_1 \int_0^{t_1} dt_2 \int_0^{t_2} dt_3 \int_0^{t_3} dt_4 \, \delta(t_1 - t_3) \, \delta(t_2 - t_4) \, ,$$

and,

$$\int_0^t dt_1 \int_0^{t_1} dt_2 \int_0^{t_2} dt_3 \int_0^{t_3} dt_4 \, \delta(t_1 - t_4) \, \delta(t_2 - t_3) \, .$$

The first of these four-fold integrals is equal to,

$$\int_0^t dt_1 \int_0^{t_1} dt_2 \int_0^{t_2} dt_3 \int_0^{t_3} dt_4 \, \delta(t_1 - t_2) \, \delta(t_3 - t_4) = \left(\frac{1}{2}\right)^2 \, \frac{1}{2} \, t^2 \, ,$$

where the factor $(1/2)^2$ originates from integration of delta functions ranging over half the domain of their arguments, as explained above. By inspection, the other two four-fold integrals turn out to be zero, because the arguments of the delta functions are non-zero in the entire integration range. Only products with the consecutive time ordering $t_1 \rightarrow t_2 \rightarrow t_3 \rightarrow \cdots \rightarrow t_n$ contribute. Using the expression (123) for the rotational fluctuation strength, we thus arrive at the following result,

$$\int_0^t dt_1 \int_0^{t_1} dt_2 \int_0^{t_2} dt_3 \int_0^{t_3} dt_4 \quad < \mathbf{A}(t_1) \cdot \mathbf{A}(t_2) \cdot \mathbf{A}(t_3) \cdot \mathbf{A}(t_4) > \cdot \hat{\mathbf{u}}(0)$$
$$= \left(-\frac{4}{\beta\gamma_r}\right)^2 \, \left(\frac{1}{2}\right)^2 \, \frac{1}{2} \, t^2 \, \hat{\mathbf{u}}(0) \, .$$

In the next higher order terms in the ensemble average of the iterative solution (139), the product with the consecutive time ordering is likewise the only surviving one. Along similar lines one shows that, for even n's,

$$\int_0^t dt_1 \cdots \int_0^{t_{n-1}} dt_n < \mathbf{A}(t_1) \cdot \, \cdots \, \cdot \mathbf{A}(t_n) >= \left(-\frac{4}{\beta\gamma_r}\right)^{n/2} \, \left(\frac{1}{2}\right)^{n/2} \, \frac{1}{\frac{n}{2}!} \, t^{n/2} \, \hat{\mathbf{I}} \, .$$

The iterative solution is thus,

$$< \hat{\mathbf{u}}(t) > = \left[\sum_{n=0}^{\infty} \frac{1}{n!} (-2D_r)^n \, t^n \right] \hat{\mathbf{u}}(0) \; = \; \exp\{-2D_r t\} \, \hat{\mathbf{u}}(0) \; , \tag{144}$$

where the *rotational diffusion coefficient* D_r is defined by the Einstein relation,

$$D_r \; = \; k_B T / \gamma_r \; . \tag{145}$$

The *rotational mean squared displacement* is thus equal to,

$$W_{rot}(t) \; = \; 2 \, [\, 1 - \exp\{-2D_r t\} \,] \; . \tag{146}$$

For small times this result is quite similar to eq.(130) for the mean squared displacement of the center of mass of a rod,

$$W_{rot}(t) \; = < | \; \hat{\mathbf{u}}(t) - \hat{\mathbf{u}}(t=0) \; |^2 > = \; 4 \, D_r \, t \quad , \quad D_r \, t \ll 1 \; . \tag{147}$$

This corresponds to diffusion of a point in two dimensions. Rotational Brownian motion may be visualized as a point on the unit spherical surface, representing the tip of the unit vector $\hat{\mathbf{u}}$, which exerts Brownian motion (see fig.11a). For small times this is Brownian motion on a two dimensional flat surface (see fig.11b). For larger times the tip experiences the curvature of the unit spherical surface, leading to the more complex behaviour as described by eq.(146).

0.7 Equations of Motion for Interacting Rods

So far, we have considered rods which do not interact with other rods. For systems of interacting rods, properties are most easily studied by means of probability density functions (pdf's) of positions and orientations. In this section we shall derive the fundamental equation of motion for the probability density function of the positions and orientations of an assembly of N interacting rods. This equation of motion is commonly referred to as *the Smoluchowski equation*. An essential ingredient in the derivation of this equation of motion is the neglect of inertia on the Brownian time scale, as discussed before. The Smoluchowski equation also describes the dynamics of non-interacting rods, and is shown to reproduce results obtained in previous sections. In addition, the behaviour of non-interacting rods in shear flow is discussed at the end of this section.

0.7.1 The N-particle Smoluchowski equation

Consider a single cylindrically symmetric, rigid rod embedded in solvent. The position coordinate of the rod will be denoted by $\mathbf{r}$, while its orientation is characterized by the unit vector $\hat{\mathbf{u}}$ which is directed along the long axis of the rod. The "microstate" of the rod is thus set by a point in $\Re^3$ (the position vector $\mathbf{r}$) and a point on the unit spherical surface (the tip of the vector $\hat{\mathbf{u}}$), as depicted in fig.12. The points in $\Re^3$ and on the unit spherical surface exhibit chaotic motion due to translational- and rotational Brownian motion, respectively. Consider now an ensemble of $\mathcal{N}$ containers, where each container is filled with solvent and contains

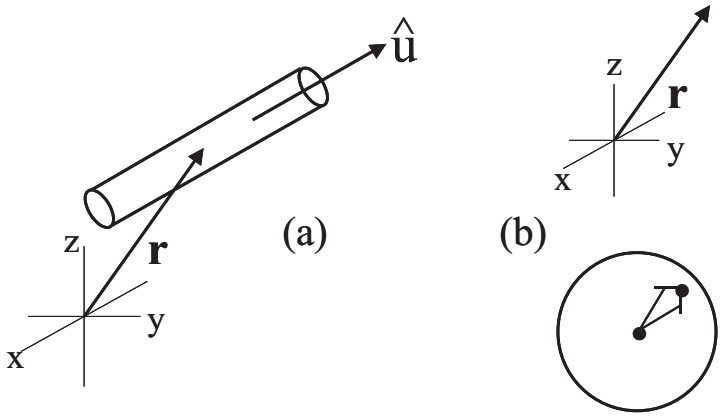

Figure 12: (a) Definition of the position coordinate $\mathbf{r}$ and the orientation $\hat{\mathbf{u}}$ of a rod. (b) The "microstate" of a single rod is set by a point in $\Re^3$ (the position coordinate) and a point on the unit spherical surface (the orientation).

just a single Brownian rod. The "microstate" of this ensemble (as far as the colloidal rod is concerned) is set by $\mathcal{N}$ points in $\Re^3$ (for the positions) and $\mathcal{N}$ points on the unit spherical surface (for the orientations). Let $\mathcal{W}$ denote an arbitrary volume in $\Re^3$, and $\mathcal{A}$ an arbitrary surface area on the unit spherical surface (see fig.13). The density of points at a certain position and orientation is proportional to the probability of finding a rod in that microstate. To find an equation of motion for that probability, we shall ask for the time rate of change of the number of points inside $\mathcal{W}$ and $\mathcal{A}$. The time dependent "number of points" $N(t)$ is related to the probability density function $P(\mathbf{r}, \hat{\mathbf{u}}, t)$ for the position $\mathbf{r}$ and orientation $\hat{\mathbf{u}}$, as,

$$N(t) \;=\; \int_{\mathcal{W}} d\mathbf{r} \int_{\mathcal{A}} d\hat{\mathbf{u}}\; P(\mathbf{r}, \hat{\mathbf{u}}, t)\;, \tag{148}$$

where $d\hat{\mathbf{u}}$ denotes an infinitesimally small surface element on the unit spherical surface (in spherical coordinates this surface element is equal to $\sin\{\Theta\}\, d\Theta\, d\varphi$). The time rate of change of the number of points in $\mathcal{W}$ and $\mathcal{A}$ is thus given by,

$$\frac{d\,N(t)}{dt} \;=\; \int_{\mathcal{W}} d\mathbf{r} \int_{\mathcal{A}} d\hat{\mathbf{u}}\; \frac{\partial}{\partial t}\, P(\mathbf{r}, \hat{\mathbf{u}}, t)\;. \tag{149}$$

The rate of change of the number of points is related to the in- and out-flux of points through the boundaries $\partial\mathcal{W}$ and $\partial\mathcal{A}$ of $\mathcal{W}$ and $\mathcal{A}$, respectively.

Consider first the flux through $\partial\mathcal{W}$. Let $\mathbf{v}$ denote the translational velocity of the center of mass of the rod. The only component of $\mathbf{v}$ that contributes to in- or out-flux through $\partial\mathcal{W}$ is the component that is perpendicular to $\mathcal{W}$: when $\mathbf{v}$ is locally parallel to $\partial\mathcal{W}$, there is no local in- nor out-flux contribution. The component of $\mathbf{v}$ that is perpendicular to $\partial\mathcal{W}$ is equal to $\hat{\mathbf{n}} \cdot \mathbf{v}$, where $\hat{\mathbf{n}}$ is the unit normal (which is chosen to be directed outward of $\mathcal{W}$). The local contribution to the rate of change of the number of points in $\mathcal{W}$ is equal to the local density

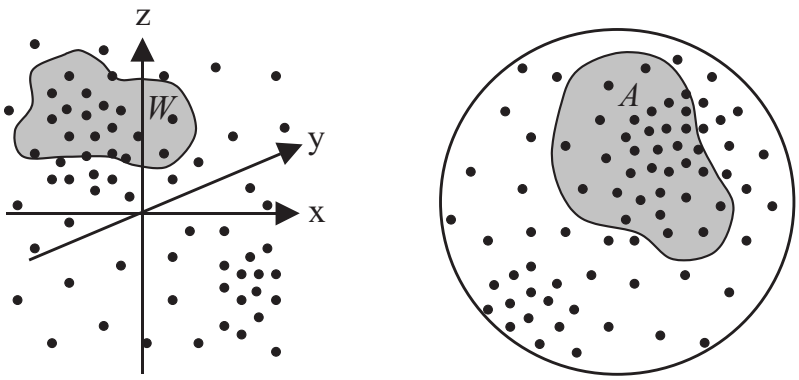

Figure 13: The "microstate" of the ensemble is given by a point distribution in $\Re^3$ and on the unit spherical surface. $\mathcal{W}$ and $\mathcal{A}$ are arbitrary subspaces in $\Re^3$ and on the unit spherical surface, respectively.

of points $P(\mathbf{r}, \hat{\mathbf{u}}, t)$, multiplied by the perpendicular component $\hat{\mathbf{n}} \cdot \mathbf{v}$ of $\mathbf{v}$. The total rate of change $dN_{\mathcal{W}}(t)/dt$ of the number of points due to in- and out-flux through $\partial\mathcal{W}$ is thus equal to (with $d\mathbf{S} = \hat{\mathbf{n}}\, dS$, where dS is an infinitesimally small surface element on $\partial\mathcal{W}$; see fig.14a),

$$\frac{d\,N_{\mathcal{W}}(t)}{dt} \;=\; -\oint_{\partial\mathcal{W}} d\mathbf{S} \;\cdot\; \int_{\mathcal{A}} d\hat{\mathbf{u}}\;\left[\,\mathbf{v}\,P(\mathbf{r},\hat{\mathbf{u}},t)\,\right]\;. \tag{150}$$

The minus sign here is due to the fact that the direction of $\hat{\mathbf{n}}$ is pointing outward of $\mathcal{W}$: when $\mathbf{v} \sim \hat{\mathbf{n}}$, so that $\hat{\mathbf{n}}\cdot\mathbf{v} > 0$, the number points in $\mathcal{W}$ decreases in time. Applying *Gauss's integral theorem* it is found that,

$$\frac{d\,N_{\mathcal{W}}(t)}{dt} \;=\; -\int_{\mathcal{W}} d\mathbf{r} \int_{\mathcal{A}} d\hat{\mathbf{u}}\,\nabla\cdot\left[\,\mathbf{v}\,P(\mathbf{r},\hat{\mathbf{u}},t)\,\right]\;. \tag{151}$$

Next consider the contribution $dN_{\mathcal{A}}(t)/dt$ of the rate of change due to in- and out-flux through the boundary $\partial\mathcal{A}$ of $\mathcal{A}$. This boundary is a closed curve on the unit spherical surface. Since $\hat{\mathbf{u}}$ is always perpendicular to the unit spherical surface, the vector that is locally perpendicular to $\partial\mathcal{A}$ is equal to $d\mathbf{l} \times \hat{\mathbf{u}}$, where $d\mathbf{l}$ is the infinitesimally small vector that is locally tangential to the curve $\partial\mathcal{A}$ (see fig.14b). The component of the velocity $d\hat{\mathbf{u}}/dt$ that is perpendicular to $\partial\mathcal{A}$ is thus equal to $(d\mathbf{l}\times\hat{\mathbf{u}})\cdot d\hat{\mathbf{u}}/dt$, which is the component that determines the in- and out-flux. Since this is equal to $d\mathbf{l}\cdot(\hat{\mathbf{u}}\times d\hat{\mathbf{u}}/dt)$, the total rate of change $dN_{\mathcal{A}}(t)/dt$ of the number of points in $\mathcal{A}$ is thus equal to,

$$\frac{d\,N_{\mathcal{A}}(t)}{dt} \;=\; -\int_{\mathcal{W}} d\mathbf{r} \oint_{\partial\mathcal{A}} d\mathbf{l}\;\cdot\;\left(\hat{\mathbf{u}}\times\frac{d\hat{\mathbf{u}}}{dt}\right)\,P(\mathbf{r},\hat{\mathbf{u}},t)\;. \tag{152}$$

Applying *Stokes's integral theorem*, it is found that,

$$\frac{d\,N_{\mathcal{A}}(t)}{dt} \;=\; -\int_{\mathcal{W}} d\mathbf{r} \int_{\mathcal{A}} d\hat{\mathbf{u}}\;\hat{\mathbf{u}}\cdot\left\{\nabla_{\hat{\mathbf{u}}}\times\left(\hat{\mathbf{u}}\times\frac{d\hat{\mathbf{u}}}{dt}\right)\,P(\mathbf{r},\hat{\mathbf{u}},t)\right\}\;, \tag{153}$$

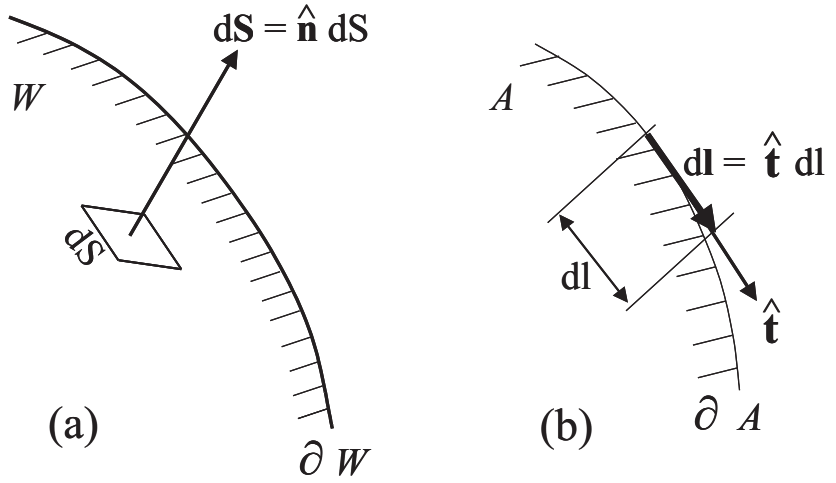

Figure 14: Part of the boundary $\partial\mathcal{W}$ (a) and of the boundary $\partial\mathcal{A}$ (b). For an explanation of the symbols in these figures, see the main text.

where $\nabla_{\hat{\mathbf{u}}}$ is the gradient operator with respect to the cartesian components of $\hat{\mathbf{u}}$. Using eq.(88) for the angular velocity, and using that $\hat{\mathbf{u}} \cdot \nabla_{\hat{\mathbf{u}}} \times (\cdots) = (\hat{\mathbf{u}} \times \nabla_{\hat{\mathbf{u}}}) \cdot (\cdots)$, eq.(153) can be rewritten as,

$$\frac{d\,N_{\mathcal{A}}(t)}{dt} \;=\; -\int_{\mathcal{W}} \int_{\mathcal{A}} d\hat{\mathbf{u}}\; (\hat{\mathbf{u}} \times \nabla_{\hat{\mathbf{u}}}) \cdot [\,\boldsymbol{\Omega}\, P(\mathbf{r}, \hat{\mathbf{u}}, t)\,] \;. \tag{154}$$

Combining eqs.(151,154) we thus find that,

$$\begin{aligned} \frac{dN(t)}{dt} \;&=\; \frac{d\,N_{\mathcal{A}}(t)}{dt} + \frac{d\,N_{\mathcal{W}}(t)}{dt} \\ &=\; -\int_{\mathcal{W}} d\mathbf{r} \int_{\mathcal{A}} d\hat{\mathbf{u}}\; \Big\{ \nabla \cdot [\,\mathbf{v}\, P(\mathbf{r}, \hat{\mathbf{u}}, t)\,] + \hat{\mathcal{R}} \cdot [\,\boldsymbol{\Omega}\, P(\mathbf{r}, \hat{\mathbf{u}}, t)\,] \Big\} , \end{aligned} \tag{155}$$

where the *rotation operator* $\hat{\mathcal{R}}$ is introduced for convenience as,

$$\hat{\mathcal{R}}\,(\cdots) \;=\; \hat{\mathbf{u}} \times \nabla_{\hat{\mathbf{u}}}\,(\cdots) \;. \tag{156}$$

The differentiation with respect to $\hat{\mathbf{u}}$ should be taken at constant length of $\hat{\mathbf{u}}$. Fortunately, the outer product with $\hat{\mathbf{u}}$ eliminates the component along $\hat{\mathbf{u}}$ of $\nabla_{\hat{\mathbf{u}}}$. Hence, the differentiation in eq.(156) can be done with respect to the unconstrained cartesian coordinates of $\hat{\mathbf{u}}$. Note the similarity between the translational and rotational contributions to the rate of change : instead of the translational velocity $\mathbf{v}$, the angular velocity $\boldsymbol{\Omega}$ appears in the rotational contribution, and instead of the gradient operator ∇ the rotation operator $\hat{\mathcal{R}}$ appears. From eqs.(149,155) it is now found that,

$$\int_{\mathcal{W}} d\mathbf{r} \int_{\mathcal{A}} d\hat{\mathbf{u}}\; \Big\{ \frac{\partial}{\partial t} P(\mathbf{r}, \hat{\mathbf{u}}, t) + \nabla \cdot [\,\mathbf{v}\, P(\mathbf{r}, \hat{\mathbf{u}}, t)\,] + \hat{\mathcal{R}} \cdot [\,\boldsymbol{\Omega}\, P(\mathbf{r}, \hat{\mathbf{u}}, t)\,] \Big\} \;=\; 0 \;. \tag{157}$$

Since this holds for arbitrary volumes $\mathcal{W}$ and surface areas $\mathcal{A}$, the integrand must be equal to 0. Hence,

$$\frac{\partial}{\partial t} P(\mathbf{r}, \hat{\mathbf{u}}, t) \;=\; -\nabla \cdot [\, \mathbf{v}\, P(\mathbf{r}, \hat{\mathbf{u}}, t)\,] - \hat{\mathcal{R}} \cdot [\, \mathbf{\Omega}\, P(\mathbf{r}, \hat{\mathbf{u}}, t)\,] \;. \tag{158}$$

Here, we considered a system that contained just a single rod. For a suspension that contains N rods, instead of just $\{\mathbf{r}, \hat{\mathbf{u}}\}$, the relevant phase space coordinates are,

$$\{\mathbf{r}_1, \mathbf{r}_2, \cdots, \mathbf{r}_N, \hat{\mathbf{u}}_1, \hat{\mathbf{u}}_2, \cdots, \hat{\mathbf{u}}_N\} \;,$$

where $\mathbf{r}_j$ is the position of the j^{th} rod, and $\hat{\mathbf{u}}_j$ its orientation. The equation of motion for the probability density function P of these phase space coordinates is found from eq.(158) by simply adding the in- and out-fluxes over all rods,

$$\frac{\partial}{\partial t}\, P(\mathbf{r}_1, \cdots, \mathbf{r}_N, \hat{\mathbf{u}}_1, \cdots, \hat{\mathbf{u}}_N, t) = -\sum_{j=1}^{N} \Big\{ \nabla_j \cdot [\, \mathbf{v}_j\, P\,] + \hat{\mathcal{R}}_j \cdot [\, \mathbf{\Omega}_j\, P\,] \Big\} \;. \tag{159}$$

The full phase space coordinate dependence of P is not denoted here on the right-hand side for brevity. Here, $\hat{\mathcal{R}}_j$ is defined as in eq.(156), with $\hat{\mathbf{u}}$ is replaced by $\hat{\mathbf{u}}_j$. This is an exact result, since it merely expresses conservation of the number of rods.

As a last step, the translational- and rotational velocities have to be expressed in terms of functions of the phase space coordinates. In doing so, we shall neglect hydrodynamic interactions between the rods. The reason for this neglect is two-fold. First of all, as will be seen later, the volume fractions of interest scale as D/L (with D the thickness and L the length of the rods). That is, the volume fraction where the isotropic-nematic phase transition occurs scales as D/L. For the study of dynamics in the isotropic phase and the isotropic-nematic phase transition, volume fractions are thus very low. This implies that on average two arbitrary surface elements of distinct rods are very far apart. Therefore, hydrodynamic interactions are probably much less important than for suspensions of spherical particles. Secondly, the precise form of hydrodynamic interaction functions for rods is unknown, even on the two-body level.

The key relation to express the velocities in terms of phase functions is the force balance equation. As has been seen before, translational and angular momentum coordinates are relaxed to equilibrium with the heat bath of solvent molecules on the Brownian time scale, so that the total force (and torque) on each Brownian particle is zero. There are three non-inertial forces (and torques) working on each rod : the hydrodynamic force $\mathbf{F}_j^h$ (torque $\mathbf{T}_j^h$) that the solvent exerts on the rod, the direct interaction force $\mathbf{F}_j^I$ (torque $\mathbf{T}_j^I$) and the Brownian force $\mathbf{F}_j^{Br}$ (torque $\mathbf{T}_j^{Br}$), which will be discussed and specified later. Hence,

$$\begin{aligned} \text{Total force} \;&=\; \mathbf{0} \;=\; \mathbf{F}_j^h + \mathbf{F}_j^I + \mathbf{F}_j^{Br} \;, \\ \text{Total torque} \;&=\; \mathbf{0} \;=\; \mathbf{T}_j^h + \mathbf{T}_j^I + \mathbf{T}_j^{Br} \;. \end{aligned} \tag{160}$$

The direct force is minus the gradient of the total potential energy Φ of the assembly of Brownian particles,

$$\mathbf{F}_j^I \;=\; -\nabla_j\, \Phi(\mathbf{r}_1, \cdots, \mathbf{r}_N, \hat{\mathbf{u}}_1, \cdots, \hat{\mathbf{u}}_N) \;, \tag{161}$$

while the direct torque is related to Φ as,

$$\mathbf{T}_j^I \;=\; -\hat{\mathcal{R}}_j \Phi \;. \tag{162}$$

With the neglect of hydrodynamic interactions, the hydrodynamic torque and force are just the friction forces of a single rod with the solvent. This friction force is equal to (see eq.(44)),

$$\mathbf{F}_j^h \;=\; \left(\gamma_\parallel \hat{\mathbf{u}}\hat{\mathbf{u}} + \gamma_\perp \left[\hat{\mathbf{I}} - \hat{\mathbf{u}}\hat{\mathbf{u}}\right]\right) \cdot (\mathbf{v}_c - \mathbf{G}\cdot\mathbf{r}_c) \;. \tag{163}$$

The torque due to friction with the solvent is equal to (see eq.(48)),

$$\mathcal{T}_j^h \;=\; -\gamma_r \left[\, \mathbf{\Omega}_j - \hat{\mathbf{u}}_j \times \mathbf{G}\cdot\hat{\mathbf{u}}_j \,\right] . \tag{164}$$

As discussed before, in case of simple shear flow, the second term in the square brackets is $\mathbf{0}$ when the rod's orientation is along the flow direction. To correctly describe Jeffery orbits of non-Brownian rods we therefore had to add the small torque that acts on rods with such an orientation (see eq.(55)). For Brownian rods this small torque is irrelevant, since rods oriented parallel to the flow direction will attain other orientations due to Brownian motion before the mentioned small torque became active.

The translational velocity can be found from eqs.(160,163) as,

$$\mathbf{v}_j \;=\; \left(D_\parallel \hat{\mathbf{u}}_j\hat{\mathbf{u}}_j + D_\perp \left[\hat{\mathbf{I}} - \hat{\mathbf{u}}_j\hat{\mathbf{u}}_j\right]\right) \cdot \left\{-\beta\nabla_j\Phi + \beta\mathbf{F}_j^{Br}\right\} + \dot\gamma\,\hat{\mathbf{G}}\cdot\mathbf{r}_j \;, \tag{165}$$

while the rotational velocity is found from eqs.(160,164) as,

$$\mathbf{\Omega}_j \;=\; D_r \left\{-\beta\hat{\mathcal{R}}_j\Phi + \beta\mathbf{T}_j^{Br}\right\} + \dot\gamma\,\hat{\mathbf{u}}_j \times \left(\,\hat{\mathbf{G}}\cdot\hat{\mathbf{u}}_j\,\right) \;. \tag{166}$$

Here, $\hat{\mathbf{G}} = \mathbf{G}/\dot\gamma$ is the "normalized" velocity gradient tensor,

$$D_\parallel \;=\; k_BT/\gamma_\parallel \;\;,\;\; D_\perp \;=\; k_BT/\gamma_\perp \;. \tag{167}$$

are the translational diffusion coefficients for motion parallel and perpendicular to the rods long axis, respectively, and,

$$D_r \;=\; k_BT/\gamma_r \;, \tag{168}$$

is *the rotational diffusion coefficient*. These diffusion coefficients depend on the length L and thickness D of the rod, and the shear viscosity η_0 of the solvent (see eqs.(40,42,49)),

$$\begin{aligned} D_r &= \frac{3k_BT\ln\{L/D\}}{\pi\,\eta_0\,L^3} \\ D_\parallel &= \frac{k_BT\ln\{L/D\}}{2\pi\,\eta_0\,L} \;, \\ D_\perp &= \tfrac{1}{2}\,D_\parallel \;. \end{aligned} \tag{169}$$

Note that due to the last two equations here, eq.(165) can be rewritten as,

$$\mathbf{v}_j \;=\; \tfrac{3}{4}\bar{D}\left[\hat{\mathbf{I}} + \hat{\mathbf{u}}_j\hat{\mathbf{u}}_j\right] \cdot \left\{-\beta\nabla_j\Phi + \beta\mathbf{F}_j^{Br}\right\} + \dot\gamma\,\hat{\mathbf{G}}\cdot\mathbf{r}_j \;, \tag{170}$$

where *the translational diffusion coefficient* $\bar{D}$ is equal to,

$$\bar{D} \;=\; \tfrac{1}{3}\left[D_\parallel + 2D_\perp\right] \;=\; \tfrac{4}{3}\,D_\perp \;=\; \tfrac{2}{3}\,D_\parallel \;=\; \frac{k_BT\ln\{L/D\}}{3\pi\,\eta_0\,L} \;. \tag{171}$$

The reason for referring to D_r and $\bar{D}$ as "diffusion coefficients" will become clear in the following section, where diffusion of non-interacting rods is considered. The above expressions

for diffusion coefficients are valid for very long and thin rods. For shorter rods, corrections to these limiting expressions are given by de la Torre and Bloomfield (1981).

We still have to express the Brownian contributions to the total force and torque in terms of phase functions. This is achieved as follows. In the absence of flow, for infinite time $t \to \infty$, when the suspension attains equilibrium, the probability density function P is proportional to the Boltzmann exponential $\exp\{-\beta\,\Phi\}$, and $\partial P/\partial t = 0$. From the long-time limit of eq.(159), together with eqs.(166,170) in the absence of shear flow, it follows that,

$$\begin{aligned} \mathbf{F}_j^{Br} &= -k_B T \nabla_j \ln\{P\}\,, \\ \mathbf{T}_j^{Br} &= -k_B T \hat{\mathcal{R}}_j \ln\{P\}\,. \end{aligned} \tag{172}$$

These Brownian contributions to the total force and torque are the result of the fact that the force balance equations (160) are only valid on the diffusive time scale. On such a coarsened time scale, not only the purely microscopic forces $\mathbf{F}_j^h$ and $\mathbf{F}_j^I$ (and the corresponding torques) act on the colloidal particles. The additional Brownian force (and torque) arises from interactions of the colloidal particle with the solvent molecules, averaged with respect to the equilibrium probability density function for the phase space coordinates of the fluid molecules in the external field imposed by the colloidal particles with prescribed positions and orientations. Even in a very dilute system of colloidal particles (an "ideal gas"), where interactions between the colloidal particles can be neglected, the equilibrium state is one where the macroscopic density is constant, independent of position. The forces that drive such an ideal gas to the homogeneous state are the Brownian forces.

In this way the following equation of motion for the probability density function P of the phase space coordinates $\{\mathbf{r}_1, \cdots, \mathbf{r}_N, \hat{\mathbf{u}}_1, \cdots, \hat{\mathbf{u}}_N\}$ is obtained,

$$\begin{aligned} \frac{\partial P}{\partial t} &= \sum_{j=1}^{N} \Big\{ \tfrac{3}{4}\bar{D}\,\nabla_j \cdot \Big(\hat{\mathbf{I}} + \hat{\mathbf{u}}_j\hat{\mathbf{u}}_j\Big) \cdot [\nabla_j P + \beta\, P \nabla_j \Phi] - \dot{\gamma}\,\nabla_j \cdot \Big[P\,\hat{\mathbf{G}}\cdot\mathbf{r}_j\Big] \\ &\qquad + D_r \hat{\mathcal{R}}_j \cdot \Big[\hat{\mathcal{R}}_j P + \beta\, P \hat{\mathcal{R}}_j \Phi\Big] - \dot{\gamma}\,\hat{\mathcal{R}}_j \cdot \Big[P\,\hat{\mathbf{u}}_j \times \Big(\hat{\mathbf{G}}\cdot\hat{\mathbf{u}}_j\Big)\Big] \Big\}\,. \end{aligned} \tag{173}$$

This is the *Smoluchowski equation* for very long and thin, rigid rods, where hydrodynamic interactions are neglected.

An alternative, perhaps more satisfying derivation of the Smoluchowski equation, is to start from the Liouville equation for a binary mixture : the solvent molecules and the colloidal particles. The Smoluchowski equation is then found after integrating over the fast phase space variables (the phase space coordinates of the solvent molecules and the momentum coordinates of the colloidal particles). Such an approach has been taken, for spherical colloids, by Deutch and Oppenheim (1971) and Murphy and Aquirre (1972). The Smoluchowski equation for spherical particles has been used as a starting point to derive the Smoluchowski equation for rods by Erpenbeck and Kirkwood (1963).

0.7.2 Translational and rotational diffusion of non-interacting rods without shear flow

Consider the mean squared center of mass displacement of a freely diffusing rod. Its position at time $t = 0$ will be chosen at the origin : $\mathbf{r}(t = 0) = \mathbf{0}$. Free diffusion occurs in suspensions

where the concentration of colloidal particles is so small, that on average, rods do not notice each other. In that case, the interaction potential in the Smoluchowski equation (173) may be neglected ($\Phi = 0$), and N can be taken equal to 1, resulting in,

$$\frac{\partial}{\partial t}P(\mathbf{r},\hat{\mathbf{u}},t) \;=\; \tfrac{3}{4}\bar{D}\nabla\cdot\left[\hat{\mathbf{I}}+\hat{\mathbf{u}}\hat{\mathbf{u}}\right]\cdot\nabla P \;+\; D_r\hat{\mathcal{R}}^2 P\;, \tag{174}$$

where $\hat{\mathcal{R}}^2 \;=\; \hat{\mathcal{R}}\cdot\hat{\mathcal{R}}$. For the highly diluted systems under consideration each orientation has equal probability, $P(\mathbf{r},\hat{\mathbf{u}},t)$ is independent of $\hat{\mathbf{u}}$, and is simply proportional to $P(\mathbf{r},t)$. Equation 174 thus reduces to,

$$\frac{\partial}{\partial t}P(\mathbf{r},t) \;=\; \tfrac{3}{4}\bar{D}\nabla\cdot\left[\hat{\mathbf{I}}+\hat{\mathbf{u}}\hat{\mathbf{u}}\right]\cdot\nabla P(\mathbf{r},t)\;. \tag{175}$$

Integration of both sides with respect to $\hat{\mathbf{u}}$, using that, [1]

$$\oint d\hat{\mathbf{u}}\,\left[\hat{\mathbf{I}}+\hat{\mathbf{u}}\hat{\mathbf{u}}\right] \;=\; \tfrac{4}{3}\,\hat{\mathbf{I}}\;,$$

thus leads to,

$$\frac{\partial}{\partial t}P(\mathbf{r},t) \;=\; \bar{D}\,\nabla^2 P(\mathbf{r},t)\;. \tag{176}$$

The equation of motion for the dyadic product $<\mathbf{r}(t)\mathbf{r}(t)>$ is obtained by multiplying both sides with **r r** and integrating,

$$\begin{aligned}\frac{d}{dt}\int d\mathbf{r}\;\mathbf{r}\,\mathbf{r}\;P(\mathbf{r},t) \;\equiv\; \frac{d}{dt}<\mathbf{r}(t)\mathbf{r}(t)> \;&=\; \bar{D}\int d\mathbf{r}\;\mathbf{r}\mathbf{r}\nabla^2 P(\mathbf{r},t)\\ &=\; \bar{D}\int d\mathbf{r}\,P(\mathbf{r},t)\nabla^2\mathbf{r}\mathbf{r} = 2\bar{D}\,\hat{\mathbf{I}}\;,\end{aligned}$$

where Gauss's integral theorem has been used twice in the second line. Since $<\mathbf{r}(t=0)\mathbf{r}(t=0)>=\mathbf{0}$, time-integration immediately leads to,

$$<\mathbf{r}(t)\mathbf{r}(t)> = \;2\bar{D}t\,\hat{\mathbf{I}}\;,$$

and hence,

$$W(t) \;\equiv <r^2(t)> = \;6\bar{D}t\;, \tag{177}$$

in accordance with the result (130) as obtained from the Langevin equation. Note that on taking the Trace of the dyadic product, each spatial dimension (3 in this case) gives rise to a factor 2 on the right-hand side in the mean squared displacement in eq.(177). Diffusion in two dimensions gives a prefactor of 4 instead of 6, in accordance with the result in eq.(147) for short-time rotational diffusion.

Let us now consider the time dependence of the orientation $<\hat{\mathbf{u}}(t)>$, given that $\hat{\mathbf{u}}(t=0)=\hat{\mathbf{u}}(0)$. For a homogeneous system, $P(\mathbf{r},\hat{\mathbf{u}},t)$ is independent of $\mathbf{r}$, so that eq.(174) reduces to,

$$\frac{\partial}{\partial t}P(\hat{\mathbf{u}},t) \;=\; D_r\,\hat{\mathcal{R}}^2 P(\hat{\mathbf{u}},t)\;. \tag{178}$$

[1] The integral $\oint d\hat{\mathbf{u}}\,(\cdots)$ stands for integration over the unit spherical surface. In terms of the angular spherical coordinates Θ and φ of $\hat{\mathbf{u}}$ this integral is $\int_0^\pi d\Theta\int_0^{2\pi} d\varphi\,\sin\{\Theta\}\,(\cdots)$.

Multiplying both sides with $\hat{\mathbf{u}}$ and integrating over the unit spherical surface gives,

$$\frac{d}{dt} < \hat{\mathbf{u}}(t) > = \; D_r \oint d\hat{\mathbf{u}}\, \hat{\mathbf{u}}\, \hat{\mathcal{R}}^2\, P(\hat{\mathbf{u}}, t) \; .$$

From Stokes's integral theorem it follows that for any two (well behaved) functions f and g of $\hat{\mathbf{u}}$,

$$\oint d\hat{\mathbf{u}}\, f(\hat{\mathbf{u}}) \hat{\mathcal{R}} g(\hat{\mathbf{u}}) \; = \; - \oint d\hat{\mathbf{u}}\, g(\hat{\mathbf{u}}) \hat{\mathcal{R}} f(\hat{\mathbf{u}}) \; . \tag{179}$$

Applying this result twice leads to,

$$\oint d\hat{\mathbf{u}}\, \hat{\mathbf{u}} \hat{\mathcal{R}}^2\, P(\hat{\mathbf{u}}, t) \; = \; \oint d\hat{\mathbf{u}}\, P(\hat{\mathbf{u}}, t) \hat{\mathcal{R}}^2\, \hat{\mathbf{u}} = -2 < \hat{\mathbf{u}}(t) > \, ,$$

where it is used that $\hat{\mathcal{R}}^2 \hat{\mathbf{u}} \; = \; -2\hat{\mathbf{u}}$. The equation of motion we were after thus reads,

$$\frac{d}{dt} < \hat{\mathbf{u}}(t) > = \; -2D_r \; < \hat{\mathbf{u}}(t) > \, ,$$

the solution of which is,

$$< \hat{\mathbf{u}}(t) > = \; \exp\{-2D_r t\}\, \hat{\mathbf{u}}(0) \; . \tag{180}$$

in accordance with eqs.(133,146) as obtained from the Langevin equation. As discussed in the section on the Langevin-equation approach, for small times where $D_r t \ll 1$, this result can be interpreted as translational diffusion of the tip of $\hat{\mathbf{u}}$ on a two-dimensional surface.

0.8 The Orientational Order Parameter

At higher concentrations, where interactions between rods are important, a transition from an isotropic distribution of orientations to an orientationally ordered nematic state can occur (as will be discussed in more detail later). Orientational order is also induced by shear flow in otherwise isotropic suspensions. For such ordered states the degree of orientational order varies, depending on the concentration of rods and the shear rate. In the present section the so-called *orientational order parameter* will be defined, which measures the degree of orientational order.

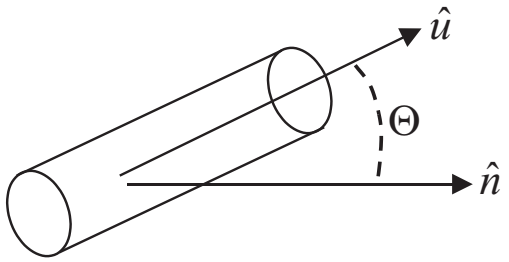

Figure 15: Definition of the angle Θ between the orientation $\hat{\mathbf{u}}$ of a rod and the director $\hat{\mathbf{n}}$.

The preferred orientation $\hat{\mathbf{n}}$ of the rods is referred to as *the director*. The most simple measure for the degree of orientation that comes to mind is $<\cos\{\Theta\}>=<\hat{\mathbf{u}}>\cdot\hat{\mathbf{n}}$, where Θ is the angle of the orientation $\hat{\mathbf{u}}$ of a given rod and the director $\hat{\mathbf{n}}$ (see fig.15). However, due to symmetry, an orientation $\hat{\mathbf{u}}$ is equally likely to occur as the orientation $-\hat{\mathbf{u}}$, so that $<\hat{\mathbf{u}}>=\mathbf{0}$. The next most simple measure would then be $<\cos^2\{\Theta\}>=<\hat{\mathbf{u}}\hat{\mathbf{u}}>:\hat{\mathbf{n}}\hat{\mathbf{n}}$. [2]. Hence, the most simple quantity that characterizes the orientational state is the so-called *orientational order parameter tensor*,

$$\mathbf{S} \equiv <\hat{\mathbf{u}}\,\hat{\mathbf{u}}> \equiv \oint d\hat{\mathbf{u}}\,\hat{\mathbf{u}}\,\hat{\mathbf{u}}\,P(\hat{\mathbf{u}})\,, \tag{181}$$

where the integration ranges over the unit spherical surface (see 1). Furthermore, $P(\hat{\mathbf{u}})$ is the probability density function (pdf) for the orientation $\hat{\mathbf{u}}$ of a rod, which can in principle be obtained from the solution of the N-particle Smoluchowski equation (173), noting that,

$$P(\hat{\mathbf{u}}) = \int d\mathbf{r}_1 \cdots \int d\mathbf{r}_N \oint d\hat{\mathbf{u}}_2 \cdots \oint d\hat{\mathbf{u}}_N\; P(\mathbf{r}_1,\cdots,\mathbf{r}_N,\hat{\mathbf{u}},\hat{\mathbf{u}}_2,\cdots,\hat{\mathbf{u}}_N)\,. \tag{182}$$

The pdf of $\hat{\mathbf{u}}$ can be time dependent, in which case orientational dynamics can be studied.

What information can be distilled from a specified $\mathbf{S}$? To answer this question, let $\hat{\mathbf{e}}$ be a unit vector, and let φ denote the angle between the orientation $\hat{\mathbf{u}}$ of a given rod and $\hat{\mathbf{e}}$. Consider the function,

$$f \equiv <\cos^2\{\varphi\}> = \mathbf{S}:\hat{\mathbf{e}}\hat{\mathbf{e}} = \sum_{m,n} S_{mn}\,\hat{e}_m\,\hat{e}_n\,, \tag{183}$$

where S_{nm} is the nm^{th} component of $\mathbf{S}$, and $\hat{e}_n$ the n^{th} component of $\hat{\mathbf{e}}$. Since the maximum value of $\cos^2\{\varphi\}$ is attained when $\varphi = 0$, and the most likely direction of $\hat{\mathbf{u}}$ is along the director, it is evident that the unit vector $\hat{\mathbf{e}}$ that maximizes f is the director. Maximization of f has to be performed under the constraint that $\hat{\mathbf{e}}$ is a unit vector, that is $\hat{\mathbf{e}}\cdot\hat{\mathbf{e}} = 1$. According to Lagrange's principle, we therefore have to maximize the function,

$$f^* = f - \lambda\,\hat{\mathbf{e}}\cdot\hat{\mathbf{e}} = \sum_{mn}\{S_{mn} - \lambda\,\delta_{mn}\}\;\hat{e}_m\,\hat{e}_n\,, \tag{184}$$

where λ is the Lagrange multiplier, and δ_{nm} is the Kronecker delta ($\delta_{mn} = 0$ when $m \neq n$ and $\delta_{mn} = 1$ when $m = n$). From $\partial f/\partial\hat{e}_m = 0$ it is easily found that,

$$\mathbf{S}\cdot\hat{\mathbf{e}} = \lambda\,\hat{\mathbf{e}}\,,\ \text{maximizes or minimizes } f^*\,. \tag{185}$$

By taking the inner product on both sides it follows that,

$$\lambda = \mathbf{S}:\hat{\mathbf{e}}\hat{\mathbf{e}}\,,\ \text{when}\ \hat{\mathbf{e}}\ \text{maximizes or minimizes}\ f^*\,. \tag{186}$$

We thus find that,

The eigenvector of $\mathbf{S}$ *with the largest eigenvalue is the director* $\hat{\mathbf{n}}$ *and the largest eigenvalue is equal to* $<\cos\{\Theta\}^2>=\mathbf{S}:\hat{\mathbf{n}}\hat{\mathbf{n}}$.

[2] The contraction symbol ":" stands for summation over two adjacent indices, that is, for two tensors $\mathbf{A}$ and $\mathbf{B}$, by definition, $\mathbf{A}:\mathbf{B} = \sum_{n,m} A_{nm}B_{mn}$

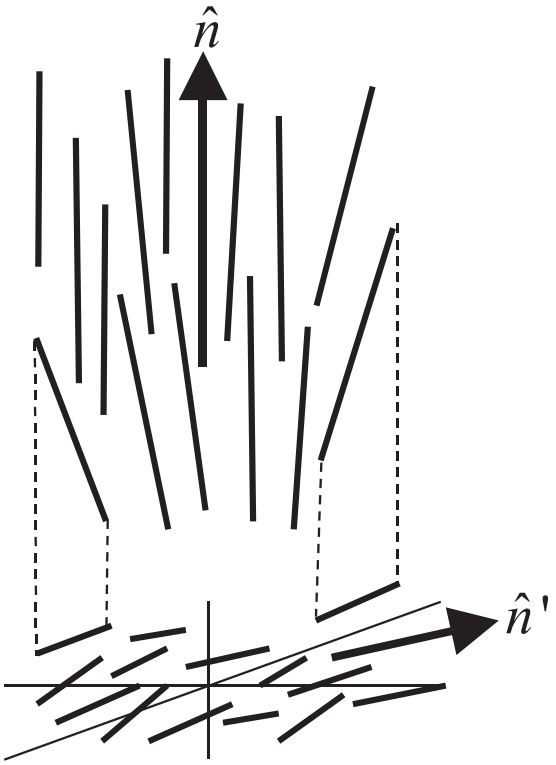

Figure 16: For a bi-axial nematic, the projections of the rods onto the plane perpendicular to the director $\hat{\mathbf{n}}$ have a preferred orientation $\hat{\mathbf{n}}'$ as well. For a uni-axial nematic, the order in this plane is isotropic.

According to eqs.(183,186), the largest eigenvalue of $\mathbf{S}$ characterizes the degree of alignment, and is referred to as *the scalar orientational order parameter*. Note that the largest eigenvalue of $\mathbf{S}$ is equal $1/3$ in the isotropic state (since then $\mathbf{S} = \frac{1}{3}\hat{\mathbf{I}}$), and equal to 1 for a perfectly aligned state (since then $\mathbf{S} = \hat{\mathbf{n}}\hat{\mathbf{n}}$). A commonly used equivalent measure is the so-called P_2-order parameter, which is defined as,

$$P_2 \equiv < P_2(\cos\{\Theta\}) > = \frac{1}{2}\left\{3 < \cos^2\{\Theta\} > -1\right\} = \frac{1}{2}\left\{3\lambda - 1\right\} , \tag{187}$$

where $P_2(x)$ is the second order Legendre polynomial. The reason for introducing this "rescaled" scalar order parameter P_2 is that it is 0 for an isotropic state and equal to 1 for a perfectly aligned state.

When for a particular nematic suspension the remaining two smaller eigenvalues are equal, the nematic is referred to as "uni-axial" *Uni-axial nematic*. When they are unequal, the nematic is referred to as "bi-axial" *Bi-axial nematic*. For a uni-axial nematic, the projections of the rods onto the plane perpendicular to the director are isotropically distributed, while for a bi-axial nematic the orientations of the rods in this projection have a second preferred direction $\hat{\mathbf{n}}'$ (see fig.16).

Bi-axiality of nematic ordering is found, for example, when a suspension of rigid rods is

subjected to simple shear flow. A nematic state of cylindrically shaped rods, in the absence of an external field, is expected to be uni-axial.

The procedure to find the order parameter is to calculate the tensor $\mathbf{S}$ and determine its eigenvalues. The largest eigenvalue measures the degree of orientational order and the corresponding eigenvector gives the preferred direction of alignment. We shall derive an equation of motion for $\mathbf{S}$ from the Smoluchowski equation later in this chapter.

0.9 Non-interacting Brownian Rods in Shear Flow

In the present section we shall discuss probability density functions (pdf's) and orientational order parameter matrices for a single Brownian rod subjected to flow. On applying a stationary flow, the orientational pdf of a single rod attains a stationary form. This stationary, time independent pdf is determined by the interplay of the aligning effect of the flow and isotropy-restoring rotational diffusion.

The stationary form of the Smoluchowski equation (173) for a single rod reads,

$$0 \;=\; \hat{\mathcal{R}}^2 P(\hat{\mathbf{u}}) \;-\; Pe_r\, \hat{\mathcal{R}} \cdot \Big[P(\hat{\mathbf{u}})\; \hat{\mathbf{u}} \times \Big(\hat{\mathbf{G}} \cdot \hat{\mathbf{u}} \Big) \Big] \;, \tag{188}$$

where the dimensionless parameter Pe_r is commonly referred to as the *rotational Peclet number*, which is defined as,

$$Pe_r \;=\; \frac{\dot{\gamma}}{D_r} \,. \tag{189}$$

This Peclet number is a measure for the effect of the shear flow relative to isotropy-restoring rotational diffusion. For small Peclet numbers, rotational diffusion is relatively fast, so that the pdf is only slightly anisotropic.

As explained below eq.(156), the differentiation in $\hat{\mathcal{R}}$ is with respect to the cartesian coordinates of $\hat{\mathbf{u}}$, without the constraint that $\hat{\mathbf{u}}$ is unit vector.

The stationary equation of motion can be solved in closed analytical form when the velocity gradient tensor $\mathbf{G}$ is symmetric (as for elongational flow). This solution is discussed in the next subsection. When the velocity gradient tensor is not symmetric (as for simple shear flow), the solution cannot be obtained in a simple closed analytical form, but must be obtained by numerical methods. However, expansion of the orientational pdf for small Peclet numbers is feasible.

0.9.1 Elongational flow

For pure straining motion, the velocity gradient tensor $\hat{\mathbf{G}}$ is equal to the symmetric tensor $\hat{\mathbf{E}}$ in eq.(2). A symmetric velocity gradient tensor admits a solution of the simpler equation,

$$\mathbf{0} \;=\; \hat{\mathcal{R}} P(\hat{\mathbf{u}}) \;-\; Pe_r \,\Big[P(\hat{\mathbf{u}})\; \hat{\mathbf{u}} \times \Big(\hat{\mathbf{E}} \cdot \hat{\mathbf{u}} \Big) \Big] \;, \tag{190}$$

where one of the $\hat{\mathcal{R}}$-operators in eq.(188) is removed. Division by $P(\hat{\mathbf{u}})$ thus yields,

$$\mathbf{0} \;=\; \hat{\mathcal{R}} \ln\{P(\hat{\mathbf{u}})\} \;-\; Pe_r\; \hat{\mathbf{u}} \times \Big(\hat{\mathbf{E}} \cdot \hat{\mathbf{u}} \Big) \;. \tag{191}$$

From one of the relations in appendix B, it follows immediately that the solution is given by,

$$P(\hat{\mathbf{u}}) \;=\; \frac{1}{C(Pe_r)}\,\exp\left\{\frac{1}{2}\,Pe_r\,(\hat{\mathbf{u}}\cdot\hat{\mathbf{E}}\cdot\hat{\mathbf{u}})\right\}\;, \tag{192}$$

where C is the Pe_r-dependent normalization constant,

$$\begin{aligned} C(Pe_r) \;&=\; \oint d\hat{\mathbf{u}}\,\exp\left\{\frac{1}{2}\,Pe_r\,(\hat{\mathbf{u}}\cdot\hat{\mathbf{E}}\cdot\hat{\mathbf{u}})\right\} \\ &=\; \int_0^{2\pi} d\varphi \int_0^{\pi} d\Theta\,\sin\{\Theta\}\,\exp\left\{Pe_r\,\sin^2\{\Theta\}\,\sin\{\varphi\}\,\cos\{\varphi\}\right\}. \end{aligned} \tag{193}$$

This normalization constant may be determined, as a function of Pe_r by numerical integration. Alternatively, $C(Pe_r)$ may be expanded for small Pe_r in a power series in Pe_r, or its asymptotic form for large Pe_r may be calculated. Taylor expansion of the exponential in eq.(193) with respect to Pe_r readily gives,

$$C(Pe_r) \;=\; 4\pi + \frac{2\pi}{15}Pe_r^2 + \frac{\pi}{630}Pe_r^4 + \mathcal{O}\left(Pe_r^6\right)\;. \tag{194}$$

For large (positive) Peclet numbers, asymptotic forms for $C(Pe_r)$ can be obtained by a saddle point analysis, which we shall not discuss here. For intermediate values of Pe_r, the integral in eq.(193) for $C(Pe_r)$ must be evaluated numerically.

The orientational order parameter tensor can be calculated from the above given forms for the pdf $P(\hat{\mathbf{u}})$ and eq.(181), and from that the scalar orientational order parameter P_2 as defined in eq.(187) and the angle χ between the director and the flow direction. These are plotted as functions of Pe_r in fig.17. Solid lines are obtained from numerical integration of eq.(193), while the dotted lines correspond to the limiting analytical results in eq.(194) for small Peclet numbers (including the corresponding expansion of the exponential in eq.(192) for the pdf). For elongational flow, χ is always equal to 45^0, which is obvious from the flow field as sketched in fig.1 : rods will orient along the extensional axis.

0.9.2 Simple shear flow

In case of pure shearing motion, the velocity gradient tensor $\hat{\mathbf{G}}$ is equal to the tensor $\hat{\mathbf{\Gamma}}$ in eq.(1). For such a non-symmetric velocity gradient tensor the above method of solution cannot be copied, since the corresponding eq.(190) has no solutions for a non-symmetric tensor $\mathbf{G}$.

For small rotational Peclet numbers the deviation of the pdf from isotropy is small, so that the solution of the stationary equation of motion (188) can be expanded as,

$$P(\hat{\mathbf{u}}) \;=\; \frac{1}{4\pi} \;+\; Pe_r\,P_1(\hat{\mathbf{u}}) \;+\; Pe_r^2\,P_2(\hat{\mathbf{u}}) \;+\; \cdots\;. \tag{195}$$

Substitution of this expansion into eq.(188) and equating coefficients of equal powers of Pe_r, one readily finds the following recursive set of differential equations for the as yet unknown functions P_j,

$$\hat{\mathcal{R}}^2\,P_j(\hat{\mathbf{u}}) \;=\; \hat{\mathcal{R}}\cdot\left[P_{j-1}(\hat{\mathbf{u}})\,\hat{\mathbf{u}}\times\left(\hat{\mathbf{\Gamma}}\cdot\hat{\mathbf{u}}\right)\right] \quad,\quad j\geq 1\,, \tag{196}$$

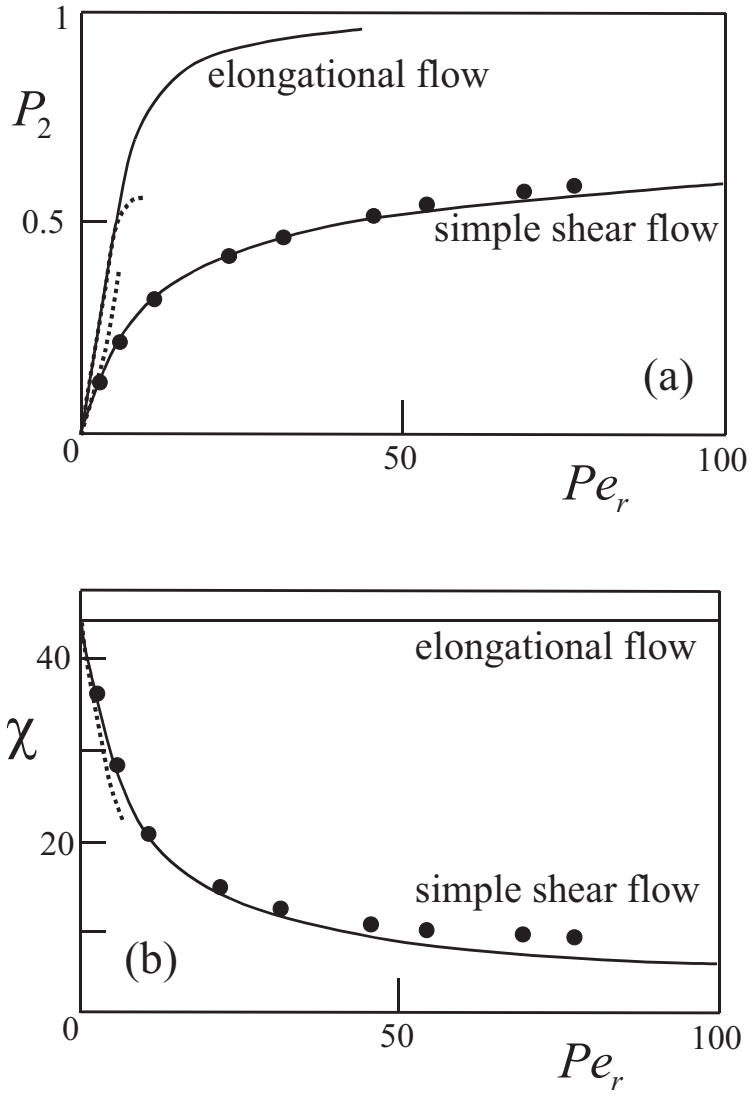

Figure 17: (a) The scalar orientational order parameter $P_2 = \frac{1}{2}\{3\lambda - 1\}$, with λ the largest eigenvalue of $\mathbf{S}$ (see eq.(187)) as a function of the rotational Peclet number $Pe_r = \dot{\gamma}/D_r$ for elongational flow and simple shear flow. Solid lines are numerical results, dotted lines correspond to the limiting analytical solutions (194) and (202) for elongational and simple shear, respectively, and data points are computer simulation results by Winkler et al. (2004a,b). (b) The angle χ between the director and the flow direction. The dotted line is the angle that follows from the limiting form (202) of the pdf for simple shear flow.

where $P_0(\hat{\mathbf{u}}) = 1/4\pi$ is the isotropic pdf without shear flow. Normalization requires that,

$$\oint d\hat{\mathbf{u}}\, P_j(\hat{\mathbf{u}}) \;=\; 0 \quad , \quad j \geq 1\,. \tag{197}$$

Let us consider the first two corrections from isotropy in the expansion (195).

For $j = 1$, using that $P_0(\hat{\mathbf{u}}) = 1/4\pi$, eq.(196) reads,

$$\hat{\mathcal{R}}^2\, P_1(\hat{\mathbf{u}}) \;=\; \frac{1}{4\pi}\,\hat{\mathcal{R}}\cdot\Big[\hat{\mathbf{u}}\times\Big(\hat{\mathbf{\Gamma}}\cdot\hat{\mathbf{u}}\Big)\Big] \;=\; -\,\frac{3}{4\pi}\,(\hat{\mathbf{u}}\cdot\hat{\mathbf{E}}\cdot\hat{\mathbf{u}})\,, \tag{198}$$

where $\hat{\mathbf{E}}$ is the symmetric part of the gradient velocity tensor $\hat{\mathbf{\Gamma}}$, that is, $\hat{\mathbf{E}} = \frac{1}{2}(\hat{\mathbf{\Gamma}} + \hat{\mathbf{\Gamma}}^T)$. The above equation follows from the relations given in appendix B [3]. Using these relations once more immediately leads to,

$$P_1(\hat{\mathbf{u}}) \;=\; \frac{1}{8\pi}\,(\hat{\mathbf{u}}\cdot\hat{\mathbf{E}}\cdot\hat{\mathbf{u}}) \;=\; \frac{1}{8\pi}\,\sin^2\{\Theta\}\,\sin\{\varphi\}\,\cos\{\varphi\}\,. \tag{199}$$

Substitution of this solution for P_1 into eq.(196) for $j = 2$ yields gives,

$$\hat{\mathcal{R}}^2\, P_2(\hat{\mathbf{u}}) \;=\; \frac{1}{8\pi}\,\hat{\mathcal{R}}\cdot\Big[(\hat{\mathbf{u}}\cdot\hat{\mathbf{E}}\cdot\hat{\mathbf{u}})(\hat{\mathbf{u}}\times\hat{\mathbf{\Gamma}}\cdot\hat{\mathbf{u}})\Big] \;=\; \frac{1}{8\pi}\Big[\hat{u}_2^2 - 5(\hat{\mathbf{u}}\cdot\hat{\mathbf{E}}\cdot\hat{\mathbf{u}})^2\Big]\,. \tag{200}$$

From the relations in appendix B one readily verifies that, $\hat{\mathcal{R}}^2(\hat{\mathbf{u}}\cdot\hat{\mathbf{E}}\cdot\hat{\mathbf{u}})^2 = 2\hat{u}_1^2 + 2\hat{u}_2^2 - 20(\hat{\mathbf{u}}\cdot\hat{\mathbf{E}}\cdot\hat{\mathbf{u}})^2$. The third equation in the appendix now shows that the solution to eq.(200) is given by,

$$\begin{aligned} P_2(\hat{\mathbf{u}}) \;&=\; \frac{1}{32\pi}\left[(\hat{\mathbf{u}}\cdot\hat{\mathbf{E}}\cdot\hat{\mathbf{u}})^2 + \frac{1}{3}(\hat{u}_1^2 - \hat{u}_2^2) - \frac{1}{15}\right] \\ &= \frac{1}{32\pi}\left[\sin^4\{\Theta\}\sin^2\{\varphi\}\cos^2\{\varphi\} + \frac{1}{3}\sin^2\{\Theta\}(\cos^2\{\varphi\} - \sin^2\{\varphi\}) - \frac{1}{15}\right]\,. \end{aligned} \tag{201}$$

The constant $1/15$ between the square brackets has been subtracted in order that P_2 satisfies the normalization constraint (197).

Collecting results, we thus obtain the following small Peclet number expansion (valid up to $\mathcal{O}(Pe_r^3)$),

$$P(\hat{\mathbf{u}}) \;=\; \frac{1}{4\pi} + Pe_r\,\frac{1}{8\pi}\,(\hat{\mathbf{u}}\cdot\hat{\mathbf{E}}\cdot\hat{\mathbf{u}}) + Pe_r^2\,\frac{1}{32\pi}\left[(\hat{\mathbf{u}}\cdot\hat{\mathbf{E}}\cdot\hat{\mathbf{u}})^2 + \frac{1}{3}(\hat{u}_1^2 - \hat{u}_2^2) - \frac{1}{15}\right]\,. \tag{202}$$

The corresponding scalar orientational order parameter P_2 and the angle χ between the director and the flow direction are plotted in fig.17, together with the numerical solution of eq.(188). The dotted lines in fig.17 correspond to asymptotic solutions for small Peclet numbers. The solid lines correspond to numerical solutions of eqs.(188), while the data points are simulation results by Winkler et al. (2004) and Winkler and Gompper (2004). In these simulations, the aspect ratio of the rods is $L/D = 15$, and there is a finite flexibility (the average end-to-end distance is 98% of the contour length). This may be the reason for the small deviations at higher Peclet numbers. For short rods the order parameter is expected to be smaller than for long rods. In fig.17a, however, the simulation results for the order parameter are slightly

[3] Notice that in the combination $\hat{\mathbf{u}}\cdot\mathbf{M}\cdot\hat{\mathbf{u}}$, one can replace the tensor $\mathbf{M}$ by its symmetric part $\frac{1}{2}(\mathbf{M} + \mathbf{M}^T)$, since $\hat{\mathbf{u}}\cdot\big(\mathbf{M} - \mathbf{M}^T\big)\cdot\hat{\mathbf{u}} = 0$.

above those corresponding to the numerical solution of the Smoluchowski equation. This is an indication for a sensitive dependence of orientational order induced by shear flow on the flexibility of rods.

Contrary to elongational flow, rods subjected to simple shear flow will rotate in the velocity-gradient plane. The orientational order parameter for elongational flow is therefore large as compared to simple shear flow. For small Peclet numbers, rods in simple shear flow spend most of their time during rotation in a direction where $\chi = 45^0$. This is the result of an interplay between the Brownian torque on the rod and the torque that the fluid exerts on the rod. A preferred alignment along the flow direction implies a strongly peaked orientational pdf. In that case the Brownian torque, being equal to $-k_B T \hat{\mathcal{R}} \ln\{P(\hat{\mathbf{u}})\}$, would be very large. The Brownian torque thus tends to diminish the strongly peaked pdf in the flow direction. This competition leads, according to the above analysis, to a preferred alignment along the extensional axis of the shear flow at very small shear rates. For larger Peclet numbers, where the torque that the fluids exerts on the rod is dominant, the angle χ tends to 0, that is, rods are on average aligned along the flow direction.

0.10 The Doi-Edwards Equation of Motion and the Maier-Saupe Potential

In this section we shall derive an equation of motion for the orientational order parameter tensor $\mathbf{S}$ for homogeneous systems of long and thin rods with short-ranged repulsive interactions subjected to shear flow. This equation of motion is known as the Doi-Edwards equation (see Doi and Edwards (1986)), which is derived here from the Smoluchowski equation (173). In such a microscopic derivation, the assumptions under which the Doi-Edwards equation holds will become clear. For the very long and thin rods under consideration here, the stationary equation of motion for the pdf $P(\hat{\mathbf{u}})$ for the orientation $\hat{\mathbf{u}}$ of a rod, as obtained from the Smoluchowski equation, complies with Onsager's free energy functional (Onsager (1933), Onsager (1942), Onsager (1949)). Expanding the interaction term in the equation of motion with respect to the orientational order parameter leads in a natural way to the Maier-Saupe potential (Maier and Saupe (1958), Maier and Saupe (1959), Maier and Saupe (1960)).

0.10.1 The equation of motion for $P(\hat{\mathbf{u}}, t)$

Let us first derive the equation of motion for $P(\hat{\mathbf{u}}, t)$. According to eqs.(182) (where P is now time dependent), such an equation of motion can be obtained from the Smoluchowski equation (173) by integration with respect to $\mathbf{r}_1, \cdots, \mathbf{r}_N, \hat{\mathbf{u}}_2, \cdots, \hat{\mathbf{u}}_N$.

Analytical progress can be made by assuming a pair-wise additive total potential, that is,

$$\Phi(\mathbf{r}_1, \cdots, \mathbf{r}_N, \hat{\mathbf{u}}_1, \cdots, \hat{\mathbf{u}}_N) \;=\; \sum_{i<j} V(\mathbf{r}_i - \mathbf{r}_j, \hat{\mathbf{u}}_i, \hat{\mathbf{u}}_j) \;, \tag{203}$$

with V the pair-interaction potential. This is exact for rods with hard-core interactions (or rods with very short-ranged repulsive interactions) that we shall consider. According to the

integral theorems of Gauss and Stokes, we have, respectively,

$$\int d\mathbf{r}_j \, \nabla_j \cdot (\cdots) \; = \; 0 \;\; , \;\; \text{and} \;\; , \;\; \oint d\hat{\mathbf{u}}_j \, \hat{\mathcal{R}}_j \cdot (\cdots) \; = \; 0 \; . \tag{204}$$

Using the above relations, integration of both sides of the Smoluchowski equation (173) with respect to $\mathbf{r}_1, \cdots, \mathbf{r}_N$ and $\hat{\mathbf{u}}_2, \cdots, \hat{\mathbf{u}}_N$, leads to (with $\hat{\mathbf{u}} = \hat{\mathbf{u}}_1$),

$$\frac{\partial}{\partial t} P(\hat{\mathbf{u}}, t) \; = \; D_r \hat{\mathcal{R}} \cdot \Big\{ \hat{\mathcal{R}} P(\hat{\mathbf{u}}, t) - \beta \, P(\hat{\mathbf{u}}, t) \, \bar{\mathbf{T}}(\hat{\mathbf{u}}, t) \Big\} - \hat{\mathcal{R}} \cdot \{ P(\hat{\mathbf{u}}, t) \, \hat{\mathbf{u}} \times (\mathbf{\Gamma} \cdot \hat{\mathbf{u}}) \} \tag{205}$$

The torque $\bar{\mathbf{T}}$ is defined as (with $\mathbf{R} = \mathbf{r}_1 - \mathbf{r}_2$ and $\hat{\mathbf{u}}' = \hat{\mathbf{u}}_2$),

$$\bar{\mathbf{T}}(\hat{\mathbf{u}}, t) \; = \; -\bar{\rho} \int d\mathbf{R} \oint d\hat{\mathbf{u}}' \, P(\hat{\mathbf{u}}', t) \, g(\mathbf{R}, \hat{\mathbf{u}}, \hat{\mathbf{u}}', t) \hat{\mathcal{R}} V(\mathbf{R}, \hat{\mathbf{u}}, \hat{\mathbf{u}}') \; , \tag{206}$$

where $\bar{\rho} = N/V$ is the number density of rods, and where the pair-correlation function g is defined as (with $\mathbf{r} = \mathbf{r}_1$ and $\mathbf{r}' = \mathbf{r}_2$),

$$\begin{aligned} P(\mathbf{r}, \mathbf{r}', \hat{\mathbf{u}}, \hat{\mathbf{u}}', t) \; &\equiv \int d\mathbf{r}_3 \cdots \int d\mathbf{r}_N \oint d\hat{\mathbf{u}}_3 \cdots \oint d\hat{\mathbf{u}}_N P(\mathbf{r}, \mathbf{r}', \mathbf{r}_3, \cdots, \mathbf{r}_N, \hat{\mathbf{u}}, \hat{\mathbf{u}}', \hat{\mathbf{u}}_3, \cdots, \hat{\mathbf{u}}_N, t) \\ &\equiv \; \frac{1}{V^2} \, P(\hat{\mathbf{u}}, t) \, P(\hat{\mathbf{u}}', t) \, g(\mathbf{r}, \mathbf{r}', \hat{\mathbf{u}}, \hat{\mathbf{u}}', t) \, , \end{aligned} \tag{207}$$

with $P(\mathbf{r}, \mathbf{r}', \hat{\mathbf{u}}, \hat{\mathbf{u}}', t)$ the pdf for the positions and orientations of two rods. Since the product $\frac{1}{V} P(\hat{\mathbf{u}}', t) g(\mathbf{r}, \mathbf{r}', \hat{\mathbf{u}}, \hat{\mathbf{u}}')$ is the conditional pdf for the position $\mathbf{r}'$ and orientation $\hat{\mathbf{u}}'$ of a rod, given the orientation $\hat{\mathbf{u}}$ and position $\mathbf{r}$ of the other rod, the torque in eq.(206) is the torque on a rod, with prescribed orientation $\hat{\mathbf{u}}$ and position $\mathbf{r}$, averaged over the orientations and positions of the other rods. In fact, eq.(205) is nothing but the one-particle Smoluchowski equation with the addition of an "external torque" $\bar{\mathbf{T}}$.

A closed equation of motion for $P(\hat{\mathbf{u}}, t)$ is obtained when g is known. For equilibrium suspensions of very long and thin, rigid and repulsive rods, similar arguments as used by Onsager (1933) lead to (see subsection 10.3 for details),

$$g(\mathbf{r} - \mathbf{r}', \hat{\mathbf{u}}, \hat{\mathbf{u}}', t) \; = \; \exp\{-\beta \, V(\mathbf{r} - \mathbf{r}', \hat{\mathbf{u}}, \hat{\mathbf{u}}')\} \; , \tag{208}$$

where V is the pair-interaction potential. This expression is valid in the isotropic and nematic states (provided the degree of alignment is not too high). That eq.(208) is a good approximation for suspensions of very long and thin rods in equilibrium even at high concentrations is shown in subsection 10.3. What is neglected in using eq.(208) are dynamic contributions to correlations and the influence of shear flow. So far, nothing is known about dynamic correlations, and we shall assume here that these contributions can be neglected. Furthermore, the effect of shear flow is to align rods, that is, shear flow strongly affects the singlet pdf $P(\hat{\mathbf{u}}, t)$. Correlations between centers-of-mass of the very long and thin rods, measured by the pair-correlation function g, are much less affected by flow.

In case of hard-core interactions we have the identity,

$$\begin{aligned} \exp\left\{-\beta V(\mathbf{r}-\mathbf{r}', \hat{\mathbf{u}}, \hat{\mathbf{u}}')\right\} \hat{\mathcal{R}} V(\mathbf{r}-\mathbf{r}', \hat{\mathbf{u}}, \hat{\mathbf{u}}') \; &= \; -\beta^{-1} \hat{\mathcal{R}} \left[\exp\left\{-\beta V(\mathbf{r}-\mathbf{r}', \hat{\mathbf{u}}, \hat{\mathbf{u}}')\right\} - 1\right] \\ &= \; \beta^{-1} \, \hat{\mathcal{R}} \, \chi(\mathbf{r} - \mathbf{r}', \hat{\mathbf{u}}, \hat{\mathbf{u}}') \; , \end{aligned} \tag{209}$$

with χ the characteristic function of the excluded volume for two rods : $\chi = 1$ when the cores of the two rods overlap and $\chi = 0$ otherwise. The torque (206) can now be written as,

$$\bar{\mathbf{T}}(\hat{\mathbf{u}}, t) \; = \; -\hat{\mathcal{R}} \, V^{eff}(\hat{\mathbf{u}}, t) \; , \tag{210}$$

where *the effective potential* V^{eff} is equal to (with $\mathbf{R} = \mathbf{r}' - \mathbf{r}$),

$$\begin{aligned} V^{eff}(\hat{\mathbf{u}}, t) &= \beta^{-1}\bar{\rho} \int d\mathbf{R} \oint d\hat{\mathbf{u}}' \, P(\hat{\mathbf{u}}', t) \, \chi(\mathbf{R}, \hat{\mathbf{u}}, \hat{\mathbf{u}}') \\ &= 2DL^2\beta^{-1}\bar{\rho} \oint d\hat{\mathbf{u}}' \, P(\hat{\mathbf{u}}', t) \; |\, \hat{\mathbf{u}} \times \hat{\mathbf{u}}' \,| \,, \end{aligned} \tag{211}$$

where in the last equation it is used that,

$$\int d\mathbf{R} \; \chi(\mathbf{R}, \hat{\mathbf{u}}, \hat{\mathbf{u}}') \;=\; 2DL^2 \,|\, \hat{\mathbf{u}} \times \hat{\mathbf{u}}' \,| \,, \tag{212}$$

for very long and thin rods. The effective potential V^{eff} is commonly referred to as *the Doi-Edwards potential*. We thus find the following closed equation of motion for $P(\hat{\mathbf{u}}, t)$,

$$\begin{aligned} \frac{\partial}{\partial t} P(\hat{\mathbf{u}}, t) &= D_r \hat{\mathcal{R}} \cdot \left\{ \hat{\mathcal{R}} P(\hat{\mathbf{u}}, t) + 2DL^2\bar{\rho} \, P(\hat{\mathbf{u}}, t) \, \hat{\mathcal{R}} \oint d\hat{\mathbf{u}}' \, P(\hat{\mathbf{u}}', t) \; |\, \hat{\mathbf{u}} \times \hat{\mathbf{u}}' \,| \right\} \\ &\qquad -\dot{\gamma} \, \hat{\mathcal{R}} \cdot \left\{ P(\hat{\mathbf{u}}, t) \; \hat{\mathbf{u}} \times \left(\hat{\mathbf{\Gamma}} \cdot \hat{\mathbf{u}} \right) \right\} \,. \end{aligned} \tag{213}$$

Note that this equation is non-linear in $P(\hat{\mathbf{u}}, t)$.

We note here, for those who are familiar with Onsager's work (Onsager (1933), Onsager (1942), Onsager (1949)), that the stationary solution $P(\hat{\mathbf{u}})$ of the equation of motion (213) without shear flow satisfies,

$$\ln\{P(\hat{\mathbf{u}})\} + 2DL^2\bar{\rho} \oint d\hat{\mathbf{u}}' \, P(\hat{\mathbf{u}}', t) \; |\, \hat{\mathbf{u}} \times \hat{\mathbf{u}}' \,| = \; C \,, \tag{214}$$

where C is an integration constant. This is precisely the Euler-Lagrange equation that complies with the Onsager free energy functional for very long and thin rods with excluded volume interactions.

An important thing to notice is that the outer product $\hat{\mathbf{u}} \times (\mathbf{\Gamma} \cdot \hat{\mathbf{u}})$ in eq.(213) can not be written in the form $\hat{\mathcal{R}} f$, with f a scalar field. Therefore, the simple shear contribution to the equation of motion (213) for $P(\hat{\mathbf{u}}, t)$ can not be incorporated as a potential. Simple shear flow is thus a non-conservative external field. Since no potential for shear flow can be defined, one can not define a free energy. Thermodynamic considerations for systems under shear flow are therefore questionable. It has yet to be seen how accurate thermodynamic approaches for systems under shear flow are. To describe coexistence under shear flow conditions, one must in principle resort to equations of motion, and time integrate these up to the stationary state. Since sharp interfaces may exist in such stationary states, equations of motion should accurately describe situations where strong gradients in concentration and orientational order parameter are present.

0.10.2 The equation of motion for $\mathbf{S}(t)$

Following Doi and Edwards, Doi and Edwards (1986), an equation of motion for $\mathbf{S}$ can be obtained by operating on both sides of eq.(213) with $\oint d\hat{\mathbf{u}} \, (\hat{\mathbf{u}}\hat{\mathbf{u}}) \, (\cdots)$ (see eq.(181), where P is now time dependent). The first term on the right hand-side of eq.(213) is easily found to render,

$$\oint d\hat{\mathbf{u}} \, (\hat{\mathbf{u}} \, \hat{\mathbf{u}}) \hat{\mathcal{R}}^2 P(\hat{\mathbf{u}}, t) \;=\; \oint d\hat{\mathbf{u}} \, P(\hat{\mathbf{u}}, t) \hat{\mathcal{R}}^2 (\hat{\mathbf{u}} \, \hat{\mathbf{u}}) \;=\; 2\hat{\mathbf{I}} - 6\mathbf{S} \,, \tag{215}$$

where in the first equation two partial integrations have been done, and in the second equation it is used that $\hat{\mathcal{R}}^2(\hat{\mathbf{u}}\,\hat{\mathbf{u}}) = 2\hat{\mathbf{I}} - 6\hat{\mathbf{u}}\,\hat{\mathbf{u}}$. To make further analytical progress, we shall expand the second term in the equation of motion (213) up to third order in the orientational order parameter. That is, we shall expand with respect to the eigenvalues of matrices like $\mathbf{q} = \hat{\mathbf{u}}\hat{\mathbf{u}} - \frac{1}{3}\hat{\mathbf{I}}$, whose eigenvalues are in between $-1/3$ and $2/3$. Such a third order Ginzburg-Landau expansion complies with a fourth order expansion of the free energy in the absence of flow. Since the outer product in eq.(213) for the effective potential can be written as (with $\mathbf{q}' = \hat{\mathbf{u}}'\hat{\mathbf{u}}' - \frac{1}{3}\hat{\mathbf{I}}$),

$$|\,\hat{\mathbf{u}} \times \hat{\mathbf{u}}'\,| = \sqrt{1 - \hat{\mathbf{u}}\hat{\mathbf{u}} : \hat{\mathbf{u}}'\hat{\mathbf{u}}'} \;=\; \sqrt{\tfrac{2}{3} - \mathbf{q} : \mathbf{q}'}\;,$$

we can Taylor expand up to leading order with respect to $\mathbf{q}$ and $\mathbf{q}'$,

$$|\,\hat{\mathbf{u}} \times \hat{\mathbf{u}}'\,| \approx \sqrt{\tfrac{2}{3}}\;\left[\,1 - \tfrac{3}{4}\,\mathbf{q} : \mathbf{q}'\,\right]\;. \tag{216}$$

Since the next higher order term in this Taylor expansion is of fourth order, this truncation leads to a Ginzburg-Landau expansion up to third order of the equation of motion for $\mathbf{S}$. Since $\sqrt{2/3}$ differs by only $3.8\,\%$ from the exact value $\pi/4$ for the isotropic average value of $|\,\hat{\mathbf{u}} \times \hat{\mathbf{u}}'\,|$, we shall replace $\sqrt{2/3}$ in eq.(216) by $\pi/4$. Errors due to truncation of the Taylor expansion in eq.(216) are probably larger. Re-substitution of the definition of the $\mathbf{q}$'s in terms of bilinear products of $\hat{\mathbf{u}}$'s then leads to,

$$|\,\hat{\mathbf{u}} \times \hat{\mathbf{u}}'\,| \approx \tfrac{5\pi}{16}\;\left[\,1 - \tfrac{3}{5}\,\hat{\mathbf{u}}\hat{\mathbf{u}} : \hat{\mathbf{u}}'\hat{\mathbf{u}}'\,\right]\;. \tag{217}$$

The effective potential (211) within this Ginzburg-Landau expansion can be written as,

$$V^{eff}(\hat{\mathbf{u}}, t) \;=\; \tfrac{5\pi}{8}\,\beta^{-1} D L^2 \bar{\rho}\,\{1 - \tfrac{3}{5}\,\mathbf{S} : \hat{\mathbf{u}}\hat{\mathbf{u}}\}\;, \tag{218}$$

known as the *Maier-Saupe potential* Maier-Saupe potential (Maier and Saupe (1958), Maier and Saupe (1959), Maier and Saupe (1960)). Using the Ginzburg-Landau expansion (218) in the Smoluchowksi equation (213), and operating on both sides with $\oint d\hat{\mathbf{u}}\,(\hat{\mathbf{u}}\hat{\mathbf{u}})\,(\cdots)$, leads to the Doi-Edwards equation of motion,

$$\frac{d}{dt}\mathbf{S} = -6D_r\left\{\mathbf{S} - \tfrac{1}{3}\hat{\mathbf{I}} - \tfrac{L}{D}\,\varphi\,\left(\mathbf{S}\cdot\mathbf{S} - \mathbf{S}^{(4)} : \mathbf{S}\right)\right\} + \dot{\gamma}\left\{\hat{\mathbf{\Gamma}}\cdot\mathbf{S} + \mathbf{S}\cdot\hat{\mathbf{\Gamma}}^T - 2\,\mathbf{S}^{(4)} : \hat{\mathbf{E}}\right\}\;, \tag{219}$$

where the concentration is now expressed in terms of the volume fraction $\varphi = \frac{\pi}{4} D^2 L \bar{\rho}$, and, as before, $\hat{\mathbf{\Gamma}} = \mathbf{\Gamma}/\dot{\gamma}$ is the normalized velocity gradient tensor, which is introduced to make the shear-rate dependence more explicit. Furthermore, $\mathbf{S}^{(4)}$ is a fourth order polyadic tensor, defined as,

$$\mathbf{S}^{(4)} \;\equiv < \hat{\mathbf{u}}\,\hat{\mathbf{u}}\,\hat{\mathbf{u}}\,\hat{\mathbf{u}} > \;. \tag{220}$$

In order to obtain a closed equation of motion for $\mathbf{S}$, the fourth order tensor $\mathbf{S}^{(4)}$ should be expressed in terms of $\mathbf{S}$. Such a closure relation is discussed below.

0.10.3 Density Expansion of the Pair Correlation Function

Before deriving an orientational closure relation, we will discuss the reason why eq.(208) is a good approximation in equilibrium for very long and thin rods with short-ranged repulsive interactions, even for high concentrations.

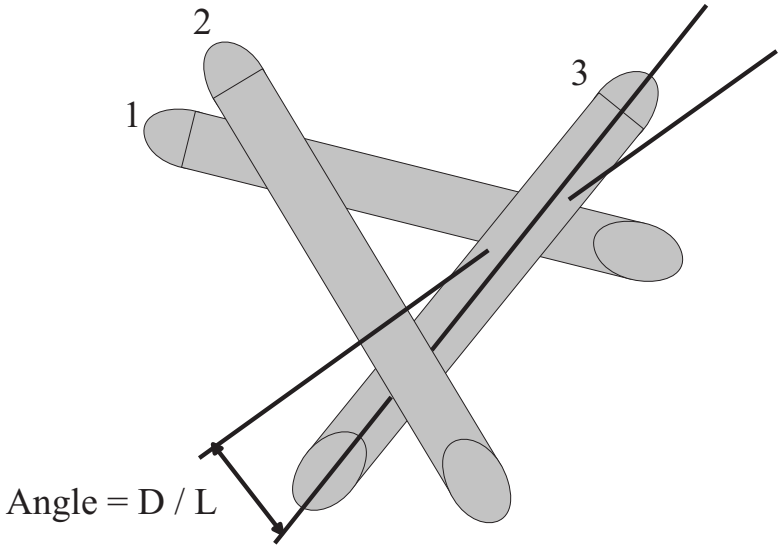

Figure 18: The effective angular integration range corresponding to the orientation of rod 3.

The first two terms in the density expansion of the equilibrium pair-correlation function are,

$$g(\mathbf{r}_1 - \mathbf{r}_2, \hat{\mathbf{u}}_1, \hat{\mathbf{u}}_2) \quad = \quad \exp\{-\beta V(\mathbf{r}_1 - \mathbf{r}_2, \hat{\mathbf{u}}_1, \hat{\mathbf{u}}_2)\} \times \tag{221}$$
$$\left\{1 + \bar{\rho} \int d\mathbf{r}_3 \oint d\hat{\mathbf{u}}_3 \; \chi(\mathbf{r}_1 - \mathbf{r}_3, \hat{\mathbf{u}}_1, \hat{\mathbf{u}}_3)\, \chi(\mathbf{r}_3 - \mathbf{r}_2, \hat{\mathbf{u}}_3, \hat{\mathbf{u}}_3) \; + \cdots \right\}.$$

Since the characteristic functions in the integrand are only non-zero when the core of rod number 3 overlaps with both the cores of rods 1 and 2, the integration with respect to $\hat{\mathbf{u}}_3$ effectively extends over an angular range of the order D/L (see fig.18). The integration with respect to $\mathbf{r}_3$ contributes at most $\sim DL^2$. Hence, the second term in the above expression is at most of order $(D/L)\, DL^2\, \bar{\rho} \sim \varphi$. Since the volume fractions of interest scale like D/L (see Onsager (1933), Onsager (1942), Onsager (1949) and later in this chapter), the first order in density contribution to the pair-correlation function is negligibly small for very long and thin rods. Higher order terms are similarly very small.

The above arguments as far as the $\hat{\mathbf{u}}_3$-integration is concerned only hold when the angle between $\hat{\mathbf{u}}_1$ and $\hat{\mathbf{u}}_2$ is much larger than $\sim D/L$, as is clear from fig.18. Otherwise, the $\hat{\mathbf{u}}_3$-integration extends over a much larger angular range than just $\sim D/L$. Hence, the expression

(208) for the pair-correlation function is valid for high concentrations, provided that the degree of alignment is not very high. Scaling of the angular integration range with D/L does not hold for all configurations of the three rods. A more careful analysis shows that the second term in eq.(221) is of order $(D/L)\ln\{L/D\}$ instead of D/L.

0.10.4 An Orientational Closure Relation

There are a number of orientational closure relations for the contraction in eq.(220) that can be used in eq.(219) to obtain a closed equation of motion for $\mathbf{S}(t)$ (for an overview, see Forest and Wang (2003)). Here we will derive a simple closure relation which is shown to be reasonably accurate. It turns out that the various tumbling and wagging phenomena where rods coherently rotate under stationary shear flow (not to be confused with the Jeffery orbits discussed before) can not be accurately described by most of the existing closure relations. Such periodic solutions for the orientational order should be analyzed on the basis of eq.(213) without using a Ginzburg-Landau expansion for $\mid \hat{\mathbf{u}} \times \hat{\mathbf{u}}' \mid$.

The fourth order average in eq.(220) occurs in the form of a double contraction,

$$\mathbf{A} \equiv \mathbf{S}^{(4)} : \mathbf{M} \, , \tag{222}$$

where $\mathbf{M}$ is equal to $\mathbf{S}$. As pointed out by Hinch and Leal (1976), orientational order increases monotonically with increasing shear-rate, so that interpolation between the known forms for $\mathbf{S}^{(4)}$ in the isotropic state and in the perfectly aligned state will probably lead to quite accurate closures. The four point average $\mathbf{S}^{(4)}$ is known exactly for the two extreme cases of perfect alignment (along the director $\hat{\mathbf{n}}$) and for the isotropic state,

$$\begin{aligned} < \hat{\mathbf{u}}\,\hat{\mathbf{u}}\,\hat{\mathbf{u}}\,\hat{\mathbf{u}} >_{ijkl} &= \hat{\mathbf{n}}_i\hat{\mathbf{n}}_j\hat{\mathbf{n}}_k\hat{\mathbf{n}}_l \quad , \qquad \text{perfect alignment} \, , \\ &= \tfrac{1}{15}\left[\, \delta_{ij}\delta_{kl} + \delta_{ik}\delta_{jl} + \delta_{ik}\delta_{jl} \,\right] \quad , \quad \text{isotropic} \, , \end{aligned} \tag{223}$$

with δ_{ij} the Kronecker delta ($\delta_{ij} = 1$ when $i = j$, and $\delta_{ij} = 0$ when $i \neq j$). Furthermore, we have the following trivial identities,

$$\begin{aligned} A_{ij} &\equiv \sum_{n,m} < \hat{\mathbf{u}}_i\,\hat{\mathbf{u}}_j\,\hat{\mathbf{u}}_n\,\hat{\mathbf{u}}_m > \mathbf{M}_{mn} = A_{ji} \, , \\ \sum_i A_{ii} &= \sum_i \sum_{n,m} < \hat{\mathbf{u}}_i\,\hat{\mathbf{u}}_i\,\hat{\mathbf{u}}_n\,\hat{\mathbf{u}}_m > \mathbf{M}_{mn} = \sum_{n,m} \mathbf{S}_{nm}\mathbf{M}_{mn} \equiv \mathbf{S} : \mathbf{M} \, . \end{aligned} \tag{224}$$

The latter identity is especially important in order to ensure that the trace of $\mathbf{S}$ remains equal to 1 on time integration of the equation of motion (219). Using closures which do not satisfy (224) violate the time invariance of the trace of the order parameter. Furthermore,

$$\mathbf{A} = < \hat{\mathbf{u}}\,\hat{\mathbf{u}}\,\hat{\mathbf{u}}\,\hat{\mathbf{u}} > : \overline{\mathbf{M}} \, , \tag{225}$$

with,

$$\overline{\mathbf{M}} \equiv \tfrac{1}{2}\left[\mathbf{M} + \mathbf{M}^T\right] \, , \tag{226}$$

the symmetric part of $\mathbf{M}$, where the superscript "T" stands for "the transpose of". This equation implies that the closure relation must be a function of $\overline{\mathbf{M}}$.

Since order parameters tend to increase monotonically with shear rate, an accurate closure relation can be found by constructing an interpolation form between the exact results (223)

such that the conditions (224,225) are satisfied. Substitution of the most general form of linear combinations of first and second order terms in $\mathbf{S}$ (insisting that no isotropic contributions $\sim \hat{\mathbf{I}}$ contribute),

$$\begin{aligned}\mathbf{A} &= c_1\mathbf{S}\cdot\overline{\mathbf{M}} + c_2\overline{\mathbf{M}}\cdot\mathbf{S} + c_3\mathbf{S}\,\hat{\mathbf{I}}:\overline{\mathbf{M}} \\ &\quad + c_4\mathbf{S}\cdot\mathbf{S}\cdot\overline{\mathbf{M}} + c_5\mathbf{S}\cdot\overline{\mathbf{M}}\cdot\mathbf{S} + c_6\overline{\mathbf{M}}\cdot\mathbf{S}\cdot\mathbf{S} + c_7\mathbf{S}\,\mathbf{S}:\overline{\mathbf{M}} + c_8\overline{\mathbf{M}}\,\mathbf{S}:\mathbf{S}\,,\end{aligned}$$

into eqs.(223-226) renders algebraic equations for the coefficients c_j, leading to,

$$<\hat{\mathbf{u}}\,\hat{\mathbf{u}}\,\hat{\mathbf{u}}\,\hat{\mathbf{u}}>:\ \mathbf{M} = \tfrac{1}{5}\left\{\mathbf{S}\cdot\overline{\mathbf{M}} + \overline{\mathbf{M}}\cdot\mathbf{S} - \mathbf{S}\cdot\mathbf{S}\cdot\overline{\mathbf{M}} - \overline{\mathbf{M}}\cdot\mathbf{S}\cdot\mathbf{S} + 2\mathbf{S}\cdot\overline{\mathbf{M}}\cdot\mathbf{S} + 3\mathbf{S}\,\mathbf{S}:\overline{\mathbf{M}}\right\}\ . \quad (227)$$

Substitution of the closure relation (227) into the equation of motion (219) finally leads to a closed equation of motion for the orientational order parameter tensor.

The accuracy of the closure relation (227) is discussed in appendix C. Comparison of exact numerical solutions of the Smoluchowski equation (205) for non-interacting rods, shows that the closure approximation (227) with $\mathbf{M} = \mathbf{S}$ and with $\mathbf{M} = \mathbf{E}$ are accurate to within 1% and 10%, respectively. Computer simulations show that this accuracy extends to interacting rods.

0.11 Paranematic-Nematic Spinodals and the Binodal under Shear Flow

Since shear flow tends to align rods, it will affect the location of isotropic-nematic phase transition lines. The shear induced shift of spinodals is theoretically more easily calculated as the shift of binodals. For the prediction of the location of binodals as a function of shear rate, equations of motion must be time-integrated up to the stationary state where two bulk phases coexist. These equations of motion must accurately account for the usually sharp interface between both bulk phases. Equations of this sort have been derived in Dhont and Briels (2002) and Dhont and Briels (2003) (see also the next section in this chapter as far as the stress tensor is concerned), but remain to be analyzed. On the basis of approaches that partly rely on thermodynamic arguments, similar equations of motion can be derived to predict the phase behaviour of rods under shear flow Olmsted and Lu (1999), Olmsted (1999), Olmsted et al. (2000), Lu et al. (2000) and Fielding and Olmsted (2003). These equations of motion are in principle valid for small gradients in concentration and orientational order parameter, and are therefore probably not able to accurately predict of the location of the binodal. Nevertheless, the analysis of such equations of motion reveals interesting behaviour like gradient banding, which will be discussed later in this chapter.

In the absence of flow, computer simulations where free energies are calculated can be used to obtain binodal concentrations for arbitrary aspect ratios Bolhuis and Frenkel (1997).

The experimental situation is different : here it is much more difficult to measure the location of spinodals as compared to binodals. In the following we shall first discuss how the shear-rate dependence of spinodals can be calculated, and an experiment is discussed where a line in between the paranematic-nematic and nematic-paranematic spinodals is probed. As far as the binodal is concerned, there are no theoretical (nor simulation) results available yet. We shall discuss an experiment where the location of the binodal is measured by means of time resolved rheology experiments.

0.11.1 Spinodals

A spinodal point is defined as a point in the shear rate versus concentration diagram (the so-called *non-equilibrium phase diagram*), where a stable stationary solution of the equation of motion (219) for the orientational order parameter turns into an unstable solution. In the absence of shear flow, such spinodal points can also be found by means of thermodynamics. Once a solution becomes unstable, the system will start to phase separate without any time delay. In order to describe such spinodal decomposition kinetics, one needs to consider the extension of the equation of motion (213) or (219) to inhomogeneous systems, where gradient contributions stabilize the system against formation of very large gradients. In the absence of shear flow, such equations of motion are analyzed by Doi et al. (1988), Shimada et al. (1988) and Winters et al. (2000). For spinodal decomposition kinetics under shear flow, these equations of motion must be supplemented by an effective Navier-Stokes equation beyond the initial stage of demixing. Spinodal decomposition of rod-like systems will be strongly affected by flow, since flow affects orientational order. Analyzing such coupled equations of motion as derived by Dhont and Briels (2002), Dhont and Briels (2003) is in progress. In the present section we shall limit the discussion to the shear induced shift of spinodals.

As far as the location of spinodals is concerned, the non-equilibrium phase diagram can most conveniently be understood on the basis of so-called *bifurcation diagrams*. A bifurcation diagram is a plot in the orientational-order-parameter versus concentration plane, where, for a given shear rate, the order parameter for the stationary solutions of the equation of motion (219) is indicated. There are two possible stationary solutions : stable- and unstable solutions. Let $\mathbf{S}_0$ denote a stationary solution of eq.(219), that is, the right-hand side of eq.(219) vanishes for $\mathbf{S} = \mathbf{S}_0$. Let $\delta\mathbf{S}$ be a small perturbation. The stationary solution $\mathbf{S}_0$ is referred to as a stable solution when an initial state $\mathbf{S}_0 + \delta\mathbf{S}$ relaxes back to $\mathbf{S}_0$ in time, provided $\delta\mathbf{S}$ is small enough. The state $\mathbf{S}_0$ is referred to as unstable, when $\delta\mathbf{S}$ does not relax to $\mathbf{0}$, no matter how small this perturbation is chosen. A linear stability analysis is required to decide whether a stationary solution is either stable or unstable. Such a stability analysis for the stationary isotropic state $\mathbf{S}_0 = \frac{1}{3}\hat{\mathbf{I}}$ in the absence of shear flow can be performed analytically. Using the closure relation (227) in eq.(219) with $\dot{\gamma} = 0$, substitution of,

$$\mathbf{S}(t) \;=\; \tfrac{1}{3}\hat{\mathbf{I}} \,+\, \delta\mathbf{S}(t) \;, \tag{228}$$

and linearization with respect to $\delta\mathbf{S}(t)$ readily leads to,

$$\frac{d}{dt}\delta\mathbf{S} \;=\; -6D_r^{eff}\,\delta\mathbf{S} \tag{229}$$

where,

$$D_r^{eff} \;=\; D_r\,\{\,1 - \tfrac{1}{5}\,\tfrac{L}{D}\,\varphi\,\}\;, \tag{230}$$

is an effective rotational diffusion coefficient. The solution of eq.(229) reads,

$$\delta\mathbf{S}(t) \;=\; \exp\left\{-6D_r^{eff}t\right\}\,\delta\mathbf{S}(t=0)\;. \tag{231}$$

The perturbation $\delta\mathbf{S}$ thus grows exponentially in time when $D_r^{eff} < 0$, that is when $\frac{L}{D}\varphi > 5$. For $\frac{L}{D}\varphi > 5$, the isotropic phase becomes unstable, and the new stable state is the nematic state with a relatively large value for λ. On subsequently lowering the concentration, the nematic state becomes unstable at $\frac{L}{D}\varphi < 40/9 = 4.44\cdots$, and the system returns to the isotropic state.

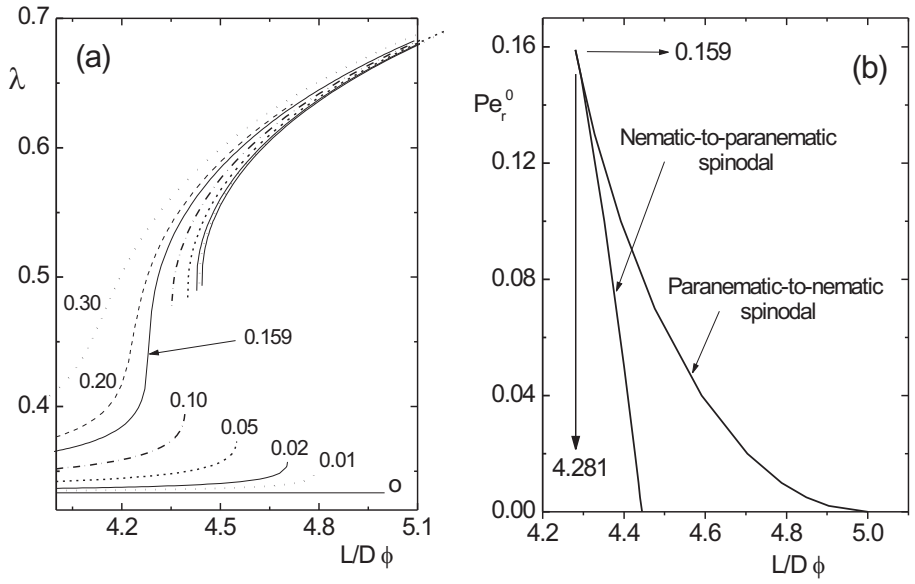

Figure 19: (a) Bifurcation diagrams, where only stable stationary solutions $\mathbf{S}_0$ of eq.(219) (together with the closure relation (227)) are shown. Here, λ is the largest eigenvalue of $\mathbf{S}_0$ and φ is the volume fraction of rods. The numbers in the plot refer to $Pe_r^0 \equiv \dot{\gamma}/D_r$. (b) Spinodal points as found from the bifurcation diagrams.

A stability analysis can in principle be done once S_0 is known, and hence an effective rotational diffusion coefficient can be defined also for non-zero shear rates. For non-zero shear rates this effective diffusion coefficient is generally a tensor rather than a scalar. An important thing to note is that the largest eigenvalue of this diffusion tensor becomes 0 at a spinodal point. Rotational diffusion therefore becomes very slow in the neighbourhood of a spinodal point, which is reminiscent of critical slowing down.

The isotropic-to-nematic spinodal concentration $\frac{L}{D}\varphi = 5$ should be compared to the exact value 4 found by Onsager (1933), or equivalently, from a linear stability analysis of eq.(213), without performing a Ginzburg-Landau expansion on $\mid \hat{\mathbf{u}} \times \hat{\mathbf{u}}' \mid$. The difference between our result and the exact result for the location of the isotropic-to-nematic spinodal point in the absence of shear flow is mainly due to the Ginzburg-Landau expansion (217), and to a lesser extent to the closure relation (227) (which is accurate to within $1\,\%$ for $\mathbf{M} = \mathbf{S}$).

Note that D_r^{eff} is a collective diffusion coefficient since it describes the collective relaxation (or growth) of an initially misaligned state, where each rod contributes to the misalignment relative to the isotropic state. This diffusion coefficient is only weakly concentration dependent because such a relaxation (or initial growth) requires very small, collective reorien-

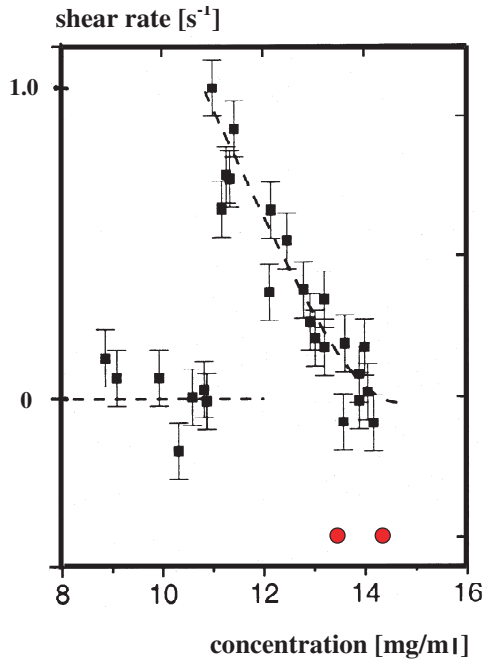

Figure 20: The shear-induced shift of spinodal concentrations as probed with time resolved birefringence measurements by Lenstra et al. (2001). The tilted line is located in between the two spinodal concentrations. The circles below indicate the binodal concentrations in the absence of shear flow.

tations of the rods. The concentration dependence of the tracer rotational diffusion coefficient considered by Doi and Edwards (1986), on the contrary, is much more pronounced due to "entanglements", since now large reorientations of the rods are important. As will be shown in section 12, the effective rotational diffusion coefficient does not depend in a linear fashion on concentration. This is due to the neglect of dynamic correlations.

Spinodals will be shifted to lower concentrations on applying simple shear-flow, since shear flow tends to align the rods, and therefore stabilizes the nematic state over the paranematic state. These spinodal points must be obtained numerically from eqs.(219,227), since generally the stationary solution $\mathbf{S}_0$ is not known analytically. In fig.19a, bifurcation diagrams are given for various values of the bare Peclet number $Pe_r^0 \equiv \dot{\gamma}/D_r$.

We note here that an otherwise isotropic stable state is aligned by shear flow. Such an aligned state is referred to as a *paranematic state* . Similarly, an otherwise stable nematic state is more strongly aligned by shear flow.

The shear-rate dependent paranematic-to-nematic spinodal (where the paranematic phase becomes unstable on increasing the concentration) and nematic-to-paranematic spinodal (where the nematic phase becomes unstable on lowering the concentration), as obtained from the bifurcation diagram in fig.19a, are plotted in fig.19b. In the absence of shear flow, as discussed above, the isotropic-to-nematic spinodal concentration is located at $\frac{L}{D}\varphi = 5$, while the

nematic-to-isotropic spinodal concentration is found to be equal to $\frac{L}{D}\varphi = 40/9 = 4.44\cdots$.

For a critical rotational Peclet number $Pe_r^0 = 0.159\cdots$, the two spinodals meet in a non-equilibrium critical point. For larger shear-rates, where $Pe_r^0 > 0.159\cdots$, there is a continuous and reversible transition between the paranematic and nematic state : here, shear forces are so large that rod-rod interactions are not able anymore to induce a discontinuous transition.

An important thing to note is that the concentration always enters through the combination $\frac{L}{D}\varphi$. For long and thin rods, the volume fractions of interest thus scale as $\sim \frac{D}{L} \ll 1$. This is the reason why hydrodynamic interactions become less important for very long and thin rods, as mentioned before. The strength of direct interactions, on the contrary, is not small, since at $\frac{L}{D}\varphi = \mathcal{O}(1)$, these interactions are sufficiently strong to induce a phase transition.

Recent time resolved birefringence experiments by Lenstra et al. (2001) confirm a shear induced shift of paranematic-nematic phase boundary lines (see fig.20). Here, the shear rate is gradually changed from a high shear rate (where the one-phase state is stable) to a lower shear rate (possibly in the two-phase region), followed by the reverse. During such a shear-rate sweep the birefringence is probed. Due to slowing down of the orientational dynamics close to a spinodal line, the birefringence will exhibit a hysteresis, the magnitude of which depends on the sweep rate. Such time resolved birefringence measurements probe a line in the non-equilibrium phase diagram that is in between the two spinodal concentrations (see Lenstra et al. (2001)). The system that is used here consists of dispersions of fd virus, which has been used for the first time for systematic studies on phase behaviour and phase separation kinetics by et al. (1989), Tang and Fraden (1993), Tang and Fraden (1995) and Grelet and Fraden (2003), including suspensions of Tobacco Mosaic Virus (see also the chapter by Fraden and Dogic in this book). Paranematic-nematic phase separation for this system is slow enough to perform a shear-rate sweep during a time interval where phase separation does not play a role for the measured birefringence. Fd-virus is a semi-flexible rod rather then a perfectly rigid rod, and the potential between the rods is not a perfect hard-core potential. The contour length of a fd-virus particle is $880\ nm$, while its persistence length is $2200\ nm$. This is the reason why, in the absence of shear flow, the experimental binodal concentrations (indicated by the two dots in fig.20) are found not to agree quantitatively with those predicted by Onsager. As can be seen in fig.20, the shear-induced shift of spinodals is much more pronounced as compared to the prediction in fig.19b. The origin of this discrepancy is most probably the flexibility of fd virus. The critical shear rate, however, is in reasonable agreement with the predicted critical shear rate $Pe_r^0 \approx 0.159$ (the bare rotational diffusion coefficient of fd is known to be $10 - 20\ s^{-1}$). So far, there is no theory dealing with the dynamics of semi-flexible Brownian particles on the same level as the Smoluchowski approach for stiff rods outlined above.

0.11.2 The binodal

An experimental binodal of a fd-virus suspension is given in fig.21. Binodal points are determined from time-dependent viscosity measurements after a shear-rate quench from a high shear rate, where the one-phase state is stable, to a lower shear rate, $\dot{\gamma}_-$ say. Whenever $\dot{\gamma}_-$ is within the paranematic-nematic two-phase region, demixing will occur after the quench into a paranematic and a nematic phase. Developing inhomogeneities give rise to a temporal change of the viscosity, the amplitude of which increases with the depth of the quench. The amplitude of the time dependent response of the viscosity vanishes on the binodal. A point on the

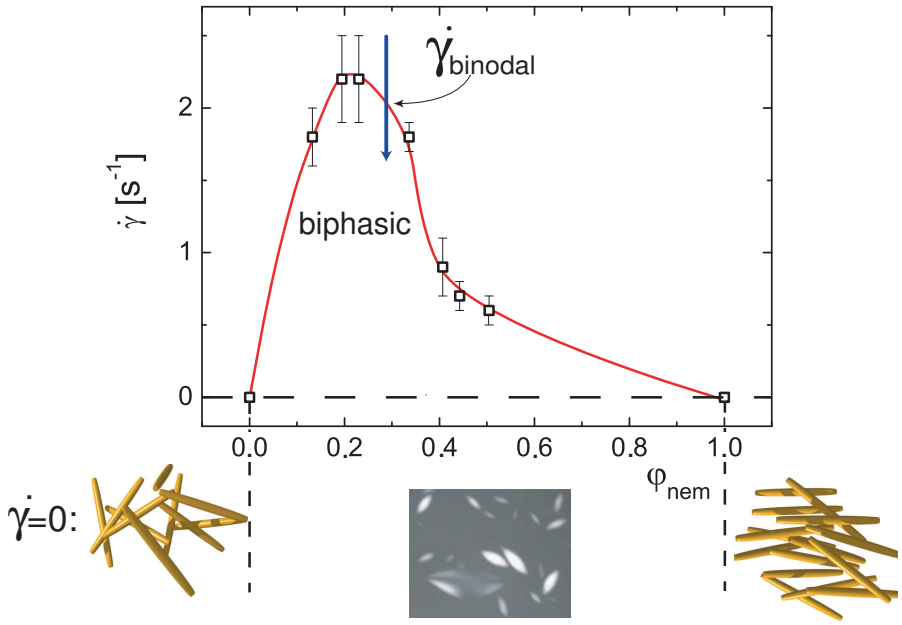

Figure 21: The paranematic-nematic binodal of a fd-virus suspensions, where dextran is added to induced attractions between the rods, leading to faster phase separation. Here, φ_{nem} is the fraction of coexisting nematic that is mixed with the corresponding isotropic bulk phase (at zero shear rate). The lower figures depict (from left to right) the isotropic state, polarization microscopy image of tactoids that form during phase separation (courtesy of Kyongok Kang) and the nematic state. The vertical line indicates a possible shear-rate quench.

binodal can thus be obtained by interpolation of the amplitude as a function of $\dot{\gamma}_-$ to zero. For more details see Lettinga and Dhont (2004). Contrary to the experiments on the location of the spinodal as described in the previous subsection, here dextran is added to the fd-virus suspension in order to enhance phase separation, which renders these experiments feasible.

0.11.3 A remark on pattern formation and time-periodic states

There are two regions in the non-equilibrium phase diagram to be distinguished that are related to pattern formation and time-periodic states. As will be seen later, shear flow can induce pattern formation within the two-phase region, that is, the region bounded by the paranematic-nematic binodal. Here "bands" are alternately stacked in the vorticity direction, where the average orientational order within the bands differ. This type of shear-induced pattern formation is referred to as *vorticity banding*. In addition, coherent rotation of rods in the otherwise nematic state leads to oscillations of the director under stationary shear flow. Such *tumbling and wagging states* have been analyzed in great detail by Marrucci and Maffettone (1990a), Marrucci and Maffettone (1990b), Rienäcker and Hess (1999), Forest and Wang (2003) and Hess and Kröger (2004). As stated before, the closure relation that is employed for the fourth

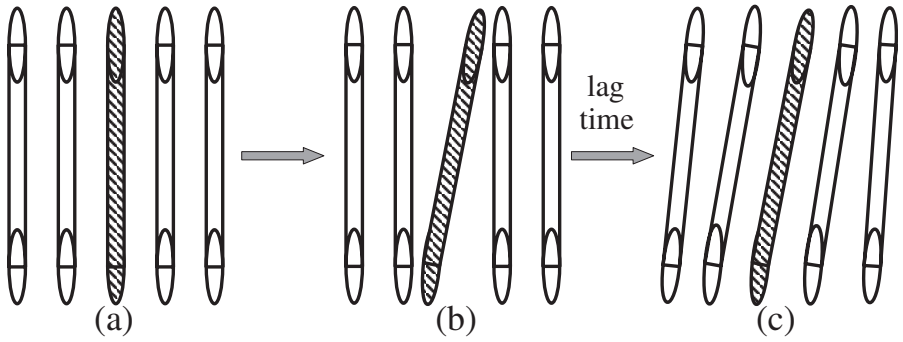

Figure 22: A sketch to explain the origin of "dynamic correlations". (a) depicts an initial configuration of rods, which for simplicity is taken as a perfectly aligned state. The orientational dynamics of the shaded rod is considered in the main text. (b) After a small time, the shaded rod has moved to a different orientation due to Brownian motion. For clarity, the corresponding movements of the other rods is not depicted here. (c) the surrounding rods need a finite time to adjust to the new orientation of the shaded rod.

order tensor in eq.(220) in terms of $\mathbf{S}$ sensitively determines whether these periodic states are correctly described. Our closure relation (227), although accurate to within about 10%, does not give rise to tumbling and wagging at all, like many other closures. Instead it is more appropriate to analyze eq.(213) as such. A numerical analysis of this equation of motion indeed predicts tumbling and wagging regimes in the non-equilibrium phase diagram, although the time-periodic states as predicted by eq.(213) are not yet fully explored. In all of these equations of motion, however, dynamic correlations are neglected. As will be discussed in section 12, such correlations might play some role of importance.

0.12 How important are dynamic correlations?

Dynamic correlations find their origin in the finite time that it takes for the surroundings of a given particle to adjust to the changing position and orientation of that particle. Consider for example an assembly of rods as depicted in fig.22a. For convenience, the orientations of all rods in this figure are taken equal in the initial state. Suppose that one is interested in the orientational dynamics of the rod in fig.22 that is depicted as a shaded cylinder. During a small time interval, the shaded rod moves to a new orientation due to rotational Brownian motion, as depicted in fig.22b. If one would then freeze the orientation of the shaded rod, the surrounding rods will change their average orientation to adjust to the field imposed by the frozen shaded rod, as depicted in fig.22c. This adjustment takes a finite time. The shaded rod thus experiences a surrounding configuration of other rods that is always "lagging behind" the configuration that would have existed in case of "coexistence" with the shaded rod. The surrounding rods therefore act with a finite torque on the shaded rod, even in an isotropic suspension, due to such dynamic correlations. This is not what is found from eq.(206), when the pdf $P(\hat{\mathbf{u}}', t)$ of surrounding rods is taken equal to the its isotropic form $1/4\pi$ *and* g is approx-

imated by the Boltzmann exponential (208). In order to describe *self rotational diffusion* of a rod on the basis of eq.(206), dynamic correlations are essential.

The neglect of dynamic correlations in the derivation of the Doi-Edwards equation (219) becomes more clear on calculating the correlation function $< \hat{\mathbf{u}}(t) \cdot \hat{\mathbf{u}}(0) >$ for an isotropic dispersion. Thus, consider a rod (the dashed rod in fig.22) with a specified orientation $\hat{\mathbf{u}}(0)$ at time $t = 0$. Noting that,

$$\frac{d}{dt} < \hat{\mathbf{u}}(t) \cdot \hat{\mathbf{u}}(0) > = \hat{\mathbf{u}}(0) \cdot \oint d\hat{\mathbf{u}}\, \hat{\mathbf{u}}\, \frac{\partial P(\hat{\mathbf{u}}, t)}{\partial t}$$

multiplying both sides of the Smoluchowski equation (206) with $\hat{\mathbf{u}} \cdot \hat{\mathbf{u}}(0)$ and integrating with respect to $\hat{\mathbf{u}}$ readily leads to,

$$\frac{d}{dt} < \hat{\mathbf{u}}(t) \cdot \hat{\mathbf{u}}(0) > = -2\, D_s^{eff}(t) < \hat{\mathbf{u}}(t) \cdot \hat{\mathbf{u}}(0) >, \tag{232}$$

where the effective self-rotational diffusion coefficient is equal to,

$$D_s^{eff}(t) \equiv D_r \left\{ 1 - \tfrac{1}{2}\beta \frac{< \bar{\mathbf{T}}(\hat{\mathbf{u}}(t)) \cdot (\hat{\mathbf{u}}(t) \times \hat{\mathbf{u}}(0)) >}{< \hat{\mathbf{u}}(t) \cdot \hat{\mathbf{u}}(0) >} \right\}, \tag{233}$$

where the torque $\bar{\mathbf{T}}(\hat{\mathbf{u}}(t))$ is given by eq.(206) with an obvious change of notation. The pdf $P(\hat{\mathbf{u}}', t)$ in the expression (206) for the torque is that of the other rods (the non-dashed rods in fig.22). When the pdf $P(\hat{\mathbf{u}}', t)$ of the other rods is taken equal to $1/4\pi$ and approximating the pair-correlation function with the Boltzmann exponential (208), one finds that $\bar{\mathbf{T}}(\hat{\mathbf{u}}(t)) = \mathbf{0}$. Hence, $D_s^{eff}(t) = D_r$ which is obviously wrong, since rotational motion of the dashed rod is certainly hindered by the presence of other rods. A non-zero torque results from dynamic correlations : $P(\hat{\mathbf{u}}', t)$ of rods in the neighbourhood of the dashed rod differs from $1/4\pi$ due to the presence of the moving dashed rod, and the pair-correlation function is not equal to the equilibrium Boltzmann exponential for the same reason.

The linear concentration dependence of the effective diffusion coefficient (230), which is a *collective diffusion coefficient*, is entirely due to the neglect of dynamic correlations. MD computer simulations, where the tail of the orientational correlation function is fitted to obtain the effective diffusion coefficient, show a strong non-linear concentration dependence Tao et al. (2004), as is shown in fig.23. This indicates that dynamic correlations are of importance. As yet, no attempt has been made to incorporate dynamic correlations in the analysis of the Smoluchowski equation (206). As will be seen later, computer simulations do predict a linear concentration dependence of the shear viscosity. It thus seems that dynamic correlations. are of minor importance for the viscoelastic response of suspensions of rods, contrary to diffusive behaviour.

0.13 The Stress Tensor for Rod Suspensions

In addition to the orientational order of rods in shear flow, the viscous behaviour of these systems is of interest. In this section we shall derive a microscopic expression for the stress tensor and express it in terms of the orientational order parameter tensor (see also Dhont and Briels (2002) and Dhont and Briels (2003)). Viscoelastic response functions can then be calculated once the equation of motion (219) for $\mathbf{S}(t)$ is solved.

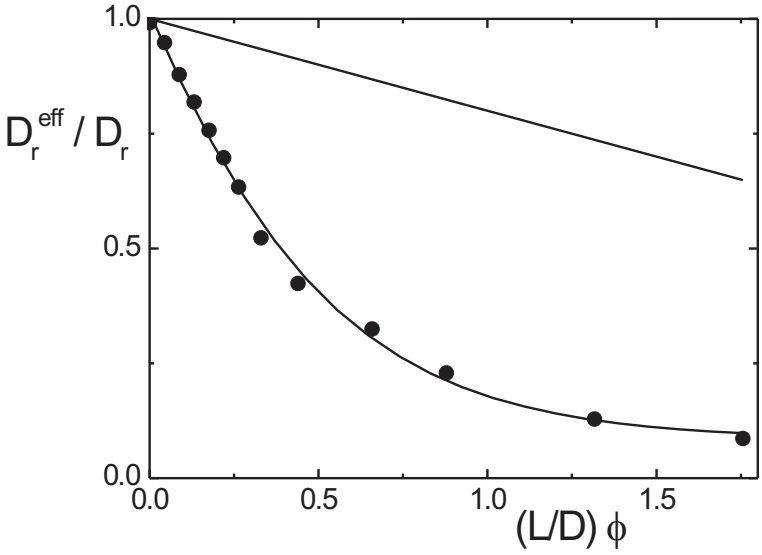

Figure 23: The effective diffusion coefficient as defined in the previous section from the theory eq.(230) where dynamic correlations are neglected and from simulations by Tao et al. (2004) (the solid line through simulation data points are a guide to the eye.)

0.13.1 The basic idea

Let $\mathbf{U}(\mathbf{r},t)$ and $\rho_m(\mathbf{r},t)$ denote the suspension velocity and mass density, respectively. The velocity satisfies the Navier-Stokes equation (13), were the divergence of the stress tensor is averaged over the phase space coordinates $\mathbf{\Gamma}$ of the colloidal rods,

$$\rho_m(\mathbf{r},t)\left[\frac{\partial \mathbf{U}(\mathbf{r},t)}{\partial t}+\mathbf{U}(\mathbf{r},t)\cdot\nabla\mathbf{U}(\mathbf{r},t)\right] = <\nabla\cdot\sigma(\mathbf{r}\mid\mathbf{\Gamma}(t))> \ . \tag{234}$$

Here, σ is the stress tensor of the solvent in which the rods are embedded, or of the core material of the rods, depending on whether $\mathbf{r}$ is within the solvent or inside the core of a rod. Clearly, σ depends on the phase space coordinates $\mathbf{\Gamma}$ of all the rods.

The fundamental quantity in hydrodynamics is the momentum density $\rho\,\mathbf{v}$, with ρ and $\mathbf{v}$ the microscopic density and velocity, respectively. Therefore, the appropriate definition of the macroscopic velocity $\mathbf{U}$ is,

$$\rho_m(\mathbf{r},t)\,\mathbf{U} = <\rho\,\mathbf{v}> \ . \tag{235}$$

It can be shown (see Dhont and Briels (2002)) that if the mass density between the fluid and the core material of which the rods consist and/or the volume fraction of colloidal material is very small, the definition in eq.(235) reduces simply to,

$$\mathbf{U}(\mathbf{r},t) = <\mathbf{v}(\mathbf{r}\,|\,\mathbf{\Gamma}(t))> , \tag{236}$$

where $\mathbf{u}$ is equal to the fluid velocity or the velocity of a piece of colloidal material, depending on whether $\mathbf{r}$ is within the solvent or inside the core of a colloidal rod.

Let $P(\mathbf{\Gamma}, t)$ denote the probability density function of $\mathbf{\Gamma}$, which is the solution of the Smoluchowski equation (173). By definition we then have,

$$\mathbf{U}(\mathbf{r}, t) \; = \; \int d\mathbf{\Gamma} \, P(\mathbf{\Gamma}, t) \, \mathbf{v}(\mathbf{r} \, | \, \mathbf{\Gamma}) \; . \tag{237}$$

In the derivation of the general expression for the divergence of the stress tensor, we shall encounter the ensemble average,

$$< \nabla^2 \mathbf{v}(\mathbf{r}) > = \int d\mathbf{\Gamma} \, P(\mathbf{\Gamma}, t) \, \nabla^2 \mathbf{v}(\mathbf{r} \, | \, \mathbf{\Gamma}) \; .$$

Since the Laplace operator can be taken in front of the phase-space integral, and the suspension flow velocity is given by eq.(236), it trivially follows that,

$$< \nabla^2 \mathbf{v}(\mathbf{r}) > = \; \nabla^2 \mathbf{U}(\mathbf{r}, t) \; . \tag{238}$$

This result will be of importance later in this section.

In order to obtain an explicit Navier-Stokes equation, the ensemble average of the body force $\nabla \cdot \sigma(\mathbf{r} \mid \mathbf{\Gamma})$ should be expressed in terms of suspension properties. To this end, consider a rectangular volume element δV located at $\mathbf{r}$, with linear dimensions δ_x, δ_y and δ_z in the $x-$, $y-$ and $z-$direction, respectively. In the formal limit that the size of the volume element vanishes, the ensemble averaged total force per unit volume of the surrounding material on the volume element is nothing but the divergence of the stress tensor that should be used in the Navier-Stokes equation (234). This force consists of three parts : forces that arise from interactions between colloidal particles outside on those within the rectangular volume element, from interactions between solvent molecules and colloidal particles, and from interactions between solvent molecules on either side of the boundary of the volume element. The corresponding stress tensors will be referred to as the "particle-particle stress tensor" $\mathbf{\Sigma}^{pp}$, the "particle-solvent stress tensor" $\mathbf{\Sigma}^{ps}$, and the "solvent-solvent stress tensor" $\mathbf{\Sigma}^{ss}$, respectively. The divergence of the suspension stress tensor $\mathbf{\Sigma}$ is the sum of these three body forces,

$$\nabla \cdot \mathbf{\Sigma} \; \equiv < \nabla \cdot \sigma(\mathbf{r} \mid \mathbf{\Gamma}(t)) > = \; \nabla \cdot \mathbf{\Sigma}^{pp} + \nabla \cdot \mathbf{\Sigma}^{ps} + \nabla \cdot \mathbf{\Sigma}^{ss} \; . \tag{239}$$

These three contributions will be calculated explicitly in the next subsections. First of all, a general expression for the ensemble averaged body force $\nabla \cdot \mathbf{\Sigma}$ will be derived, after which this expression will be expressed in terms of a probability density density function. Finally, this expression will be simplified by means of the same Ginsburg-Landau expansion used to derive the Doi-Edwards equation (219), which leads to an expression for the stress tensor involving the concentration and the orientational order parameter tensor $\mathbf{S}$.

The particle-particle stress tensor $\mathbf{\Sigma}^{pp}$

The force that colloidal particles outside the volume element exert on those within the volume element is equal to,

$$\sum_j^{\star} \mathbf{F}_j \; ,$$

where $\mathbf{F}_j$ is the force that all colloidal particles exert on colloidal particle j, and the $\star$ on the summation is used to indicate that the summation ranges only over those colloidal particles that are inside the volume element, that is, for which $\mathbf{r}_j \in \delta V$. Note that mutual interactions between colloidal particles within the volume element can not give rise to a net force on that volume element. The force per unit volume, for formally vanishing size of the volume element, is thus equal to,

$$\nabla \cdot \mathbf{\Sigma}^{pp} \;=\; \lim_{\delta_x,\delta_y,\delta_z \to 0} \frac{1}{\delta_x\,\delta_y\,\delta_z} \sum_{j=1}^{N} < \chi_{\mathbf{r}}(\mathbf{r}_j)\,\mathbf{F}_j \;> \,, \tag{240}$$

where N is the total number of colloidal particles in the system under consideration, $\mathbf{r}_j$ is the position coordinate of a colloidal particle and $\chi_{\mathbf{r}}$ is the characteristic function of the rectangular volume element that was introduced in the previous section. The characteristic function is defined as,

$$\begin{aligned} \chi_{\mathbf{r}}(\mathbf{R}) \;&=\; 1 \;\text{ when }\; \mathbf{R} \in \delta V \;, \\ &=\; 0 \;\text{ otherwise .} \end{aligned} \tag{241}$$

The subscript "$\mathbf{r}$" on the characteristic function is used to indicate that the volume element δV is located at position $\mathbf{r}$. The characteristic function effectively limits the summation to colloidal particles that are inside δV, that is, for which $\mathbf{r}_j \in \delta V$. Furthermore, as discussed before, the total force $\mathbf{F}_j$ on the j^{th} colloidal particle due to interactions with all other colloidal particles is equal to,

$$\mathbf{F}_j \;=\; -\nabla_j \Phi - k_B T \nabla_j \ln\{P\} \;, \tag{242}$$

where Ψ is the total potential energy of the assembly of N rods in the suspension, and P is the probability density function of the phase space coordinates of all the colloidal rods : $-\nabla_j \Phi$ is the force due to potential interactions, and $-k_B T \nabla_j \ln\{P\}$ is the Brownian force, where ∇_j is the gradient operator with respect to $\mathbf{r}_j$. Since (with $\delta(\mathbf{r}-\mathbf{r}_j)$ the 3-dimensional delta distribution),

$$\lim_{\delta_x,\delta_y,\delta_z \to 0} \chi_{\mathbf{r}}(\mathbf{r}_j)/\delta_x\,\delta_y\,\delta_z \;=\; \delta(\mathbf{r}-\mathbf{r}_j) \;, \tag{243}$$

as is easily verified by integration of both sides with respect to $\mathbf{r}_j$, this immediately leads to,

$$\nabla \cdot \mathbf{\Sigma}^{pp} \;=\; \sum_{j=1}^{N} <\; \delta(\mathbf{r}-\mathbf{r}_j)\,\mathbf{F}_j \;> \;. \tag{244}$$

Together with eq.(242) for the forces, this is the microscopic expression for the contribution to the divergence of the stress tensor which is due to inter-colloidal particle forces.

The particle-solvent stress tensor $\mathbf{\Sigma}^{ps}$

The particle-solvent stress arises from forces on the volume element due to interactions between colloidal particles and solvent molecules. These forces are mediated to the volume element by colloidal particles that intersect with the surface enclosing the rectangular volume element. Consider first the force that is mediated to the solvent within the volume element by

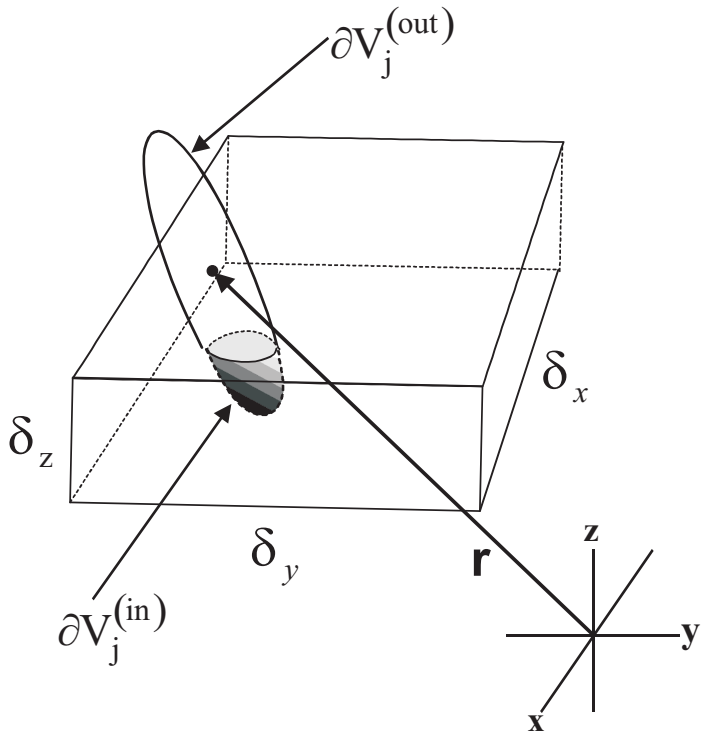

Figure 24: The rectangular volume element δV at position $\mathbf{r}$ intersects with the core of colloidal rod j with its position coordinate $\mathbf{r}_j$ outside the volume element. $\partial V^{(out)}$ is that part of the surface area ∂V_j of the rod that is outside the volume element, and $\partial V_j^{(in)}$ is the part inside.

a colloidal particle with its position coordinate outside the volume element (see fig.24). The instantaneous force that the colloidal particle exerts on the solvent inside the volume element is equal to,

$$-\int_{\partial V_j^{(in)}(\mathbf{r}_j,\hat{\mathbf{u}}_j)} d\mathbf{S}' \cdot \sigma(\mathbf{r}') \ .$$

Here, the surface area $\partial V_j^{(in)}$ is that part of the surface area of the colloidal particle that is inside the volume element (see fig.24). This range of integration depends both on the position $\mathbf{r}_j$ of colloidal particle j and its orientation $\hat{\mathbf{u}}_j$. Furthermore, $d\mathbf{S}'$ is the normal surface element on the surface area of the colloidal particle, and σ is the stress tensor of the solvent. The minus sign in eq.(245) arises from the fact that $d\mathbf{S}' \cdot \sigma(\mathbf{r}')$ is equal to $dS'\ \mathbf{f}^h(\mathbf{r}')$, with $\mathbf{f}^h(\mathbf{r}')$ the force per unit area that the fluid exerts on the surface element $d\mathbf{S}'$, which is minus the force that this surface element exerts on the fluid. In terms of this hydrodynamic force, eq.(245) is more conveniently written as,

$$-\int_{\partial V_j^{(in)}(\mathbf{r}_j,\hat{\mathbf{u}}_j)} dS'\ \mathbf{f}^h(\mathbf{r}') \ .$$

The ensemble averaged force $\mathbf{F}^{out}$ of all colloidal particles outside the volume element on the solvent inside the element, is thus equal to,

$$\mathbf{F}^{out} \;=\; - \,<\sum_{j=1}^{N}\,[1-\chi_{\mathbf{r}}(\mathbf{r}_j)]\,\oint_{\partial V_j(\mathbf{r}_j,\hat{\mathbf{u}}_j)} dS'\,\mathbf{f}^h(\mathbf{r}')\,\chi_{\mathbf{r}}(\mathbf{r}')>\,, \tag{245}$$

where, as before, $\chi_{\mathbf{r}}$ is the characteristic function of the volume element. The characteristic function $1-\chi_{\mathbf{r}}(\mathbf{r}_j)$ for the volume outside the volume element assures that in the summation over all colloidal particles, only those are counted which are outside the volume element. Furthermore, the characteristic function $\chi_{\mathbf{r}}(\mathbf{r}')$ assures that only points $\mathbf{r}'$ on the surface of the colloidal particle inside the volume element are taken into account. Including the characteristic function in the integrand in eq.(245) allows for the extension of the integration range to the entire surface area $\partial V_j(\mathbf{r}_j,\hat{\mathbf{u}}_j)$ of the j^{th} colloidal particle.

Similarly, in case a colloidal particle is located inside the volume element, that is, when $\mathbf{r}_j \in \delta V$, the instantaneous force that the colloidal particle exerts on the solvent outside the volume element is equal to,

$$-\int_{\partial V_j^{(out)}(\mathbf{r}_j,\hat{\mathbf{u}}_j)} dS'\,\mathbf{f}^h(\mathbf{r}')\;,$$

with $\partial V_j^{(out)}$ the part of the surface area of the colloidal particle located outside the volume element (see fig.24. This is minus the force that is exerted on the colloidal particle by the solvent outside the volume element. Hence, similarly as before, the ensemble averaged force $\mathbf{F}^{in}$ on the volume element due to interactions between solvent molecules outside and colloidal particles inside the volume element is found to be equal to,

$$\mathbf{F}^{in} \;=<\sum_{j=1}^{N}\chi_{\mathbf{r}}(\mathbf{r}_j)\,\oint_{\partial V_j(\mathbf{r}_j,\hat{\mathbf{u}}_j)} dS'\,\mathbf{f}^h(\mathbf{r}')\;[1-\chi_{\mathbf{r}}(\mathbf{r}')]>\,, \tag{246}$$

where it is used again that $1-\chi_{\mathbf{r}}(\mathbf{r}')$ is the characteristic function for the volume outside the volume element. From the representation (243) of the delta distribution it is thus found that,

$$\begin{aligned}\nabla\cdot\boldsymbol{\Sigma}^{ps} \;&=\; \lim_{\delta_x,\delta_y,\delta_z\to 0}\left[\mathbf{F}^{out}+\mathbf{F}^{in}\right]/\delta_x\,\delta_y\,\delta_z \qquad (247)\\ &=\; <\sum_{j=1}^{N}\delta(\mathbf{r}-\mathbf{r}_j)\,\mathbf{F}_j^h>\,-\,<\sum_{j=1}^{N}\oint_{\partial V_j(\mathbf{r}_j,\hat{\mathbf{u}}_j)} dS'\,\delta(\mathbf{r}-\mathbf{r}')\,\mathbf{f}^h(\mathbf{r}')\;>\,,\end{aligned}$$

where,

$$\mathbf{F}_j^h \;=\; \oint_{\partial V_j(\mathbf{r}_j,\hat{\mathbf{u}}_j)} dS'\,\mathbf{f}^h(\mathbf{r}')\;, \tag{248}$$

is the total force that the solvent exerts on the j^{th} colloidal particle.

The solvent-solvent stress tensor $\boldsymbol{\Sigma}^{ss}$

The force per unit volume that the solvent outside the volume element δV exerts on the solvent inside, for formally vanishing size of the volume element, is equal to,

$$\nabla\cdot\boldsymbol{\Sigma}^{ss} \;=\; \lim_{\delta_x,\delta_y,\delta_z\to 0}\frac{1}{\delta_x\,\delta_y\,\delta_z}<\int_{A_s} d\mathbf{S}'\cdot\sigma(\mathbf{r}')>\,, \tag{249}$$

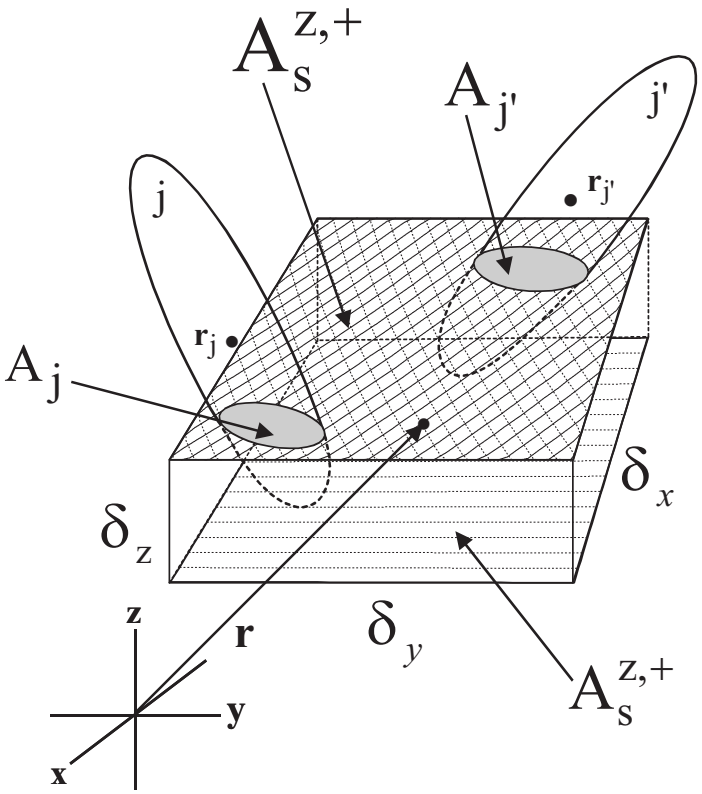

Figure 25: The part of the surface area $\partial\delta V$ of the volume element that is occupied by solvent is denoted as A_s. This is $\partial\delta V$ minus the areas A_j of intersection of $\partial\delta V$ with the core of colloidal rod j. The part of A_s on the upper z-side of the volume is denoted as $A_s^{z,+}$, and on the lower side as $A_s^{z,-}$.

where A_s is the part of the surface area of the volume element that is occupied by solvent, which is the surface area of the volume element minus the part that is cut by cores of colloidal particles (see fig.25). Here, $d\mathbf{S}'$ points outward of δV. The subscript "s" on the integration A_s refers to "solvent". For an incompressible solvent we have,

$$\sigma(\mathbf{r}') \;=\; \eta_0 \left[\nabla' \mathbf{v}(\mathbf{r}') + (\nabla' \mathbf{v}(\mathbf{r}'))^T \right] - p(\mathbf{r}')\, \hat{\mathbf{I}} \,, \tag{250}$$

with η_0 the solvent shear viscosity and $\mathbf{v}$ the solvent flow velocity. Furthermore, p is the mechanical pressure in the solvent, and $\hat{\mathbf{I}}$ is the identity tensor. The superscript "T" stands for the transpose of a tensor. Note that since $\nabla^2 p(\mathbf{r}) = 0$ within the incompressible solvent, p is entirely determined by the boundary conditions for the solvent flow imposed by surfaces of the colloidal particles and the container walls. Hence, $p(\mathbf{r}')$ depends implicitly on the position and orientations of all rods. Substitution of eq.(250) into eq.(249) leads to,

$$\nabla \cdot \mathbf{\Sigma}^{ss} \;=\; \mathbf{M}^{(1)} + \mathbf{M}^{(2)} \,, \tag{251}$$

where,

$$\mathbf{M}^{(1)} \equiv \lim_{\delta_x,\delta_y,\delta_z\to 0} \frac{\eta_0}{\delta_x\,\delta_y\,\delta_z} < \int_{A_s} d\mathbf{S}' \cdot \Big[\nabla'\mathbf{v}(\mathbf{r}') + (\nabla'\mathbf{v}(\mathbf{r}'))^T \Big] > , \tag{252}$$

and,

$$\mathbf{M}^{(2)} \equiv - \lim_{\delta_x,\delta_y,\delta_z\to 0} \frac{1}{\delta_x\,\delta_y\,\delta_z} < \int_{A_s} d\mathbf{S}'\, p(\mathbf{r}') > , \tag{253}$$

Consider first the contribution $\mathbf{M}^{(1)}$. We can rewrite the integral as,

$$< \int_{A_s} d\mathbf{S}' \cdot \big[\nabla'\mathbf{v}(\mathbf{r}') + (\nabla'\mathbf{v}(\mathbf{r}'))^T\big] > = < \left[\oint_{\partial\delta V} - \sum_{j=1}^{N} \int_{A_j} \right] d\mathbf{S}' \cdot \Big[\nabla'\mathbf{v}(\mathbf{r}') + (\nabla'\mathbf{v}(\mathbf{r}'))^T\Big] >, \tag{254}$$

where A_j is the area of intersection of the surface area $\partial\delta V$ of the volume element and the core of colloidal particle j (see fig.25). For a rigid colloidal particle, the velocity inside the core is given by,

$$\mathbf{v}(\mathbf{r}') \;=\; \mathbf{v}_j + \mathbf{\Omega}_j \times (\mathbf{r}' - \mathbf{r}_j) \;\;,\;\; \mathbf{r}' \in \text{core of particle } j \;, \tag{255}$$

where $\mathbf{v}_j$ is the translational velocity and $\mathbf{\Omega}_j$ the rotational velocity of colloidal particle j. Hence (with ϵ the Levi-Cevita tensor, and $\Omega_{j,p}$ the p^{th} component of $\mathbf{\Omega}_j$),

$$\nabla'_m\, v_n \;=\; \nabla_m \left[\, \mathbf{\Omega}_j \times (\mathbf{r}' - \mathbf{r}_j) \,\right]_n \;=\; \nabla'_m\, \epsilon_{npq}\, \Omega_{j,p}\, r'_q \;=\; \epsilon_{npm}\, \Omega_{j,p} \;,$$

where summation over repeated indices is assumed. From the anti-symmetry of the Levi-Cevita tensor, it is thus found that,

$$\int_{A_j} d\mathbf{S}' \cdot \Big[\nabla'\mathbf{v}(\mathbf{r}') + (\nabla'\mathbf{v}(\mathbf{r}'))^T \Big] \;=\; \mathbf{0} \;. \tag{256}$$

Using Gauss's integral theorem, we thus find from eqs.(254,256), for incompressible solvents,

$$< \int_{A_s} d\mathbf{S}' \cdot \Big[\nabla'\mathbf{v}(\mathbf{r}') + (\nabla'\mathbf{v}(\mathbf{r}'))^T \Big] > = < \int_{\delta V} d\mathbf{r}'\, \nabla'^2 \mathbf{v}(\mathbf{r}') > \;,$$

Hence, eq.(252) reduces to,

$$\mathbf{M}^{(1)} \;=\; \lim_{\delta_x,\delta_y,\delta_z\to 0} \frac{\eta_0}{\delta_x\,\delta_y\,\delta_z} < \int_{\delta V} d\mathbf{r}'\, \nabla'^2 \mathbf{v}(\mathbf{r}') > = \; \eta_0 < \nabla^2 \mathbf{v}(\mathbf{r}) > \;.$$

From eq.(238), it is thus finally found that,

$$\mathbf{M}^{(1)} \;=\; \eta_0\, \nabla^2 \mathbf{U}(\mathbf{r}, t) \;. \tag{257}$$

The contribution $\mathbf{M}^{(2)}$ can be expressed in terms of suspension properties as follows. Let $A_s^{z,+}$ denote the top-side of A_s, and similarly $A_s^{z,-}$ the lower-side, as indicated in fig.25. Furthermore, let $\hat{\mathbf{e}}_z$ denote the unit vector along the positive z-axis. Since the unit normal on $A_s^{z,+}$ is $\hat{\mathbf{e}}_z$ while the unit normal on $A_s^{z,-}$ is $-\hat{\mathbf{e}}_z$, the contribution $\mathbf{M}_z^{(2)}$ from the top- and lower-side of A_s to $\mathbf{M}^{(2)}$ is equal to,

$$\mathbf{M}_z^{(2)} \;=\; -\hat{\mathbf{e}}_z \lim_{\delta_x,\delta_y,\delta_z\to 0} \frac{1}{\delta_x\,\delta_y\,\delta_z} < \left[\int_{A_s^{z,+}} - \int_{A_s^{z,-}} \right] dS'\, p(\mathbf{r}') > \;.$$

For small sizes of the volume element, the scalar,

$$P^{ss}(\mathbf{r} + \tfrac{1}{2}\delta_z\,\hat{\mathbf{e}}_z, t) \;\equiv\; \frac{1}{\delta_x\,\delta_y} < \int_{A_s^{z,+}} dS'\,p(\mathbf{r}') > , \tag{258}$$

defines the contribution to the suspension pressure due solvent-solvent interactions at the position of the top-side of the volume element. A similar expression can be written down for P^{ss} at the lower-side. It thus follows that,

$$\mathbf{M}_z^{(2)} \;=\; -\hat{\mathbf{e}}_z \lim_{\delta_z \to 0} \frac{1}{\delta_z}\,[P^{ss}(\mathbf{r} + \tfrac{1}{2}\delta_z\,\hat{\mathbf{e}}_z, t) - P^{ss}(\mathbf{r} - \tfrac{1}{2}\delta_z\,\hat{\mathbf{e}}_z, t)] \;=\; -\hat{\mathbf{e}}_z\,\frac{\partial P^{ss}(\mathbf{r}, t)}{\partial z}\;.$$

In the same way the contribution to $\mathbf{M}^{(2)}$ from the left- and right-sides, and front- and backsides of the volume element are obtained. Adding these contributions leads to,

$$\mathbf{M}^{(2)} \;=\; -\nabla\,P^{ss}(\mathbf{r}, t)\;. \tag{259}$$

We thus find from eqs.(251,257,259) the following expression for the divergence of the stress tensor that arises from solvent-solvent interactions,

$$\nabla \cdot \boldsymbol{\Sigma}^{ss} \;=\; \eta_0\,\nabla^2\mathbf{U}(\mathbf{r}, t) - \nabla\,P^{ss}(\mathbf{r}, t)\;. \tag{260}$$

Note that P^{ss} is not just determined by boundary conditions when the suspension is inhomogeneous.

0.13.2 The total stress tensor

On the Smoluchowski time scale, as discussed before, the interaction force $\mathbf{F}_j$ in eq.(242) balances with the hydrodynamic force in eq.(248), that is,

$$\mathbf{F}_j + \mathbf{F}_j^h \;=\; \mathbf{0}\;. \tag{261}$$

The first term in eq.(247) for the particle-solvent stress thus cancels against the particle-particle stress in eq.(244). Adding eqs.(244,247,260) therefore leads to the following expression for the divergence of the total stress tensor,

$$\nabla \cdot \boldsymbol{\Sigma} \;=\; \eta_0\,\nabla^2\mathbf{U}(\mathbf{r}, t) - \nabla P^{ss}(\mathbf{r}, t) - \sum_{j=1}^{N} < \oint_{\partial V_j(\mathbf{r}_j, \hat{\mathbf{u}}_j)} dS'\,\delta(\mathbf{r} - \mathbf{r}')\,\mathbf{f}^h(\mathbf{r}') > \;. \tag{262}$$

This seemingly simple expression is valid for homogeneous suspensions as well as systems with large gradients in shear rate, concentration and orientational order parameter. Suspension properties should not vary significantly over distances equal to the thickness of the rods, but may vary significantly over distances equal to the length of the rods.

0.13.3 The stress tensor for homogeneous suspensions

Since $\mathbf{r}' \in \partial V_j$ in the integrand in eq.(262), the magnitude of $\mathbf{r}' - \mathbf{r}_j$ is never larger than the linear dimension of the rigid colloidal particles. Hence, for not too large gradients of suspension properties, the delta distribution $\delta(\mathbf{r} - \mathbf{r}')$ can be Taylor expanded around $\mathbf{r}' = \mathbf{r}_j$,

$$\delta(\mathbf{r} - \mathbf{r}') \;=\; \delta(\mathbf{r} - \mathbf{r}_j) + \sum_{n=1}^{\infty} \frac{1}{n!}\,(\mathbf{r}_j - \mathbf{r}')^n \odot \nabla^n \delta(\mathbf{r} - \mathbf{r}_j)\;,$$

where $(\mathbf{r}_j - \mathbf{r}')^n$ and ∇^n are polyadic products, and $\odot$ is the n-fold contraction of these two products. Substitution of this expansion into eq.(262) gives,

$$\nabla \cdot \mathbf{\Sigma} \;=\; \eta_0 \, \nabla^2 \mathbf{U}(\mathbf{r},t) - \nabla P^{ss}(\mathbf{r},t) - \sum_{j=1}^{N} < \delta(\mathbf{r}-\mathbf{r}_j)\, \mathbf{F}_j^h > \tag{263}$$

$$- \sum_{n=1}^{\infty} \frac{1}{n!} \nabla^n \sum_{j=1}^{N} < \delta(\mathbf{r}-\mathbf{r}_j) \odot \oint_{\partial V_j(\mathbf{r}_j,\hat{\mathbf{u}}_j)} dS' \, (\mathbf{r}_j - \mathbf{r}')^n \, \mathbf{f}^h(\mathbf{r}') > \; .$$

Consider a flow in the x-direction with its gradient in the y-direction (see fig.1a). Since all suspension properties, including the suspension flow velocity, do not vary on xz-planes, the stress tensor is a function of y only. Hence,

$$\nabla \cdot \mathbf{\Sigma}(\mathbf{r}) \;=\; \hat{\mathbf{e}}_2 \cdot \frac{d\mathbf{\Sigma}(y)}{dy} \; .$$

where $\hat{\mathbf{e}}_2$ is the unit vector in the y-direction. Since in a homogeneous system the force $< \delta(\mathbf{r}-\mathbf{r}_j)\, \mathbf{F}_j^h >$ on rod j at $\mathbf{r}$ is independent of $\mathbf{r}$, it follows that the contribution $\Delta\mathbf{\Sigma}$ to the stress tensor corresponding to the last term in the first line in eq.(263) is equal to,

$$\hat{\mathbf{e}}_2 \cdot \Delta\mathbf{\Sigma}(y) \;=\; -y \sum_{j=1}^{N} < \delta(\mathbf{r}-\mathbf{r}_j)\, \mathbf{F}_j^h > = \; - \hat{\mathbf{e}}_2 \cdot \sum_{j=1}^{N} < \delta(\mathbf{r}-\mathbf{r}_j)\, \mathbf{r}_j \, \mathbf{F}_j^h > \; .$$

Here, the integration constant is set equal to 0, since it does not contribute to the force on a given volume element, and is therefore irrelevant. Hence,

$$\Delta\mathbf{\Sigma} \;=\; -\sum_{j=1}^{N} < \delta(\mathbf{r}-\mathbf{r}_j)\, \mathbf{r}_j \, \mathbf{F}_j^h > \; . \tag{264}$$

In the last term in eq.(263), only the leading order gradient contribution is non-zero for homogeneous suspensions, so that,

$$\sum_{n=1}^{\infty} \frac{1}{n!} \nabla^n \sum_{j=1}^{N} < \delta(\mathbf{r}-\mathbf{r}_j) \odot \oint_{\partial V_j(\mathbf{r}_j,\hat{\mathbf{u}}_j)} dS' \, (\mathbf{r}_j - \mathbf{r}')^n \, \mathbf{f}^h(\mathbf{r}') > =$$

$$- \nabla \cdot \sum_{j=1}^{N} < \delta(\mathbf{r}-\mathbf{r}_j) \oint_{\partial V_j(\mathbf{r}_j,\hat{\mathbf{u}}_j)} dS' \, (\mathbf{r}' - \mathbf{r}_j)\, \mathbf{f}^h(\mathbf{r}') > \; . \tag{265}$$

From eqs.(263,264,265), the stress tensor is found to be equal to,

$$\mathbf{\Sigma} \;=\; \eta_0 \left[\nabla\mathbf{U} + (\nabla\mathbf{U})^T \right] - P^{ss}\, \hat{\mathbf{I}} - \sum_{j=1}^{N} < \delta(\mathbf{r}-\mathbf{r}_j)\, \mathbf{r}_j \, \mathbf{F}_j^h >$$

$$+ \sum_{j=1}^{N} < \delta(\mathbf{r}-\mathbf{r}_j) \oint_{\partial V_j(\mathbf{r}_j,\hat{\mathbf{u}}_j)} dS' \, (\mathbf{r}' - \mathbf{r}_j)\, \mathbf{f}^h(\mathbf{r}') > \; . \tag{266}$$

On volume averaging, one recovers the expression for the stress tensor as derived by Batchelor (1970) and later by Strating (1995) in different ways. Note that a divergence-less contribution to the stress tensor is of no significance, since the suspension flow velocity is determined solely by the body force that is equal to the divergence of the stress tensor.

0.13.4 Explicit evaluation of the stress tensor for very Long and thin rods

Within the bead model for the rods (see fig.3), the surface integral that appears in eq.(262) for the stress tensor can be written as a sum over beads as (with ∂V_α the surface area of bead α),

$$\oint_{\partial V_j(\mathbf{r}_j,\hat{\mathbf{u}}_j)} dS'\,\delta(\mathbf{r}-\mathbf{r}')\,\mathbf{f}^h(\mathbf{r}') \;=\; \sum_\alpha \delta(\mathbf{r}-\mathbf{r}_j-\alpha\,D\hat{\mathbf{u}}_j)\,\mathbf{F}^h_{j,\alpha}\;,$$

where $\mathbf{F}^h_{j,\alpha}$ is the force that the fluid exerts on the α'th bead of rod j. Hence,

$$\nabla\cdot\mathbf{\Sigma} \;=\; \eta_0\nabla^2\mathbf{U}(\mathbf{r},t) - \nabla P^{ss}(\mathbf{r},t) - \sum_{j=1}^{N}\sum_\alpha < \delta(\mathbf{r}-\mathbf{r}_j-\alpha\,D\,\hat{\mathbf{u}}_j)\,\mathbf{F}^h_{j,\alpha} > \;. \qquad (267)$$

In order to evaluate the summation over beads, an explicit expression for $\mathbf{F}^h_{j,\alpha}$ must be found. Consider the flow velocity $\mathbf{u}_{0,\alpha}$ of the fluid that would have existed in the absence of bead α. This velocity is equal to, according to eq.(18),

$$\mathbf{u}_{0,\alpha} \;=\; \mathbf{U}^\star_\alpha - \sum_{\beta\neq\alpha}\int_{\partial V_\beta} dS'\,\mathbf{T}(\mathbf{r}_\alpha-\mathbf{r}')\cdot\mathbf{f}^{h,\star}_\beta(\mathbf{r}')\;, \qquad (268)$$

where the $\star$ is used to indicate the absence of bead α. Here, $\mathbf{U}^\star$ is the fluid flow velocity at the position of bead α that is due to the presence of the remaining rods and the externally imposed flow field, in the absence of bead α. The force $\mathbf{f}^{h,\star}_\beta(\mathbf{r}')$ is the force per unit area that the fluid exerts on the surface element at $\mathbf{r}'$ on the surface ∂V_β of bead β, again in the absence of bead α. For very long and thin rods, the majority of beads β experience a flow and force that is only a little different from those in the absence of bead α. We shall therefore set $\mathbf{f}^{h,\star}_\beta$ equal to the actual force $\mathbf{f}^h_\beta$ in the presence of bead α. Within the bead model for the rod, eq.(268) then reads,

$$\mathbf{u}_{0,\alpha} \;=\; \mathbf{U}^\star_\alpha - \sum_{\beta\neq\alpha}\mathbf{T}(\mathbf{r}_\alpha-\mathbf{r}_\beta)\cdot\mathbf{F}^h_\beta\;, \qquad (269)$$

where, as before, $\mathbf{F}^h_\beta$ is the total force that the fluid exerts on bead β. When gradients in the fluid flow velocity $\mathbf{U}^\star_\alpha$, stemming from other rods and an externally imposed field, are negligible on the length scale equal to the thickness D of the rod, the force on bead α is simply equal to $\mathbf{F}^h_\alpha = -\gamma\,[\,\mathbf{v}_\alpha - \mathbf{u}_{0,\alpha}\,]$, where $\gamma = 3\pi\eta_0 D$ is the Stokes friction coefficient of a single bead and $\mathbf{v}_\alpha$ is the translational velocity of bead α. Hence, from eq.(269) and eq.(23) for the Oseen tensor,

$$\mathbf{F}^h_{j,\alpha} \;=\; -\gamma\,\left[\,\mathbf{v}_{j,\alpha} - \mathbf{U}^\star_{j,\alpha}\,\right] - \tfrac{3}{8}\,\left[\,\hat{\mathbf{I}} + \hat{\mathbf{u}}_j\,\hat{\mathbf{u}}_j\,\right]\cdot\sum_{\beta\neq\alpha}\frac{1}{\mid\alpha-\beta\mid}\,\mathbf{F}^h_{j,\beta}\;. \qquad (270)$$

Now consider summations of the form,

$$\sum_\alpha G(\alpha)\,\mathbf{F}^h_{j,\alpha}\;. \qquad (271)$$

Multiplying both sides of eq.(270) with $G(\alpha)$ and summing over α leads to,

$$\sum_{\alpha} G(\alpha)\mathbf{F}^{h}_{j,\alpha} = -\gamma \sum_{\alpha} G(\alpha)\left[\,\mathbf{v}_{j,\alpha} - \mathbf{U}^{\star}_{j,\alpha}\,\right] - \tfrac{3}{8}\left[\hat{\mathbf{I}} + \hat{\mathbf{u}}_j\,\hat{\mathbf{u}}_j\right]\cdot \sum_{\alpha}\sum_{\beta\neq\alpha} \frac{G(\alpha)}{\mid \alpha-\beta \mid}\,\mathbf{F}^{h}_{j,\beta}\ . \tag{272}$$

In appendix D it is shown that for specific functions $G(\alpha)$ it follows from the above relation that,

$$\sum_{\alpha} G(\alpha)\mathbf{F}^{h}_{j,\alpha} \;=\; -\tfrac{4}{3}\,\frac{\gamma}{\ln\{L/D\}}\,\left[\hat{\mathbf{I}} - \tfrac{1}{2}\,\hat{\mathbf{u}}_j\,\hat{\mathbf{u}}_j\right]\cdot \sum_{\alpha} G(\alpha)\,\left[\,\mathbf{v}_{j,\alpha} - \mathbf{U}^{\star}_{j,\alpha}\,\right]\ . \tag{273}$$

For the sum in eq.(267), the function $G(\alpha)$ is identified in appendix D, and the validity of eq.(272) for that particular $G(\alpha)$ is proven. Using this result in eq.(267) immediately leads to,

$$\begin{aligned}\nabla\cdot\mathbf{\Sigma} \;&=\; \eta_0\nabla^2\mathbf{U}(\mathbf{r},t) - \nabla P^{ss}(\mathbf{r},t) \\ &\quad + \tfrac{4}{3}\tfrac{\gamma}{\ln\{L/D\}} < \sum_{j=1}^{N}\left[\hat{\mathbf{I}} - \tfrac{1}{2}\hat{\mathbf{u}}_j\hat{\mathbf{u}}_j\right]\cdot\sum_{\alpha}\delta(\mathbf{r}-\mathbf{r}_j-\alpha\,D\hat{\mathbf{u}}_j)\left[\mathbf{v}_{j,\alpha}-\mathbf{U}^{\star}_{j,\alpha}\right] > \ .\end{aligned} \tag{274}$$

For each j, the ensemble average that involves the solvent velocity $\mathbf{U}^{\star}$, can be written as,

$$\begin{aligned}&< \left[\hat{\mathbf{I}} - \tfrac{1}{2}\hat{\mathbf{u}}_j\hat{\mathbf{u}}_j\right]\cdot\sum_{\alpha}\delta(\mathbf{r}-\mathbf{r}_j-\alpha\,D\hat{\mathbf{u}}_j)\mathbf{U}^{\star}_{j,\alpha} > \;\; = \\ &\qquad \int d\mathbf{r}_j \oint d\hat{\mathbf{u}}_j\, P(\mathbf{r}_j,\hat{\mathbf{u}}_j,t)\,\left[\hat{\mathbf{I}} - \tfrac{1}{2}\hat{\mathbf{u}}_j\hat{\mathbf{u}}_j\right]\cdot\sum_{\alpha}\delta(\mathbf{r}-\mathbf{r}_j-\alpha\,D\hat{\mathbf{u}}_j) < \mathbf{U}^{\star}_{j,\alpha} >^{(c)}\ ,\end{aligned}$$

where $< \cdots >^{(c)}$ denotes ensemble averaging with respect to the conditional pdf $P^{(c)}$ of $\{\mathbf{r}_1,\cdots,\mathbf{r}_{j-1},\mathbf{r}_{j+1},\cdots,\mathbf{r}_N,\hat{\mathbf{u}}_2,\cdots,\hat{\mathbf{u}}_{j-1},\hat{\mathbf{u}}_{j+1},\cdots,\hat{\mathbf{u}}_N\}$ for prescribed $\mathbf{r}_j$ and $\hat{\mathbf{u}}_j$, which is equal to,

$$\begin{aligned}P^{(c)}(\mathbf{r}_1,\cdots,\mathbf{r}_{j-1},\mathbf{r}_{j+1},\cdots,\mathbf{r}_N,\hat{\mathbf{u}}_1,\cdots,\hat{\mathbf{u}}_{j-1},\hat{\mathbf{u}}_{j+1},\cdots,\hat{\mathbf{u}}_N\,|\,\mathbf{r}_j,\hat{\mathbf{u}}_j,t) \;&\equiv \\ P(\mathbf{r}_1,\cdots,\mathbf{r}_N,\hat{\mathbf{u}}_1,\cdots,\hat{\mathbf{u}}_N,t)/P(\mathbf{r}_1,\hat{\mathbf{u}}_1,t)\ .&\end{aligned}$$

We can thus rewrite the eq.(267) for the divergence of the stress tensor as,

$$\begin{aligned}\nabla\cdot\mathbf{\Sigma} \;&=\; \eta_0\nabla^2\mathbf{U}(\mathbf{r},t) - \nabla P^{ss}(\mathbf{r},t) + \tfrac{4}{3}\tfrac{\gamma}{\ln\{L/D\}}\frac{1}{N}\sum_{j=1}^{N}\int d\mathbf{r}_j\oint d\hat{\mathbf{u}}_j\,\rho(\mathbf{r}_j,\hat{\mathbf{u}}_j,t) \\ &\qquad \left[\hat{\mathbf{I}} - \tfrac{1}{2}\hat{\mathbf{u}}_j\hat{\mathbf{u}}_j\right]\cdot\sum_{\alpha}\delta(\mathbf{r}-\mathbf{r}_j-\alpha\,D\hat{\mathbf{u}}_j)\left[\mathbf{v}_{j,\alpha} - < \mathbf{U}^{\star}_{j,\alpha} >^{(c)}\right]\ ,\end{aligned} \tag{275}$$

where $\rho(\mathbf{r},\hat{\mathbf{u}},t)$ is the density of rods with orientation $\hat{\mathbf{u}}$ at position $\mathbf{r}$,

$$\rho(\mathbf{r},\hat{\mathbf{u}},t) \;=\; N\,P(\mathbf{r},\hat{\mathbf{u}},t)\ . \tag{276}$$

The conditional ensemble average $< \mathbf{U}^{\star}_{j,\alpha} >^{(c)}$ is the contribution to the solvent flow velocity at the position of bead α of rod j, in the absence of that bead, that originates from the presence of other rods and the externally imposed flow, averaged over the positions and orientations of all other rods with a prescribed position and orientation of rod j. This average is to a good

approximation equal to the suspension flow velocity $\mathbf{U}_{j,\alpha}$ at the position of bead α of rod j, that is,

$$< \mathbf{U}^{\star}_{j,\alpha} >^{(c)} = \mathbf{U}_{j,\alpha} \; . \tag{277}$$

Using that the bead velocity is given by,

$$\mathbf{v}_{j,\alpha} \; = \; \mathbf{v}_j + \alpha \, D \, \mathbf{\Omega}_j \times \hat{\mathbf{u}}_j \; , \tag{278}$$

together with eqs.(170,166) for the translational and rotational velocity of a rod, eq.(275) for the divergence of the stress tensor thus leads to (mathematical details are given in appendix E),

$$\begin{aligned}
\nabla \cdot \mathbf{\Sigma}(\mathbf{r},t) \;\; &= \;\; \eta_0 \nabla^2 \mathbf{U}(\mathbf{r},t) - \nabla P^{ss}(\mathbf{r},t) \\
&\quad + \tfrac{k_B T}{L^2} \oint d\hat{\mathbf{u}} \int_{-L/2}^{L/2} dx \left\{ 12 \frac{x}{L} \, \hat{\mathbf{u}} \times \Big[\hat{\mathcal{R}} \rho(\mathbf{r} - x\hat{\mathbf{u}}_0, \hat{\mathbf{u}}, t) \Big]_{\hat{\mathbf{u}}_0 = \hat{\mathbf{u}}} - L \nabla \rho(\mathbf{r} - x\hat{\mathbf{u}}, \hat{\mathbf{u}}, t) \right\} \\
&+ \tfrac{2D \, k_B T}{L^2} \oint d\hat{\mathbf{u}} \oint d\hat{\mathbf{u}}' \int_{-L/2}^{L/2} dx \int_{-L/2}^{L/2} dl \int_{-L/2}^{L/2} dl' \; \rho(\mathbf{r} - x\hat{\mathbf{u}}, \hat{\mathbf{u}}, t) \\
&\left\{ 12 \, \frac{x}{L} \, \hat{\mathbf{u}} \times \Big[\hat{\mathcal{R}} \, | \, \hat{\mathbf{u}} \times \hat{\mathbf{u}}' \, | \, \rho(\mathbf{r} - x\hat{\mathbf{u}}_0 - l\hat{\mathbf{u}} - l'\hat{\mathbf{u}}', \hat{\mathbf{u}}', t) \Big]_{\hat{\mathbf{u}}_0 = \hat{\mathbf{u}}} - \, | \, \hat{\mathbf{u}} \times \hat{\mathbf{u}}' \, | \, L \nabla \rho(\mathbf{r} - (x+l)\hat{\mathbf{u}} - l'\hat{\mathbf{u}}', \hat{\mathbf{u}}', t) \right\} \\
&+ \tfrac{4\pi\eta_0}{L \, \ln\{L/D\}} \oint d\hat{\mathbf{u}} \int_{-L/2}^{L/2} dx \int_{-L/2}^{L/2} dx' \, \rho(\mathbf{r} - x\hat{\mathbf{u}}, \hat{\mathbf{u}}, t) \\
&\qquad \Big[\hat{\mathbf{I}} - \tfrac{1}{2} \hat{\mathbf{u}}\hat{\mathbf{u}} \Big] \cdot \left\{ \mathbf{U}(\mathbf{r} + (x' - x)\hat{\mathbf{u}}, t) - \mathbf{U}(\mathbf{r}, t) - 12 \frac{x \, x'}{L^2} \hat{\mathbf{u}} \times [\hat{\mathbf{u}} \times \mathbf{U}(\mathbf{r} + (x' - x)\hat{\mathbf{u}}, t)] \right\} \; .
\end{aligned} \tag{279}$$

Here, summations over bead indices α and β are replaced by integrals with respect to x and x', respectively (see eqs.(321,324) in appendix E). The notation $\Big[\hat{\mathcal{R}}(\cdots) \Big]_{\hat{\mathbf{u}}_0 = \hat{\mathbf{u}}}$ is used to indicate that the differentiation with respect to $\hat{\mathbf{u}}$ should be performed first, after which $\hat{\mathbf{u}}_0$ should be taken equal to $\hat{\mathbf{u}}$.

The first two contributions to the stress tensor are solvent contributions. The third term stems from Brownian forces, the fourth term from direct interactions, while the last term accounts for the suspension flow.

Contrary to commonly used expressions for the stress tensor for inhomogeneous suspensions, eq.(279) contains convolution-type integrals. An expression that is similar to commonly used expressions for the stress tensor is obtained by gradient expanding the convolution-type integrals and truncating this expansion after the fourth order in ∇-contributions. Such a truncation is expected to work only when gradients are not very large. Our expression (279) for the divergence of the stress tensor, however, is valid even in the presence of large gradients.

0.13.5 The stress tensor for a homogeneous system expressed in terms of the order parameter

For a homogeneous system, where the concentration, the orientational order parameter and the shear rate are independent of position, the probability density function ρ in the integrals in

eq.(279) can be gradient expanded up to leading order in gradients that survives the convolution type of integrals. For example,

$$\rho(\mathbf{r}-x\hat{\mathbf{u}},\hat{\mathbf{u}},t) \;=\; \rho(\mathbf{r},\hat{\mathbf{u}},t)-x\,\hat{\mathbf{u}}\cdot\nabla\rho(\mathbf{r},\hat{\mathbf{u}},t)+\tfrac{1}{2}\,x^2\,\hat{\mathbf{u}}\hat{\mathbf{u}}:\nabla\nabla\,\rho(\mathbf{r},\hat{\mathbf{u}},t)+"\mathcal{O}(\nabla^3)"\;. \tag{280}$$

Using the same Ginzburg-Landau expansion (217) as before, a lengthy but straightforward calculation leads to the following expression for the stress tensor (where the fourth order tensor $\mathbf{S}^{(4)}$ is defined in eq.(220)),

$$\boldsymbol{\Sigma} \;=\; -P\,\hat{\mathbf{I}}+\boldsymbol{\Sigma}_D\;, \tag{281}$$

with $\boldsymbol{\Sigma}_D$ the deviatoric part of the stress tensor,

$$\begin{aligned}\boldsymbol{\Sigma}_D \;&=\; 2\,\eta_0\,\dot\gamma\,\hat{\mathbf{E}}\;+\\ &3\,\bar\rho k_BT\left[\mathbf{S}-\tfrac{1}{3}\hat{\mathbf{I}}+\tfrac{L}{D}\varphi\left\{\mathbf{S}^{(4)}:\mathbf{S}-\mathbf{S}\cdot\mathbf{S}\right\}+\tfrac{1}{6}\,Pe_r\left\{\mathbf{S}^{(4)}:\hat{\mathbf{E}}-\tfrac{1}{3}\,\hat{\mathbf{I}}\,\mathbf{S}:\hat{\mathbf{E}}\right\}\right]\;,\end{aligned} \tag{282}$$

where eq.(169) for D_r has been used. Here, $\bar\rho = N/V$ is the number density of the homogeneous system, $\varphi = \frac{\pi}{4}D^2L\bar\rho$ is the volume fraction of rods, and $Pe_r = \dot\gamma/D_r$ is the same *bare rotational Peclet number* that we encountered before. The tensor $\hat{\mathbf{E}}$ is, as before, equal to $\mathbf{E}/\dot\gamma$. Furthermore,

$$P \;=\; P^{ss}+\bar\rho\,k_BT\left[1+\tfrac{5}{4}\,\tfrac{L}{D}\varphi\,\{1-\tfrac{3}{5}\,\mathbf{S}:\mathbf{S}\}-\tfrac{1}{6}\,Pe_r\,\mathbf{S}:\hat{\mathbf{E}}\right]. \tag{283}$$

is the pressure.

The first term $\mathbf{S}-\frac{1}{3}\hat{\mathbf{I}}$ stems from the Brownian contribution in eq.(279), the second term $\sim \frac{L}{D}$ from the direct interaction terms, and the term $\sim Pe_r$ from the suspension flow terms.

Note that from eq.(219), using the expression (169) for D_r, the deviatoric stress tensor can be rewritten more elegantly as,

$$\boldsymbol{\Sigma}_D = 2\,\eta_0\,\dot\gamma\,\left[\hat{\mathbf{E}}+\frac{(L/D)^2}{3\ln\{L/D\}}\,\varphi\left\{\hat{\boldsymbol{\Gamma}}\cdot\mathbf{S}+\mathbf{S}\cdot\hat{\boldsymbol{\Gamma}}^T-\mathbf{S}^{(4)}:\hat{\mathbf{E}}-\tfrac{1}{3}\,\hat{\mathbf{I}}\,\mathbf{S}:\hat{\mathbf{E}}-\frac{1}{\dot\gamma}\frac{d\mathbf{S}}{dt}\right\}\right]\;. \tag{284}$$

This form makes the proportionality of the stress tensor with the shear-rate more explicit.

A similar expression for the stress tensor has been derived by Doi and Edwards (1978a), Doi and Edwards (1978b), Doi (1981), Kuzuu and Doi (1983) and Marrucci and Maffettone (1989). For non-interacting rods, that is, for $\frac{L}{D}\varphi = 0$, Hinch and Leal (1976) found a constitutive relation similar to eq.(284) by interpolating between known expressions for low and high shear-rates.

0.14 Viscoelastic Response Functions

In the present section we shall analyze the viscous behaviour of rod suspensions on the basis of the equation of motion (219) for $\mathbf{S}(t)$ and the Navier-Stokes equation with eq.(284) for

the stress tensor (together with the closure relation (227)). The equations (219) and (284) are quite similar to those derived on the basis of phenomenological arguments by Doi and Edwards (1978a), Doi and Edwards (1978b), Doi (1981), Kuzuu and Doi (1983) and Doi and Edwards (1986). We shall refer to this latter theory as the DEK-theory, where DEK stands for "Doi, Edwards, Kuzuu". Our predictions will be compared to those of the DEK-theory.

The DEK theory appears in literature in various forms. Sometimes an effective rotational diffusion coefficient is used in the Smoluchowski equation and the equation of motion (219) instead of the bare diffusion coefficient D_r. This effective diffusion coefficient is calculated independently as a function of the order parameter and concentration. The present approach shows that this is not correct : the bare diffusion coefficient should be used in the equation of motion (219) and expressions (282,284) for the stress tensor. Interactions between rods are explicitly accounted for in these expressions. Sometimes the interaction contributions are omitted, and the above mentioned effective diffusion coefficient is used. The effective diffusion coefficient is then assumed to account for interactions between rods. Either the interaction contributions are kept as they stand and the bare diffusion coefficient is used, or the interaction contributions are omitted and an effective diffusion coefficient should be used.

Viscoelastic response functions will be discussed both for low shear rates, where analytic expressions can be derived, and high shear rates, where numerical results will be given. For higher shear rates, shear thinning curves and non-linear oscillatory response functions will be discussed. These results will be compared to other theories, computer simulations and experiments. A remarkable feature is that the shear viscosity is predicted to vary linear with concentration up to the isotropic-nematic phase transition, which is confirmed by computer simulations. Comparing theory with experimental data on fd-virus suspensions, it turns out that a slight degree of flexibility has a large effect on viscoelastic response functions.

0.14.1 Shear viscosity and normal stresses for low shear-rates

In order to obtain analytic results for the leading order shear rate dependence of the zero-frequency shear viscosity and normal stress differences, the orientational order parameter tensor is expanded up to third power in the shear rate,

$$\mathbf{S} \;=\; \tfrac{1}{3}\,\hat{\mathbf{I}} + \dot\gamma\,\Delta\mathbf{S}_1 + \dot\gamma^2\,\Delta\mathbf{S}_2 + \dot\gamma^3\,\Delta\mathbf{S}_3 + \cdots\;. \tag{285}$$

Substitution of this expansion into the stationary form of the equation of motion (219) and noting that $\hat{\mathbf{I}} : \Delta\mathbf{S}_j = 0$, a straightforward but somewhat lengthy calculation leads to the following expressions for the $\Delta\mathbf{S}_j$'s,

$$\begin{aligned}
\dot\gamma\,\Delta\mathbf{S}_1 &= \frac{1}{15}\frac{\dot\gamma}{D_r^{eff}}\,\hat{\mathbf{E}}\,,\\
\dot\gamma^2\,\Delta\mathbf{S}_2 &= \frac{1}{450}\left(\frac{\dot\gamma}{D_r^{eff}}\right)^2\left[\begin{pmatrix}3&0&0\\0&-2&0\\0&0&-1\end{pmatrix} + \frac{1}{10}\frac{D_r}{D_r^{eff}}\,\frac{L}{D}\,\varphi\begin{pmatrix}1&0&0\\0&1&0\\0&0&-2\end{pmatrix}\right],\\
\dot\gamma^3\,\Delta\mathbf{S}_3 &= \frac{1}{1125}\left(\frac{\dot\gamma}{D_r^{eff}}\right)^3\left[-\frac{7}{3} + \frac{3}{10}\frac{D_r}{D_r^{eff}}\,\frac{L}{D}\,\varphi + \frac{1}{50}\left(\frac{D_r}{D_r^{eff}}\,\frac{L}{D}\,\varphi\right)^2\right]\hat{\mathbf{E}}\,.
\end{aligned} \tag{286}$$

The concentration dependent, effective rotational diffusion coefficient D_r^{eff} is given in eq.(230).

As can be seen from the above expressions, the actual expansion parameter is *the dressed rotational Peclet number*,

$$Pe_r^{eff} \;=\; \dot{\gamma}/D_r^{eff} \;. \tag{287}$$

The expansion (285) is therefore valid only when $\dot{\gamma}/D_r^{eff}$ is small. For concentrations close to the spinodal line, where D_r^{eff} is much smaller than the free rotational diffusion coefficient D_r, the shear-rate should be equally smaller in order for the expansion (285) to be valid. Substitution of eqs.(286) into eq.(284) for the deviatoric part of the stress tensor leads to,

$$\mathbf{\Sigma}_D \;=\; 2\,\eta^{eff}\,\dot{\gamma}\,\hat{\mathbf{E}} + \eta_0\,\frac{1}{120}\,\frac{\dot{\gamma}^2}{D_r^{eff}}\,\alpha\,\varphi \begin{pmatrix} 19 & 0 & 0 \\ 0 & -11 & 0 \\ 0 & 0 & -8 \end{pmatrix}, \tag{288}$$

where the coefficient α is equal to,

$$\alpha \;=\; \frac{8}{45}\,\frac{(L/D)^2}{\ln\{L/D\}} \;, \tag{289}$$

and the suspension shear viscosity η^{eff} is found to be equal to,

$$\eta^{eff} \;=\; \eta_0 \left[1 + \left\{ 1 - \frac{1}{50}\left(\frac{\dot{\gamma}}{D_r^{eff}}\right)^2 \right\} \alpha\,\varphi + \frac{1}{1500}\,\frac{\dot{\gamma}^2\,D_r}{\left(D_r^{eff}\right)^3}\,\alpha\,\frac{L}{D}\,\varphi^2 \right], \tag{290}$$

up to second order in the shear-rate. Expanding the dressed Peclet number with respect to the concentration yields, up to second order in concentration,

$$\eta^{eff} \;=\; \eta_0 \left[1 + \left\{ 1 - \frac{1}{50}\left(\frac{\dot{\gamma}}{D_r}\right)^2 \right\} \alpha\,\varphi - \frac{11}{1500}\left(\frac{\dot{\gamma}}{D_r}\right)^2 \alpha\,\frac{L}{D}\,\varphi^2 \right]. \tag{291}$$

Note that the Huggins coefficient vanishes at zero shear-rates. There is a non-zero Huggins coefficient at zero shear-rates when hydrodynamic interactions would have been taken into account. As discussed before, hydrodynamic interactions are not so important for the very long and thin rods under consideration here.

For zero shear-rate, eq.(291) for the effective viscosity is the rigid-rod analogue of Einstein's equation $\eta^{eff} = \eta_0[1 + \frac{5}{2}\varphi]$ for the viscosity of very dilute suspensions of spheres. Note, however, that eq.(291) is valid also for larger concentrations. That is, higher order concentration contributions to the zero shear viscosity are absent. This linear concentration dependence of the zero shear suspension viscosity is the result of the use of the form (208) for the pair-correlation function and the neglect of hydrodynamic interactions. As will be seen later in this section, such a linear concentration dependence is also seen in computer simulations for very long and thin rods.

Normal stress differences due to a weak shear flow follow immediately from eq.(288) as,

$$\begin{aligned} N_1 \;&\equiv\; \Sigma_{11} - \Sigma_{22} \;=\; \eta_0\,\frac{1}{4}\,\frac{\dot{\gamma}^2}{D_r^{eff}}\,\alpha\,\varphi \;, \\ N_2 \;&\equiv\; \Sigma_{22} - \Sigma_{33} \;=\; -\,\eta_0\,\frac{1}{40}\,\frac{\dot{\gamma}^2}{D_r^{eff}}\,\alpha\,\varphi \;. \end{aligned} \tag{292}$$

Note that $\alpha\,\varphi$ can be large for very long and thin rods, even at low volume fractions φ, so that normal stress differences are predicted to be quite significant.

Expressions for linear response functions to oscillatory shear flow can be obtained by substitution of,

$$\mathbf{S}(t) \;=\; \tfrac{1}{3}\,\hat{\mathbf{I}} + \dot{\gamma}_0\,[\;\Delta\mathbf{S}_c\;\cos\{\omega t\} + \Delta\mathbf{S}_s\;\sin\{\omega t\}\;]\;, \tag{293}$$

into the equation of motion (219). Linearization with respect to the in- and out-of-phase response functions $\Delta\mathbf{S}_c$ and $\Delta\mathbf{S}_s$, respectively, keeping only linear terms in $\dot{\gamma}_0$, and using eq.(6) for the shear rate $\dot{\gamma}$, one readily finds in dimensionless form,

$$\mathbf{S}(t) \;=\; \frac{1}{3}\,\hat{\mathbf{I}} + \frac{2}{5}\,\frac{\dot{\gamma}_0}{\omega}\,F(\Omega^{eff}/6)\,\big[\,\cos\{\omega t\} + \tfrac{1}{6}\Omega^{eff}\;\sin\{\omega t\}\,\big]\;\hat{\mathbf{E}}\;, \tag{294}$$

where,

$$F(x) \;\equiv\; \frac{x}{1+x^2} \quad , \quad \text{and} \quad , \quad \Omega^{eff} \;=\; \omega/D_r^{eff}\;. \tag{295}$$

The dimensionless frequency Ω^{eff} is a dressed, concentration dependent *rotational Deborah number*. Substitution of eqs.(294,295) into eq.(284) for the stress tensor, gives,

$$\mathbf{\Sigma}_D \;=\; 2\,\dot{\gamma}_0\hat{\mathbf{E}}\,[\;\eta'\;\cos\{\omega t\} + \eta''\;\sin\{\omega t\}\;]\;, \tag{296}$$

where the dissipative and storage shear viscosity are respectively equal to,

$$\begin{aligned}
\eta' \;&=\; \eta_0\;\left[1 + \left(\frac{1}{4} + \frac{9}{2}\,\frac{F(\Omega^{eff}/6)}{\Omega^{eff}}\right)\;\alpha\,\varphi\right]\;, \\
\eta'' \;&=\; \eta_0\;\frac{3}{4}\,F(\Omega^{eff}/6)\;\alpha\,\varphi\;.
\end{aligned} \tag{297}$$

To leading order in shear-rate, we thus find a Maxwellian behaviour of the viscoelastic response function, with a concentration dependent relaxation time that is set by the effective rotational diffusion coefficient. Note that,

$$\frac{\eta^{eff} - \eta_\infty^{eff}}{\eta_0} \;=\; \frac{3}{4}\,\alpha\,\varphi \;=\; 6\,\lim_{\Omega\to\infty}\,\frac{\eta''}{\Omega^{eff}}\;. \tag{298}$$

where $\eta^{eff} = \eta_0[\,1 + \alpha\,\varphi\,]$ shear viscosity (291) at zero shear rate, and $\eta_\infty^{eff} \equiv \eta'(\Omega^{eff} \to \infty)$ is the high frequency, zero shear-rate viscosity. These are relationships that could be tested experimentally. As before, the predicted linear concentration dependence in eq.(297) should hold over the entire concentration regime (up to the isotropic-nematic phase transition concentration), and could serve as an experimental test for the validity of the approximation (208) for the pair-correlation function.

0.14.2 Viscoelastic response at high shear-rates

For larger shear-rates no analytical results can be obtained in view of the complexity of the equation of motion (219). Instead, eq.(219) must be time-integrated numerically, either with a stationary or an oscillating shear-rate, until transients have relaxed. The resulting solution is substituted into eq.(284) for the stress tensor, from which viscoelastic response functions can be deduced.

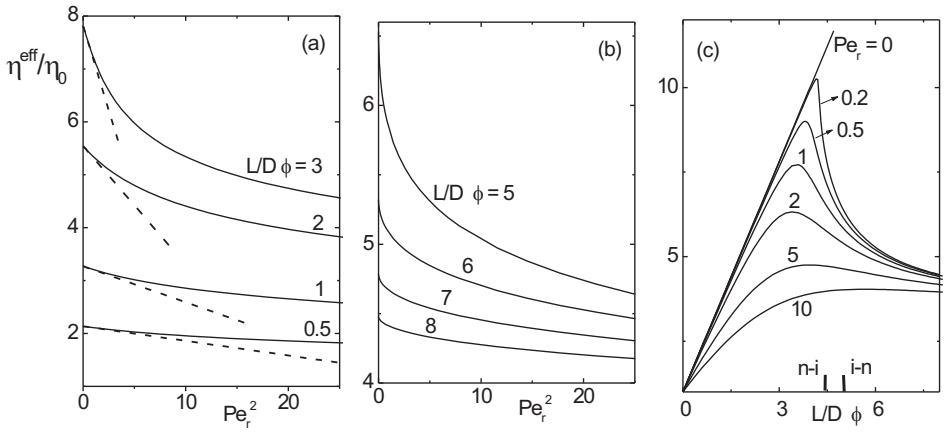

Figure 26: (a) The suspension viscosity η^{eff} for the otherwise isotropic state, normalized with the solvent shear viscosity η_0, as a function of the squared Peclet number for several concentrations, as indicated in the figure. The dashed lines correspond to the low shear-rate expansion (290). Here, and in the other figures, $L/D = 50$. (b) The same as (a) for the nematic state. (c) The shear viscosity as a function of the concentration for various shear-rates, as indicated in the figure. The isotropic-to-nematic and nematic-to-isotropic spinodal concentrations are also indicated.

The dimensionless numbers on which stress response functions under stationary shear flow conditions depends are $\frac{L}{D}$, $\frac{L}{D}\varphi$, and the bare rotational Peclet number (189) for dilute systems or the dressed Peclet number (287) for strongly interacting systems. As will turn out, under oscillatory shear flow, the same Peclet numbers are of interest, except that the shear-rate is replaced by the shear-amplitude $\dot{\gamma}_0$ in eq.(6). The frequency dependence is expressed in terms the dressed Deborah number in eq.(295) or the bare Deborah number,

$$\Omega \; = \; \omega / D_r \; . \tag{299}$$

Numerical results are shown here for $\frac{L}{D} = 50$ as functions of the other dimensionless numbers : essential features of viscoelastic response functions do not depend on the aspect ratio for aspect ratios larger than about 10.

In figs.26a,b, the suspension viscosity is plotted as a function of the squared rotational Peclet number for various concentrations, both in the otherwise isotropic phase (in fig.26a) and for the nematic state (in fig.26b). The dashed lines in fig.26a correspond to the small Peclet number expansion (290). The range of validity of this expansion is seen to decrease for larger concentrations. The reason for this is that eq.(290) is actually an expansion with respect to the dressed rotational Peclet number (287), while the effective rotational diffusion coefficient (230) becomes smaller on approach of the isotropic-to-nematic spinodal point. Note that for a nematic there seems to be no regime at small shear-rates where the viscosity varies linearly with $\dot{\gamma}^2$, contrary to a paranematic. Furthermore, the suspension viscosity of a nematic

decreases with increasing concentration : the rise in stress on adding rods is smaller than its decrease due to the increase of degree of orientational order. In fig.26c, the dependence of the viscosity on concentration is shown for various shear-rates. For shear-rates close to the critical shear-rate $Pe_r = 0.159\cdots$, the viscosity sharply decreases with increasing concentration due to the sharp increase of the degree of alignment as the corresponding branch in the bifurcation diagram fig.19a is traced. For shear-rates below the critical shear-rate, the curves in fig.26c develop discontinuous jumps. Such jumps are probably of no experimental relevance, since phase separation will occur during an experiment. In the limit of zero shear-rate, the viscosity depends linearly on concentration (see eq.(290) with $\dot{\gamma} = 0$).

The normal stress differences N_1 and N_2 (normalized with $\eta_0\,\dot{\gamma}$), are plotted as functions of the shear-rate for various concentrations in figs.27a and b, respectively, for the paranematic state and in figs.27c and d for the nematic state. The dashed lines in figs.27a,b correspond to the low shear-rate expansions (292). Note the strong shear-rate dependencies in the otherwise isotropic state. As for the suspension viscosity, absolute values of normal stress differences for the nematic decrease on increasing the concentration. In figs.27e and f, the normal stress differences are given as functions of the concentrations for various shear-rates. The dashed lines correspond, as before, to the low shear-rate expansions (292). For the same reason as with the suspension viscosity discussed above, there is a very strong concentration dependence for shear-rates close to the critical shear-rate.

0.14.3 Non-linear viscoelastic response

Dynamic response functions can be obtained from a Fourier analysis of the time dependence of eq.(284) for the stress tensor after substitution of solutions of eq.(219) under oscillatory shear flow, when transients have relaxed. The frequency dependence of η' and η'' for the otherwise isotropic state are given in figs.28a,b, respectively, for various values of the Peclet number,

$$Pe_{r,0} \;=\; \dot{\gamma}_0/D_r \;, \tag{300}$$

where $\dot{\gamma}_0$ is the shear-amplitude as defined in eq.(6). Response functions are plotted as functions of the dimensionless bare Deborah number (299). The dashed curves correspond to the leading Peclet number expansions (297). As soon as $Pe_{r,0} > 1$ (or rather, $Pe^{eff}_{r,0} = \dot{\gamma}_0/D^{eff}_r > 1$), there are deviations from the leading order expansions (297). Higher order, non-linear response functions now come into play as well. For these higher shear-amplitudes, the time dependent stress tensor can be Fourier expanded as,

$$\mathbf{\Sigma}_D \;=\; 2\,\dot{\gamma}_0\,\hat{\mathbf{E}}\,\sum_{n=0}^{\infty}\,[\;\eta'_n\;\cos\{n\omega t\} + \eta''_n \sin\{n\omega t\}\;]\;. \tag{301}$$

where η'_0 and η''_0 are henceforth simply denoted as η' and η'', respectively. The non-linear dissipative- and elasticity response functions η'_n and η''_n are plotted for $n = 3$ and 5 in figs.28c-f, for the paranematic state. The response functions for even n are zero. The non-linear response functions exhibit oscillatory behaviour as functions of the frequency. Note the very different frequency dependence of third and fifth order functions. Except for the maximum in η''_3, the third order response functions behave qualitatively similar to those for near-critical

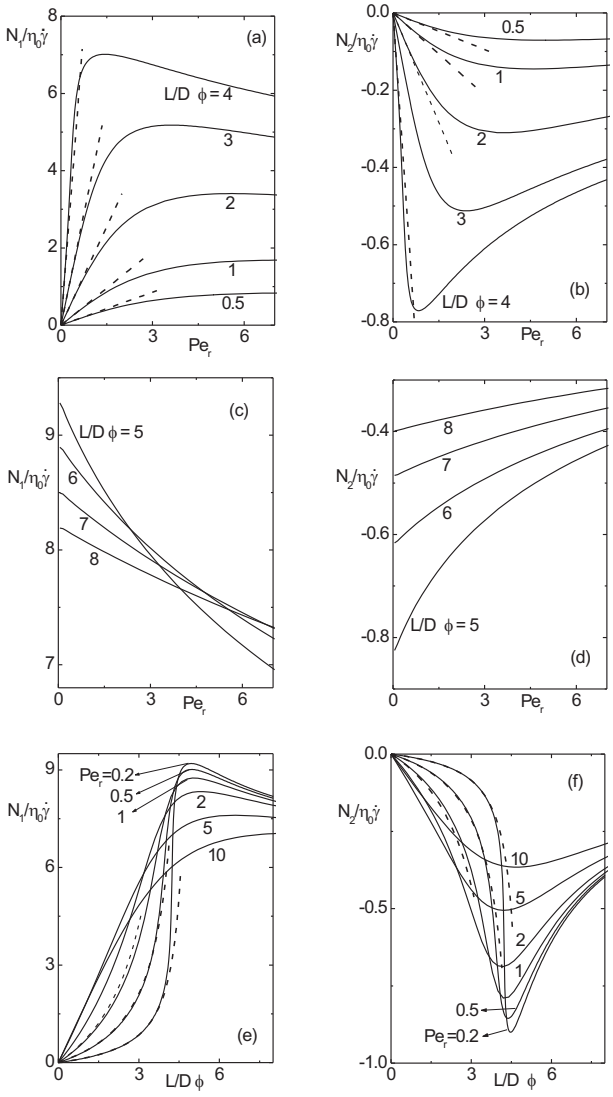

Figure 27: (a) The normal stress difference N_1 for the otherwise isotropic state, normalized by $\eta_0\dot{\gamma}$ as a function of shear-rate for various concentrations, as indicated in the figure. The dashed lines correspond to the low shear-rate expansion (292). Here, and in the other figures, $L/D = 50$. (b) The same as in (a) for the normal stress difference N_2. The dashed lines correspond to the expansion (292). (c) The same as in (a) for the nematic state. (d) The same as in (b) for the nematic state. (e) The normal stress difference N_1 as a function of concentration for various shear-rates, as indicated in the figure. The dashed lines correspond to the low shear-rate expansion (292). (f) The same as in (e) for the normal stress difference N_2. The dashed lines correspond to the low shear-rate expansion (292).

systems of spherical colloids (see Dhont and Nägele (1998)). The corresponding response functions for the nematic state are given in figs.29a-f. There are pronounced differences between the viscoelastic response of the paranematic and nematic state. First of all, the response functions for the nematic state are only non-zero in a much smaller frequency range. The response functions for the nematic state are strongly varying functions of frequency in this small frequency range. Furthermore, the frequency dependence of, for example η'', changes with $Pe_{r,0}$ in a quite different fashion as compared to the paranematic state. In a paranematic, η'' decreases on increasing $Pe_{r,0}$ without changing the location of its maximum too much, contrary to the nematic state, where the predominant effect of increasing $Pe_{r,0}$ is to shift the location of the maximum value of η'', while the maximum value itself does not change that drastically.

The present approach allows for the straightforward (numerical) calculation of response functions for superimposed oscillatory shear flow as well. We shall not discuss such response functions here.

0.14.4 Comparison with other theories, simulations and experiments

An expression for the effective viscosity η^{eff}_{ellips} at zero shear rate for non-interacting ellipsoidally shaped rods is due to Kuhn and Kuhn (1945) and Simha (1940) (see Larson (1999) for an extensive overview). They found,

$$\eta^{eff}_{ellips} \;=\; \eta_0 \left[1 + \left\{ \frac{8}{5} + \frac{p_e^2}{5} \left(\frac{1}{3(\ln\{2p_e\} - 3/2)} + \frac{1}{\ln\{2p_e\} - 1/2} \right) \right\} \varphi \right] \;. \qquad (302)$$

where $p_e = L_e/D_e$ is the total length (L_e) over total thickness (D_e) ratio of the ellipsoidal rod. Expanding to leading order in p_e gives,

$$\eta^{eff}_{ellips} \;=\; \eta_0 \left[1 + \frac{3}{2}\,\frac{8}{45}\,\frac{p_e^2}{\ln\{p_e\}}\,\varphi \right] \;. \qquad (303)$$

In order to compare this result with eq.(291) for $\dot\gamma = 0$, note that for cylindrical rods (with $\bar\rho = N/V$ the number density of rods),

$$\left(\frac{L}{D}\right)^2 \varphi \;=\; \left(\frac{L}{D}\right)^2 \frac{\pi}{4} D^2 L\,\bar\rho \;=\; \frac{\pi}{4}\,L^3\,\bar\rho\,,$$

while for ellipsoidal rods,

$$\left(\frac{L_e}{D_e}\right)^2 \varphi \;=\; \left(\frac{L_e}{D_e}\right)^2 \frac{\pi}{6} D_e^2 L_e\,\bar\rho \;=\; \frac{\pi}{6}\,L_e^3\,\bar\rho\,.$$

When we choose the lengths of the cylindrical and ellipsoidal rods to be equal, that is,

$$L \;=\; L_e\,, \qquad (304)$$

it follows, for equal volume fractions, that our result (291) is identical to eq.(303) (note that $\ln\{p_e\} \;=\; \ln\{L/D\} + \mathcal{O}(1)$). This identification also applies to the rotational and translational diffusion coefficients of free, non-interacting cylinders and ellipsoids : the leading order expressions for these diffusion coefficients are identical for very long and thin cylinders

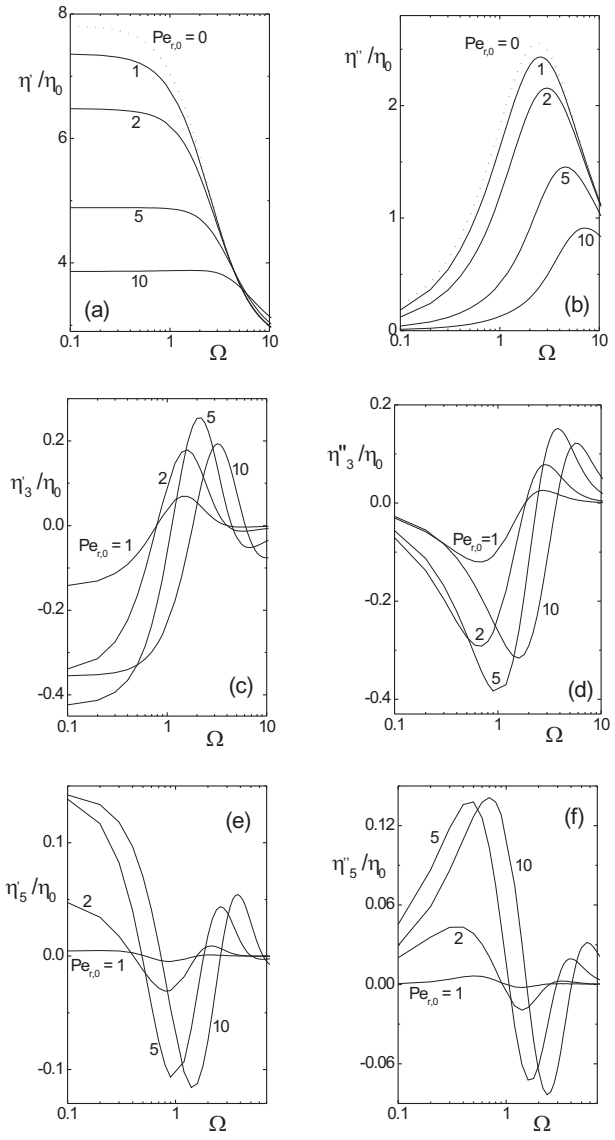

Figure 28: Non-linear response functions for the otherwise *isotropic state* : (a) The dissipative response function η' as a function of the Deborah number (299) for various values of the Peclet number (300), as indicated in the figure. The dashed line corresponds to the leading order expansion (297). Here, and in the other figures, $L/D = 50$. (b) The same for the elasticity response function η'', where the dashed line corresponds to the eq.(297). (c) The same for the leading order non-linear dissipative response function η_3'. (d) The leading order non-linear elasticity response function η_3''. (e), (f) The same as figures (c) and (d) for the response functions η_5' and η_5'', respectively.

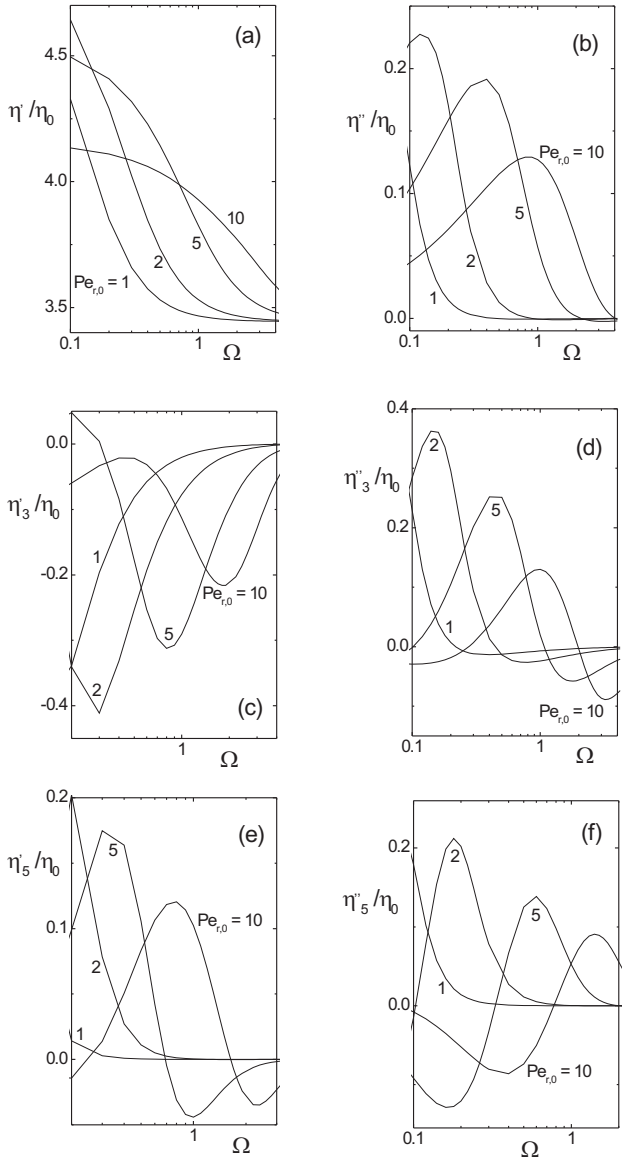

Figure 29: The same as in fig.28, now for the *nematic state*.

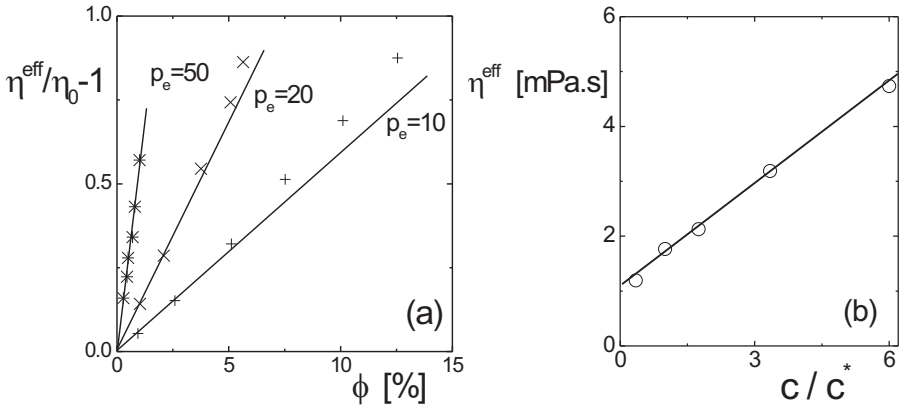

Figure 30: (a) Brownian dynamics simulation data from Claeys et al. (1993) for the suspension shear viscosity (at zero shear-rate and infinite frequency) of ellipsoidal rods as a function of their volume fraction for various aspect ratios p_e, as indicated in the figure. (b) Linear concentration dependence of the shear viscosity as found in simulations by Yamane et al. (1994).

and ellipsoids, when their lengths are taken equal. In the above we have chosen equal volume fraction and number density of the cylindrical and ellipsoidal rods. This implies equal volumes of the rods, from which a relation between the thickness of the rods follows as,

$$D_e/D \;=\; \sqrt{3/2}\,. \tag{305}$$

Other choices for mapping results for ellipsoidal rods onto those for cylindrical rods can be used. The above mapping is simple, and correctly compares not only viscosity coefficients but also diffusion coefficients.

The leading shear thinning behaviour of the zero frequency shear viscosity as found in eq.(291) may be compared to the result obtained by Berry and Russel (1987), which reads in our notation,

$$\eta^{eff} \;=\; \eta_0 \left[1 + \left\{ 1 - \frac{1}{50} \left(\frac{\dot\gamma}{D_r} \right)^2 \right\} \alpha\,\varphi + \frac{2}{5} \left\{ 1 - 0.0342 \left(\frac{\dot\gamma}{D_r} \right)^2 \right\} \alpha^2\,\varphi^2 \right] . \tag{306}$$

up to second order in concentration and shear-rate. This result is valid in the dilute regime, where $\left(\frac{L}{D}\right)^2 \varphi \ll 1$. To first order in volume fraction this agrees with our result (291). There are serious differences, however, for the φ^2-contribution. First of all, as discussed in the previous section, we predict a linear volume fraction dependence of the shear viscosity at zero shear-rate. From eqs.(290), and from eq.(297) at infinite frequency, we obtain,

$$\eta^{eff} \;=\; \eta_0\,[\,1 + \alpha\,\varphi\,] \quad , \quad \eta_\infty^{eff} \;=\; \eta_0\,[\,1 + \tfrac{1}{4}\,\alpha\,\varphi\,] \;, \tag{307}$$

where, as before, η^{eff} is the zero frequency and η_∞^{eff} the high frequency viscosity. The above result (306) for zero frequency of Berry and Russel predicts on the other hand, at zero-shear-

rates and up to second order in concentration,

$$\eta^{eff} \;=\; \eta_0 \left[1 + \alpha\,\varphi + \frac{2}{5}\alpha^2\,\varphi^2\right] . \tag{308}$$

On the basis of this latter prediction, a pronounced φ^2-dependence for long and thin rods is expected, since $\alpha\varphi \sim \frac{L}{D}/\ln\{\frac{L}{D}\} \to \infty$ as $\frac{L}{D} \to \infty$, for a given value of $\frac{L}{D}\varphi$. For zero shear-rates, we may compare the above predictions with computer simulations by Claeys and Brady (1993) on ellipsoidal rods. In fig.30a, simulation data from Claeys and Brady (1993) for the effective zero shear-rate viscosities at infinite frequencies are plotted for three aspect ratios p_e of the ellipsoidal rods : $p_e = 50,\ 20$ and 10. There is a remarkable linear concentration dependence over a large concentration range, especially for the longer rods. In fact, Claeys and Brady (1993) remark that "Somewhat surprisingly, the dispersion containing 1% rods of aspect ratio 50 still responds hydrodynamically as if it were dilute, even though $n_\phi \frac{4}{3}\pi a^3 = 25$" (in their notation, n_ϕ is the number density of rods and $a = L/2$). Such a linear concentration dependence is also found in computer simulations on non-Brownian rods by et al. (1994) (see fig.30b). They state that "$\cdots$ the excess viscosity is proportional to the number density n even in the region $nL^3 \approx 40, \cdots$". The magnitude of the second order in volume fraction contribution in the Berry-Russel equation (306), relative to the first order contribution is $\frac{2}{5}\alpha\varphi \approx 50\%$ for the highest concentration shown in fig.30 for both $p_e = 20$ and 50. The large second order in concentration contributions predicted by Berry and Russel are thus in disagreement with the linear relationship found in fig.30. A decrease of the Huggins coefficient with increasing aspect ratio is confirmed in experiments on spindle-type colloidal hematite rods by Solomon and Boger (1998) (see fig.2 and table III in this reference).

The slope of the simulation results for the high frequency viscosity η_∞^{eff} versus the volume fraction in fig.30, taken from Claeys and Brady (1993), may be compared to the slope $\alpha/4$ as predicted in eq.(307). Noting that the volume fraction of ellipsoids in fig.30a is equal to $\frac{\pi}{6}\,DL^2\,\bar{\rho}$ while for the cylindrical particles under consideration here the volume fraction is equal to $\frac{\pi}{4}\,DL^2\,\bar{\rho}$, a slope of 36 is found from the simulation data for $L/D = 50$, whereas from eq.(289) we find a slope of 29. For $L/D = 20$ one finds a slope of 9 from fig.30, while $\alpha/4 = 6$, and for $L/D = 10$ one finds 3.8 and $\alpha/4 = 1.9$. The slope found from simulations thus seems to converge to the asymptotic result in eq.(307) when the aspect ratio is large enough.

The linear concentration dependence of the zero-shear viscosity is not found within the DEK-theory (Doi and Edwards (1986)), where the concentration dependence originates from the assumed state dependence of the rotational tracer diffusion coefficient.

The experiments by Graf et al. (1993) and Schmidt et al. (2000) on fd-virus suspensions do not show a linear concentration dependence of the zero-shear and zero-frequency viscosity (except maybe for the salt free case in fig.3 of Graf et al. (1993), which result should not be taken as proof of the present theory in view of the not well understood behaviour of fd-virus at very low ionic strength). The higher order concentration dependence as found for fd-virus, however, is much weaker than for hard-spheres, indicating that, in accordance with our findings, elongated objects tend to diminish non-linear concentration dependence. Similarly, a considerable second order concentration dependence of the shear viscosity is found experimentally for Xanthan gum by Chauveteau (1982). It is known that fd-virus is relatively stiff (contour length is 880 nm, intrinsic persistence length is 2200 nm), but nevertheless behaves

quite non-Onsager like, in the sense that the relative isotropic-nematic bi-phasic gapwidth in the absence of shear flow is much narrower than the width for very long and thin, truely rigid rods (see Tang and Fraden (1995)). Hence, even for relatively stiff rod like particles, the approximation (208) for the pair-correlation function is not very good. Xanthan and "stiff" polymers like PBLG (Yang (1987) and Mead and Larson (1990)), are even more flexible than fd-virus. The non-zero Huggins coefficient at zero shear-rate found experimentally for fd-virus by Graf et al. (1993), Xanthan gum by Chauveteau (1982) and PBLG by Yang (1987) and Mead and Larson (1990) is probably due to flexibility. In view of this sensitivity on flexibility, it would be very interesting to include flexibility (even up to leading order in the inverse persistence length) in stress calculations. The sensitivity on slight flexibility obscures the comparison of theories for truly stiff rods with experiments.

The difference between the experimental rods mentioned above and the model rods in computer simulations, is their degree of stiffness. The advantage of computer simulations is that the persistence length of rods can be made infinite. In the computer simulations mentioned above, hydrodynamics are taken into account. The different concentration dependence of the zero shear viscosity (at least for long and thin rods) found in experiments as compared to simulations, as far as the Huggins coefficient is concerned, is therefore most likely due to flexibility.

Despite the sensitivity of viscoelastic response functions on flexibility, we shall nevertheless compare experimental data with our theoretical predictions. This comparison should be taken seriously only on a qualitative level. Fig.31 shows experimental data for the shear-rate dependence of the shear viscosity of Xanthan (Chauveteau (1982)) with two different molar weights, PBLG (Yang (1987)) and a salt free fd-virus suspension (Graf et al. (1993)). Plotted is the intrinsic viscosity $[\eta] = \eta/\eta_0 - 1$, with η_0 the solvent shear viscosity, relative to its value $[\eta]_0$ at zero shear-rate. For Xanthan we took $D_r = 133\, s^{-1}$ and $103\, s^{-1}$ for the low and high molecular weight, respectively, as reported by Berry and Russel (1987), for PBLG we took $D_r = 167\, s^{-1}$, as reported by Larson (1999), and for salt free fd we took $D_r = 11\, s^{-1}$ (see Graf et al. (1993)). The solid lines refer to the present theory with $L/D = 50$ (the precise form of these curves is insensitive to the aspect ratio). The Xanthan and PBLG suspensions are dilute, and are seen to be in reasonable agreement with theory. The concentration of the salt free fd-virus suspension is equal to $6\, c^*$, where c^* is the overlap concentration. There is some deviation from the fd-data in comparison to theory, which may be either due to flexibility or aggregation at low ionic strength.

The linear concentration dependence in eq.(307) holds up to the isotropic-nematic phase transition. Within the nematic state this result is no longer valid, since in deriving eq.(307) we linearized around the isotropic state (see eq.(285)). As can be seen from fig.26b, the viscosity decreases with increasing concentration for a nematic. As was mentioned before, this is the result of an increase in alignment on increasing the concentration. Such a decrease of the shear viscosity with increasing concentration is indeed observed experimentally (see for example fig.10.5 in Doi and Edwards (1986) and fig.1 in Kiss and Porter (1978)). Furthermore, the type of concentration dependence of the shear viscosity at higher shear-rates as found in fig.26c is also seen in experiments (see for example fig.10.9 in Doi and Edwards (1986)).

To leading order in concentration, the low shear limiting expressions (292) for normal stress differences are also found by Hinch and Leal (1972), except that instead of the prefactor

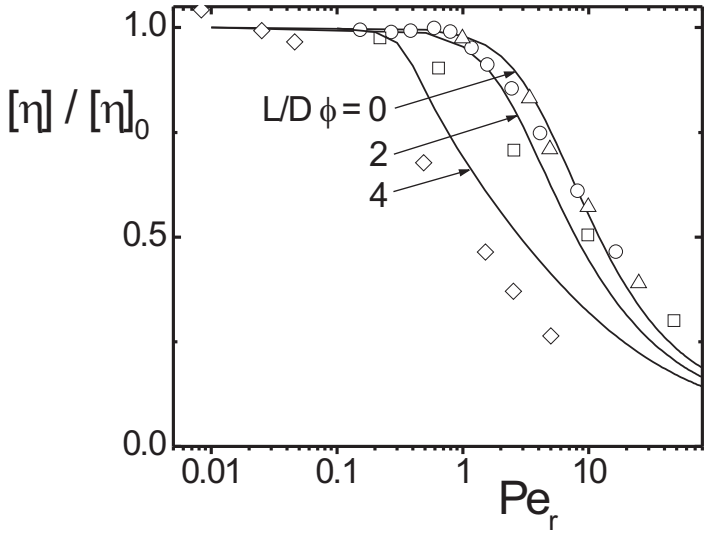

Figure 31: The intrinsic viscosity $[\eta] = \eta/\eta_0 - 1$, relative to its value $[\eta]_0$ at zero shear-rate, as a function of the bare rotational Peclet number. The solid line are theoretical predictions for various values of $\frac{L}{D}\varphi$, as indicated in the figure, for $L/D = 50$ (the theoretical curves are insensitive to the precise value of the aspect ratio). The symbols relate to experimental data for Xanthan by Chauveteau (1982) (O-small molecular weight, $\triangle$-large molecular weight), for PBLG by Yang (1987) ($\Box$) and for salt-free fd by Graf et al. (1993) ($\Diamond$).

$-1/40$ they find $-1/28$. Within the DEK-theory, it is found that, to leading order in shear-rate,

$$N_1 = \eta_0 \frac{1}{30} \bar{\rho}\, k_B T \frac{\dot{\gamma}^2}{\tilde{D}_r^2} ,$$

$$N_2 = -\eta_0 \frac{1}{105} \bar{\rho} k_B T \frac{\dot{\gamma}^2}{\tilde{D}_r^2} ,$$

where $\bar{\rho}$ is the number concentration of rods and $\tilde{D}_r$ is their state dependent rotational tracer diffusion coefficient. Using that $D_r = 3k_BT \ln\{L/D\}/\pi\eta_0 L^3$ in the expression (289) for α, we find from eqs.(292) that,

$$N_1 = \eta_0 \frac{1}{30} \bar{\rho}\, k_B T \frac{\dot{\gamma}^2}{D_r\, D_r^{eff}} ,$$

$$N_2 = -\eta_0 \frac{1}{300} \bar{\rho} k_B T \frac{\dot{\gamma}^2}{D_r\, D_r^{eff}} ,$$

where the effective rotational, collective diffusion coefficient D^{eff} is given in eq.(230). The prefactor for N_2 is almost a factor of 3 smaller than in the DEK-theory, and in both expressions we find the combination $D_r\, D_r^{eff}$ instead of $\tilde{D}_r^2$. Experimental results for normal stress differences on fibers are reported by Zirnsak et al. (1994). Here, Brownian motion is very weak as compared to shear forces, so that one should compare with the high shear-rate results as plotted in fig.27. One should be careful in comparing, since inertial effects in fiber suspensions may play a role. As can be seen from figs.27a,b, both normal stress differences become linear functions of the shear-rate for high shear-rates (since $N_1/\dot{\gamma}$ and $N_2/\dot{\gamma}$ tend to constant, shear-rate independent values). This remarkable linear shear-rate dependence is indeed typically found in experiments on fibers (see, for example, fig.11 in Zirnsak et al. (1994)). In addition, in figs.16,17 of the same reference, it is found that the first normal stress difference varies linearly with concentration. This is also found in our fig.27e for high shear-rates, for concentrations where $\frac{L}{D}\varphi$ is less than about 3. The concentrations in the experiments on fibers is indeed well within this range.

Normal stress differences that change from being positive to negative on increasing the shear-rate, and for larger shear-rates from negative to positive again, were reported by Iizuka (1978), Kiss and Porter (1978), Kiss (1996) and Larson (1996) for PBLG solutions in m-cresol, and later for the same polymer by Magda et al. (1991). Marrucci and Maffettone (1989) predict, on the basis of a two-dimensional DEK-like approach for a homogeneous nematic, that the normal stress difference N_1 is negative at low shear-rates and becomes positive at higher shear-rates (see their fig.10). This behaviour is found for shear-rates which are large enough to assure that stationary solutions of equations of motion exist, that is, where tumbling or wagging are absent. Larson (1990) analyzed the full 3-dimensional DEK-theory (using closures as obtained by Hinch and Leal (1976)), and suggests that the experimentally observed sign changes of normal stress differences are due to the existence of tumbling or wagging nematic domains. By time-averaging of stresses generated by tumbling domains over a number of oscillations, he indeed finds the kind of sign changes for normal stress differences that are observed experimentally. This kind of behaviour is essentially also found within the two-dimensional DEK-like approach by Marrucci and Maffettone (1990a), Marrucci and Maffettone (1990b). Magda et al. (1991) suggested that polydomain nematics may exhibit apparent steady flow behaviour, even though each individual domain exhibits tumbling or wagging, since in a rheometer averages over many independent tumbling domains are probed. Tumbling and wagging can be observed in an experiments by flow reversal, which renders the various domains coherently tumbling/wagging for some time. As mentioned before, whether a theory predicts tumbling and wagging is very sensitive to the closure relation that is used. Our closure relation (227) is not suited to describe tumbling and wagging. Other closure relations can be used to study these time-periodic states (see Marrucci and Maffettone (1989), Larson (1990), Marrucci and Maffettone (1990a), Marrucci and Maffettone (1990b) and Forest and Wang (2003)). Due to the sensitivity for the prediction of time-periodic states on the closure relation, the most sensible thing to do seems to employ the original equation of motion (213), before introducing a Ginzburg-Landau expansion.

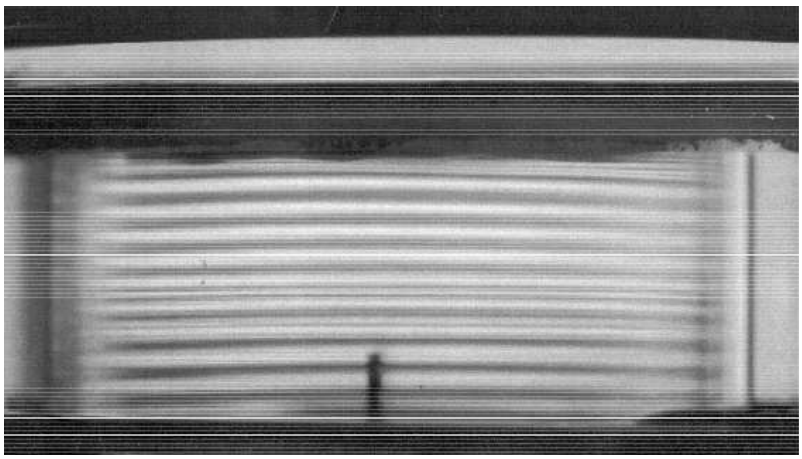

Figure 32: A photograph from the side of an optical couette cell between two crossed polarizers. The couette cell contains an fd-virus suspensions in a vorticity banded state. The width of the shear cell is about $5\ cm$, while the height of the bands is about $1\ mm$.

0.15 Current Research Topics

Some of the current research interests related to what has discussed in the present chapter will be briefly described in this last section. Current research interests include,

(i) shear-banding transitions,

(ii) the non-equilibrium phase behaviour under shear flow,

and,

(iii) phase separation kinetics under flow conditions.

0.15.1 Shear-banding transitions

There are essentially two types of banding transitions observed experimentally in various types of systems containing mesoscopic entities : vorticity banding and gradient banding. Here, "bands" refer to coexisting regions under stationary flow which have different microstructural order and can sustain different shear rates and/or stresses. In case of vorticity banding, regularly stacked bands in the vorticity direction are observed, which differ in their average orientational order. For gradient banding, two regions coexists, extending along the gradient direction, each with a different shear rate.

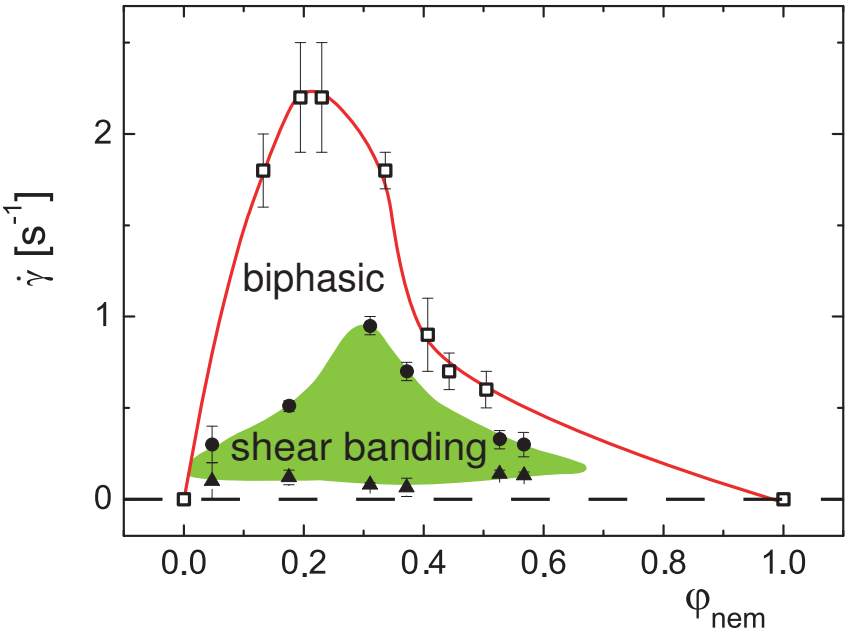

Figure 33: Experimental phase diagram of fd virus (with added dextran) including the vorticity banding region.

Vorticity banding Within part of the two-phase region (the region enclosed by the binodal), fd-virus suspensions exhibit vorticity banding, where regularly stacked bands are formed along the vorticity direction. The height of these bands can be up to $mm's$. A photograph of such a banded state in an optical couette cell between two crossed polarizers is given in fig.32. The difference in contrast of the two types of bands between crossed polarizers is due to the different orientational order in the bands. The director has different orientations in the two bands. The concentration difference in the two bands has been shown to be zero to within experimental error. The region in the phase diagram where vorticity banding is found is indicated in fig.33. At lower concentrations, the boundary of the region where vorticity banding occurs coincides exactly with the binodal. It thus seems that inhomogeneities that are formed right after a shear-rate quench into the two-phase region (the region bounded by the paranematic-nematic binodal) are necessary to render normal stresses such that they induce an instability along the vorticity direction leading to banding. If this is indeed the case, equations of motion need to be analyzed which account for large gradients in concentration, orientational order parameter and/or shear rate. For stiff colloidal rods, such equations of motions have been derived by Dhont and Briels (2002), Dhont and Briels (2003). The particular normal stress behaviour that leads to vorticity banding and the role of inhomogeneities leading to that behaviour is not yet understood (see, however Olmsted and Lu (1999), where vorticity banding is assumed to occur whenever the velocity-gradient stress versus the shear rate relation is multi-valued). At higher concentrations, there are indications that banding ceases to

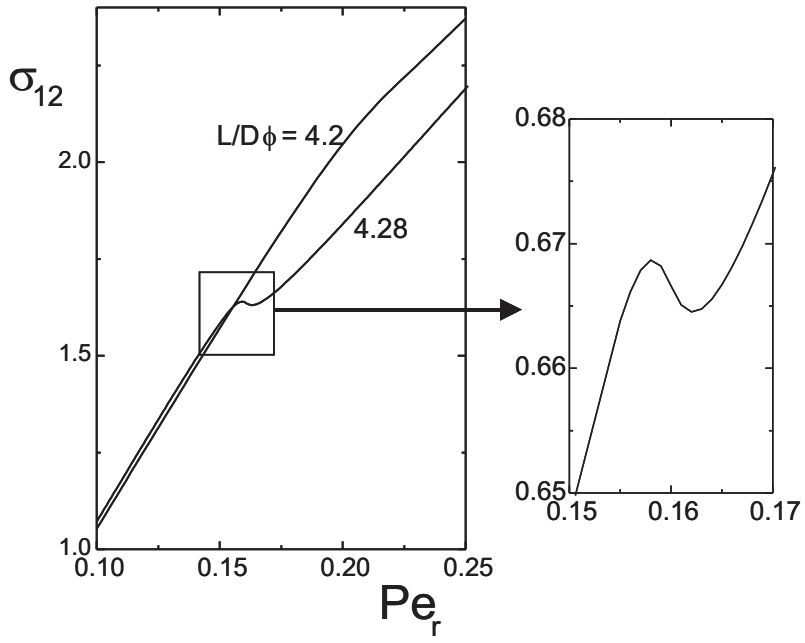

Figure 34: The dimensionless flow-gradient component $\sigma_{12} \equiv \Sigma_{12}/\eta_0\, D_r$ of the stress tensor as a function of the shear-rate for concentrations close to the critical concentration $\frac{L}{D}\varphi = 4.281\cdots$; see fig.19b. The smaller figure on the right side is a blow-up of the van der Waals loop.

occur when tumbling/wagging sets in.

Gradient banding On the basis of the stationary forms of the equation of motion (219) and the expression (284) for the deviatoric stress tensor (where D_r is the bare, state-independent rotational diffusion coefficient), a non-monotonic behaviour of the shear-stress as a function of shear-rate is found. Such a "van der Waals loop-like" behaviour is only found for concentrations very close to the critical concentration $\frac{L}{D}\varphi = 4.281\cdots$, as can be seen in fig.34, where the dimensionless flow-gradient component $\sigma_{12} = \Sigma_{12}/\eta_0\, D_r$ of the stress tensor is plotted as a function of shear-rate. Such a decrease of the stress in a certain shear-rate interval implies that the usual linear flow profile as depicted in fig.1a is unstable. The stable flow profile is now a banded flow, where two regions with different shear rates are in coexistence. Within these two regions (the "bands"), the shear rate is constant, independent of position. The shear rates within the two bands can be found from a modified equal area construction on the van der Waals loop in fig.34 (see Olmsted and Lu (1999), Olmsted (1999), Olmsted et al. (2000), Lu et al. (2000), Fielding and Olmsted (2003) and Dhont (1999)). As can be seen, the difference between these shear rates is very small. Since the concentration range where gradient banding is expected to occur and the difference in shear rates as sustained in the two bands is very small, gradient banding in suspensions of stiff rods will be difficult to detect experimentally. In addition, passing the critical point at a fixed concentration by increasing the shear rate, the

two-phase region is also probed (see figs.19b and 21), as a result of which phase separation will occur during a rheological experiment. It is possible, however, that gradient banding also occurs within the two-phase region (the region bounded by the paranematic-nematic binodal), which has not been studied experimentally yet. The situation for worm-like micellar systems is different. Here strong gradient banding has been observed outside the two-phase region. The reason for such pronounced gradient banding is probably that shear flow enhances alignment, which enhances head-to-tail collisions leading to longer worms, leading in turn to a higher degree of alignment. This mechanism probably renders wormlike micellar systems much more strongly shear thinning as compared to, for example, fd-virus suspensions, giving rise to a more pronounced van der Waals loop like behaviour of the stress versus shear rate.

Although gradient banding of suspensions of stiff rods is experimentally possibly less relevant, these systems do allow to gain in understanding on the microscopic origin of the van der Waals loop-like behaviour of the stress tensor. The reason for the strong shear-thinning behaviour on passing the critical point is that rotational motion is very slow at the critical point (since there $D_r^{eff} = 0$, as discussed in subsection 11.1), so that shear-aligning forces are not counterbalanced any more by rotational diffusion. A small increase in shear-rate near the critical point therefore results in an appreciable increase of the degree of alignment, leading to strong shear thinning, giving rise to the van der Waals loop like behaviour of the stress tensor. It may be a general feature for the origin of gradient banding, that the dynamics of a variable, that strongly couples to the stress, becomes very slow on increasing the shear rate.

0.15.2 The non-equilibrium phase diagram under shear flow

A sketch of a possible complete phase diagram of rods subjected to simple shear flow, for concentrations below the nematic-to-smectic transition, is given in fig.35. As discussed before, the location of the binodal and the region within the two-phase region (as enclosed by the binodal) where vorticity banding occurs has been obtained experimentally for an fd-virus suspension with added dextran that induced slight attractions between the rods. At lower concentrations, the region where vorticity banding ceases to occur coincides with the binodal. There are indications that the vorticity-banding ceases to occur at higher concentrations where non-stationary, time-periodic states become stable. Gradient banding is expected to occur in a very small concentration interval close to the critical point (as discussed above), but has so far not been observed experimentally.

Characteristic features of vorticity bands have not been investigated yet. It is not known how the band height varies with shear rate and concentration, the internal orientational order within the bands has not been investigated, and it is not known whether or not there is a dependence on the gap width of the shear cell.

The various types of non-stationary states as described in detail by Rienäcker and Hess (1999) and Hess and Kröger (2004). These various types of time-periodic states are difficult to distinguish experimentally. So far, only tumbling and wagging states have been seen in fd-virus suspensions by Lettinga and Dhont (2004). The phase diagram in fig.35 may, however, be more complicated as far as these time-periodic states are concerned.

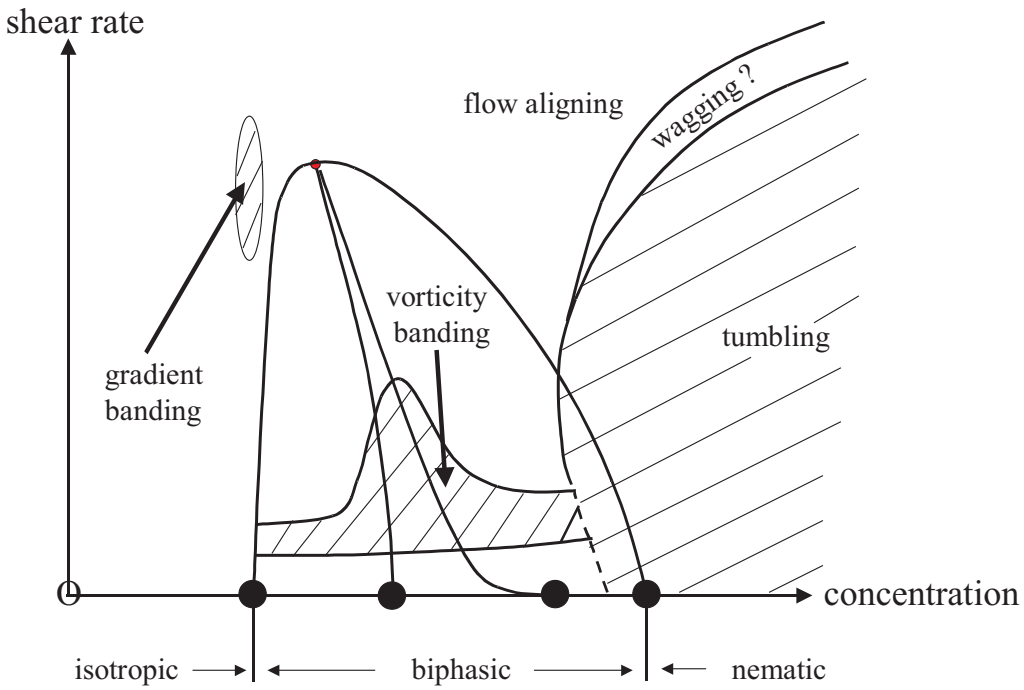

Figure 35: A sketch of the possible non-equilibrium phase diagram of stiff rods.

0.15.3 Phase separation kinetics under flow conditions

No experimental results for demixing kinetics of colloidal systems consisting of either spherical or rod-like colloids under shear flow have been published so far. An analysis of a simplified Smoluchowski equation in the initial stage of spinodal demixing of *suspensions of rods in the absence of flow* has been discussed by Winters et al. (2000). Initial spinodal decomposition of *suspensions of spheres in the presence of shear flow* has been analyzed by Dhont (1996), which analysis reproduces features that are seen experimentally for fluid mixtures by Baumberger et al. (1991). There are as yet no theories on spinodal decomposition of suspensions of rod-like colloids *under shear flow*, although much work has been done on polymer blend demixing under flow conditions.

There are regions in the phase diagram where decomposition proceeds through spinodal demixing or by nucleation and growth, depending on the degree of orientational order of the initial state. These regions are most conveniently identified by means of the bifurcation diagrams as discussed in section 11.

The kinetics of vorticity-band formation has not been studied so far. Experiments indicate

that these bands are formed from an unstable state, that is, by means of a spinodal type of demixing, with a time constant that varies with shear rate and concentration. The same experiments show a remarkably strong dependence of the height of the bands and the rate with which bands are formed on the gapwidth of the shear cell (Kang et al. (2004)).

Appendix A

This appendix deals with the mathematical details of how bead index summations can be calculated by means of integration.

Consider the function appearing in eq.(35),

$$f(L/D) = \sum_{j=-\frac{1}{2}n}^{\frac{1}{2}n} \sum_{i=-\frac{1}{2}n\ ,\ i\neq j}^{\frac{1}{2}n} \frac{1}{\mid i-j \mid} .$$

Let us first evaluate the sum,

$$\sum_{i=-\frac{1}{2}n\ ,\ i\neq j}^{\frac{1}{2}n} \frac{1}{\mid i-j \mid} .$$

This sum equals the surface area of all the rectangles in fig.36. It can be replaced by an integral, when the summation range $(-\frac{1}{2}n, \frac{1}{2}n)$ is large,

$$\sum_{i=-\frac{1}{2}n\ ,\ i\neq j}^{\frac{1}{2}n} \frac{1}{\mid i-j \mid} \approx \left[\int_{-\frac{1}{2}(n+1)}^{j-\frac{1}{2}} + \int_{j+\frac{1}{2}}^{\frac{1}{2}(n+1)} \right] di\, \frac{1}{\mid i-j \mid} . \tag{309}$$

The difference between the sum and the integral is the sum of the dashed surface areas in fig.36 (with their proper sign). For increasing L/D-ratios, this difference tends to a constant, while the sum itself goes to infinity. The relative error that is made by replacing the sum by

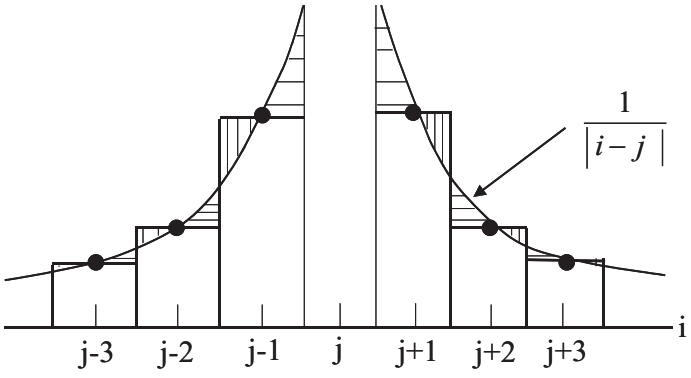

Figure 36: The sum in eq.(309) equals the surface area of all rectangles, and the integral is the surface area under the solid curve.

an integral thus tends to zero as L/D tends to infinity. The leading terms in the above integral are,

$$\ln\{j+\frac{1}{2}(n+1)\}+\ln\{\frac{1}{2}(n+1)-j\}\,.$$

This expression is substituted into eq.(309), where the sum over j is again replaced by an integral. Using the standard integral,

$$\int dz\, z^m \ln\{z\} \;=\; z^{m+1}\left[\frac{\ln\{z\}}{m+1}-\frac{1}{(m+1)^2}\right]\,,$$

one ends up, to leading order in D/L, with the result given in eq.(36). The two values of $j=\pm n/2$ do not contribute to leading order, so that in the evaluation of summations, j may always be assumed in the interior of the summation range.

Appendix B : Useful mathematical identities

Useful mathematical identities which are frequently used in the present chapter are,

$$\begin{aligned}
\hat{\mathcal{R}}^2(\cdots) &= -2\hat{\mathbf{u}}\cdot\nabla_u(\cdots)-\hat{\mathbf{u}}\hat{\mathbf{u}}:\nabla_u\nabla_u(\cdots)+\nabla_u^2(\cdots)\,,\\
\hat{\mathcal{R}}^2(\mathbf{a}\cdot\hat{\mathbf{u}})^2 &= 2\left[a^2-3(\mathbf{a}\cdot\hat{\mathbf{u}})^2\right]\,,\\
\hat{\mathcal{R}}^2(\hat{\mathbf{u}}\cdot\mathbf{M}\cdot\hat{\mathbf{u}}) &= -6\,(\hat{\mathbf{u}}\cdot\mathbf{M}\cdot\hat{\mathbf{u}})+2\,Tr\{\mathbf{M}\}\,,\\
\hat{\mathcal{R}}^2(\hat{\mathbf{u}}\hat{\mathbf{u}}) &= -6\hat{\mathbf{u}}\hat{\mathbf{u}}+2\hat{\mathbf{I}}\,,\\
(\hat{\mathbf{u}}\times\mathbf{M}\cdot\hat{\mathbf{u}})\cdot\hat{\mathcal{R}}(\cdots) &= [\nabla_u(\cdots)]\cdot(\mathbf{M}\cdot\hat{\mathbf{u}})-(\hat{\mathbf{u}}\cdot[\nabla_u(\cdots)])(\hat{\mathbf{u}}\cdot\mathbf{M}\cdot\hat{\mathbf{u}})\,,\\
\hat{\mathcal{R}}\cdot[\hat{\mathbf{u}}\times(\mathbf{M}\cdot\hat{\mathbf{u}})] &= -3(\hat{\mathbf{u}}\cdot\mathbf{M}\cdot\hat{\mathbf{u}})+Tr\{\mathbf{M}\}\,,\\
\hat{\mathcal{R}}\cdot((\cdots)(\hat{\mathbf{u}}\cdot\mathbf{M}\cdot\hat{\mathbf{u}})) &= [Tr\{\mathbf{M}\}-3(\hat{\mathbf{u}}\cdot\mathbf{M}\cdot\hat{\mathbf{u}})]\,(\cdots)+(\mathbf{M}\cdot\hat{\mathbf{u}})\cdot\left[\hat{\mathbf{I}}-\hat{\mathbf{u}}\hat{\mathbf{u}}\right]\cdot\nabla_u(\cdots)\,,\\
\hat{\mathcal{R}}\cdot(\hat{\mathbf{u}}\times\mathbf{a}) &= -2(\hat{\mathbf{u}}\cdot\mathbf{a})\,,\\
\hat{\mathcal{R}}(\hat{\mathbf{u}}\cdot\mathbf{M}\cdot\hat{\mathbf{u}}) &= \hat{\mathbf{u}}\times\left[\mathbf{M}\cdot\hat{\mathbf{u}}+\mathbf{M}^T\cdot\hat{\mathbf{u}}\right]\,,\\
\mathbf{a}\cdot\hat{\mathcal{R}}\hat{\mathbf{u}} &= \mathbf{a}\times\hat{\mathbf{u}}\,.
\end{aligned}$$

Here, $\mathbf{M}$ and $\mathbf{a}$ denote $\hat{\mathbf{u}}$-independent tensor and vector, respectively, and $(\cdots)$ denotes an arbitrary, but differentiable, scalar or vector field. The above identities are easily verified by explicit differentiation.

Appendix C : On the accuracy of the closure relation (227)

In order to asses the accuracy of the closure relation (227), we numerically solve the Smoluchowski equation (213) for a single rod in shear flow, that is, without the interaction term. From the stationary numerical solution $P(\hat{\mathbf{u}},t\to\infty)$, both $\mathbf{S}$ and $\mathbf{S}^{(4)}$ can be obtained by numerical integration. This allows to compare the approximation (227) with the exact form of $\mathbf{S}^{(4)}$. Note that the stationary solution of eq.(213) is a function of the shear rate through the dimensionless rotational Peclet number $Pe_r=\dot{\gamma}/D_r$.

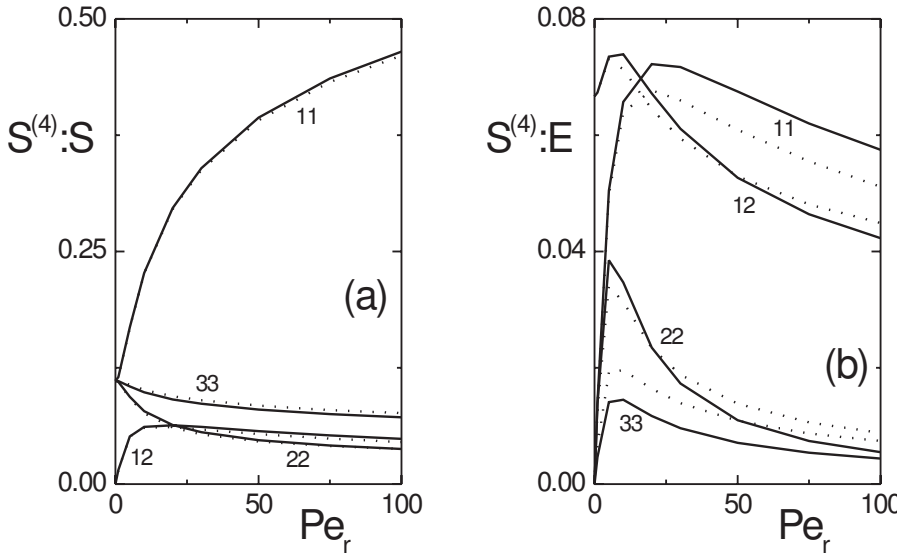

Figure 37: A test of the accuracy of the closure relation (227) for (a) $\mathbf{M} = \hat{\mathbf{S}}$ and (b) $\mathbf{M} = \hat{\mathbf{E}}$. Solid lines are obtained from numerical solution of the Smoluchowski equation (213), and dotted lines are obtained from $\mathbf{S}$ using the closure relation (227). The numbers indicate the tensor elements. Tensor elements that are not shown are 0.

A comparison between the exact values (solid lines) and values obtained from the closure relation (227) (dotted lines) for the non-zero components of the tensors $\mathbf{S}^{(4)} : \mathbf{S}$ and $\mathbf{S}^{(4)} : \hat{\mathbf{E}}$ are given in figs.37a,b, respectively. As can be seen, the shear-rate dependence of the various components is well reproduced by the closure relation. Moreover, the accuracy of the closure relation (227) is seen to be accurate to within 1% for $\mathbf{M} = \mathbf{S}$, and about 10% in case $\mathbf{M} = \hat{\mathbf{E}}$. Computer simulations indicate the same accuracy for larger concentrations.

Appendix D : Evaluation of sums over bead index numbers

Consider the evaluation of eq.(272) to obtain an explicit expression for the sum in eq.(271). As a first step, the double summation in eq.(272) is rewritten as,

$$\sum_{\alpha}\sum_{\beta\neq\alpha}\frac{G(\alpha)}{|\,\alpha-\beta\,|}\,\mathbf{F}^{h}_{j,\beta} \;=\; \sum_{\alpha}\sum_{\beta\neq\alpha}\frac{G(\beta)}{|\,\alpha-\beta\,|}\,\mathbf{F}^{h}_{j,\beta} + \sum_{\alpha}\sum_{\beta\neq\alpha}\frac{G(\alpha)-G(\beta)}{|\,\alpha-\beta\,|}\,\mathbf{F}^{h}_{j,\beta}\,. \tag{310}$$

The last term in this equation can be rewritten, by first interchanging the summation indices α and β, and subsequently interchanging the order of summations, as,

$$\sum_{\alpha}\sum_{\beta\neq\alpha}\frac{G(\alpha)-G(\beta)}{|\,\alpha-\beta\,|}\,\mathbf{F}^{h}_{j,\beta} = \sum_{\beta}\sum_{\alpha\neq\beta}\frac{G(\beta)-G(\alpha)}{|\,\alpha-\beta\,|}\,\mathbf{F}^{h}_{j,\alpha} = \sum_{\alpha}\mathbf{F}^{h}_{j,\alpha}\sum_{\beta\neq\alpha}\frac{G(\beta)-G(\alpha)}{|\,\beta-\alpha\,|}\,. \tag{311}$$

After a similar interchange of the order of summation in the first term on the right hand-side of eq.(310), substitution of eqs.(310,311) into eq.(272) gives,

$$\sum_\alpha G(\alpha)\,\mathbf{F}^h_{j,\alpha} = -\gamma \sum_\alpha G(\alpha)\,[\mathbf{v}_{j,\alpha} - \mathbf{U}_{j,\alpha}] - \tfrac{3}{8}\left[\hat{\mathbf{I}} + \hat{\mathbf{u}}_j\hat{\mathbf{u}}_j\right]\cdot\left[\sum_\alpha G(\alpha)\,\mathbf{F}^h_{j,\alpha}\sum_{\beta\neq\alpha}\frac{1}{|\,\alpha-\beta\,|} + \Delta\right], \tag{312}$$

where,

$$\Delta \;=\; \sum_\alpha \mathbf{F}^h_{j,\alpha}\sum_{\beta\neq\alpha}\frac{G(\beta)-G(\alpha)}{|\,\beta-\alpha\,|}\;. \tag{313}$$

Consider the first contribution between the square brackets in eq.(312),

$$\sum_\alpha G(\alpha)\,\mathbf{F}^h_\alpha \sum_{\beta\neq\alpha}\frac{1}{|\,\alpha-\beta\,|}\;. \tag{314}$$

The sum $S(\alpha) \equiv \sum_{\beta\neq\alpha} 1/|\,\alpha-\beta\,|$ can be approximated by an integral. To leading order one finds,

$$S(\alpha) \;\equiv\; \sum_{\beta\neq\alpha}\frac{1}{|\,\alpha-\beta\,|} \;=\; \left[\int_{-\frac{1}{2}\,(\frac{L}{D}-1)}^{\alpha-\frac{1}{2}} + \int_{\alpha+\frac{1}{2}}^{\frac{1}{2}\,(\frac{L}{D}-1)}\right] dx\,\frac{1}{|\,x-\beta\,|}\;.$$

The integrals are easily evaluated to yield,

$$S(\alpha) \;=\; 2\ln\{2\} + \ln\{\tfrac{1}{2}(\tfrac{L}{D}-1)+\alpha\} + \ln\{\tfrac{1}{2}(\tfrac{L}{D}-1)-\alpha\}\;.$$

Except for α's close to the ends of the rod, this gives to leading order,

$$S(\alpha) \;\approx\; 2\,\ln\{\tfrac{L}{D}\}\;. \tag{315}$$

In fig.38a, $S(\alpha)/2\,\ln\{L/D\}$ is plotted as a function of α/m, with $2m+1$ the number of beads (so that α/m ranges from -1 to $+1$). As can be seen, the approximation (315) is good to within about $10\,\%$, except at the very ends of the rod. In fact, the width of the region at the tips of the rod where eq.(315) is not a good approximation asymptotically vanishes in the limit where $L/D \to \infty$. Hence, except when $G(\alpha)\,\mathbf{F}^h_{j,\alpha}$ in eq.(314) peaks at the ends of rod j, eq.(315) can be used as a good approximation. For our purpose, there is no reason for the function $G(\alpha)\,\mathbf{F}^h_{j,\alpha}$ to peak at the very ends of the rod. A quantitative estimate for the error made in using eq.(315), is the differences between the sums $\sum_\alpha S(\alpha)$ and $\sum_\alpha 2\ln\{L/D\} = 2(L/D-1)\,\ln\{L/D\}$. These sums are plotted as functions of L/D in fig.38b. The relative error does not exceed $8\,\%$ (for $L/D \leq 5$), and very slowly converges to 0 with increasing aspect ratio. Hence, to within about $10\,\%$ error, we can approximate the expression in eq.(314) by,

$$\sum_\alpha G(\alpha)\,\mathbf{F}^h_\alpha \sum_{\beta\neq\alpha}\frac{1}{|\,\alpha-\beta\,|} \;=\; 2\,\ln\{L/D\}\sum_\alpha G(\alpha)\,\mathbf{F}^h_{j,\alpha}\;. \tag{316}$$

The term on the left hand-side in eq.(312) can be neglected against this contribution, which is logarithmically larger.

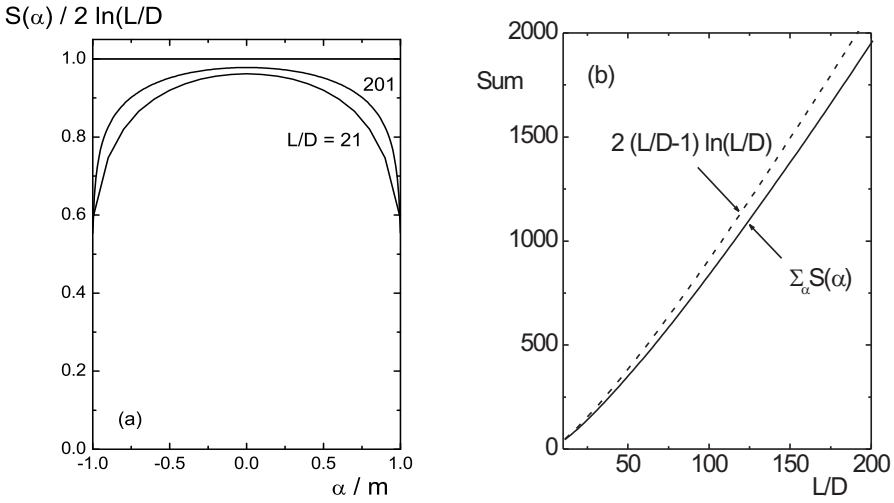

Figure 38: (a) $S(\alpha)/2\ln\{L/D\}$ as a function of α/m with $2m+1$ the total number of beads (where $S(\alpha) \equiv \sum_{\beta\neq\alpha} 1/\mid \alpha-\beta \mid$). The lower curve is for $L/D=20$, the upper curve for $L/D=201$. (b) the sums $\sum_\alpha S(\alpha)$ and $\sum_\alpha 2ln\{L/D\} = 2(L/D-1)\ln\{L/D\}$ as a function of L/D. The relative error between the two sums never exceeds 8%, and very slowly converges to 0 with increasing L/D.

For the divergence of the stress tensor in eq.(267) we need to evaluate the sum,

$$S \;\equiv\; \sum_\alpha < \delta(\mathbf{r}-\mathbf{r}_1-\alpha\, D\,\hat{\mathbf{u}}_1)\,\mathbf{F}^h_{1,\alpha} > \;\;.$$

where j is taken equal to 1 for convenience. Writing the ensemble average in terms of an integral with respect to the probability density function (pdf) P, of all phase space coordinates of the colloidal rods, the integration with respect to $\mathbf{r}_1$ can be done immediately due to the delta distribution, leading to,

$$S \;=\; \oint d\hat{\mathbf{u}}_1 \int d\mathbf{\Gamma} \sum_\alpha \; P(\mathbf{r}_1=\mathbf{r}-\alpha\, D\hat{\mathbf{u}}_1,\hat{\mathbf{u}}_1,\mathbf{\Gamma},t)\,\mathbf{F}^h_{1,\alpha}(\mathbf{r}_1=\mathbf{r}-\alpha\, D\hat{\mathbf{u}}_1,\hat{\mathbf{u}}_1,\mathbf{\Gamma}),$$

where $\mathbf{\Gamma}$ stands for the phase space coordinates $\mathbf{r}_2,\cdots,\mathbf{r}_N,\hat{\mathbf{u}}_2,\cdots,\hat{\mathbf{u}}_N$. The integrand is of the form of the left hand-side of eq.(272), except that in $\mathbf{F}^h_{1,\alpha}$ the position $\mathbf{r}_1$ is taken equal to $\mathbf{r}-\alpha\, D\hat{\mathbf{u}}_1$, which does not affect the present analysis leading to eq.(273). The function $G(\alpha)$ is now equal to,

$$G(\alpha) \;=\; P(\mathbf{r}_1=\mathbf{r}-\alpha\, D\hat{\mathbf{u}}_1,\hat{\mathbf{u}}_1,\mathbf{\Gamma},t)\;.$$

Since the pdf is a continuous differentiable function of $\mathbf{r}_1$, there is a scalar z between α and β, such that,

$$\frac{G(\beta)-G(\alpha)}{\beta-\alpha} \;=\; \frac{dG(z)}{dz} \;\equiv\; \frac{dP(\mathbf{r}_1=\mathbf{r}-z\, D\hat{\mathbf{u}}_1,\hat{\mathbf{u}}_1,\mathbf{\Gamma},t)}{dz}\;.$$

The latter derivative is just the change of P on changing the position of rod number 1 by $D\,\hat{\mathbf{u}}_1$, that is, its center is shifted over a distance D in the direction of its orientation. Since for the very large aspect ratios under consideration, suspension properties are essentially constant over distances of the order D, so that this is a very small number. The number $R = (L/D)d\ln\{G(z)\}/dz$ measures the change of "the entropy" $\ln\{P\}$ over distances of the order of the length of the rods. In terms of this number we have the order of magnitude estimate,

$$\Delta \sim R \sum_\alpha G(\alpha)\mathbf{F}^h_{1,\alpha} .$$

Hence, according to eq.(316), as long as relative changes of suspension properties over the contour of the rods are much smaller than $\ln\{L/D\}$, Δ can be neglected against the first term between the square brackets in eq.(312). This justifies the step from eqs.(267) to eq.(273,274).

Appendix E : Derivation of eq.(279)

After substitution of eqs.(278,170,166,172,277) into eq.(275) it is immediately found that,

$$\nabla\cdot\mathbf{\Sigma} = \eta_0\nabla^2\mathbf{U}(\mathbf{r},t) - \nabla P^{ss}(\mathbf{r},t) + \mathbf{I}_r + \mathbf{I}_t + \mathbf{I}_u , \tag{317}$$

where,

$$\mathbf{I}_r = -\tfrac{\gamma\,\bar{D}\,D_r}{\ln\{L/D\}} < \sum_{j=1}^{N}\sum_\alpha \alpha\,\delta(\mathbf{r}-\mathbf{r}_j-\alpha\,D\hat{\mathbf{u}}_j)\left[\beta\hat{\mathcal{R}}_j\Psi + \hat{\mathcal{R}}_j\ln\{P\}\right]\times\hat{\mathbf{u}}_j > , \tag{318}$$

$$\mathbf{I}_t = -\tfrac{\gamma\,\bar{D}}{\ln\{L/D\}} < \sum_{j=1}^{N}\sum_\alpha \delta(\mathbf{r}-\mathbf{r}_j-\alpha\,D\hat{\mathbf{u}}_j)\,[\beta\nabla_j\Psi + \nabla_j\ln\{P\}] > , \tag{319}$$

and,

$$\begin{aligned}\mathbf{I}_u &= \tfrac{4}{3}\tfrac{\gamma}{\ln\{L/D\}} < \sum_{j=1}^{N}\left[\hat{\mathbf{I}} - \tfrac{1}{2}\hat{\mathbf{u}}_j\hat{\mathbf{u}}_j\right]\cdot\sum_\alpha \delta(\mathbf{r}-\mathbf{r}_j-\alpha\,D\hat{\mathbf{u}}_j) \\ &\quad\times\left[\tfrac{D}{L}\sum_\beta \mathbf{U}_{j,\beta} - \mathbf{U}_{j,\alpha} - 12\,\alpha\,(\tfrac{D}{L})^3\,\hat{\mathbf{u}}_j\times\{\hat{\mathbf{u}}_j\times\sum_\beta \beta\,\mathbf{U}_{j,\beta}\}\right] > .\end{aligned} \tag{320}$$

First consider the relatively simple contribution,

$$\begin{aligned}\mathbf{I} &\equiv < \sum_{j=1}^{N}\sum_\alpha \alpha\,\delta(\mathbf{r}-\mathbf{r}_j-\alpha\,D\hat{\mathbf{u}}_j)\,\hat{\mathbf{u}}_j\times\hat{\mathcal{R}}_j\ln\{P\} > \\ &= \sum_{j=1}^{N}\sum_\alpha \alpha\int d\mathbf{r}_1\cdots\int d\mathbf{r}_N\oint d\hat{\mathbf{u}}_1\cdots\oint d\hat{\mathbf{u}}_N\,\delta(\mathbf{r}-\mathbf{r}_j-\alpha\,D\hat{\mathbf{u}}_j)\,\hat{\mathbf{u}}_j\times\hat{\mathcal{R}}_j\,P .\end{aligned}$$

that appears in eq.(318) for $\mathbf{I}_r$. In the second line it is used that $P\hat{\mathcal{R}}_j \ln\{P\} = \hat{\mathcal{R}}_j P$, where, $P \equiv P(\mathbf{r}_1, \cdots, \hat{\mathbf{u}}_N, t)$ is the N-particle pdf. For each j, the integrations with respect to $\mathbf{r}_m$ and $\hat{\mathbf{u}}_m$ with $m \neq j$ can be done immediately. Assuming identical rods gives,

$$\mathbf{I} \;=\; N \sum_\alpha \alpha \int d\mathbf{r}_1 \oint d\hat{\mathbf{u}}_1 \, \delta(\mathbf{r} - \mathbf{r}_1 - \alpha\, D\hat{\mathbf{u}}_1)\, \hat{\mathbf{u}}_1 \times \hat{\mathcal{R}}_1 \, P(\mathbf{r}_1, \hat{\mathbf{u}}_1, t)\,.$$

It is to be noted that the differentiation with respect to $\hat{\mathbf{u}}_1$ must be performed, after which $\mathbf{r}_1$ can be replaced by $\mathbf{r} - \alpha D\hat{\mathbf{u}}_1$ upon integration with respect to $\mathbf{r}_1$. Hence,

$$\mathbf{I} \;=\; N \sum_\alpha \alpha \oint d\hat{\mathbf{u}}_1 \, \hat{\mathbf{u}}_1 \times \Big[\hat{\mathcal{R}}_1 \, P(\mathbf{r} - \alpha\, D\hat{\mathbf{u}}_0, \hat{\mathbf{u}}_1, t)\Big]_{\hat{\mathbf{u}}_0 = \hat{\mathbf{u}}_1} \;.$$

The corresponding contribution to the divergence of the stress tensor in eq.(279) follows by replacing the summation over the bead index number α by an integral as,

$$\sum_\alpha f(\cdots - \alpha\, D\hat{\mathbf{u}}_1) \;=\; D^{-1} \int_{-L/2}^{L/2} dx\, f(\cdots - x\, \hat{\mathbf{u}}_1)\;. \tag{321}$$

Next consider the somewhat more complicated contribution,

$$\begin{aligned}
\mathbf{I} \;&\equiv\; \beta < \sum_{j=1}^{N} \sum_\alpha \alpha\, \delta(\mathbf{r} - \mathbf{r}_j - \alpha\, D\hat{\mathbf{u}}_j)\, \hat{\mathbf{u}}_j \times \hat{\mathcal{R}}_j \Psi \;> \\
&=\; \beta \sum_{j=1}^{N} \sum_\alpha \alpha \int d\mathbf{r}_1 \cdots \int d\mathbf{r}_N \oint d\hat{\mathbf{u}}_1 \cdots \oint d\hat{\mathbf{u}}_N \, \delta(\mathbf{r} - \mathbf{r}_j - \alpha\, D\hat{\mathbf{u}}_j)\; P\; \hat{\mathbf{u}}_j \times \hat{\mathcal{R}}_j \Psi\,,
\end{aligned}$$

which appears in eq.(318) for $\mathbf{I}_r$. Using pair-wise additivity (see eq.(203)), substitution of eq.(207) together with eq.(209), and assuming identical rods, it is readily found that,

$$\begin{aligned}
\mathbf{I} \;&=\; \sum_\alpha \alpha \int d\mathbf{r}_1 \oint d\hat{\mathbf{u}}_1 \oint d\hat{\mathbf{u}}_2 \, \delta(\mathbf{r} - \mathbf{r}_1 - \alpha\, D\hat{\mathbf{u}}_1)\, \rho(\mathbf{r}_1, \hat{\mathbf{u}}_1, t) \\
&\qquad \hat{\mathbf{u}}_1 \times \hat{\mathcal{R}}_1 \int d\mathbf{r}_2 \, \rho(\mathbf{r}_2, \hat{\mathbf{u}}_2, t)\, \chi(\mathbf{r}_1 - \mathbf{r}_2, \hat{\mathbf{u}}_1, \hat{\mathbf{u}}_2)\,.
\end{aligned} \tag{322}$$

The integration with respect to $\mathbf{r}_2$ can be performed after transforming to the integration variable $\mathbf{R} = \mathbf{r}_1 - \mathbf{r}_2$,

$$\begin{aligned}
\int d\mathbf{r}_2 \, \rho(\mathbf{r}_2, \hat{\mathbf{u}}_2, t)\, \chi(\mathbf{r}_1 - \mathbf{r}_2, \hat{\mathbf{u}}_1, \hat{\mathbf{u}}_2) \;&=\; \int d\mathbf{R}\, \rho(\mathbf{r}_1 - \mathbf{R}, \hat{\mathbf{u}}_2, t)\, \chi(\mathbf{R}, \hat{\mathbf{u}}_1, \hat{\mathbf{u}}_2) \\
&=\; 2D \;|\, \hat{\mathbf{u}}_1 \times \hat{\mathbf{u}}_2 \,| \int_{-L/2}^{L/2} dl \int_{-L/2}^{L/2} dl'\, \rho(\mathbf{r}_1 - l\, \hat{\mathbf{u}}_1 - l'\, \hat{\mathbf{u}}_2, \hat{\mathbf{u}}_2, t)\;.
\end{aligned}$$

In the second equation, the integration with respect to $\mathbf{R}$ is transformed to integration with respect to $\{l, l', l''\}$, which are defined as, ,

$$\begin{aligned}
\mathbf{R} \;&=\; l\, \hat{\mathbf{u}}_1 + l'\, \hat{\mathbf{u}}_2 + l'' \frac{\hat{\mathbf{u}}_1 \times \hat{\mathbf{u}}_2}{|\, \hat{\mathbf{u}}_1 \times \hat{\mathbf{u}}_2 \,|}\;, \\
-\tfrac{1}{2}L \le l\,, l' \le \tfrac{1}{2}L \quad &, \quad -D \le l'' \le D\;.
\end{aligned} \tag{323}$$

The Jacobian of this transformation is equal to $|\,\hat{\mathbf{u}}_1 \times \hat{\mathbf{u}}_2\,|$. Since the suspension properties do not significantly change over distances of the order of the thickness D of the rods, the integration with respect to l'' gives rise to a prefactor $2D$. Hence,

$$\mathbf{I} \;=\; 2D \sum_\alpha \alpha \int d\mathbf{r}_1 \oint d\hat{\mathbf{u}}_1 \oint d\hat{\mathbf{u}}_2 \int_{-L/2}^{L/2} dl \int_{-L/2}^{L/2} dl'\, \delta(\mathbf{r}-\mathbf{r}_1-\alpha\, D\hat{\mathbf{u}}_1)\, \rho(\mathbf{r}_1,\hat{\mathbf{u}}_1,t)$$
$$\hat{\mathbf{u}}_1 \times \hat{\mathcal{R}}_1\, |\,\hat{\mathbf{u}}_1 \times \hat{\mathbf{u}}_2\,|\;\; \rho(\mathbf{r}_1 - l\,\hat{\mathbf{u}}_1 - l'\,\hat{\mathbf{u}}_2, \hat{\mathbf{u}}_2, t)\,.$$

As before it should be noted that upon integration with respect to $\mathbf{r}_1$, the delta distribution renders $\mathbf{r}_1 = \mathbf{r} - \alpha D\hat{\mathbf{u}}_1$ after the differentiation with respect to $\hat{\mathbf{u}}_1$ has been performed. Hence,

$$\mathbf{I} \;=\; 2D \sum_\alpha \alpha \oint d\hat{\mathbf{u}}_1 \oint d\hat{\mathbf{u}}_2 \int_{-L/2}^{L/2} dl \int_{-L/2}^{L/2} dl'\, \rho(\mathbf{r} - \alpha\, D\hat{\mathbf{u}}_1, \hat{\mathbf{u}}_1, t)$$
$$\hat{\mathbf{u}}_1 \times \Big[\hat{\mathcal{R}}_1\, |\,\hat{\mathbf{u}}_1 \times \hat{\mathbf{u}}_2\,|\;\; \rho(\mathbf{r} - \alpha\, D\hat{\mathbf{u}}_0 - l\,\hat{\mathbf{u}}_1 - l'\,\hat{\mathbf{u}}_2, \hat{\mathbf{u}}_2, t)\Big]_{\hat{\mathbf{u}}_0 = \hat{\mathbf{u}}}\,.$$

The bead index summation is replaced by an integral similarly as in eq.(321), leading to (with $\hat{\mathbf{u}} = \hat{\mathbf{u}}_1$ and $\hat{\mathbf{u}}' = \hat{\mathbf{u}}_2$),

$$\mathbf{I} \;=\; \tfrac{2}{D} \oint d\hat{\mathbf{u}} \oint d\hat{\mathbf{u}}' \int_{-L/2}^{L/2} dx \int_{-L/2}^{L/2} dl \int_{-L/2}^{l/2} dl'\, x\, \rho(\mathbf{r} - x, \hat{\mathbf{u}}, t)$$
$$\hat{\mathbf{u}} \times \Big[\hat{\mathcal{R}}\;\; |\,\hat{\mathbf{u}} \times \hat{\mathbf{u}}'\,|\;\; \rho(\mathbf{r} - x\,\hat{\mathbf{u}}_0 - l\,\hat{\mathbf{u}} - l'\,\hat{\mathbf{u}}', \hat{\mathbf{u}}, t)\Big]_{\hat{\mathbf{u}}_0 = \hat{\mathbf{u}}}\,.$$

This expression can be found in eq.(279).

The contribution $\mathbf{I}_t$ to the stress tensor in eq.(319) is evaluated similarly.

The β-summations in the contribution $\mathbf{I}_u$ in eq.(320) are replaced by integrals, similar to eq.(321), as,

$$\sum_\beta \beta\, \mathbf{U}_{j,\beta} \;=\; D^{-2} \int dx'\, x'\, \mathbf{U}(\mathbf{r}_j + x'\,\hat{\mathbf{u}}_j)\,. \tag{324}$$

The prefactors in eqs.(318,319,320) are found from eqs.(169,171) to be equal to,

$$\frac{\gamma\,\bar{D}}{\ln\{L/D\}} \;=\; \tfrac{D}{L}\, k_B T\;,\;\; \text{and}\;\;,\;\; \tfrac{4}{3}\, \tfrac{\gamma\, D\, D_r}{\ln\{L/D\}} \;=\; 12 \tfrac{D^2}{L^3}\, k_B T\;.$$

This concludes the mathematical details leading to eq.(279).

Bibliography

Batchelor, G. K., 1970, *J. Fluid Mech.* **41**, 545.

Baumberger, T., Perrot, F., and Beysens, D., 1991, *Physica A* **174**, 31.

Berry, D. H. and Russel, W. B., 1987, *Fluid Mech.* **180**, 475.

Bolhuis, P. and Frenkel, D., 1997, *J. Chem. Phys.* **106**, 666.

Bretherton, F. P., 1962, *J. Fluid Mech.* **14**, 284.

Chauveteau, G., 1982, *J. Rheol.* **26**, 111.

Claeys, I. L. and Brady, J. F., 1993, *Fluid Mech.* **251**, 442.

de la Torre, J. G. and Bloomfield, V. A., 1981, *Quarterly Rev. Biophys.* **14**, 81.

Deutch, J. M. and Oppenheim, I. J., 1971, *J. Chem. Phys.* **54**, 3547.

Dhont, J. K. G., 1996, *An Introduction to Dynamics of Colloids*. Elsevier, Amsterdam.

Dhont, J. K. G., 1999, *Phys. Rev. E* **60**, 4534.

Dhont, J. K. G. and Briels, W. J., 2002, *J. Chem. Phys.* **117**, 3992.

Dhont, J. K. G. and Briels, W. J., 2003, *J. Chem. Phys.* **118**, 1466.

Dhont, J. K. G. and Nägele, G., 1998, *Phys. Rev. E* **58**, 7710.

Doi, M., 1981, *J. Pol. Sci.: Pol. Phys. Edition* **19**, 229.

Doi, M. and Edwards, S. F., 1978a, *J. Chem. Soc. Faraday Trans. 2* **74**, 560.

Doi, M. and Edwards, S. F., 1978b, *J. Chem. Soc. Faraday Trans. 2* **74**, 918.

Doi, M. and Edwards, S. M., 1986, *The Theory of Polymer Dynamics*. Oxford University Press, Oxford.

Doi, M., Shimada, T., and Okano, K., 1988, *J. Chem. Phys.* **88**, 4070.

Erpenbeck, J. J. and Kirkwood, J. G., 1963, *J. Chem. Phys.* **38**, 1023.

Fielding, S. M. and Olmsted, P. D., 2003, *Eur. Phys. J. E* **11**, 65.

Forest, M. G. and Wang, Q., 2003, *Rheol. Acta* **42**, 20.

Fraden, S., Maret, G., Caspar, D. L. D., and Meyer, R. B., 1989, *Phys. Rev. Lett.* **63**, 2068.

Graf, C., Kramer, H., Deggelmann, M., Hagenbüchle, M., Johner, C., Martin, C., and Weber, R., 1993, *J. Chem. Phys.* **98**, 4920.

Grelet, E. and Fraden, S., 2003, *Phys. Rev. Lett.* **90**, 198302.

Happel, J. and Brenner, H., 1983, *Low Reynolds Number Hydrodynamics*. Martinus Nijhoff Publishers, The Hague.

Hess, S. and Kröger, M., 2004, *J. Phys.: Condensed Matter* **38**, 3835.

Hinch, E. J. and Leal, L. G., 1972, *J. Fluid Mech.* **52**, 683.

Hinch, E. J. and Leal, L. G., 1976, *J. Fluid Mech.* **76**, 187.

Iizuka, E., 1978, *Kiss and Porter (1978) refers to a personal communication with Iizuka who apparently found negative normal stress differences before or at the same time as Kiss and Porter (1978), but never published these data.* .

Ingber, M. S. and Mondy, L. A., 1994, *J. Rheol.* **38**, 1829.

Jefferey, G. B., 1922, *Proc. R. Soc. London, Ser A* **102**, 161.

Kang, K., Lettinga, M. P., and Dhont, J. K. G., 2004, *Unpublished* .

Kiss, G., 1996, *J. Polym. Sci.: Part B : Polym. Phys.* **34**, 2263.

Kiss, G. and Porter, R. S., 1978, *J. Polym. Sci.: Polym. Symp.* **65**, 193.

Kuhn, W. and Kuhn, H., 1945, *Helv. Chim. Acta* **28**, 97 (in German).

Kuzuu, N. and Doi, M., 1983, *J. Phys. Soc. Japan* **52**, 3486.

Larson, R. G., 1990, *Macromolecules* **23**, 3983.

Larson, R. G., 1996, *J. Polym. Sci.: Part B : Polym. Phys.* **34**, 2267.

Larson, R. G., 1999, *The Structure and Rheology of Complex Fluids*. Oxford University Press, NY/Oxford.

Leal, L. G. and Hinch, E. J., 1972, *J. Fluid Mech* **55**, 161.

Lenstra, T. A. J., Dogic, Z., and Dhont, J. K. G., 2001, *J. Chem. Phys.* **114**, 10151.

Lettinga, M. P. and Dhont, J. K. G., 2004, *J. Phys.: Condensed Matter* **16**, 3929.

Lu, C.-Y., Olmsted, P. D., and Ball, R. C., 2000, *Phys. Rev. Lett.* **84**, 642.

Magda, J. J., Baek, B. S.-G., de Vries, K. L., and Larson, R. G., 1991, *Macromolecules* **24**, 4460.

Maier, W. and Saupe, A., 1958, *Z. Naturforsch.* **13A**, 564.

Maier, W. and Saupe, A., 1959, *Z. Naturforsch.* **14A**, 882.

Maier, W. and Saupe, A., 1960, *Z. Naturforsch.* **15A**, 287.

Marrucci, G. and Maffettone, P. L., 1989, *Macromolecules* **22**, 4076.

Marrucci, G. and Maffettone, P. L., 1990a, *J. Rheol.* **34**, 1217.

Marrucci, G. and Maffettone, P. L., 1990b, *J. Rheol.* **34**, 1231.

Mead, D. W. and Larson, R. G., 1990, *Macromolecules* **23**, 2524.

Murphy, T. J. and Aquirre, J. L., 1972, *J. Chem. Phys.* **57**, 2098.

Olmsted, P. D., 1999, *Europhys. Lett.* **48**, 339.

Olmsted, P. D. and Lu, C.-Y. D., 1999, *Phys. Rev. E* **60**, 4397.

Olmsted, P. D., Radulescu, O., and Lu, C.-Y. D., 2000, *J. Rheol.* **44**, 257.

Onsager, L., 1933, *Chem. Rev.* **13**, 73.

Onsager, L., 1942, *Phys. Rev.* **62**, 558.

Onsager, L., 1949, *Ann. N.Y.Acad.Sci* **51**, 627.

Oseen, C. W., 1927, *Neuere Methoden und Ergebnisse in der Hydrodynamik*. Akademische Verlagsgesellschaft, Leipzig.

Papathanasiou, T. D. and Guell, D. C., 1997, *Flow-induced alignment in composite materials*. Woodhead Publishing Ltd., Cambridge.

Rienäcker, G. and Hess, S., 1999, *Physica A* **267**, 294.

Russel, W. B., Saville, D. A., and Schowalter, W. R., 1991, *Colloidal Dispersions*. Cambridge University Press, Cambridge.

Schmidt, F. G., Hinner, B., Sackmann, E., and Tang, J. X., 2000, *Phys. Rev. E* **62**, 5509.

Shimada, T., Doi, M., and Okano, K., 1988, *J. Chem. Phys.* **88**, 7181.

Simha, R., 1940, *J. Phys. Chem.* **44**, 25.

Solomon, M. J. and Boger, D. V., 1998, *J. Rheol.* **42**, 929.

Strating, P., 1995, *J. Chem. Phys.* **103**, 10226.

Tang, J. and Fraden, S., 1993, *Phys. Rev. Lett.* **71**, 3509.

Tang, J. and Fraden, S., 1995, *Liquid Crystals* **19**, 459.

Tao, Y., den Otter, W. K., Padding, J. P., and Briels, W. J., 2004, *unpublished* .

Vermant, J., Yang, H., and Fuller, G. G., 2001, *AIChE Journal* **47**, 790.

Winkler, R. G. and Gompper, G., 2004, *unpublished* .

Winkler, R. G., Mussawisade, K., Ripoll, M., and Gompper, G., 2004, *J. Phys. Condens. Matter* **16**, S3941.

Winters, J. W., Odijk, T., and van der Schoot, P., 2000, *Phys. Rev. E* **63**, 011501.

Yamamoto, S. and Matsuoka, T., 1995, *J. Chem. Phys.* **102**, 2254.

Yamane, Y., Kaneda, Y., and Doi, M., 1994, *J. Non-Newtonian Fluid Mech.* **54**, 405.

Yang, J. T., 1987, *Dynamics of Polymeric Liquids*, vol. 2. John Wiley and Sons, Inc.

Zirnsak, M. A., Hur, D. U., and Boger, D. V., 1994, *J. Non-Newtonian Fluid Mech.* **54**, 153.